

**Formational Processes of Recent, Arsenic Rich,
Ferromanganese Lacustrine Precipitates in Nova Scotia and
Northern Ontario**

Presented by
Leah Kerkermeier

Submitted for the fulfillment of the requirements for the degree of
Master of Science in Geology

Supervisor: Dr. P. Fralick

Department of Geology
Lakehead University
Thunder Bay, Ontario, P7B 5E1

Canada

July, 2013

Table of Contents

List of Figures	3
List of Tables	6
Abstract	7
Purpose of Study	8
Introduction	
Previous Work.....	10
<i>Iron-manganese precipitates in a near neutral pH, lacustrine setting</i>	10
<i>Arsenic found in iron and manganese deposits of lacustrine and groundwater settings</i>	17
<i>Iron-manganese nanospheres</i>	20
<i>Health effects from arsenic in iron- and manganese-rich water contamination</i>	23
Site Description	
Topography and Geology.....	25
Locations and Access	32
Methodology	
Description of Methods.....	39
Results	
1. Nodule Description.....	49
2. Water Chemistry.....	66
3. Environmental Distribution of Major and Minor Elements.....	72
4. Correlation of Geochemical Elements.....	75
5. Nodule Anatomy, Sediment Geochemistry and Rare Earth Elements.....	81
6. Micro Analysis with a Scanning Electron Microscope (SEM).....	87
7. My Cove Shoreline Analysis, Lake Charlotte.....	109
8. X-Ray Diffraction (XRD) Analysis	117

Discussion

1. Chemical Correlations.....119

2. Geochemistry.....128

3. Microbiology.....131

4. Water Chemistry.....133

5. The Growth of a Nodule: Review of Past Theories.....139

6. Nodule Growth Models.....141

7. Potential Environmental Implications of Iron-Manganese Precipitate Research.....148

Conclusion.....150

Acknowledgements.....152

References.....153

Appendix Table of Contents.....162

Appendix A: Accuracy and Precision values.....appendix p. 2

Appendix B: Transect point precipitate geochemistry data and water data values.....appendix p. 3

Appendix C: Precipitate geochemistry dissection values.....appendix p. 31

Appendix D: Geochemistry of silisiclastic sediment.....appendix p.34

Appendix E: Water analysis Data.....appendix p. 38

Appendix F: Environmental distribution elemental maps.....appendix p. 54

List of Figures

Site Descriptions

Figure 1: Geologic map of Shebandowan Lake and legend.....	26
Figure 2: Geologic Map of Sowden Lake.....	28
Figure 3: Geologic map of Lake Charlotte.....	30
Figure 4: Map of Lake Shebandowan displaying site location areas.....	32
Figure 5: Southern Shore of Small Site and Island Site, Shebandowan Lake.....	33
Figure 6: Map of Sowden Lake displaying collection sites	34
Figure 7: Sowden 41 site, and Sowden 46 Site, Sowden Lake.....	35
Figure 8: Map of Lake Charlotte displaying areas of sample collection.....	36
Figure 9: Images of Lake Charlotte Shorelines.....	37

Methodology and Results

Figure 10: Water chemistry collection points at the 5 Lake Charlotte study sites.....	42
Figure 11: Water Chemistry data points from the Lake Charlotte and Shebandowan Lake Study Sites.....	43
Figure 12: Nodule sample collection points from the 5 Lake Charlotte study sites.....	44
Figure 13: Nodule sample collection points from Shebandowan and Sowden Lakes.....	45
Figure 14: Lake Charlotte, 7 Cove	50
Figure 15: Lake Charlotte, Bud's Cove nodules	52
Figure 16: Lake Charlotte, My Cove nodules.....	54
Figure 17: Lake Charlotte, Granite Islands nodules.....	56
Figure 18: Lake Charlotte, Mine Site nodules.....	58
Figure 19: Sowden Lake, Area 41 nodules	60
Figure 20: Sowden Lake, Area 46 nodules	62
Figure 21: Shebandowan Lake, Island Site	64
Figure 22: Shebandowan, Island Site nodule.....	66
Figure 23: A positive trend between the temperatures of the lake bottom and the difference between the lake bottom and sediment bottom at 7 Cove, Lake Charlotte.....	67
Figure 24: A positive trend between the lake bottom temperature and the difference between lake bottom and sediment temperatures at My Cove , Lake Charlotte.....	68
Figure 25: Example of elemental mapping.....	73

Figure 26: Arsenic vs. iron (a) and phosphorous vs. iron (b) displaying a positive correlation	77
Figure 27: Barium vs. Manganese (a) and Suphur vs. Manganese (b) and cobalt vs. Manganese (c) displaying a positive correlation to one another.....	78
Figure 28: A positive correlation between potassium vs. Aluminum, (a) magnesium vs. aluminum (b), and titanium vs. aluminum.....	79
Figure 29: A negative correlation is found between Iron and Aluminum	80
Figure 30: Graph displays a negative correlation between manganese and aluminum.....	80
Figure 31: Graph displaying as the amount of arsenic increases in a sample, the amount of phosphorous decreases.....	81
Figure 32: Graphs of Rare earth elements normalized to PAAS	85
Figure 33: Rare earth element analysis of the top portion vs. bottom portion of five samples normalized to PAAS.....	86
Figure 34: Lake Charlotte, My Cove images of the bottom portion of the nodule.....	89
Figure 35: Lake Charlotte, My Cove images of the top portion of a nodule.....	89
Figure 36: Element distribution images from the bottom portion of a Lake Charlotte sample.....	90
Figure 37: Element distribution images from the top portion of a Lake Charlotte sample.....	90
Figure 38: a) A line Scan analysis from the nodule found in Figure 33.....	91
Figure 39: SEM image map of the top (a) middle (b) and bottom (c) portion of a sample from Lake Charlotte.....	92
Figure 40: Sowden Lake, Area 46; images of the top portion of the nodule.....	95
Figure 41: Sowden Lake, Area 46; images of the bottom portion of the nodule.....	95
Figure 42: Element distribution images of Figure 39 (top section of Sowden Lake nodule).....	96
Figure 43: Element distribution images of Figure 39 (bottom section of Sowden Lake nodule).....	97
Figure 44: A line Scan analysis from a nodule found in Sowden Lake.....	98
Figure 45: SEM image of the top of a sample from Sowden Lake data provided in Table 4	99
Figure 46: Shebandowan Lake, Island Site images of the bottom top of the nodule.....	101
Figure 47: Shebandowan Lake, Island Site images of the bottom portion of the nodule.....	102
Figure 48: Element distribution images of Figure 45	102
Figure 49: Element distribution images of Figure 46	103
Figure 50: A line Scan analysis from a nodule found in Shebandoawn Lake.....	104
Figure 51: a) SEM image of the top of a sample from Shebandowan Lake.....	105
Figure 52: SEM images of the surface of a raw sample from Lake Charlotte.....	107
Figure 53: A raw sample SEM image and maps from a Lake Charlotte nodule.....	108

Figure 54: SEM image of potential nanospheres surrounded by possible extracellular polymeric substances (EPS) on the surface of a nodule from Lake Charlotte.....	109
Figure 55: Image of the My Cove shoreline pit.....	110
Figure 56: Image of layer A.....	111
Figure 57: Image of Layer B.....	111
Figure 58: Image of Layer C.....	112
Figure 59: Image of layer C-D (b) Layer C-D sediment distribution graph.....	113
Figure 60: Image of layer E (b) Layer E sediment distribution graph.....	113
Figure 61: Image of layer E-F (b) Layer E-F sediment distribution graph.....	114
Figure 62: Image of layer F (b) Layer F sediment distribution graph.....	115
Figure 63: Image of layer G (b) Layer G sediment distribution graph.....	116
Figure 64: Geochemical data from each layer of the My Cove.....	117

Discussion

Figure 65: Eh-pH diagram of phosphorous displaying how the element changes valance states depending on the pH and redox potential of the environment.....	120
Figure 66: Eh-pH diagram of arsenic displaying how the element changes valance states depending on the pH and redox potential of the environment.....	120
Figure 67: The Linear relationship between phosphorous and arsenic	122
Figure 68: A visual representation of how barium is able to attach to a manganese oxide taken from Manceau (2007).....	126
Figure 69: Average rare earth concentrations normalized to PAAS.....	129
Figure 70: A visual representation of how diatoms found in a biofilm are able to naturally remove iron and arsenic from contaminated water.....	133
Figure 71: Eh/pH diagrams displaying averages from each lake	136
Figure 72: An illustration of overturn in a dimectic lake adapted from Wetzel (1983).....	138
Figure 73: A diagram of how a potential redox boundary can be created when ground water comes into contact with lake water.....	142
Figure 74: A possible explanation as to why precipitates were found embedded in clay at Shebandowan and Sowden Lakes...146	
Figure 75: Visual representation, adapted from Dean et al (1981).....	148

List of Tables

All in Methodology and Results Section

Table 1: Average DO% values from each study site	69
Table 2: Average pH and Eh readings from all sites.....	70
Table 3: Water analysis compared to the drinking water standard.....	71
Table 4: Elements with comparable distributions to iron on the contour maps.....	74
Table 5: Elements with comparable distributions to manganese on the contour maps.....	74
Table 6: Elements with comparable distributions to aluminum on the contour maps.....	75
Table 7: Elements with comparable distributions to Carbon on the contour maps.....	75
Table 8: Percent difference values showing depletion and enrichment in elements found in the precipitate vs. the underlying sediment of a study site.....	82
Table 9: Percent difference values showing an enrichment in the lake sediment found in precipitate fields when compared to the beach sand from My Cove when has not been in contact with any precipitates.....	83
Table 10: Lake Charlotte SEM Point analysis data from Figures 38 (a-c)	93
Table 11: Sowden Lake SEM Point analysis data from Figures 44 (a and b).....	99
Table 12: Shebandowan Lake SEM Point analysis data from Figures 50 (a and b).....	105
Table 13: Representative results from SEM data	106

Abstract:

Banded iron - and manganese - rich precipitates were collected from the lake bottoms of Lake Charlotte (Nova Scotia), Lake Shebandowan (Ontario) and Sowden Lake (Ontario). Investigations of study areas at the macro, meso and micro scale were conducted to understand the iron-manganese rich-nodules in their natural environment. The nodules appear as circular precipitate bands which alternate between high concentrations of iron and manganese. Analysis of precipitates revealed that those from Lake Charlotte are highly concentrated in arsenic. Lake Shebandowan and Sowden Lake samples are highly concentrated in phosphorous.

Correlation between iron, arsenic and phosphorous suggests oxidation and precipitation of these elements in the same bands of the nodule. Iron relies on the Eh and pH of an environment to precipitate from solution. At a redox boundary in a near neutral environment, iron is able to oxidize as a sediment coating and co-precipitate arsenic and phosphorous from the water. An affiliation between manganese, barium and cobalt suggests precipitation of these elements in the alternate bands present in the nodule. Barium and cobalt are able to co-precipitate with manganese by either penetrating a manganese oxide by means of protonation, or oxidize and become interchangeable with Mn^{4+} .

The growth of the nodules at Shebandowan and the majority of Lake Charlotte sites were probably affected by a redox boundary created by the diffuse upward flow of groundwater with lower Eh than the oxidized lake water. It is likely that photosynthetic and iron and manganese oxidizing microorganisms are present in a bacterial mat covering the nodules and probably played a role in their precipitation. Analysis of the growth mechanisms of precipitates revealed in Sowden Lake and the Granite Islands site of Lake Charlotte were inconclusive.

Purpose of Study

This study was completed to understand how iron – and manganese – rich precipitates grow on freshwater lake bottoms in three Canadian lakes. In past research by Dasti (2008) and Stevens (2007), iron – and manganese – rich precipitates collected from Lake Charlotte, Nova Scotia were found to have extremely high concentrations of arsenic. Further research in Lake Shebandowan, Ontario (Sozanski and Cornan, 1978; Dasti, 2008) revealed the presence of precipitates similar in appearance and composition to those of Lake Charlotte. Accidental collection of precipitates by a fisherman in Sowden Lake, Ontario, brought to light specimens with the same nodule structure as those in Lake Shebandowan and Lake Charlotte, although no previous research on the precipitates from Sowden Lake is known.

Iron – and manganese-rich nodules appear as spherical or oblong structures. They consist of a dark brown or black precipitate surrounding a nucleus created by an object found within their environment, such as a pebble, cobble or wood, etc. They are present on the surface of lake bottoms, often occurring in shallow waters and on top of a sandy substrate (Kindle, 1932; Harris and Troup, 1969; Sozanski and Cornan, 1976; Dean et al., 1981; Boudreau, 1988; Kepkay, 1985; Sommers et al., 2002; Stevens, 2007). A cross-section of the precipitate matter from the nodules collected in this study often reveals alternating light and dark brown layering appearing as stromatolitic structures. Similar structures have also been described on the surface of ocean bottoms in both shallow and abyssal waters (Oswald and Fraser, 1973; Crerar and Barnes, 1974; Margolis and Burns, 1976; Reyss et al. 1982; Yoshikawa, 1991; Takahashi et al. 2000).

Iron and manganese are the two main elements composing the nodules. Chemically, both elements behave similarly to redox potentials and temperature. Changes to these conditions will alter the form iron and manganese take in the surrounding environment. Iron exists in solution as either a ferrous (Fe^{2+}) or ferric (Fe^{3+}) state. The amount of iron in solution is dependent on the degree of

oxidation in the aqueous environment, which will dictate the amount and rate of iron oxidation from the ferrous to ferric state (Wetzel, 2001). The most common species of ferric iron in a well aerated lacustrine environment is hydrated ferric oxide ($\text{Fe}(\text{OH})_3$), which is at equilibrium in the pH range of 5-8, appearing as a solid state due to its low solubility (Wetzel, 2001).

Manganese in particular can be difficult to interpret in a changing environment due to its oxide mineralogy. Although manganese can occur in several valence states, in a well aerated lacustrine environment Mn^{3+} becomes thermodynamically unstable and Mn^{4+} is insoluble. The divalent Mn^{2+} commonly occurs at low redox potentials and pH, however its presence is often observed in a broad range of natural environments (Wetzel, 2001).

Research involving iron, manganese and arsenic may enhance understanding of how these elements interact with one another, how they are formed, and how they are able to grow in their natural environment. Knowledge gained from understanding nodule formation can be used in environmental science practice as a means of preventing arsenic and other heavy metal contamination in surface and groundwater settings.

Introduction

Previous Work

Iron-manganese precipitates in a near neutral pH, lacustrine setting:

Ferromanganese concretions consisting of nodules composed of alternating bands rich in iron and manganese have been found in lacustrine environments with normal pH waters. The deposition of these concretions is influenced by water depth, substrate of the lake bottom, and the biotic communities of microorganisms. All factors play a role in forming the appearance of stromatolitic structures found as part of the nodule morphology (Sommers et al., 2002). By observing the setting, morphology, and microbiology where ferromanganese deposits are found, a better understanding of the processes that created them can be achieved.

Two morphologies of ferromanganese nodules have been described in Lake Vermilion, Minnesota including a “reef type” consisting of a laminated disc growing around a cobble, and an “oncoïd type” consisting of oval nodules found on muddy gravel (Sommers et al., 2002). Reef type deposits are up to 2.5cm thick, are found on a solid substrate in depths of 1-7.0m, and grow three times faster upward than they grow downward. These precipitates are laminated with alternating iron-rich and manganese-rich layers and range on the mm to cm scale. These nodules concentrate iron and manganese offering a micronutrient environment for microorganisms and some plants which require manganese for photosynthesis (Sommers et al., 2002).

Conclusions of the study from Sommers et al. (2002), primarily from the role of biogenesis, suggested that the growth rate of the precipitates is extremely slow (2.27-3.53 $\mu\text{m}/\text{yr}$) therefore making the precipitates 4250-6600 years old. Sommers et al. (2002) state that due to the amount of variability in the physical conditions of lakes, no explanation of nodule genesis could be proposed. However,

limitations to the nodule origin and development were determined to be created by biogenic processes, water depth, and substrate.

Rod and coccoidal shaped bacteria were found colonizing the surface of stromatolite structures on the nodules from Lake Vermilion and are considered to be the prime constructing agents of the stromatolitic structures concentrating in the precipitate (Sommers et al., 2002). It is suggested that the bacteria present in the stromatolitic structures allow for iron and manganese precipitation along with abiotic factors such as water chemistry (Sommers et al., 2002). The development of stromatolitic structures appears to be influenced by the substrate the precipitates are found on: either solid substrate with cobbles for “reef type”, muddy gravel for “oncoïd type” and fine mud for no stromatolite growth (Sommers et al., 2002). The water depth appears as a constricting factor in Lake Vermilion allowing for growth only between 1-7 meters depth. Sommers et al. (2002) suggested the explanation for this to be a lack of a suitable substrate elsewhere, competition from green algae, or the amount of sunlight penetrating to the lake bottom.

Approximately 80km Northwest from Thunder Bay (Ontario) in Lake Shebandowan, a similar morphology of ferromanganese deposits to those found in Lake Vermilion, Minnesota has been described. Here the deposits occur at depths of 1-12m and are underlain by sand or coarser material (Sozanski and Cornan, 1976). The precipitates are similar in structure to the “reef” concretions found in Lake Vermilion. Both deposits are observed with banded layers of either oxidized iron (Fe) precipitates such as Goethite ($\text{FeO}(\text{OH})$), or oxidized Manganese (Mn) precipitates such as MnO_2 (Sozanski and Cornan, 1976).

Sozanski and Cornan (1976) described six different morphologies found in Lake Shebandowan: a “mushroom shape” in which the nodule is found on top of a pebble or cobble, a “top ring” where the nodule ringed structure surrounds the top of the pebble; “saturine” shaped where the nodule surrounds

the center of the pebble or cobble, an “equatorial skirt” which is a saturnine shape with only a small section around the pebble, “disc with a down curl” where a flat pebble or cobble is surrounded by the precipitate with the flat part down and stromatolite structure facing the surface, and the “pulley” in which the nodule is flat except around the edges where it splits into two sections.

The precipitates appear to be concentrated in slow moving, swampy waters. This could be due to lower pH and dissolved oxygen values in the lake water, allowing for metals to travel with organic matter (Sozanski and Cornan, 1978). Sozanski and Cornan (1978) have determined there is a positive correlation between Mn and potassium (K), calcium (Ca), magnesium (Mg), copper (Cu), nickel (Ni) and cobalt (Co). The only positive correlation found for iron was with Zinc (Zn), possible due to a known presence of zinc sulphide in the area (Sozanski and Cornan, 1978).

Sozanski and Cornan (1978) described the formation of precipitates in the Shebandowan area in the following manner. Diagenesis in the substrate below the precipitate involving an upward remobilization of iron and manganese is suggested. The material supplied to create the precipitate is then derived from a lateral and upward remobilization of iron and manganese from the substrate or by being adsorbed from the lake water. The initial precipitation of iron in the form of $\text{Fe}(\text{OH})_3$ onto a pebble nucleus is followed by absorption of Mn^{2+} . As an increase in Eh-pH occurs at the lake bottom by means of groundwater coming into contact with surface water through the lake bottom sand, the Mn^{2+} becomes oxidized to Mn^{4+} and is precipitated as MnO_2 . The Eh-pH of a lake is often altered by changes in the seasons and therefore could be cause for the alternating iron and manganese banding found in the precipitate. It is suggested that due to the iron rich nature of the precipitates found in Lake Shebandowan, and the ability for iron to oxidize before manganese, distribution of the precipitates is dependent on the Eh-pH conditions of the lake bottom water.

Similar morphologies to those found in northwestern Ontario have been described in Nova Scotia, Canada. However the geological environment of Grand Lake and Ship Harbour Lake (Lake Charlotte), where the nodules are located, is different than that of northwestern Ontario (Kindle, 1932). Precipitates in Nova Scotia are found on sedimentary rock fragments in 0.5-2m of water depth and form on bottoms composed of coarse grained sand and pebbles (Harris and Troup, 1969). As with the other precipitates described, they display internal banded of iron and manganese. Harris and Troup (1969) had no explanation for the origin of precipitate formation; however, they suggest two major features which should be taken into account: the geographic distribution of precipitates in temperate vs. subarctic environments, and the presence of chemical banding. They hypothesize that a pair of bands, one iron-rich and one manganese- rich represent the annual growth increment of a precipitate. The calculated growth rate for precipitates in the Nova Scotia lakes by Harris and Troup (1969) was 1.5mm/yr.

Lake Charlotte nodules have been examined by Boudreau (1988) to further understand the rational of their growth, and the origins of heavy metals present in them. Boudreau (1988) suggested that a nodule plays the role of a strong sink for heavy metals when compared to its underlying lake bottom sediment. As the lake water passes over the nodule, gradients in metal concentrations develop in the water adjacent to its surface. This allows for the lake water coming into contact with the nodule to diffuse elements onto the nodule surface. Therefore, the concentration of iron and manganese in the precipitate would be dependent on the concentration of these elements within the lake water.

The research of Boudreau (1988) was broadly based on the work of Kepkay (1985) who suggested that the diffusion of metals is directed into the sediment from the lake water. Kepkay (1985) researched the amounts of iron and manganese present in the pore waters of sediment underlying the nodules of Lake Charlotte, Nova Scotia. It was suggested that the oxidation of heavy metals onto the sediment has a strong affiliation with the existence of microorganisms in the environment.

Iron and manganese precipitates found in Lake Charlotte, Nova Scotia were examined by Stevens (2007) to further understand their origin. Stevens (2007) suggested that when reduced groundwater comes into contact with oxidized lake water by means of a spring or diffuse flow on a lake bottom, redox sensitive elements can oxidize and precipitate out of solution coating a nucleation point such as a pebble. This idea may be used to further understand why large concentrations of other elements have been found in iron-manganese precipitates. For example, concentration of arsenic, by means of this redox method, can be high due to the ability of groundwater to leach a large area and transport ions in solution for long distances, concentrating the dissolved material in the nodules.

A final theory as to how ferromanganese precipitates form was examined by Konhauser (2007) who adapted models described by Dean et al. (1981). In this model nodules are created from a series of microbial catalyzed reactions, which are as follows (Dean et al., 1981): Firstly, cyanobacteria and algal plankton concentrate manganese and iron by catalyzed oxidation reactions. Upon their death, the bodies of these microorganisms are transported to the lake bottom sediment and are buried. This causes their bodies to be exposed to a suboxic environment, allowing iron and manganese to be reduced into solution. An upward diffusion of water at the sediment-water interface causes the iron and manganese to be re-oxidized. This reaction is continued causing accretion on an existing oxidized iron and manganese surface. The result is the formation of a nodule. Dean et al. (1981) further suggested that some of the iron- manganese precipitates could be physically transported to the anoxic zone of a lake causing reduction of redox elements to occur and allowing their ions to be introduced to the water column. Some of the reduced iron and manganese ions end up in oxic waters where they are re-precipitated. In this study, three main nodule formation concepts described by previous authors will be considered, including the ground to surface water interface, the sediment interface, or from an interface in the lake water.

Iron and manganese oxidization by bacteria in a near neutral pH environment

Iron oxidizing bacteria require ferrous iron to metabolize for their energy requirements. In near neutral waters, the immediate oxidation of ferrous iron makes it difficult for microorganisms that use this as an energy source to thrive. Bacterial oxidation is not instantaneous and therefore cannot compete when chemical oxidation is already occurring (Emerson and Moyer, 1997). Due to the potential for ferrous iron to become rapidly oxidized by abiotic (non-living) processes in an environment of high oxygen and near neutral pH, neutrophilic microorganisms, known as microaerophiles, preferentially populate the anoxic/oxic interface in sediment and groundwaters (Hedrich et al., 2011). Here they acquire the oxygen and energy (carbon) which they need for survival.

In a highly oxygenated, near neutral environment, the microaerophile *Gallionella ferruginea* sp. may act as bacterial catalyst for the oxidation of iron. The *G. ferruginea* sp. appear as elongated helical stalks composed of intertwined microfibrils covered with iron oxide precipitate sheaths. They obtain their energy by a chemolithotrophic process which uses inorganic donors such as ferrous (Fe^{2+}) iron in oxidation/reduction reactions (Ridgeway et al., 1981). *G. ferruginea* can be autotrophic, having the ability to create nutrient organic molecules from inorganic sources (light or chemical energy), or mixotrophic having the ability to gain nutrients by a combination of different energy sources, and are able to grow by using ferrous iron as an electron donor (Hallbeck and Pederson, 1991).

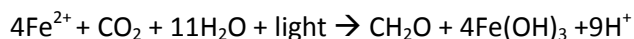
Chemolithotrophy involving ferrous iron oxidation, as in the case of the *G. ferruginea* sp., works for the organism to gain two objectives: to generate adenosine triphosphate (ATP) in the organism for use of transporting energy within cells, and to generate the reducing power of nicotinamide adenine dinucleotide (NADH) within the organism to be used as a reducing agent to donate electrons (Hedrich et al., 2011). These two objectives are fulfilled in the following equation (Miot et al., 2009):



Here the Fe^{2+} serves as both the source of ATP and the electrons electrons for NADH.

The *Leptothrix ochracea* sp. is another iron oxidizing bacteria that can be found in neutral pH environments. Both microorganisms are only able to thrive under anoxic conditions such as at the oxic-anoxic boundary of a groundwater spring (James and Ferris, 2004). The *Leptothrix* can be identified by their straw-like appearance with a sheath that commonly becomes encrusted with iron hydroxides. Though the reason is unknown, if both species occur in the same environment, the *Leptothrix* will most likely be the dominant species and most productive (James and Ferris, 2004). Dominance of *Leptothrix* could be due to its ability to act not only as a chemolithotroph or a mixotroph as with the *Gallionella*, but also as an organotroph, having the ability to obtain hydrogen from organic substrates (James and Ferris, 2004). Photoautotrophic iron oxidizing bacteria have also been found in the environment at the oxic/anoxic boundary.

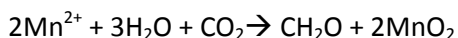
The phototrophic *Rhodobactor* sp, a kind of purple bacteria, is able to synthesize nutrients from inorganic iron sources by use of light as its energy source (Miot et al., 2009). In this case ferrous iron is used as a reducing agent for carbon dioxide, which is described in the following equation (Hedrich et al., 2011):



As with other oxidizing bacteria, an iron sheath precipitates around the bacteria. In the case of a the *Rhodobactor* sp, its sheath may become its demise due to the iron precipitate restricting the bacteria's access to light (Hedrich et al., 2011).

Precipitation of manganese in a neutral pH environment has a greater relationship with bacteria compared to iron. Unlike, iron, manganese does not oxidize quickly in a pH of below 9 and therefore precipitation benefits from that of a bacterial catalyst (Ghiorse, 1984). Even though this is the case, the

majority of Mn-oxidizing bacteria prefer to thrive at near anoxic conditions where there is less competition with chemical oxidation. The *Leptothrix sp* which is also an iron catalyst is the most prevalent Mn-oxidizer. The bacteria works the same as with iron by absorbing Mn(II) onto its sheath and then oxidizing it by a catalyst reaction (Perera and Jinno, 2009):



Once the Mn(II) is oxidized to form MnO₂, cations of heavy metals such as lead (Pb) can be adsorbed onto the sheath of the bacteria. This allows for a concentration of heavy metals. If the bacteria are used as a food source for clams and/or other primary consumers it can work its way up the food chain causing biomagnification (Jürgensen et al., 2004). Precipitation of Mn in a neutral pH environment can also be affected by the microorganism genus *Crenothrix*. These are another form of sheathed bacteria, in which the Mn (and sometimes Fe) is adsorbed onto the sheath and then oxidized (Ghiorse, 1984). They generally occur in large masses in near anoxic, neutral pH conditions.

Iron- and manganese- rich nodules are present throughout the world in lacustrine, neutral pH environments. Their morphology often occurs as banded discs of alternating iron-and-manganese-rich microlayers. By understanding the physical parameters in which these deposits are found, and the biological relationships which may contribute to their rapid deposition, knowledge can be gained of depositional processes.

Arsenic found in iron and manganese deposits of lacustrine and groundwater settings

The ability to remove arsenic from lacustrine and groundwater water can be accomplished by redox reactions involving the presence of iron and manganese in near neutral pH environments (Chen et al., 2006). In order to understand the adsorption of arsenic on these elements, the behavior of arsenic in contact with these elements must be explored. Iron and manganese oxidizing and reducing bacteria may

also be used as a tool for arsenic removal (Chen et al., 2006). Knowledge obtained from research in this field may provide new easy, low cost methods to remove arsenic from drinking water and polluted natural environments.

For arsenic to have the ability to be precipitated by iron or adsorbed onto iron hydroxide, oxidation of the environment must first occur. Reduced ferrous iron (Fe^{2+}) becomes oxidized to ferric iron (Fe^{3+}) and precipitates out of solution forming a precipitate, which commonly coats a sediment particle (Rott et al., 2006). Arsenic in the environment will then act in a similar manner to phosphate because of their chemical resemblance. Iron hydroxides have a zero charge at a pH of 8.6 making its charge in normal lake water (pH 6-8) positive (Takamatsu et al., 1985). Just as phosphate has a -3 charge in neutral pH, water so does arsenic in the form of arsenite (AsO_3^{-3}). This allows for the precipitation of oxidized As(V) with ferric iron to create the precipitate iron arsenate (AsFeO_4).

Manganese oxidation in a lake environment requires a higher redox potential (Eh) than iron due to its zero charge being at a pH of 2.3 (Takamatsu et al., 1985). This means that if manganese and iron are in solution together, iron must first be immobilized before manganese can come out of solution. If this were always the case, then the arsenic in solution would concentrate in the iron as AsFeO_4 due to iron precipitating before manganese (Rott et al., 2002). However, manganese does have the ability to precipitate with arsenic in neutral pH waters if cations such as Mn^{2+} , Sr^{2+} , Ba^{2+} and Ni^{2+} are present in solution with manganese hydroxide ($\text{Mn}(\text{OH})_2$). This allows for a change in the surface charge of $\text{Mn}(\text{OH})_2$ due to the additional cation. This increases the surface charge of the compound giving it the ability to precipitate in a neutral pH environment (Takamatsu et al., 1985). The increase in surface charge is accomplished as follows (Takamatsu et al., 1985): A divalent cation is adsorbed onto $\text{Mn}(\text{OH})_2$ by exchanging itself with an H^+ found on the oxide surface creating manganese oxide (MnO_2). This

provides H^+ in solution changing the pH around the precipitate. The manganese oxide (MnO_2) now has the ratio:

charged equivalents released (H^+) : charged equivalents adsorbed (divalent cation)

In this ratio, the release of H^+ is < the divalent cation by a charge of 1. This leads to a change in the MnO_2 surface charge to be more positive. If the binding of greater amount of divalent cations to the MnO_2 continues, the surface charge will have enough of a positive charge to absorb arsenic onto its surface (Takamatsu et al., 1985).

The ability of As to precipitate in a redox environment with a neutral pH has been described to be most effective if both Fe and Mn are found in the environment (He and Hering, 2009). He and Hering (2009) studied the ability for MnO_2 to adsorb As(V) both in the presence of iron and when iron was absent. They concluded that without ferrous iron present, MnO_2 could not adsorb As(V) onto its surface. It appears that the oxidation of ferrous iron to ferric iron allows for an increase in the amount of As(III) oxidizing to As(V) that can be precipitated with manganese. They determined that all the arsenic precipitated was concentrated in MnO_2 and not Fe (III) hydroxides. However the amount of arsenic adsorbed onto MnO_2 decreased when no iron was present. This is consistent with other research (Chen et al., 2006) demonstrating that the oxidation of As(III) was influenced by contact with MnO_2 .

Microorganisms of the *Leptothrix sp.* and to a lesser extent the *Gallionella sp.* are known to be involved in the precipitation of iron and manganese oxides (Katsoyiannis and Zouboulis, 2006). In the case of iron, bacteria play a role in the oxidation of ferrous iron to ferric oxy-hydroxides in anaerobic environments if chemical oxidation cannot readily occur. The oxidized iron is then incorporated in the surrounding sheaths of the bacteria creating a covering (Keim, 2011). Keim (2011) describes the coated iron sheaths as substrate for passing arsenate to be absorbed into. The iron and arsenic coated sheath

then can be adsorbed onto a precipitate or other solid state (such as a pebble) allowing arsenic to concentrate in one specific area (Keim, 2011).

Iron-manganese at the nano-scale:

Scanning electron microscopes (SEM) have enabled exploration of images at the nano-scale level. In microbial mineral interactions, this technology has been mostly applied to study the formation of carbonate minerals. Nano-bacteria, such as oxide-reducing bacteria, have been discussed as having the ability to mediate the formation of iron oxides. However, evidence to support micro structure formation by microbes is difficult to prove (Bontognali et al., 2008).

Among the nanoforms found between iron-manganese nano-spheres, are extracellular polymeric substances (EPS). EPS are compounds composed of polysaccharides with the ability to attach to a cell surface, or be secreted as a medium designed to support the growth of microorganisms. In the study of mineralization at the nano-scale, the existence of EPS has been considered proof of mediation by microbes. However due to variable composition and the hydration ability of EPS it is very difficult to study (Bontognali et al., 2008).

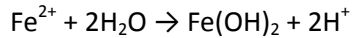
According to Vali et al. (2001), two mechanisms have been known to exist that result in the formation of nano-scale mineralization. Biomineralization, in which either bacteria induce nucleation as a result of metabolic activity, or in bacteria controlled systems where minerals will crystallize on cell walls or in an intracellular area. The mineralization of carbonates at the nanometer scale displays a unique collection of aggregates described as nano-globules. Saez-Roman et al. (2008) suggest that these structures may be the start of the nucleation of dolomite. In order for the dolomite crystals to attach to bacterial structures, they must have a charge. Microbial cell surfaces and EPS both can carry a net negative charge and therefore allow for ions to bind to their surface creating a site suitable for nucleation (Aloisi et al., 2006).

Nanostructures have been postulated to assist in the formation of Mg- rich calcite and iron hydrous oxides in the Cezallier hydrothermal springs in Massif, Central France (Casanova et al., 1999). The iron hydrous oxides were composed of dense aggregates of small rounded crystals that appear as crusts overlying organics such as twigs. These aggregates hold colonies and frameworks of bacteria known as ferruginous bacterial accretions, which are also found in acid mine drainage (Leblanc, 1996). Major and minor elements, including arsenic are concentrated on the bacterial surfaces. The evidence of nano-scale structures found in both carbonate and hydrous iron oxide environments are indications that microbial mediation is possibly contributory to mineral formation.

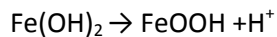
Iron oxyhydroxide nanostructures have been shown to develop in areas with microbial filaments containing polysaccharides (Chan et al., 2004). As microbial cells come in contact with iron oxyhydroxides (FeOOH) they extrude polysaccharide strands attaching to the FeOOH. Microbial cells accomplish this by acting as a catalyst to an oxidizing reaction where the cell uses the oxygen in the FeOOH for energy and in the process will precipitate iron out of solution. The attraction between the microbe and the iron is due to the net negative charge of the microbial filament and the positive Fe²⁺ (Chen et al., 2004). The microbes thus produce a polymer (polysaccharide), mineralize the polymer, and then discard the polymer so as to not become entombed by the mineral. Iron oxidizing bacteria often found in biofilms where oxidation of iron at the microscale occurs include *Leptothrix sp.* and *Gallionella sp.* (Chen et al., 2004). These bacteria oxidize iron onto an armored sheath that appears as a stalk or helix which then can be shed from the body.

The chemistry behind the entombment of a polymer can be used to further understand how bacteria oxidize iron as a source of energy. If bacteria are able to localize iron mineral precipitation, a micro-environment can be created in which there is a decrease in pH (Chan et al., 2004). The oxidation

of iron outside the surface of a cell will acidify the microenvironment adjacent to the cell membrane as described in the following equation:



Here iron generates two protons enabling a decrease in the microenvironments pH. The acidity of the environment again decreases when another proton is emitted from solution:



The H^+ is then transferred from the outside of the cell, across the proton pumping adenosine triphosphate (ATP), to the inside of the cell to be used for energy. Polysaccharides can be emitted from an iron oxidizing bacterial cell as spaghetti-like structures enabling a greater surface area for decreasing the pH in the microenvironment and enhancing the ability for iron oxidation in a microenvironment to produce energy for bacteria (Chan et al., 2004).

Nanostructures are also created with the influence of a bacterial catalyst in redox sensitive reactions. The oxidation of manganese from a 2+ to a 4+ state at the nanoscale can be achieved by a biological process. In a freshwater environment *Leptothrix discophora* have the ability to assist with the oxidation of manganese and deposit the material on an extracellular sheath (Villalobos et al., 2005). Another strain of bacteria, *Pseudomonas putida*, has the ability to produce Mn^{4+} oxides and use a biofilm consisting of extracellular polymers (EPS) to hold the oxidized manganese in place.

Pseudomonas putida assists with oxidation of manganese on the nanoscale by oxidizing the Mn^{2+} found in solution and precipitating manganese in its biofilm (Toner, B. 2005). Mn^{2+} becomes oxidized to Mn^{3+} and precipitates out of solution onto the outer portion of a bacteria's cell membrane. Manganese ions can also be oxidized to form Mn^{4+} , which can also precipitate onto or between the cell

membrane. The oxidized precipitates will then nucleate forming extra-cellular aggregates surrounding and filling in spaces between bacterial aggregates composed of bacterial membranes (Toner, 2005).

Gupta et al. (2010) researched the oxidation of iron and manganese at the nanoscale for assisting in the removal of natural arsenic concentrations in lacustrine environments. Laboratory created iron and manganese nanosphere aggregates concentrated in bulk, were used for the oxidation of arsenic, causing its precipitation out of groundwater moving through a redox boundary. The sample able to adsorb the greatest amount of arsenic had a ratio of 5:1, iron to manganese, and occurred in a pH environment of 3-7 and a temperature below 30°C. Understanding the relationship of nanoparticles related to arsenic adsorption is beneficial for implementation of effective methods of arsenic removal from freshwater, groundwater and water treatment plants.

Health Effects from Arsenic in Iron- and Manganese-Rich Water Contamination:

Arsenic can become a health concern if drinking water supplies are situated in an arsenic contaminated environment. Arsenic, a known carcinogen, is found in compounds that are tasteless, do not have an odor and readily dissolve in water (Wang and Mulligan, 2005). This creates a threat to the health of the plants, animals and humans who may use this contaminated water for consumption (Wang and Mulligan, 2005). According to the world health organization (WHO, 2012), water containing greater than 0.01mg/L of arsenic can be harmful to human health and drinking water containing 60mg/L of arsenic can be fatal.

Acute arsenic poisoning can occur within 30 minutes of ingestion and includes symptoms of gastrointestinal discomfort, vomiting, coma and death (WHO, 2012). Chronic exposure to arsenic contamination can lead to anemia, skin cancer, and other cancers of the liver, lung, nasal cavity, kidneys and prostate (WHO, 2012). Arsenic contaminated groundwater is found in areas all over the world, with areas of concern present in Bangladesh, India, Argentina, the United States, and Nepal.

In arsenic contaminated water, As(III) has a higher mobility than As(V) due to its inability to easily fit in the lattice of an oxidized solid (Thomas et al., 2001). As (III) is therefore more easily consumed by humans through contaminated water. Once consumed, As(III) is considered to be more toxic compared to As(V) because of the way it becomes utilized in the human body. Thomas et al. (2001) describe As(III) as the preferred substrate for methylation reactions which involve the addition of a methyl group (one carbon and three hydrogen atoms) onto a substrate (in this case As(III)). The As(III) methyl group is used as a coenzyme in the body's metabolism to transfer compounds to different chemical reactions occurring within the body (Thomas et al., 2001). As part of the metabolism, arsenic has the ability to create toxic and carcinogenetic effects on the large organs of the body.

The removal of arsenic along with heavy metals such as iron and manganese from drinking water supplies has become a concern. This was especially brought to the world's attention in the 1990's when millions of drinking water wells were installed in Bangladesh by agencies such as Unicef, and the World bank, only to be discovered to supply drinking water with high concentrations of naturally occurring arsenic (Smith et al., 2000). Smith et al. (2000) suggested that of the 35-77 million people potentially affected by the contaminated water source containing 500 μ g of arsenic per liter, 1 in 10 will ultimately die from cancers affecting large organs such as the lungs and skin. In order to prevent further exposure to arsenic in affected areas of Bangladesh and other countries of the world where the concentration of As is above the WHO drinking water standards, effective methods of arsenic removal from groundwater are being researched.

An example of a method being investigated to remediate areas with natural contamination of arsenic is using oxygenation of groundwater to remove arsenic. Rott et al. (2002) described a method in which groundwater passed through a well with a vacuum pump delivering atmospheric oxygen. The now oxygenated water then passed through a degassing tank which was purged of any excessive gas from

the groundwater, which then re-filtered back into the groundwater system. Oxygenation of the water will allow for the reduced iron, manganese and arsenic found in the groundwater to be precipitated out and displaced onto the surroundings of the well. This method appears to be enhanced if sediment is added to the oxygenated well which has been coated in iron and manganese oxidizing bacteria such as the *Leptothrix sp.* and *Gallionella sp.* The bacteria are able to enhance the oxygenation process specifically for the heavy metals in question (Rott et al., 2002).

Site Description

Topography and Geology

Shebandowan Lake:

Shebandowan Lake is located approximately 80km from Thunder Bay Ontario, southwest of Highway 11 at latitude 48 38' 00"N and longitude 90 20' 00"W (Figure 1). The lake is approximately 32km from east to west and is separated into three sections: Upper (west), Middle (central), and Lower (east) Shebandowan lakes. As it is easily accessible from the highway, Shebandowan is cottage country for many families of the Thunder Bay area, creating a populated northern shore. Two resorts are present on the lake, both enticing hunters and anglers to stay for the abundant fish and wildlife of the area.

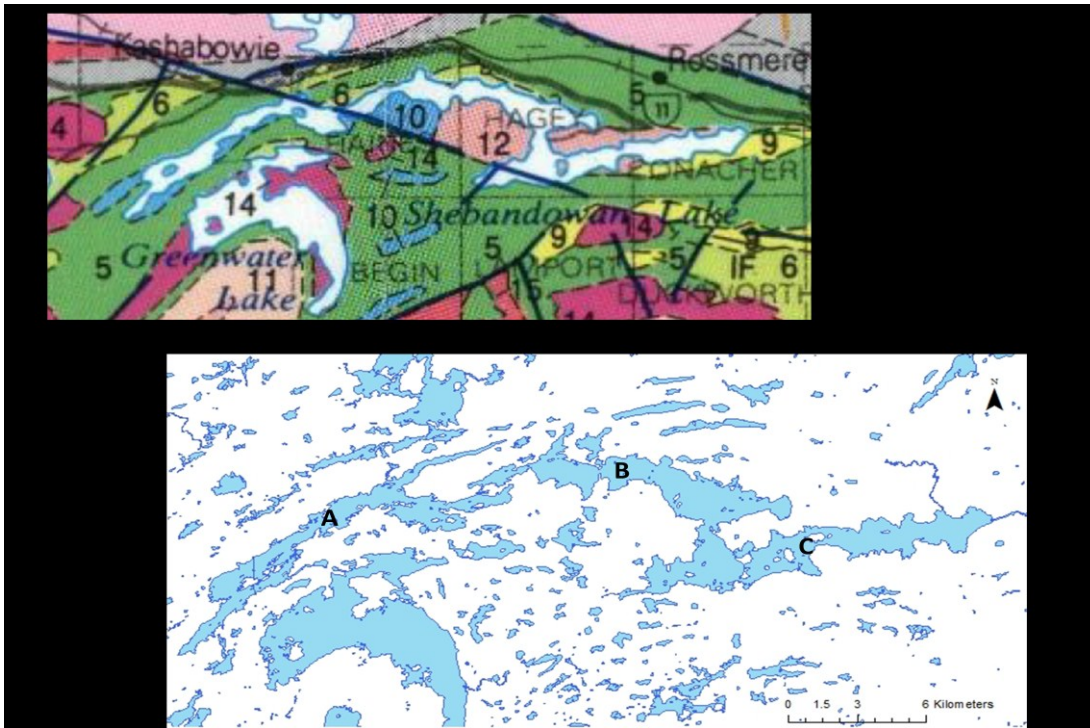


Figure 1: (a) Geologic map of Shebandowan Lake and legend. Map scale 1:1 00 000 (Ontario Geologic Survey, 1991). (b) Map of Shebandowan Lake (Natural Resources Canada, 2012) A=Upper, B=Middle, C=Lower Shebandowan

The topography of the Shebandowan Lake area consists of low undulating slopes with elevations averaging 15m in height (Morin, 1973). The drainage pattern of the area is immature creating many muskeg swamps proximal to the lake and in its surrounding area (Morin, 1973). The lake's water is supplied by six major rivers and streams including the Greenwater, Firefly, Kashabowie, Kabaigon, Harnden, and Swamp Rivers (Vander Wal and Stedwill, 1973). The only outflow from the lake is the Shebandowan River, which joins the Kamanistqua River to be discharged into Lake Superior (Vander Wal and Stedwill, 1973). The main characteristics of the area's topography are the geographic features created by past glaciation, including eskers and poorly sorted sediment (Morin, 1973). Vegetation around Lake Shebandowan consists of both coniferous and deciduous trees and various shrubs, muskeg vegetation in areas of oversaturation, and various aquatic plant life in the lake itself.

The Shebandowan Lake area is underlain by Precambrian age “Timiskaming-type” bedrock which unconformably overlies Archean “Keewatin-type” rocks, both consisting of metavolcanic and metasediments (Aubut and Campbell, 2012). The Timiskaming-type rocks range in age from 2700Ma to 2680Ma (Card, 1990). The metavolcanics are shoshonitic having high amounts of aluminum and potassium, and a titanium oxide content (Osmani, 1996). They are associated with volcanoclastic mass-flow conglomerates and tuffs re-worked in the nearshore environments by tides and waves (Osmani, 1996). All supracrustal rocks of the area are structurally deformed and chemically altered. The rocks of this area are part of the Shebandowan Greenstone Belt, which forms part of the Wawa Subprovince of the Superior Province of Canada (Osmani, 1996).

The Shebandowan Mine, located on the lower section of Shebandowan Lake, in the Shebandowan greenstone belt, operated between 1971 and 1998. During this time, the mine produced 9.29 million tonnes of ore from which nickel, copper, cobalt, platinum and silver were extracted (Inco, 2001). The North Coldstream Mine located 115km northwest of Thunder Bay on the Shebandowan greenstone belt operated between 1957 and 1967 and produced approximately 2.5 million tonnes of ore mined for copper, gold and silver (Golder Associates, 2002). Rehabilitation of both sites is currently ongoing with contamination due to acid-generating mine tailings posing the largest problem.

Sowden Lake:

Sowden Lake is located approximately 50km northeast of Ignace, Ontario at latitude 49° 32' 40''N and longitude 91° 11' 57''W (Figure 2). The lake appears as two smaller lake sections both approximately 10km from north to south. There is limited access to the lake with a public launch on the western side sharing the shoreline with a small amount of private camps, and a road to a resort on the eastern side. The resort is responsible for the greatest population on the lake, as it commercially

advertises to hunters and anglers from the United States to come for a true Northern Ontario experience.

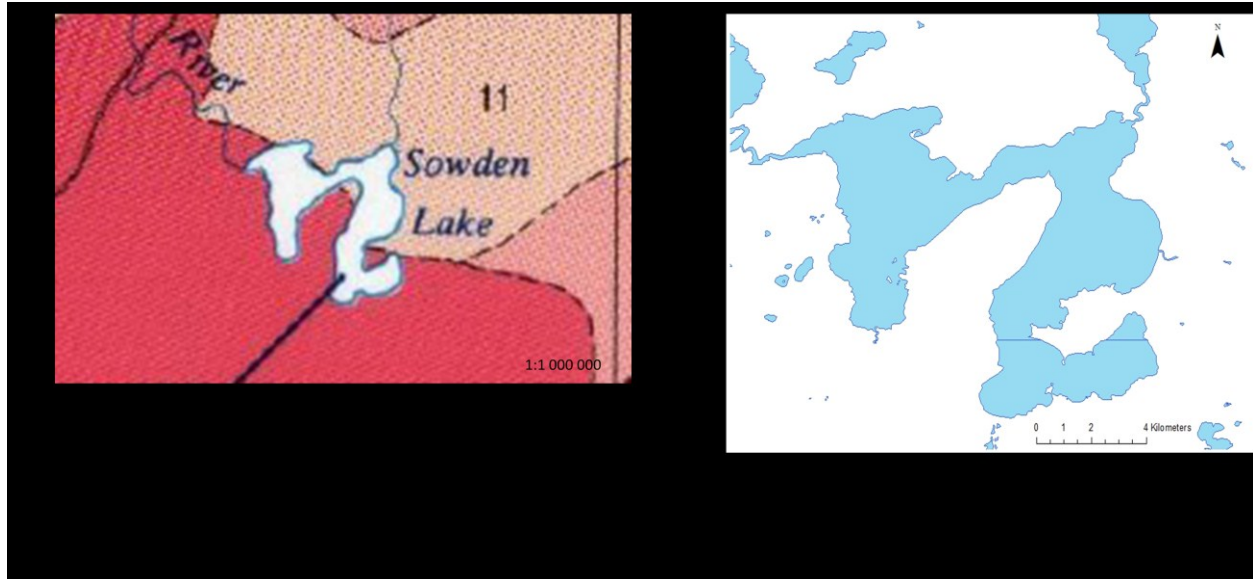


Figure 2: (a) Geologic Map of Sowden Lake and legend (Ontario Geologic Survey, 1991). (b) Map of Sowden Lake (Natural Resources Canada, 2012)

Topography of the Sowden Lake area has been affected by past glaciation in the area creating poorly sorted sediment and glacial morphologies such as kames and moraines (Proctor and Redfern, 1981). The lake is part of the English River system which eventually discharges into Hudson Bay. However, the Pleistocene glacial sediments of the area make water drainage from the lake difficult creating wetlands throughout the area. Vegetation around Sowden Lake consists of trees, mostly coniferous with some deciduous, various shrubs, muskeg vegetation in areas of oversaturation, and various aquatic plant life in the lake itself. The lack of adequate water drainage in the area has, in the past, created feasibility studies for potential peat exploitation (Proctor and Redfern, 1981).

The geology of the Sowden Lake area is composed of Archean bedrock of the central Wabigoon Subprovince of the Superior Province (Jackson, 2003). This Archean bedrock is composed of granitic and

metavolcanic rocks that have been altered by metamorphism, structurally folded and faulted, and intruded by plutons (Proctor and Redfern, 1981). The mineral assemblages surrounding the lake consist of diorite (including granodiorite to granite) on its eastern side, and tonlite on its western side (Jackson, 2003). Sediment sampling of three sites in Sowden Lake has been completed by the Ontario government for potential exploration prospects which found the sediments to contain notable values of sodium, titanium, aluminum, arsenic, barium, cobalt, iron, cerium, potassium and manganese (Jackson, 2003).

Recently the Nuclear Waste Management Organization (NWMO) has conducted an initial screening of the Ignace area to determine the possibility of nuclear waste from Southern Ontario being deposited in the areas' bedrock. It concluded that the Ignace area met all criteria of the initial screening including: having enough available land to accommodate a nuclear waste facility, being outside of any protected areas or heritage sites, not having any groundwater resources at the repository depth, not containing any exploitable natural resources, and not bearing any geological characteristics that would create potential for the site being unsafe (Shaver, 2011).

Lake Charlotte:

Lake Charlotte is located along on the eastern shore of Halifax County, Nova Scotia approximately 60km from Halifax at latitude 44° 46' 3" N and longitude 62° 57' 5" W (Figure 3Figure 3). The lake is approximately 15km from north to south and 2km east to west. The southwestern side of the lakeshore is densely populated with cottage dwelling residents, due to its easy access from Highway 7. There is also a resort on the western side of the lake enticing anglers and recreationists to stay for fishing, swimming and water sports.

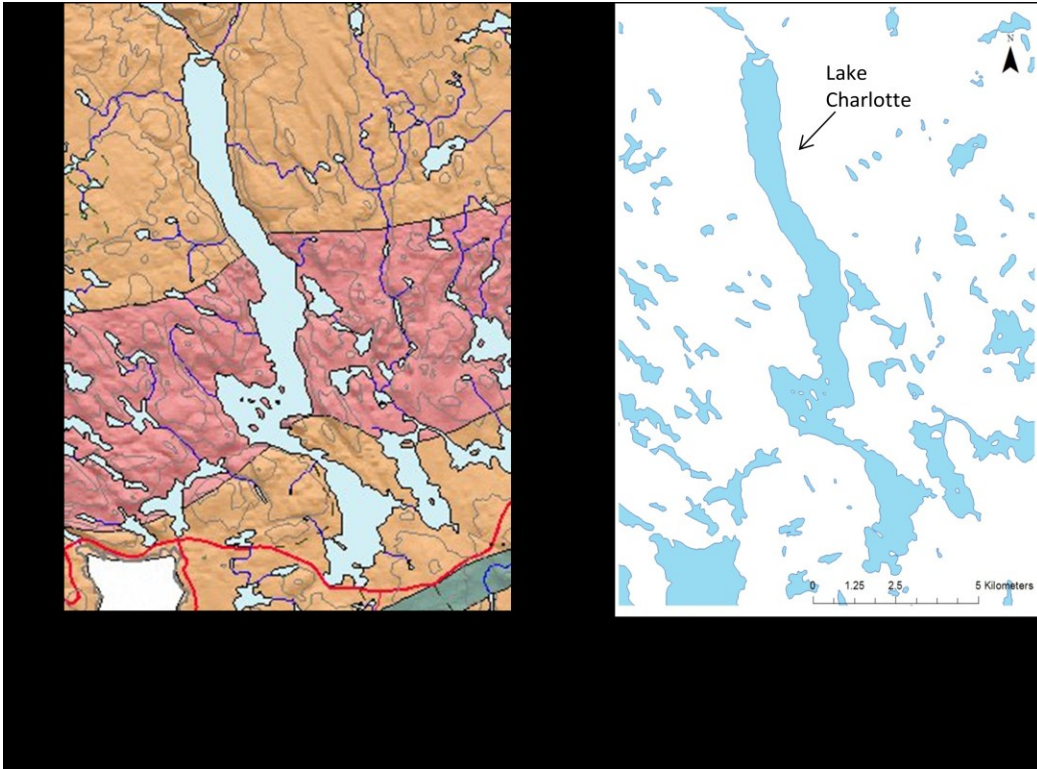


Figure 3: (a) Geologic map of Lake Charlotte (Nova Scotia, Dept. of Nat. Res. 2004). (b) Map of Lake Chartotte (Natural Resources Canada, 2012)

Topographic features of the area include glacial deposits such as drumlins and roche moutainne and the presence of eskers. Poorly sorted sediment covers the areas bedrock geology (Patrie, 1995). A lush growth of trees, such as spruce, hemlock and pine cover the topography, along with various shrubs and aquatic plant species found within the lake (Patrie, 1995). Lake Charlotte overlies the Cambrian-Ordovician age Meguma group, which is composed mainly of meta-sandstone and slate (Patrie, 1995). The Meguma group consists of a minimum of approximately 4900 meters inter-bedded quartzite and slate, with mineralized quartz veins composed of quartz, carbonate, pyrite, arsenopyrite, gold and scheelite (Fralick, 1980).

The hydrothermal system that deposited the arsenopyrite originated in the slate of the Meguma group from clay formed illite releasing water during metamorphism. The water became trapped in the impermeable slate until pore-fluid pressure caused fracturing of the slate beds. This allowed fluid into

the fracture cavity and carbonate to be deposited due to a decrease in the cavity's CO₂ pressure (Fergusson, 1972). Most of the arsenopyrite is found with the carbonate in the slate formation of the Meguma group.

The chemical composition of lake waters in Halifax County, Nova Scotia is affected by the nature of the geological substratum and the topography of the area, which controls sediment type and thickness. Climate of the area and its proximity to the Atlantic Ocean also have an effect (Gorham, 1957). Further environmental changes to the area have become evident with an increase in human activity altering the natural landscape of the area surrounding lakes in Halifax County.

The discovery of gold in Halifax County was first documented in the 1860's. A mine opened on the shore-line of northern Lake Charlotte in 1939, and was prosperous throughout the 1940's (Cudmore et al., 1945). There was a gold mining district comprised of small mining operations extracting gold-bearing quartz veins and associated mineralized wall rock. A significant association between gold and arsenopyrite was found in this area (Malcolm, 1976). The grade of the mined rock was over 2 ounces of gold per ton (Patrie, 1995). Mining of the quartz veins, along with other human activities such as quarrying and construction, enabled remobilization of arsenic in the rock mass (Fralick, 1980). Leaching from the Meguma sequence has caused the groundwater of the area to become contaminated with high concentrations of arsenic, which has been known to affect the resident drinking water wells in areas of Halifax County (Fralick, 1980).

Locations and Access

Shebandowan Lake:

Shebandowan Lake was accessed by vehicle, driving from Thunder Bay Ontario to Wilderness Discovery Family Resort, located on the northern shore of Lower Shebandowan, off of Highway 11. From the resort transport with all supplies was done in a 16ft aluminum boat with a 15hp motor. Locations of data collection sites were determined by examining past maps of the area, trial and error, and talking with locals.

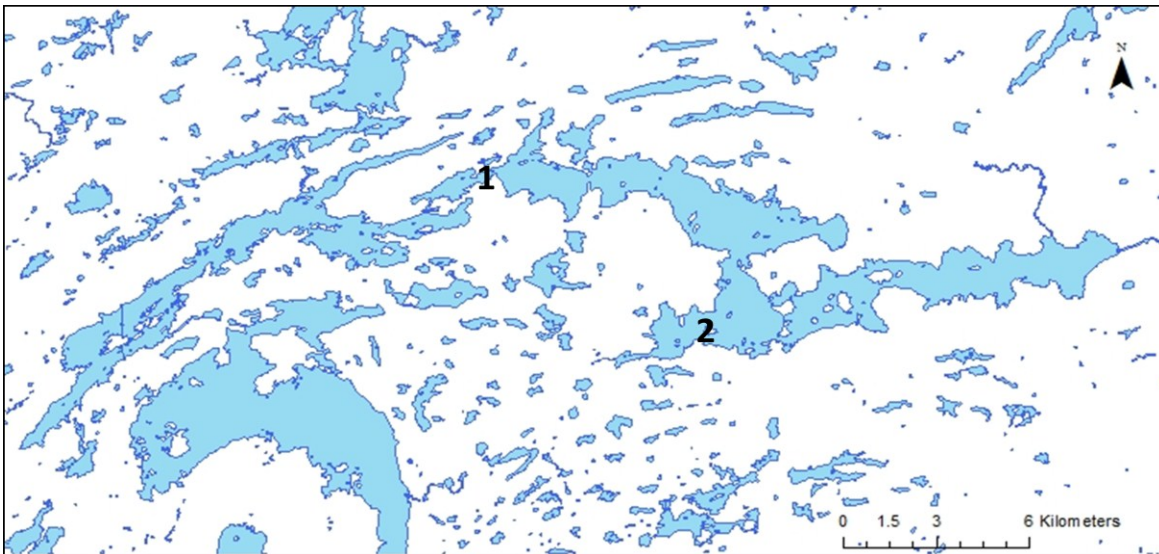


Figure 4: Map of Lake Shebandowan displaying site location areas (Natural Resources Canada 2012). Small site is labeled 1 on map and Island site is labeled 2

Small Site:

The small site is located on the south side of Middle Shebandowan Lake in a small channel connecting Middle Shebandowan to Upper Shebandowan (Figure 4) at UTM Zone 15 of WGS84 at approximately UTM 696200E and 9391800N. The channel was populated with one camp found at its northern side and had an island in its center. The nodule field was found began along the shoreline on

the south side of this channel. This shore displayed vegetation directly to the shoreline and had a bedrock point which opened into a small bay (Figure 5). Aquatic vegetation was observed sporadically throughout the lake bottom. The nodule field at Small Site was approximately 100m west to east and 50m north to south. There site as a whole displayed a gradual increase in depth from the shoreline with the greatest depth located in the centre of the channel at approximately 23m (nodules only found up to 10m).

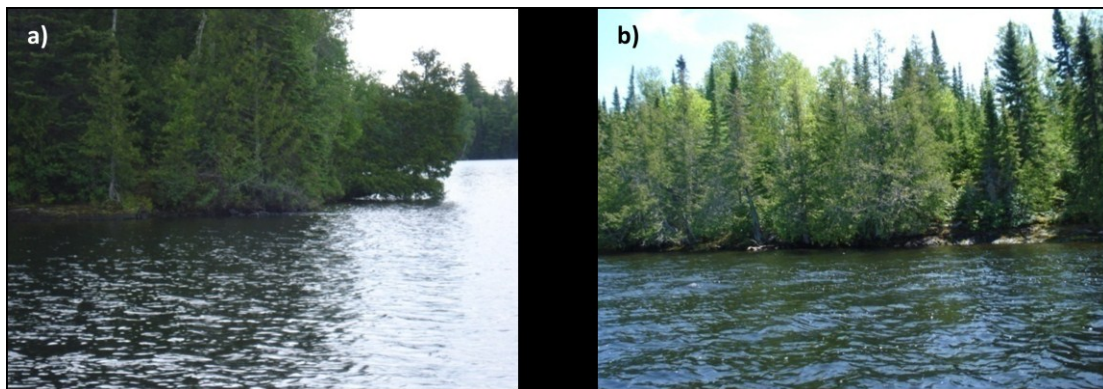


Figure 5: (a) Southern Shore of Small Site, Shebandowan Lake (b) Southern shore of the Island Site: Shebandowan Lake

Island Site:

The island site was located off the north shore of an island highly vegetated with coniferous trees on the western side of Lower Shebandowan (Figure 5b). It is found geographically in UTM Zone 16 of WGS84 at approximately 702170E and 5386280N. The site was found to have a small nodule field approximately 50m off the shore of the island. This field stretched from the islands western corner to offshore of its centre, and was approximately 100m east to west and 20m north to south. The precipitates were surrounded by a hard rock lake bottom to the west and south which was part of the island. There is a light, gritty, grey coloured silt and muddy lake bottom to its east, and a red stained, thick, dense clay to its north. The field had a sandy substrate and the lake bottom was densely populated with nodules. The nodules found in the center of the field were the largest; there size slowly

decreasing towards the fields edge. Aquatic vegetation was observed sporadically throughout the lake bottom. The site as a whole has a gradual decrease in depth from the shore of the island, the precipitate field being found at a depth between 7 and 10m.

Sowden Lake:

Sowden Lake was accessed by vehicle via highway 17 from Thunder Bay to Sowden Lake Resort, located on the southeastern side of the lake (Figure 6). From the resort, transport with all supplies was done in a 16ft aluminum boat with a 20hp motor. Locations of data collection sites were determined by trial and error, and talking with locals. At the time of sample collection, Sowden Lake was experiencing an unusually high water trend.

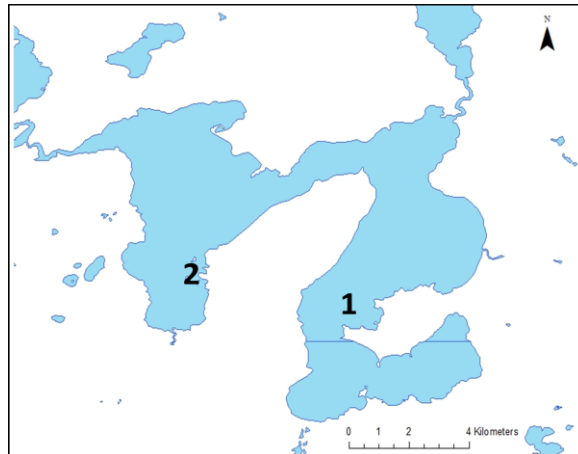


Figure 6: Map of Sowden Lake displaying collection sites (Natural resources Canada, 2012). Sowden-41 is labeled 1 on map and Sowden- 46 is labeled 2.

Sowden- 41 site:

Sowden 41 site was located away from any shoreline in the southeastern portion of the lake (Figure 7a). It is found geographically in UTM Zone 16 of WGS84 at approximately 630100E and 5482630N. The nodule field was present on the top of a shallow, steep sided reef at approximately 5-8m depth. A red gasoline can was attached to the reef to keep marine vehicles from hitting the top of the

reef with their motor. The nodules were abundant in an area approximately 30m east to west and 70m north to south. The field was located on a sandy substrate. The lake bottom surrounding the precipitate field was composed of red clay that had pebble sized Fe-Mn precipitates embedded in it. The lake bottom surrounding the clay was deeper and consisted of an organic-rich, light, squishy, grey substrate. Aquatic vegetation was observed sporadically on the lake bottom.

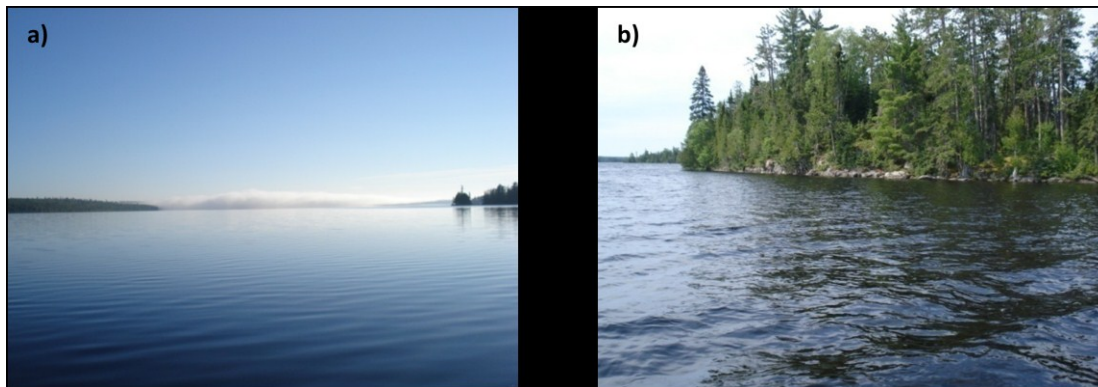


Figure 7: (a) Sowden 41 site, Sowden Lake. Picture was taken on top of nodule field facing northeast (b) Sowden 46 site, Sowden Lake. Picture illustrates the island the precipitates were found beside. This picture was taken on the eastern edge of the nodule field.

Sowden-46:

The Sowden-46 site is located off the eastern side of an island on the southwestern side of the lake. The geographic coordinates of this site are UTM Zone 16 of WGS84 at approximately 626270E and 5486700N. The island was highly vegetated with coniferous trees up to the edge of its shoreline (Figure 7b). The nodule field began almost directly off the island and spanned an area of approximately 50m north to south and 30m east to west in a depth between 2-8m. Precipitates were found in abundance on top of a sandy substrate. As with the Sowden 41 site, the lake bottom surrounding the precipitate field was composed of red coloured clay with small, pebble sized nodules embedded in the clay itself. Beyond the red clay in deeper waters was an organic-rich, light, grey coloured substrate. Aquatic vegetation was observed sporadically throughout the lake bottom.

Lake Charlotte:

Lake Charlotte was accessed by vehicle from the Halifax, Nova Scotia, airport via Highway 7 and a secondary road to a private cottage located at the My Cove Site. From the private cottage, transport with all supplies was done in a 12ft aluminum boat with a 9.9hp motor. Locations of data collection sites were determined by knowledge of past research of the area, trial and error, and talking with locals (Figure 8).



Figure 8: Map of Lake Charlotte displaying areas of sample collection. The map is numbered as follows: 7 Cove shown as 1, Bud's Cove, 2, My Cove, 3, Granite Islands, 4, Mine Site, 5.

7 Cove:

7 Cove site is located in a cove on the southern shore of the lake (Figure 9a) and is found geographically at UTM Zone 20 of WGS84 at approximately 503800E and 5957500N. The shoreline consisted of a shallow sand and pebble beach surrounded by coniferous and deciduous trees. The lake bottom of 7 Cove was occasionally scattered with debris such as old tires, remains of an old dock and

lumber. The precipitate field itself was approximately 30m from north to south and 60m east to west and located at a depth between 0.5-2m on a sandy substrate. Aquatic vegetation was observed sporadically on the lake bottom. On the north side of the precipitate field there is a steep decline where the lake bottom begins to change to fine sediments, such as silt and clay.



Figure 9: (a) The shoreline at 7 Cove, Lake Charlotte (b) Picture taken on the shoreline of My Cove, Lake Charlotte (c) Granite Island Site, Lake Charlotte. Picture was taken facing the Granite Islands site shoreline where the water depth was approximately 18m (d) Appearance of shoreline coming from the south towards the Mine site. The site was present beyond the point in the picture.

Bud's Cove:

The Bud's Cove site is located on the southwestern shore of Lake Charlotte at the UTM (WGS84, zone 20) coordinates 530650E, 4958700N. Its shoreline is a populated cove with five cottages along the beach and docks for keeping motorized vehicles. The lake bottom of Bud's Cove is occasionally littered

with foreign debris such as old tires and lumber. The area where only precipitates were found is approximately 40m north to south and 30m east to west. It is at a depth of 1-1.5m on a sandy substrate. Aquatic vegetation was observed sporadically on the lake bottom. As depth increases, the substrate beside the nodule field became fine grained and high in organic matter.

My Cove:

The My Cove Site is located on the southwestern shore of Lake Charlotte and is the first cove north from Bud's Cove (Figure 9b). It is located geographically at UTM WGS84, Zone 20, approximately 503630E and 4958980N. The shoreline of My Cove is populated with cottages and docks to facilitate motorized vehicles. The lake bottom is occasionally littered with old lumber. The area of the precipitate field is approximately 50m north to south and 40m east to west. It is at a depth of 1-1.5m on a sandy substrate. Aquatic vegetation was observed sporadically throughout the lake bottom, also on the sandy substrate. After a steady increase in depth, the substrate off shore from the nodule field became fine-grained and visually high in organic matter.

Granite Islands:

The Granite Islands site was located between two islands in the central section of Lake Charlotte where the bedrock is composed of a granitic batholith (Figure 9c). Geographically, the Granite Islands site is found at approximately UTM WGS84, Zone 20, coordinates 501700E and 496215N. The shoreline of the site is composed of granite boulders which continue below the water surface to a depth of approximately 2m. The island densely supports coniferous and deciduous vegetation. The precipitate field at the Granite islands location was larger than any other field in Lake Charlotte. Despite the use of an underwater video camera, its parameters were never completely determined, due to the existence of precipitates at a depth greater than 18m. The substrate below the nodules was sandy closer to the shoreline. However, it became finer-grained and light coloured as the depth of the field increased.

Aquatic vegetation was observed sporadically on the lake bottom. The nodules found at this site were all very similar in size and almost uniform in appearance. There were abundant and separated by approximately 10-20cm from one another.

Mine Site:

The Mine Site is located on the northwestern shoreline of Lake Charlotte offshore from a small-scale abandoned gold mine consisting of a tunnel into the steep bank going down to the shoreline (Figure9d). The approximate geographic location of the site is UTM WGS84, Zone 20, 500570E and 4966750N. The shoreline of the area was dense with vegetation including both coniferous and deciduous trees, plants and shrubs. The shore sloped at a steady grade. All aspects of the past mine were overgrown with vegetation with the exception of the adit closed off by a gate to the public which contributed water to a spring. There was a small 5m wharf composed of boulders found coming off the shoreline. The lake bottom at the Mine site was occasionally littered with debris from the mine such as pipes and other pieces of metal. The precipitates found at this site consisted of thin partial coatings on rocks, not the well developed nodules found at other sites. The lake bottom at the Mine site was sandy with cobbles close to shore but dropped off to a silt clay bottom at a depth of approximately 4-5m.

Methodology

Description of Methods

Fieldwork Data collection:

All lake fieldwork data collection was done from an aluminum boat. Nodule fields were located through the use of existing maps and publications, tips from talking to local individuals and by use of an underwater video camera. Once a nodule field was found, transect lines were established and followed

by use of points of reference on the shoreline, or with floating jugs attached to cement blocks dropped at the start and finish of each transect. The length and width between transect lines was determined by the size of the field. To keep the boat on the transect line as data was being obtained, up to three cement blocks were used as anchors depending on the strength of the wind. Each data point was given a name and Universal Transverse Mercator (UTM) coordinate using the reference datum WGS 84. Lake Charlotte values are found in UTM zone 20N and Shebandowan and Sowden Lake are found in UTM zone 15N. All transect data points for each study site can be found in Figures 10-13.

Water analysis data:

The pH, reduction potential (Eh), temperature, and dissolved oxygen (DO) data were collected using a Hanna multi-parameter water quality meter, model HI9828. The instrument was lowered off the side of the boat until the probe reached the lake bottom. The probe was then lifted off the lake bottom approximately 0.5m and was held at this location for approximately 1 minute so any disturbed sediment could settle. Data was then read off the instrument and recorded in a field notebook. Sediment temperature data recorded at My Cove, 7 Cove and Bud's Cove was collected with a waterproof thermometer pushed by hand into the sediment. All temperature values were recorded into a field notebook.

Water sample collection:

Water samples were collected using a submersible water collector. The instrument was attached to a rope and lowered from the side of the boat until it hit the lake bottom. Once on the bottom the rope was swiftly pulled on to close the instrument and then pulled to the surface. The water was then poured until overflowing into a sample bottle containing 2-3 drops of a 5% nitric acid solution to keep all elements in solution. The samples were kept in a cooler or refrigerated until brought to the laboratory. Water analysis of total metals was conducted by a professional technician by digesting the

sample with nitric acid using HTV (open) vessels and a CEM Mars Xpress microwave oven. Here, the samples were concentrated 5 to 10 fold depending on anticipated analyte levels and interferants to a final acid concentration of 4%. Total metals are measured using inductively coupled plasma atomic emission spectroscopy (ICP-AES), a Varian Vista Pro Radial analyzer which is equipped with a cyclonic spray chamber and a Seaspray nebulizer.

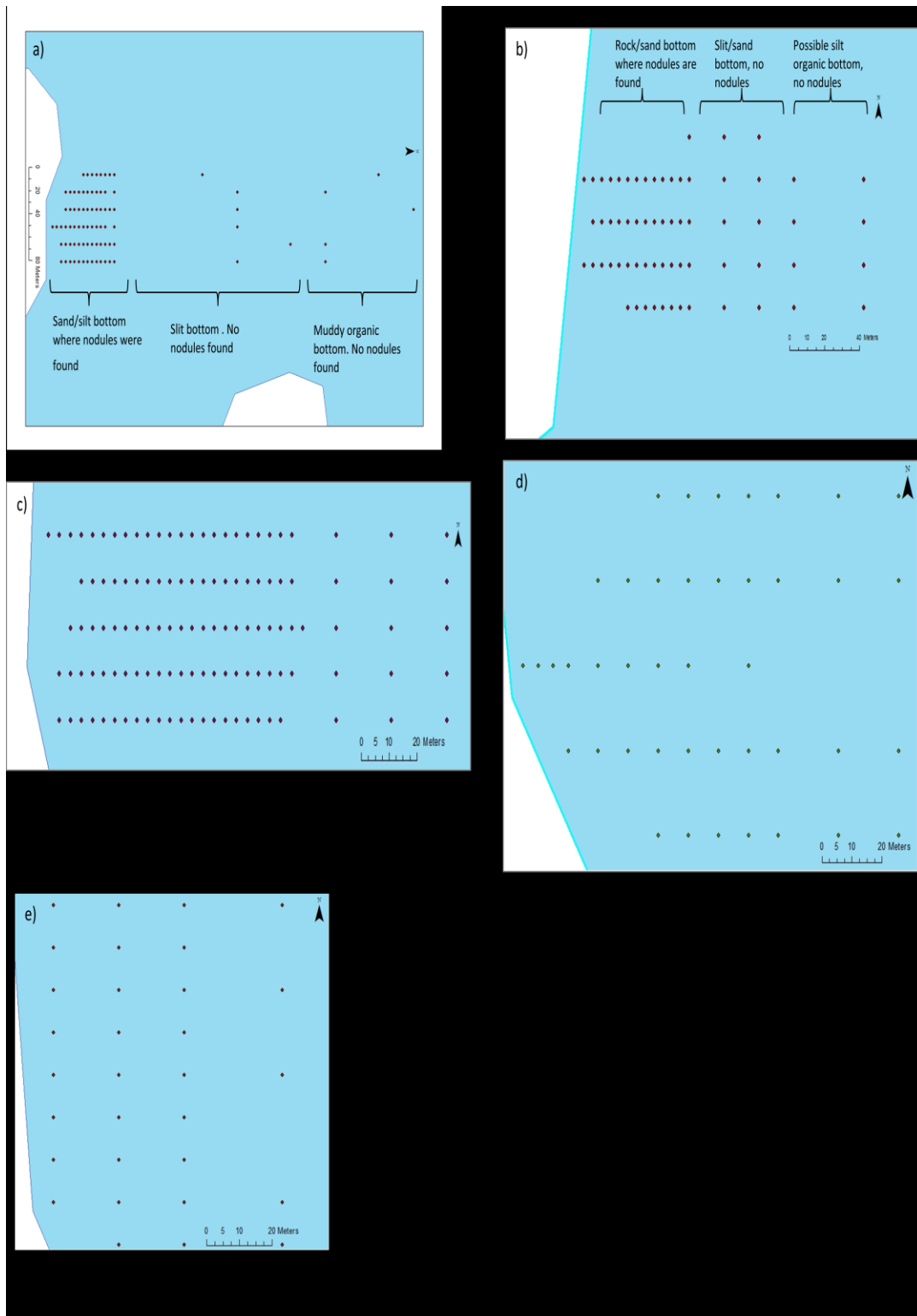


Figure 10: Water chemistry collection points at the 5 Lake Charlotte study sites. (a) 7 Cove (b) Bud's Cove (c) My Cove (d) Granite Islands (e) Mine Site. GPS co-ordinates for each point are displayed in the appendix.

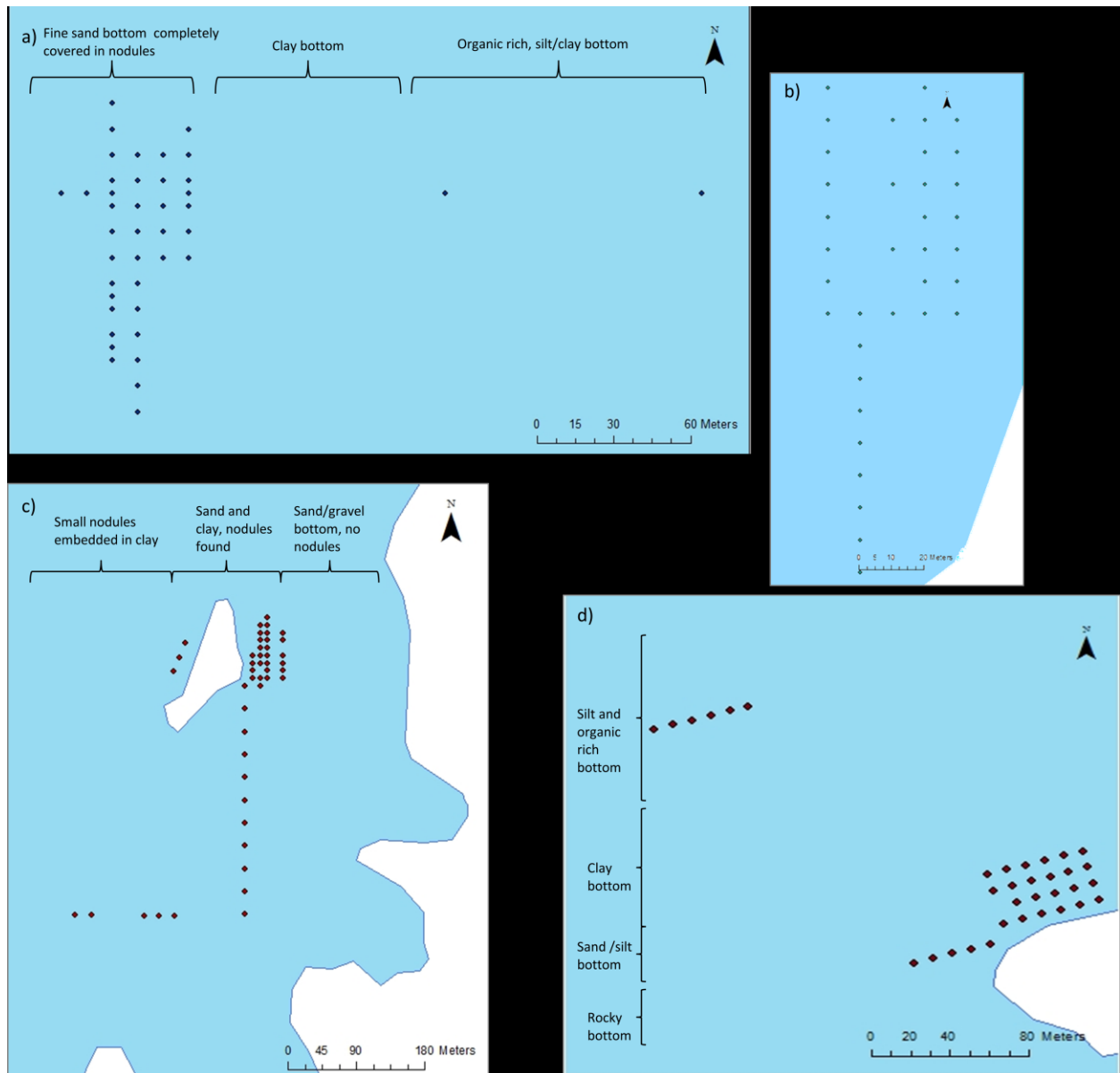


Figure 11: Water Chemistry data points from the Lake Charlotte and Shebandowan Lake Study Sites. (a) Sowden 41 site (b) Shebandowan Small Site (c) Sowden 46 study Site (d) Shebandowan Island Site. GPS co-ordinates for each point are displayed in the appendix.

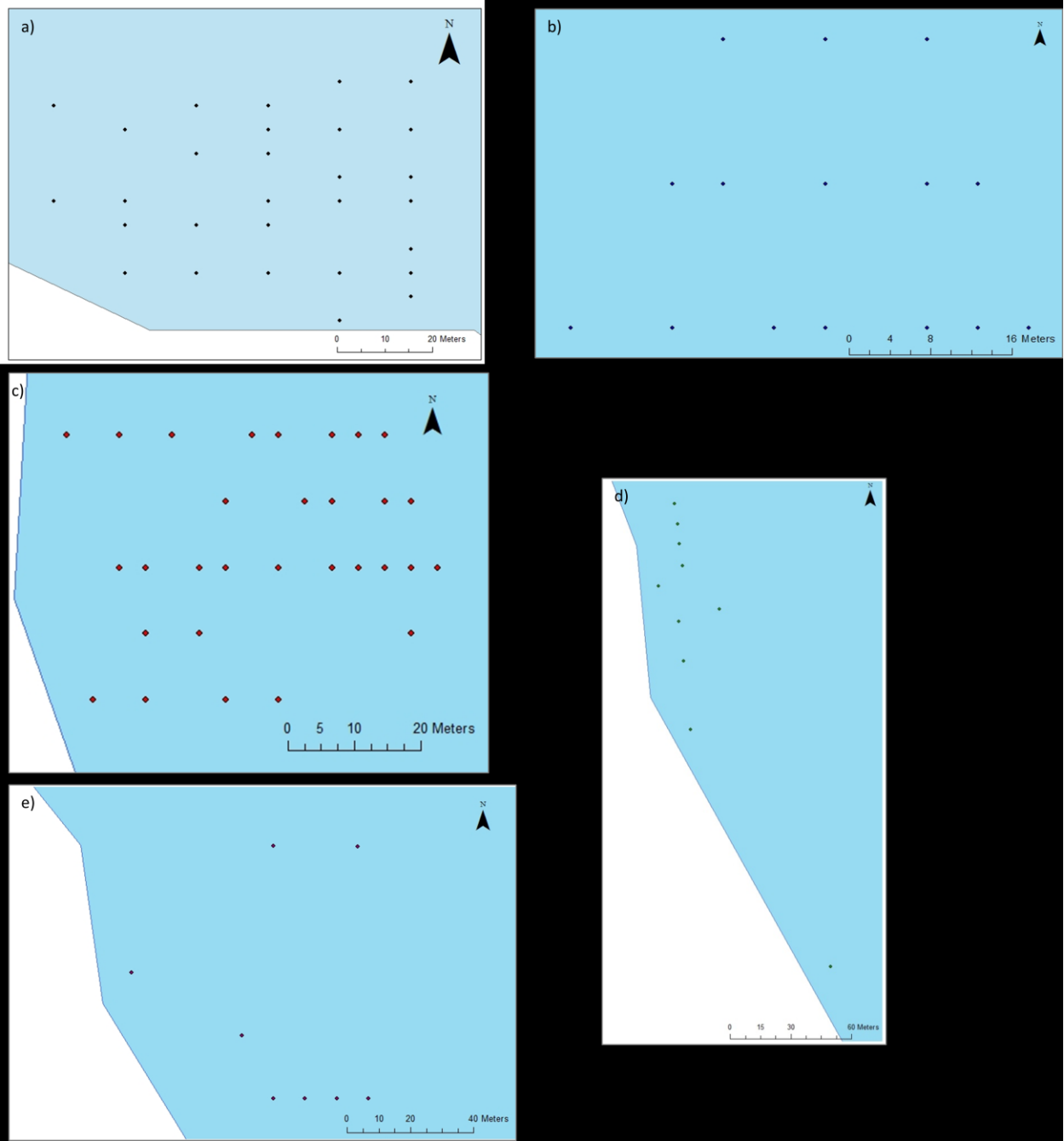


Figure 12: Nodule sample collection points from the 5 Lake Charlotte study sites. (a) 7 Cove (b) Bud's Cove (c) My Cove (d) Mine Site (e) Granite Islands. GPS co-ordinates for each point are displayed in the appendix.

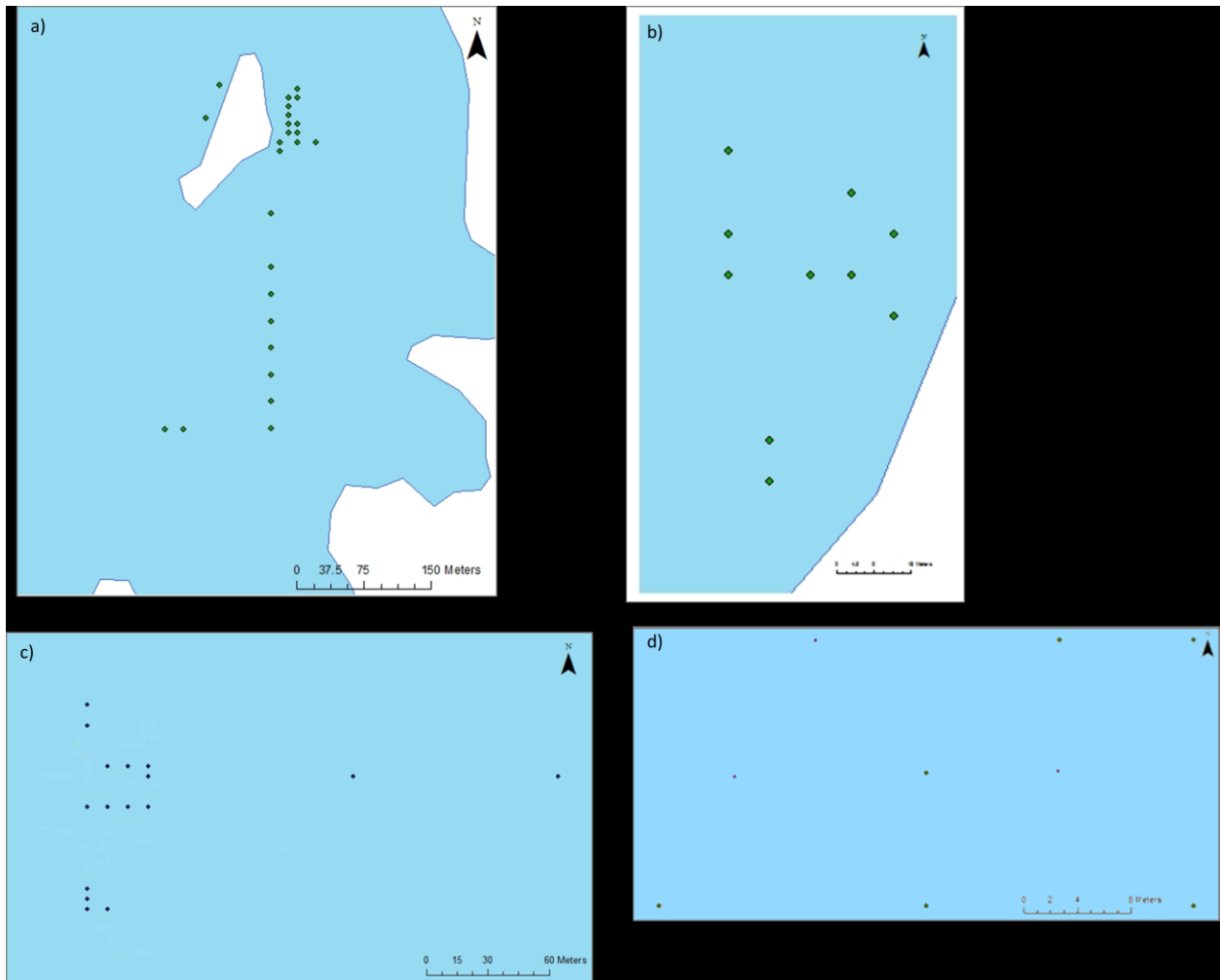


Figure 13: Nodule sample collection points from Shebandowan and Sowden Lakes. (a) Sowden 46 Site (b) Shebandowan Small Site (c) Sowden 46 Site (d) Shebandowan Island Site

Nodule sample collection and analysis:

Nodule samples were collected either by hand by an individual snorkeling, or, in deeper water were obtained from the bottom using an 11.34 kg Ponar Grab sampler with a 63.5cm³ sample storage area. The precipitates were then labeled and placed into sample bags.

Samples were crushed into a fine powder using a mortar and pestle. Each sample was then weighed to exactly 0.5000g and transferred into a Teflon beaker. The beakers were then placed on a hotplate set at 90°C, filled with 10ml double distilled water (DDW) and 5ml nitric acid and left overnight to dry. The next day the beakers were filled with 10ml nitric acid and 5ml hydrofluoric acid and heated to dryness. This step was repeated for the next three days to ensure all material was in solution. On the fifth day 5ml of hydrochloric acid was added to each beaker and allowed to boil for 20min. The beakers were then filled with 10ml of DDW and were allowed to boil for another 10min. The solution in each beaker was transferred into 100ml flasks and filled with DDW to create a 200x dilution. The flasks were allowed to boil on the hotplate (still at 90°C) for 3 hours. Five milliliters were removed and diluted 2000x. Both the 200x and 2000x dilutions were poured into laboratory sample containers and brought to the Lakehead University Instrumentation Laboratory in Thunder Bay, Ontario for analysis by a technician. Blanks and standards were run with each batch of samples.

The Varian Vista Pro Radical inductively coupled plasma atomic spectrometer (*ICP-AES*) was used to determine the major and selected minor elements found in each sample. Accuracy and precision percentages for each element can be found in Appendix A. The elements barium, cerium, cobalt, lithium, molybdenum, sodium, yttrium and zircon all have accuracy and/or precision values above 10% and therefore should be used semi-quantitatively. Accuracy values for boron, sulfur and scandium could not be determined due to no available standards of these elements.

A Carbon Hydrogen Nitrogen Sulfur [C] Elementar Vario (CHNS) analyzer was used to determine the concentration of carbon present in the sample. Samples were crushed to a fine powder using a mortar and pestle. The powder was then brought to the Lakehead University Instrumentation Laboratory for analysis.

An X-Ray Diffractor Meter Pananalytical Xpert Pro Diffractometer (XRD), was used to determine the detectable crystalline phases that occurred within selected samples. The precipitates were crushed to a fine powder using a mortar and pestle. The powder was then used for analysis at the Lakehead University Instrumentation Laboratory. Data obtained was then compared with the mineral standards from the *ICDD PDF2 2008* Database using *Bruker Topax Rietveld* software. Five samples from each lake (15 total samples) were analyzed.

An ELAN 9000 inductively-coupled plasma mass spectrometer (ICP-MS) was used for analysis of rare earth elements. Precipitates were separated using a rotary tool into top and bottom components and crushed with a mortar and pestle into a fine powder. The powder from 5 precipitates (10 samples total) was then shipped to GEOLabs at the Ontario Geological Survey in Sudbury, Ontario for analysis.

Results from the ICP-AES analysis were then analyzed using maps created by ArcGIS, Arcmap 10 software. Contours were determined by use of the program's Radial Basis Function. This method uses a series of exact interpolation techniques in which the contour line must pass through a known sample value. Each contour is dependent on the distance from a know value resulting in a smooth interpolation of the lines between known values (ESRI, 2012).

Microscopy:

Thin sections were created from nodules at each study site. The slides were then examined with an Olympus BX51 Petrographic microscope using normal and polarized light to detect similarities or differences in structure when compared to one another.

A Hitachi Su-70 Schottky Field Emission Scanning Electron Microscope (SEM) was used to examine the specimens with both secondary electron (SE) and backscatter electron (BSE) applications for enhancing imagery. SEM discs and thin sections were created and coated with carbon for use in the

instrument. Elemental chemistry analysis of each image was achieved using the Oxford Instruments Aztec software by means of mapping, linescan and point analysis techniques. Precipitate pieces were also observed and analyzed with the SEM in their pure state using SE and BSE imagery and Aztec mapping techniques. Preparation for these samples included breaking a small piece of the precipitate off with a screwdriver, gluing the sample onto a one inch SEM sample holder, coating the sample with carbon and heating the sample to 75°C to omit vapours prior to use.

Grainsize analysis and distribution of My Cove Pit:

A pit was dug using a shovel on the shoreline of the My Cove site approximately 60-80cm in depth to observe changes in sedimentary layering. Samples from each obvious layer were collected and dried to be used for grainsize analysis. This location was used due to its easy accessibility and received permission from the land owner.

Grainsize analysis procedure:

Each sample was rinsed with distilled water and filtered through a sieve to separate out any organic or non-sedimentary debris. A 4 ϕ sieve was then used to separate the clay and silt from the sand. The sand remaining on the sieve was then dried on an electric heater. Once dry, the sediment was poured into sieves stacked on a sieve shaker to obtain the weight of individual size fractions. The clay silt fraction from each grainsize analysis procedure underwent standard pipette analysis.

Results

1. Nodule Description:

Lake Charlotte, 7 Cove:

Nodules present in 7 Cove have a flat surface with a rough stromatolitic texture (Figure 14a, b) covering a ring structured underside. On both the underside and top portion of some nodules a micro-stromatolitic structure appears. The stromatolies on the underside appear to be growing upside down towards the lake bottom (Figure 14c). Of all Lake Charlotte nodules, those found in 7 Cove were the most difficult to break apart with one's hands. The interior of the nodule can be described as having a thick outer crust on the nodule surface followed by hard, dark laminae, and a loosely compacted sandy grained center (Figure 14d). The bottom of the nodules consists, again, of hard, dark laminae towards the center, and hard, orange coloured laminae that are found on the outer portion of the nodule. Some of the hard areas of the nodules were observed to have a silver-coloured sheen.

A pavement of fused nodules can be found in 7 Cove. However, this appears in isolated clusters on the lake bottom as opposed to the more continuous clusters at My Cove (Figure 14e). The sizes of the nodules, like with My Cove, changes with depth so the smallest are found closest to the shoreline at the beginning of the field and the largest are found furthest away from the shoreline. The largest nodules of Lake Charlotte were present at 7 Cove, some approaching 30cm in diameter (Figure 14f). All nodules were located under a bacterial mat 2-3cm thick.

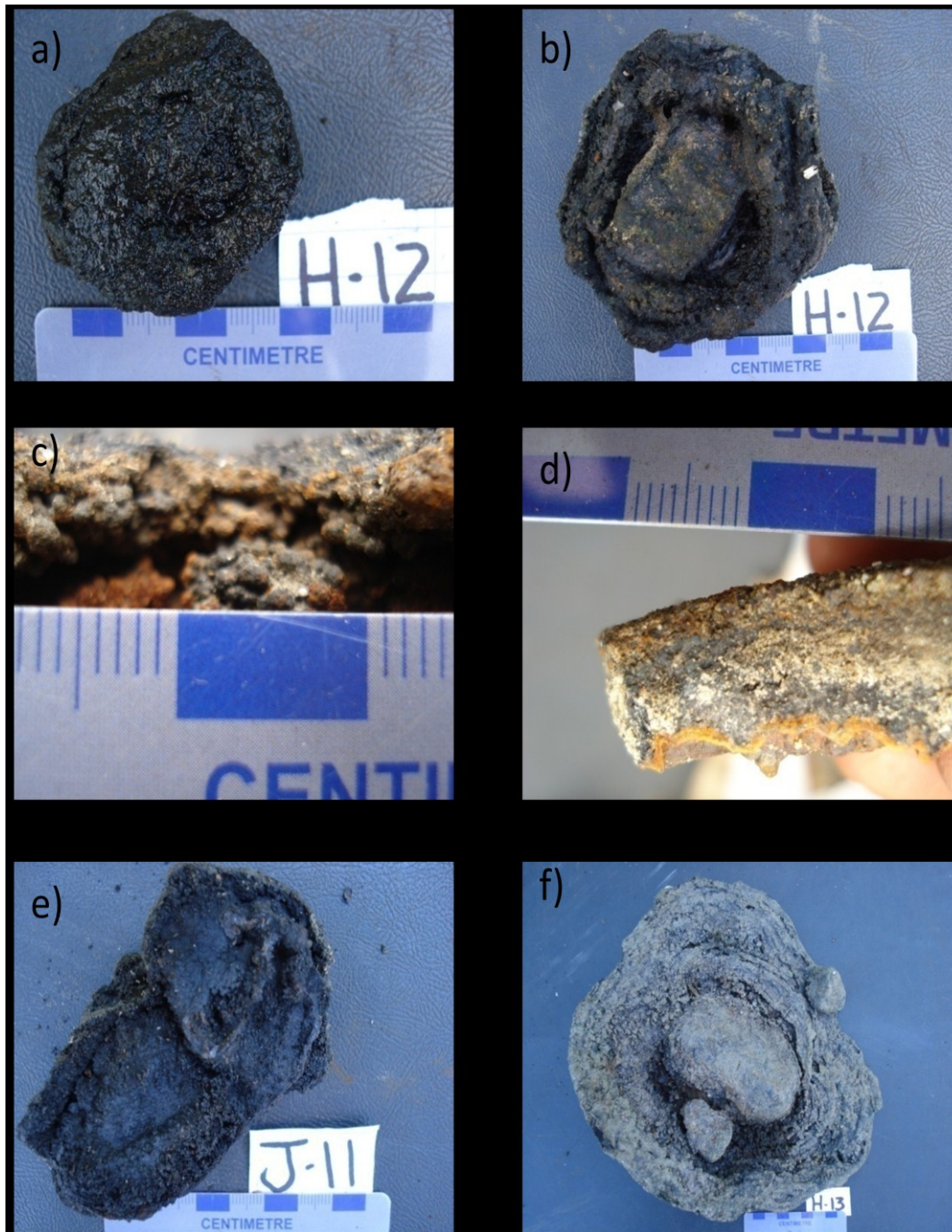


Figure 14: Lake Charlotte, 7 Cove nodules (a) Top portion of a nodule displaying small stromatolites. This was present covered by a bacterial mat (b) Underside of (a) displaying a ringed structure around a cobble (c) Stromatolitic structure present on the underside of some nodules, (d) Cross section of a nodule displaying a hard outer coating and dark coloured center (e) Two nodules fused together to form a pavement (f) The largest nodule collected in Lake Charlotte found on the outer edge of the 7 cove field.

Lake Charlotte, Bud's Cove:

The nodules found at Bud's Cove are unusual due to their extremely flat, smooth surface (Figure 15a). The center stone of each nodule is larger than those found at My Cove and 7 Cove ranging to boulder size (Figure 15b). The underside of the nodules present at Bud's Cove display smaller nodules fused underneath larger nodules creating a sort of nodule "family" (Figure 15c, d). The surface of the largest, topmost nodules of this family is seen to fuse together with other nodules found in close lateral proximity. This creates a thick, hard pavement which can at times only be broken apart with use of a tool such as flathead screwdriver (Figure 15e, f). Bud's Cove has the thickest and largest area of pavement of all study areas taking up approximately 70% of the entire nodule field. This makes it difficult to determine if the size and structure of the nodules is similar to those of My Cove and 7 Cove. The edge of the nodule field at Bud's Cove closest to the shoreline has smaller nodules present. However, the outer edge seems to abruptly end at approximately 2m depth with no further differences in nodule size.

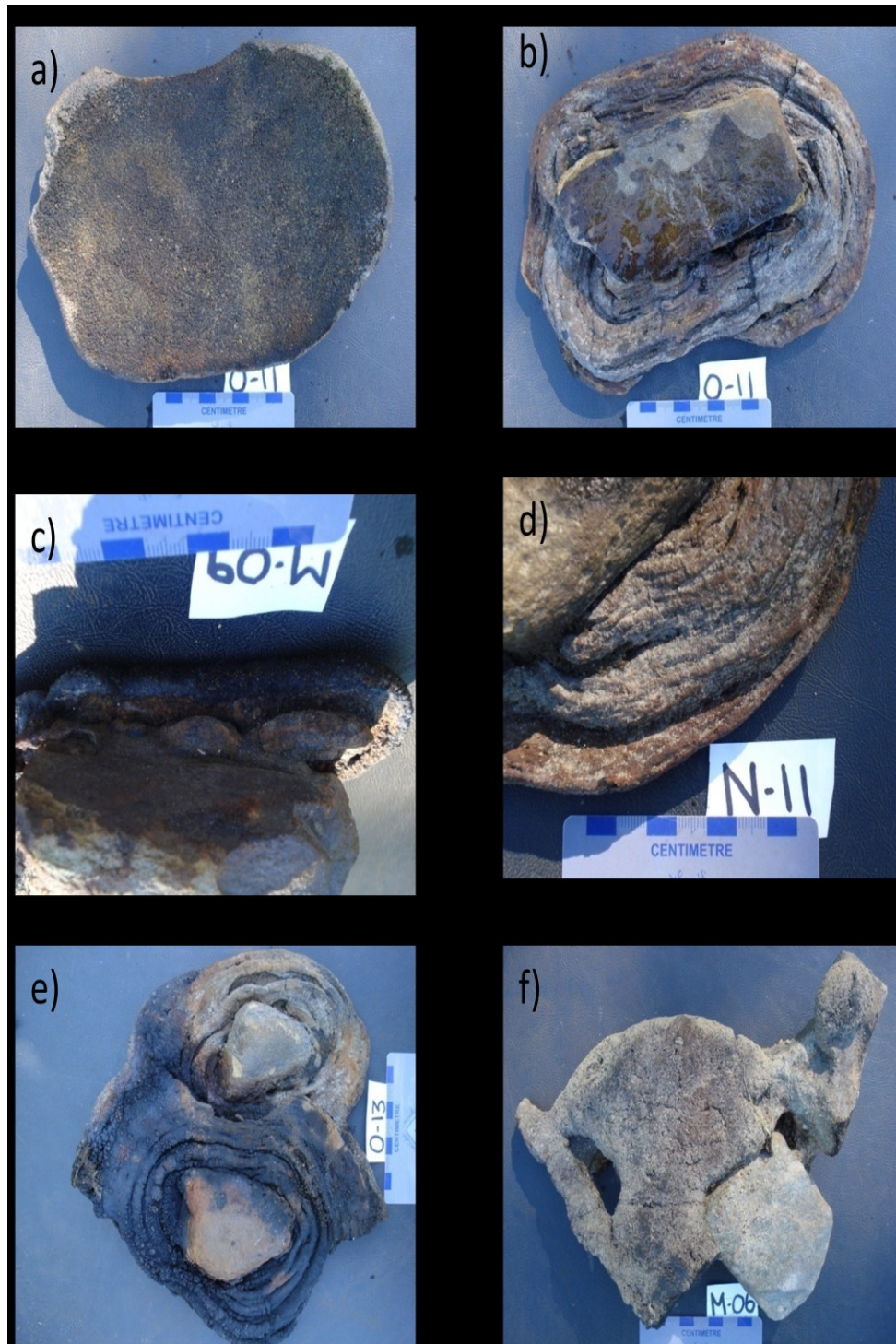


Figure 15: Lake Charlotte, Bud's Cove nodules (a) Surface of a nodule from Bud's cove depicting the sites unique flat pavement (b) underside of (a) displaying ring structure around a cobble. (c) Precipitate growth over smaller nodules of different sizes (d) Precipitate growth over smaller precipitate structures, all displaying circular rings around the center cobble (e) Underside of two nodules fused together to form a pavement (f) Surface view of the precipitate pavement structure unique to Bud's Cove

Lake Charlotte, My Cove:

Nodules formed in My Cove have a flat, smooth surface which appears as a small lump on the lake bottom (Figure 16a). On the lake bottom, the precipitates are often covered with a thick bacterial mat, commonly approximately 3cm thick, making it difficult to identify them. The underside of the nodules display ringed structures, which can be seen surrounding a pebble or cobble (Figures 16, b and c). These ringed structures appear more evident in larger nodule specimens.

The nodules at My Cove are easily broken apart with one's hands. Observation of the interior of the nodules (Figure 16d) shows a smooth top portion, and a powdery textured bottom, which appears black with small interior lineations that are red in colour. The entire nodule is covered with a dark, eggshell-like crust. Nodules found close together on the lake bottom can be seen growing large enough to fuse together and create a pavement-like structure (Figure 16e). Some of the nodules display microstromatolites on the bottom of the nodule (Figure 16f). It is interesting to note that the stromatolitic structures appear to be usually growing downwards towards the sandy lake bottom.

The size of the nodule growth is correlated to the distance it was found from shore. In shallow waters less than 1.5m in depth, only a thin coating of the precipitate can be found on pebbles and cobbles of the lake bottom. The smallest nodules, approximately 5cm in diameter, are found at the edge of the nodule field closest to the cove shoreline at a depth of 1.5-2m. As the depth of the water increases, the nodules become larger. Often, the top portions of the nodules fuse together with other precipitate nodules to create a pavement. The edge of the field furthest from the shoreline had the largest nodules found in the field being approximately 20cm in diameter. These nodules are more dispersed than those in the center of the field and become scarce on the lake bottom as the water increases in depth.



Figure 16: Lake Charlotte, My Cove nodules (a) The top portion of a nodule depicting the flat surface, which, when on the lake bottom, is covered by a bacterial mat. (b) The underside of nodule (a) displaying the ringed structure surrounding a cobble (c) A closer view of the ringed structure of (b). (d) A cross section of a nodule displaying a granular portion and a hard dark portion. (e) Pavement that can develop when two nodules found close to each other fuse together (f) Stromatolite structures found on the underside of some nodules (they appear as round balls in this image). These stromatolites grow upside down towards the lake bottom.

Lake Charlotte: Granite Islands:

Nodules present at the Granite Island site are comparatively very lightweight and higher in organic matter than those found at the other sites in Lake Charlotte. They do not always have a stone in the center of the ring structure, and are easy to break, often crumbling in ones hands. The top portion of the nodule (Figure 17a) displays a similar ring structure appearance to that of its bottom (Figure 17b). Unlike the rest of the precipitates in Lake Charlotte, those found at Granite Islands have no exterior coating present.

The distance from the shoreline and the depth at which the precipitates were found was correlated with the size and appearance of the nodule's structure. In shallow waters of approximately 1m, coatings of the precipitate are found on large boulders, which are common on the shoreline and shallow waters. There is then an abrupt change in depth as the lake bottom slopes towards deeper waters with precipitates beginning to develop on the shallow portion of this slope. The difference between those nodules found in the shallows (approximately 2m) and those found at a greater depth (approximately, 3.5m+) is their shape and proximity to one another on the lake bottom. Those found closer to the shoreline are oddly shaped, appear randomly distributed on the lake bottom, and have ringed structures surrounding a pebble or cobble (Figure 17c, d, e). A transition stage then occurs where the nodules become more uniform and a center stone was not always present (Figure 17f).

The further away from the shoreline and in greater depth the nodules began to form as almost perfect circles with more apparent ring structures and no stone in the center (Figure 17a, b). The nodules also became distinctly uniform in their distribution, appearing approximately 40cm apart from one another and basically covering almost the entire lake bottom. The edge of this field furthest from

the shoreline was never found as the video camera being used could not display a usable image deeper than 20m. At this depth, however, the field still dominated the lake bottom.

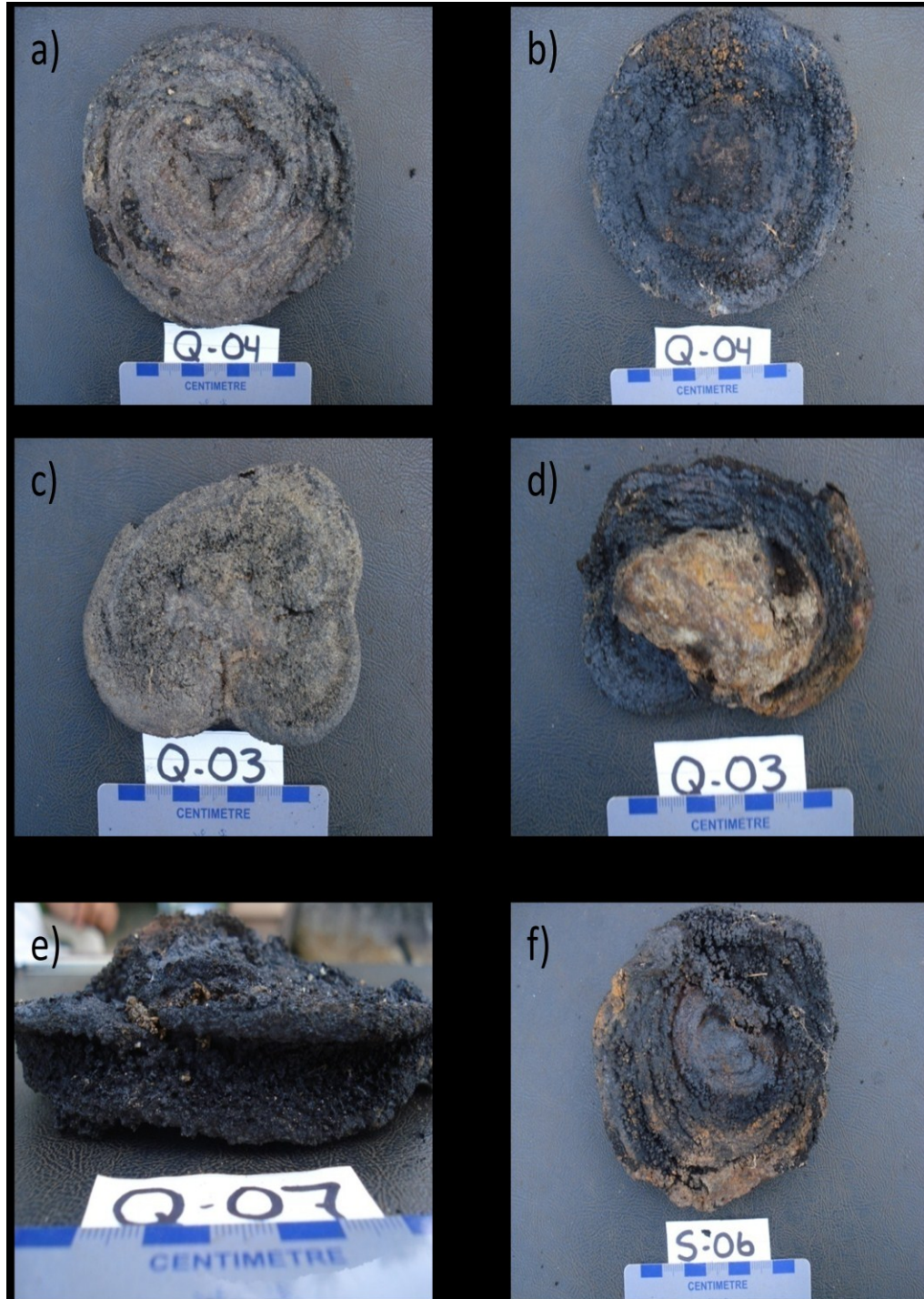


Figure 17: Lake Charlotte, Granite Islands nodules (a) Surface of a nodule from the Granite Island site. Its perfect circular appearance suggests that this sample was taken at a greater depth than sample s c-f (b) Underside of nodule in (a), (c)

Surface structure of a nodule found closer to the shoreline. (d) Underside of nodule (c), (e) Unusually shaped nodule found close to shore. (f) Transitional precipitate found between the depths of (c) and (a).

Lake Charlotte: Mine Site

The precipitates from the Mine Site are the least developed of all the Lake Charlotte study areas. The nodules found on the rocks of the lake bottom are thin with a rough texture and minimal ringed structure in the underside of the overgrowth (Figure 18a, b). The precipitate can be described as two visually unique forms. Precipitates in Figure 18, c and d are found close to the shoreline at a depth of approximately 2m. They appear brown and/or orange in colour with a fine-grained texture. These nodules were often found near and on iron or steel debris left from past mining in the area. The second type of nodules (Figure 18e, f) are dark grey in colour, have a rough, sharp texture, and only consists of very thin coating over the rocks found on the lake bottom. Both nodule types have the ability to grow on multiple rocks present in close proximity, fusing them together.

Due to the lack of precipitate growth on the lake bottom rocks in this area, no definite precipitate field is present. Like the Granite Islands site, Mine site has a drop off in water depth very close to the shoreline making it difficult to determine how far the precipitates continue away from the shoreline. At a depth of almost 5m the rocky drop-off ends in a flat, silt-rich lake bottom with no nodules.

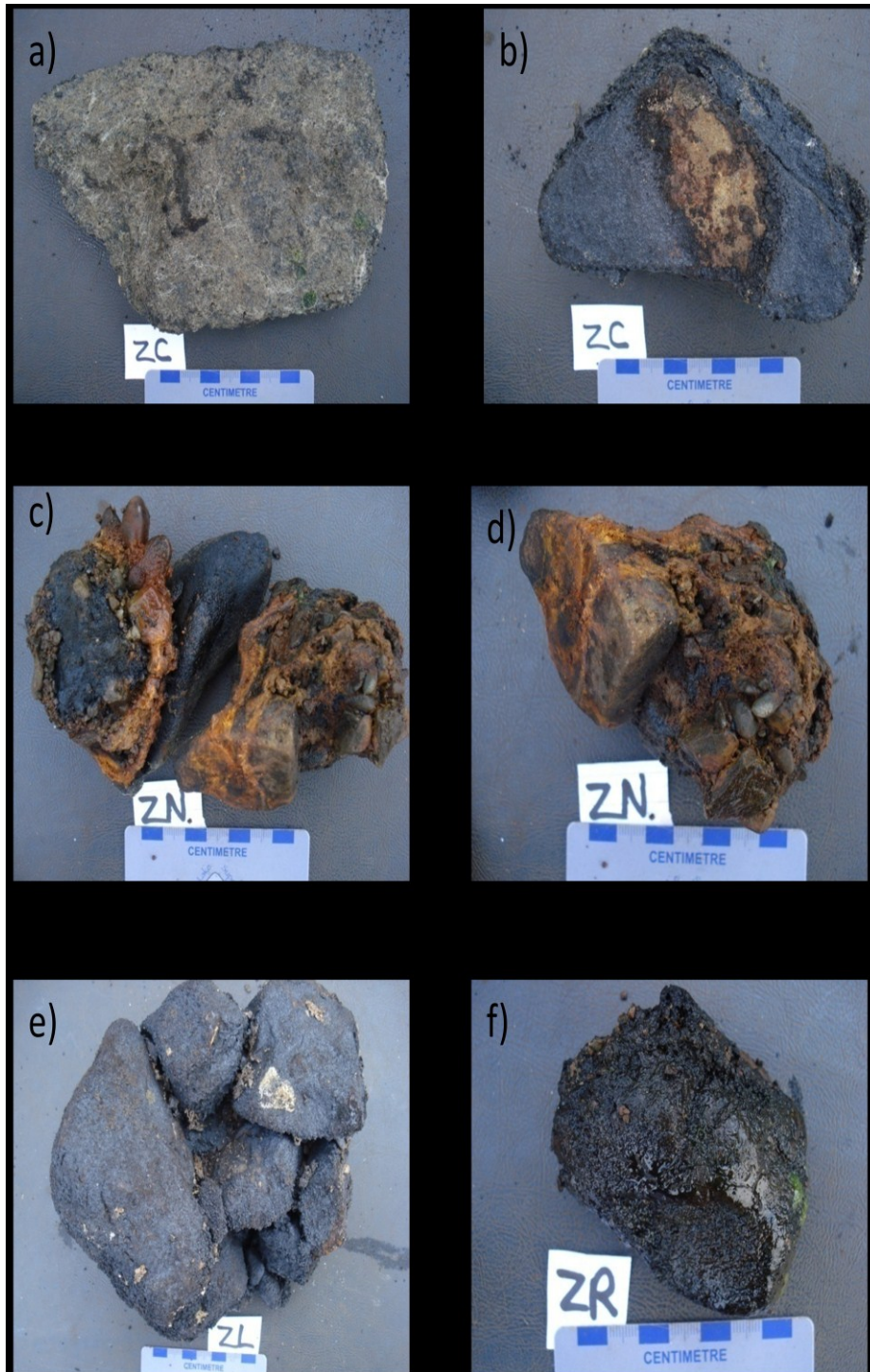


Figure 18: Lake Charlotte, Mine Site nodules. (a) Surface of a nodule found at the mine site. (b) Underside of nodule (a). Note the lack of dominant circular rings around the cobble. (c) and (d) Nodule unique to the mine site in Lake Charlotte. Note the orange brown colour and muddy texture. (e) and (f) Thin coating unique to mine site. It has a very rough, sharp texture.

Sowden Lake, Area 41

The precipitates found in Sowden Lake are comparatively different to those found at the Lake Charlotte sites. The Area 41 study site, like the majority of Sowden Lake, has precipitates forming on its entire lake bottom. In areas the amount of nodules found was so great that the actual lake bottom could not be acquired when collecting samples with the Ponar grab sampler. Nodules are found at depths of 5-9m. As the precipitates were found closer to a depth of 9m, they became smaller in size and were not only on the surface of the lake bottom, but also embedded in its reddish coloured clay. All precipitates found at the Area 41 did not contain a stone at their center.

Figure 19, (a,b), depict typical nodules found in the area. Larger nodules are generally 2-3cm in thickness and have a similar appearance on the top and bottom. They may or may not display a ringed structure circling the center, which, if observed, is present on both the surface and underside. Nodules are dark brown or black in colour, oval or semi-circular shaped and appear uniform throughout the sample. The nodules are hard and can be difficult to break apart by hand. The smaller, rounder samples are the most difficult to break requiring a tool such as a flathead screw driver.

The center of the nodule field at Area 41 had the shallowest depth of 5m. As samples were collected farther away from the center of the field in deeper water the nodules became smaller and more abundant. Figure 19c and 19d were both taken from an area of the lake bottom approximately 60cm x 60cm where the precipitates were found in greatest abundance. At the edge of the field, nodules were found embedded in clay or silty mud (Figure 19e, f). Size and structure of these nodules was similar to other nodules from the area, but the lake bottom here became a pink/red coloured clay. Nodules embedded in this clay were approximately the size of a quarter, had an oval shape and were difficult to break apart by hand (Figure 19d). The nodules in deeper waters were commonly broken or fragmented when brought into the boat for observation.



Figure 19: Sowden Lake, Area 41 nodules. (a) Surface of nodules found in Sowden Lake, Area 41 near the center of the field. (b) Underside of the nodules (a). Notice the similarity of the top and bottom of the samples. (c) Small nodules found in abundance on the lake bottom (d) Small nodules present imbedded in a pink/red clay on the outer edge of the nodule field. (e,f) Nodules found on top or imbedded in silty mud and clay.

Sowden Lake, Area 46:

Area 46 had similar types of precipitates as Area 41 and also contains a similar nodule distribution. Area 46 is located between a marsh covered lake shoreline and a rocky island shoreline. The field is found almost directly off the island on the rocks that form its shore. Here the precipitates of this field are the largest and are in depths of 1-2 meters. These nodules display ringed structures, which surround a center with a large pebble or cobble (Figure 20a,b). Moving away from the island, the nodules remain similar in size and shape, however, they no longer have a central stone resulting in a solid oval structure with rings circulating around the center (Figure 20c,d). The majority of the solid, oval nodules are found at a depth of approximately 7m. They appear with ringed structures on both the top and bottom areas of the nodule.

As the depth of the field increases to approximately 8-9m, a type of pavement is found where oval shaped nodules are fused together in red/brown clay of the lake bottom (Figure 20e). This pavement appears to cover the entire lake bottom at similar depths. It is a hard material and therefore difficult to recover from the lake even with the force of a dredge attempting to break it into fragments. Due to the inability to always collect a pavement sample it is difficult to determine exactly where the pavement ends in the nodule field.

At a depth of approximately 9m, small, smooth, oval shaped nodules can be found on the surface of the lake bottom and in the clay below (Figure 20f). These nodules commonly do not have any type of structural appearance, are dark coloured, brown or black, and have a hard texture making it difficult to break them by hand. These small nodules are found at the edge of the precipitate field. As the water depth increases, the red/brown clay lake bottom continues with tiny precipitates, generally no greater than 1cm in diameter, found embedded in the clay.

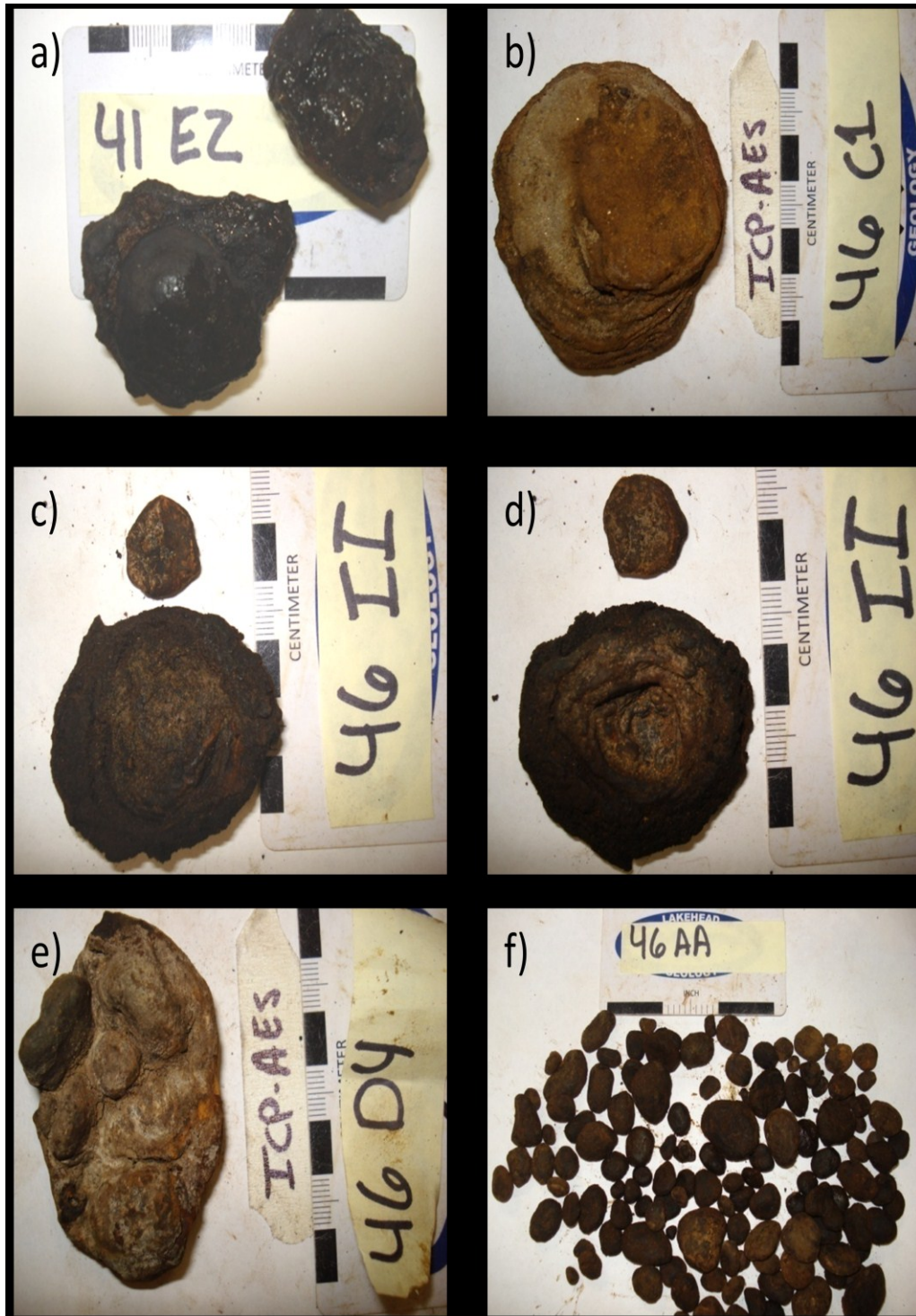


Figure 20: Sowden Lake, Area 46 nodules (a) Nodule growth around a pebble at Area 46, Sowden Lake. (b) Nodules recovered off the point of the Area 46 island near the edge of the nodule field. (c) Top portion of nodule displaying a circular ringed structure around its center. There is no stone in the center of this nodule. (d) Underside of (c) displaying a more pronounced ringed structure (e) Smaller precipitates fused together in a clay pavement. (f) Small nodules with no structural, ringed appearance recovered from the surface of red/brown lake bottom clay, or embedded in the clay.

Shebandowan, Small Site:

The Small Site study area encompasses a variety of different nodules in an area no greater than 20m². The nodules here form a variety of circular shapes and sizes. Morphology of the precipitates of Shebandowan have been described previously by Sozanski and Cronan (1976), therefore their terminology will be used to describe the precipitates found for this study.

The field begins out from the shoreline at a depth of approximately 6 meters where nodules begin to form around the pebbles or cobbles that make up the lake bottom. Figure 21 (a, b) is considered a *saturnine* (Sozanski and Cronan, 1976) shaped nodule where the precipitate appears as a thin, flat, circular ringed structure which surrounds a pebble or cobble. Also close to the shallow edge of the nodule field *mushroom* shaped (Sozanski and Cronan, 1976) nodules appear where the precipitate encircles the top portion of the pebble (Figure Figure21c).

Towards the center of the nodule field, the lake bottom begins to become sandy and nodules begin forming as an *equatorial skirt* (Sozanski and Cronan, 1976) around the central pebble (Figure 21d). Here the nodules display obvious ringed structures around the central stone. The rings are similar on both the top and underside of the structure. The *equatorial skirt* nodules are found in abundance on the lake bottom and are typically uniform in size, approximately 5-7cm in diameter. At times small precipitates appeared to be growing below the surface of the lake bottom in the sandy material (Figure 21e)

On the outer edge of the nodule field the lake bottom appears as red/brown clay and the nodules are embedded in the clay, as opposed to being present on the surface of the lake bottom (Figure 21f). The nodules here appear as small, quarter sized, brown coloured nodules. The precipitates in the clay can be structurally different either displaying no significant rings, or the typical ringed structures surrounding the center of a nodule with no pebble in the center.

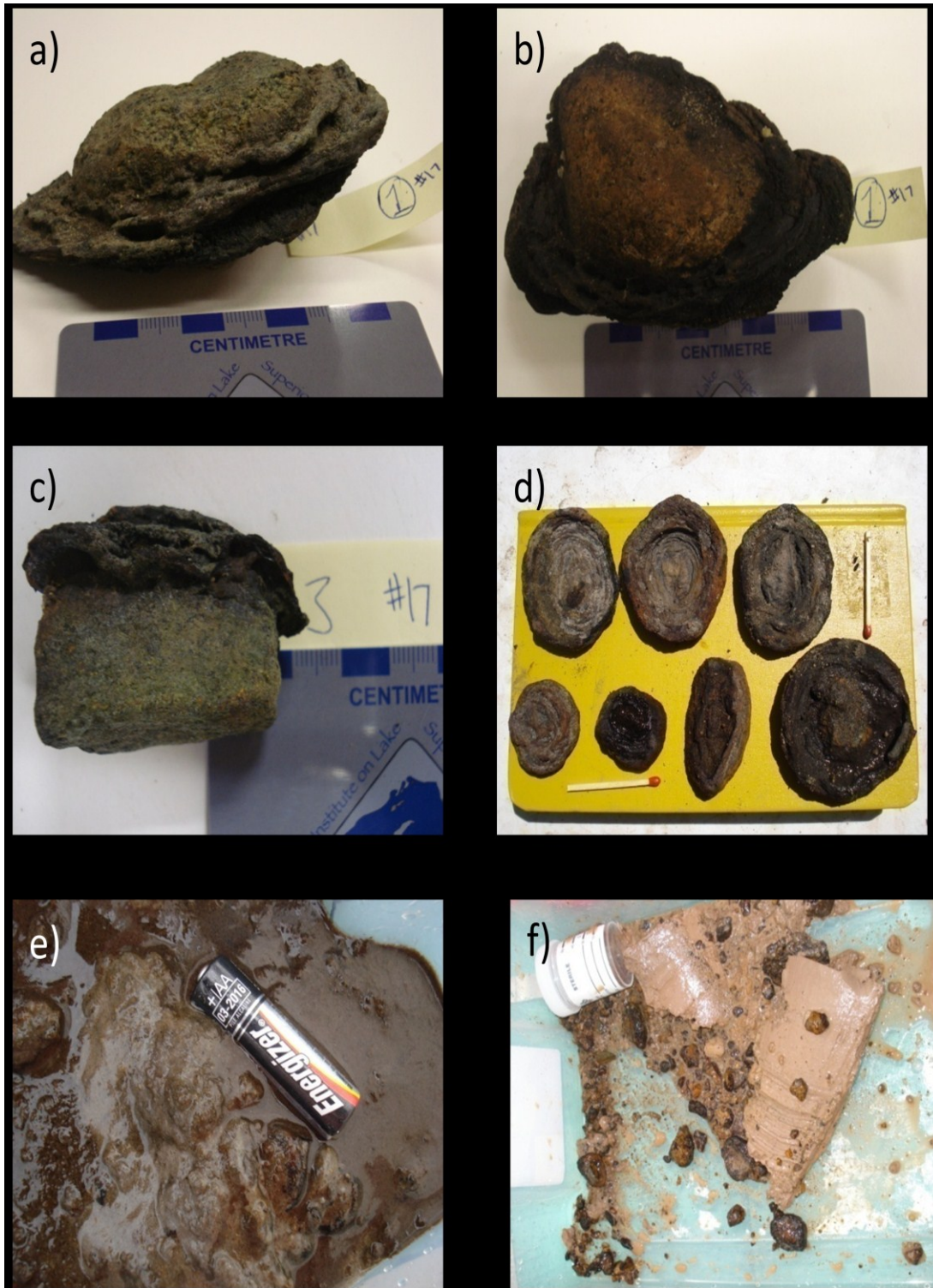


Figure 21: Shebandowan Lake, Island Site (a). A saturnine nodule structure surrounding a cobble found close to the shoreline at Small Site, Shebandowan. (b) Underside of nodule (a). (c) A mushroom shaped nodule structure found near the shoreline. (d) Equatorial skirt nodules found in great numbers on a sandy lake bottom in the center of a nodule field. (e) Sandy lake bottom material embedded with precipitates (f) Clay lake bottom forms the edge of the field embedded with precipitates.

Shebandowan, Island Site:

The Island Site is similar to the Small Site in terms of precipitate distribution, but differs in nodule morphology. The nodules of the Island Site begin close to shore at a depth of approximately 5 meters. They appear as a *disc with a down curl* (Sozanski and Cronan, 1976) where the top of the nodules is smooth with only a small portion of the ring structure visible. A central pebble is commonly present (Figure 22a). As the nodule grows outward from the stone it begins to grow downwards creating a domal structure (Figure 22c). The underside of the nodule displays prevalent ringed structures around the stone (Figure 22b). These precipitates are found on a rocky or sandy lake bottom.

As the water depth increases the precipitates become smaller and more prevalent (Figure 22d). They have a similar structure to the larger nodules found in this area. However, not all of the smaller nodules have a stone in their center. The nodules present in this area are on a silt or clay bottom, which is surrounded by a red/brown clay. In this clay small quarter sized precipitates can be found imbedded below the surface. The layout of the precipitates on the lake bottom in the Island Site appears more uniform than those present in the Small site of Shebandowan.

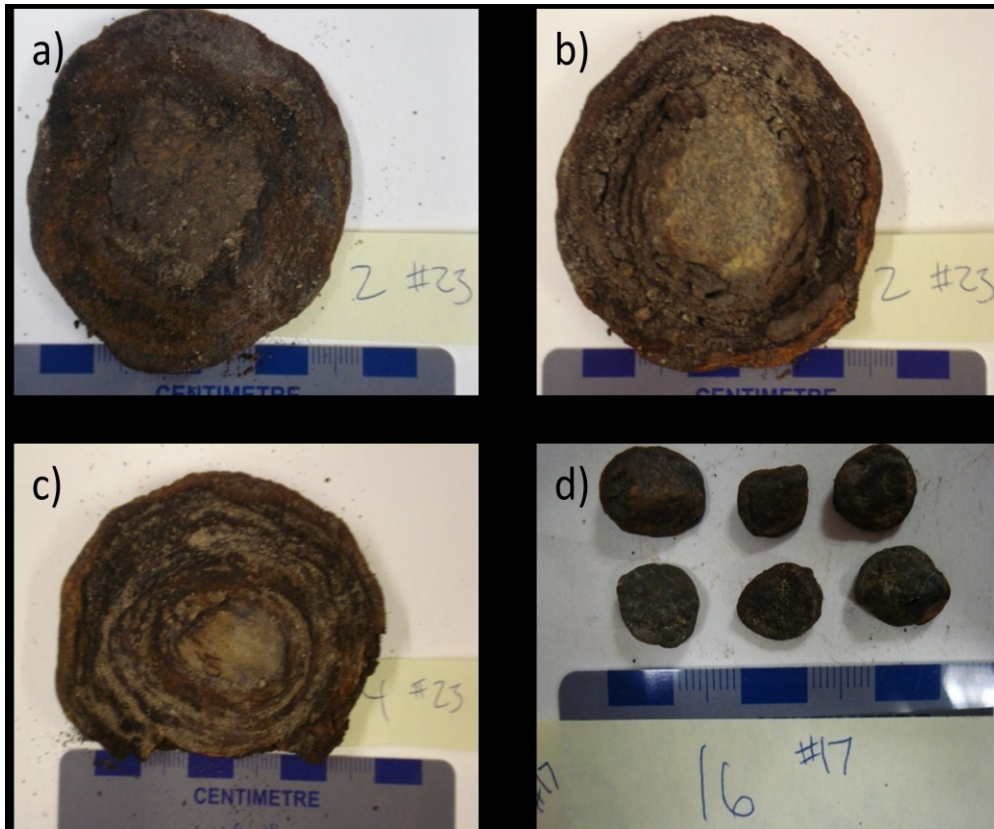


Figure 22: Shebandowan, Island Site nodules (a) The topside of a *disc with a down curl* nodule (b) the bottom side of a *disc with a down curl* nodule displaying a pebble in its center (c) a *disc with a down curl* nodule displaying a prevalent dome structure (d) smaller nodules found at greater water depth towards the edge of the field.

2. Water Chemistry

Depth and Temperature

Maps of depth for each study site can be found in the Appendix E. The study areas My Cove, 7 Cove and Bud's Cove were analyzed for differences between the water temperature of the lake bottom and the water temperature of the substrate 5cm into the lake bottom sediment. Results from Bud's Cove did not show any correlation between lake bottom temperature and water temperature, possibly

due to a malfunction with the thermometer used to collect data. Results from Bud's Cove are not included in this section.

Lake Charlotte, 7 Cove:

The average difference in water temperature to sediment temperature is 1.35°C with the colder water coming from within the sediment. There appears to be a positive trend between the temperature of the lake water and the difference of the sediment temperature to the lake water temperature (Figure 23). In the shallower areas where lake bottom temperatures are highest, the greatest difference exists between lake bottom temperature and sediment temperature. In deeper areas where the lake bottom temperatures are less, the difference is less. Numerical results from each data point can be found in the Appendix B.

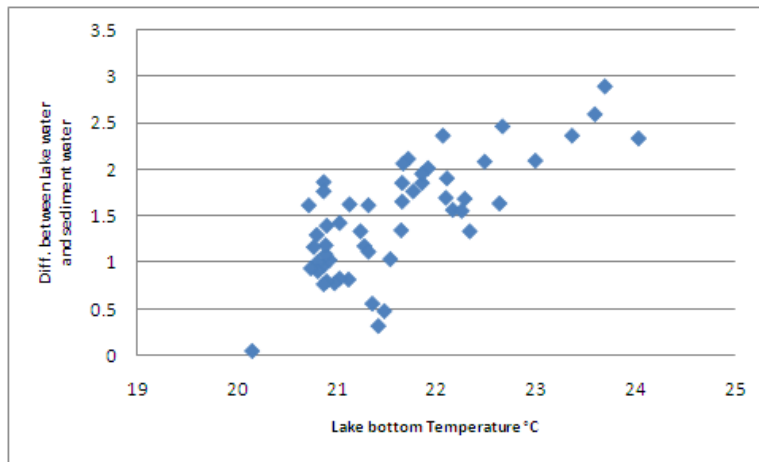


Figure 23: A positive trend is present between the temperatures of the lake bottom and the difference between the lake bottom and sediment bottom at 7 Cove, Lake Charlotte.

Lake Charlotte, My Cove:

The average difference between the lake bottom water temperature and sediment temperature at the My Cove site is 1.64°C. There appears, as with 7Cove, to be a positive trend between

the temperature of the lake water and the difference between the sediment temperature and the lake water temperature (Figure 24). Numerical results from each data point can be found in the Appendix.

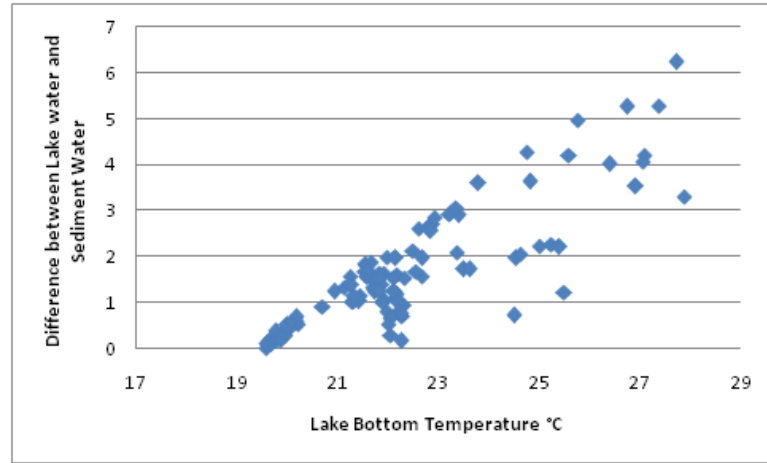


Figure 24: A positive trend can be found between the lake bottom temperature and the difference between lake bottom and sediment temperatures at My Cove, Lake Charlotte.

Analysis of lake bottom water temperature and sediment temperature was conducted to determine if a groundwater spring or diffuse flow was present in any of the study areas. Such a flow could create unique physical and chemical conditions at the lake bottom sediment interface. Two of the three study areas analyzed for sediment temperature showed a decrease in the difference between the sediment water and the lake bottom water as the lake water decreased in temperature (as the lake became deeper) suggesting a groundwater spring below the lake bottom. Due to temperature changes of the shallow lake bottom areas throughout the course of a day it can be difficult to use this comparison method as the only means of determining whether groundwater flow is present below each site.

Dissolved Oxygen (DO)

Table 1 gives the average of all values collected for dissolved oxygen at all nine study areas. It can be assumed that in deeper water there is more potential for the existence of plankton biomass. This allows for a greater amount of carbon to be deposited and therefore a greater amount of oxygen to become consumed. A decrease in the amount of oxygen by depth can be observed by comparing the average DO from deeper study sites (Granite Islands, Mine Site) to more shallow study areas from the same lake (My Cove, 7 Cove and Bud's Cove). Changes in the amount of DO present between June and July at Shebandowan Lake forms a seasonal pattern with a greater amount of oxygen found in the spring opposed to summer. Complete data and maps of DO from each study site can be found in Appendix B and E.

Table 1: Average DO% values from each study site

Site	Average DO (%)
Bud's Cove	83.32
Granite Islands	69.91
Mine Site	68.41
My Cove	92.83
7 Cove	89.32
Sowden 41	78.46
Sowden 46	82.57
Shebandowan Small Site (June)	76.95
Shebandowan Small Site (July)	38.24
Shebandowan Island (June)	79.00
Shebandowan Island (July)	51.12

pH and Redox potential (Eh) Water Chemistry

pH and Eh data were collected from the study sites on the lake bottoms of all three lakes. Results are useful for comparison with one another and understanding of precipitate formation and growth. The Eh values are used to measure the tendency for a chemical species to acquire electrons and therefore become reduced. A visual representation of the pH and Eh of each site is present in Appendix E. The average of all stat values collected of Eh and pH readings from all sites are in Table 2.

Table 2: Average pH and Eh readings from all sites

Site	pH	Eh (mV)
Bud's Cove	5.85	138.33
Granite Islands	5.81	111.22
Mine Site	5.79	93.28
My Cove	5.91	145.58
7 Cove	5.88	130.81
Sowden 41	7.3	190.68
Sowden 46	6.96	172.42
Shebandowan Small Site (June)	7.49	97.55
Shebandowan Small Site (July)	7.43	-61.4
Shebandowan Island (June)	7.62	90.53
Shebandowan Island (July)	7.54	-52.87

Water elemental analysis:

Water samples were analyzed and compared with the environmental protection agency (EPA) standards for drinking water. Any results in which the element was above the EPA drinking standard, or considered high compared with all other results, are given in Table 3. The full elemental water analyses are in Appendix E.

Table 3: Water analysis compared to the drinking water standard

Element	EPA standard (mg/L)	Site above standard (mg/L). Recorded values shown in brackets
Aluminum	0.05-2	My Cove Pit at water table(2.683)
Arsenic	0.01	Mine Site at 1.5m depth (0.257)
Iron	0.3	7 cove at 9m depth (1.261) Dug well at Bud's Cove (0.5392) My Cove pit at water table (0.7579) All Sowden Lake samples (0.4445-0.7555)
Manganese	0.05	7Cove at 9m depth (0.5707) 7 Cove at 12m depth (0.0514)
TDP (total dissolved phosphorus)	0.02	Dug well at Bud's Cove (0.035) My Cove pit at water table (0.061) Sowden 46 (DD) at 11.5m (0.024)

3. Environmental Distribution of Major and Minor elements:

Geochemistry results from ICP-AES analysis of precipitate samples from nodules collected at each site were mapped using the ArcGIS, ARcMAp10 *Radial Basis Function* for each study area. These maps allow a visual representation of how each elemental component of the precipitate concentrates in the entirety of a nodule field. Each elemental map was then compared with maps of the same area for elements known to be highly concentrated in precipitates, including iron, manganese, aluminum and carbon. An example of how this mapping technique was used as a means of comparability between iron and three minor elements can be observed in Figure 25. Comparable distributions between maps of a highly concentrated element and a minor element suggest a chemical correlation on a large-scale. A visual presentation of the three most obvious comparable elements, to each major element, at each site can be found in Appendix F. All other elemental maps are also present in Appendix F.

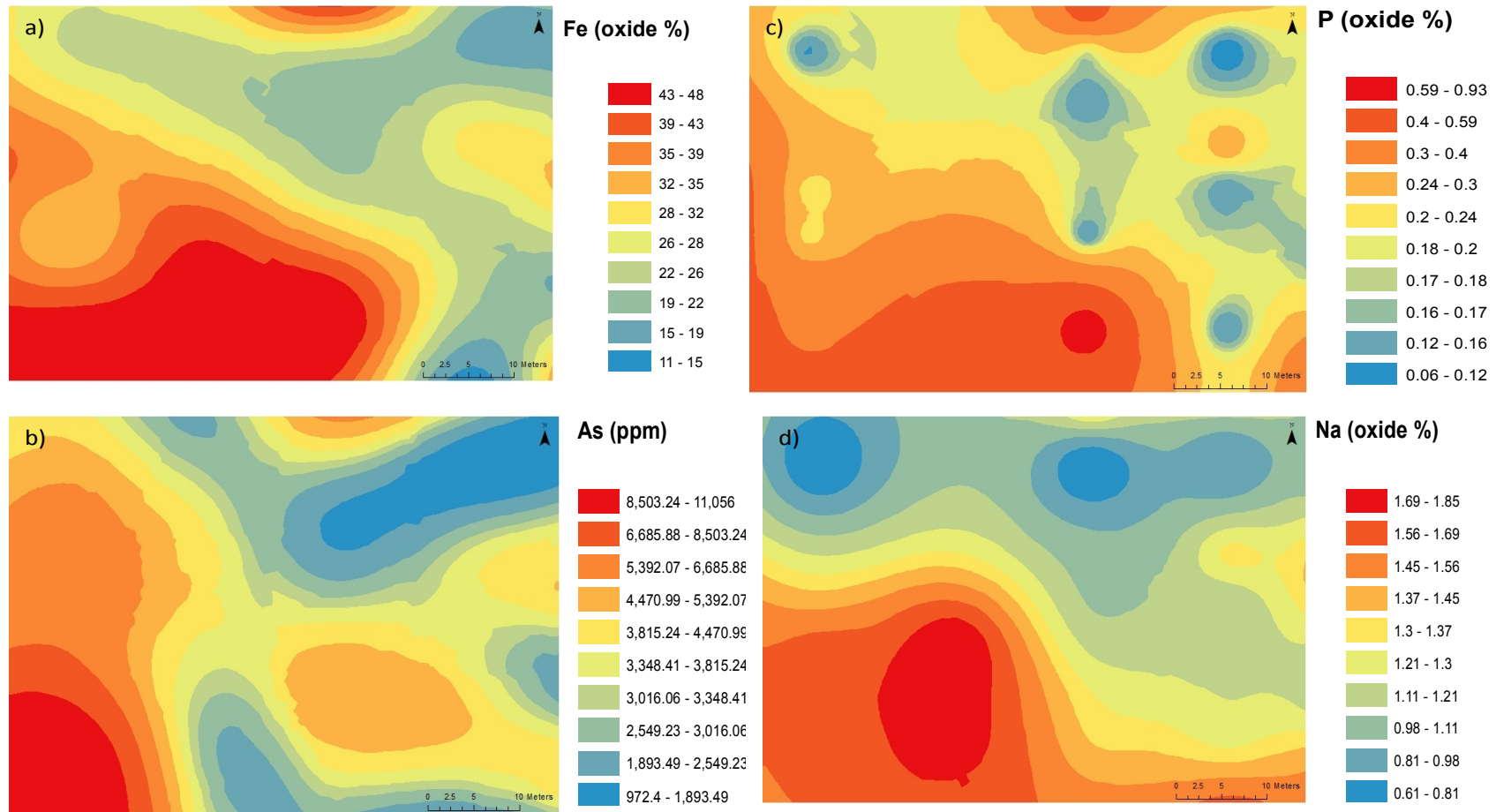


Figure 25: An example of an elemental distribution map comparison. Image's a to d are all created by the data analysis from precipitates collected from the My Cove Site. Areas of red show where an element is at its highest concentration in a precipitate field. Comparison data collected from these maps can be used to determine if any similarities exist at a large scale. This example displays the chemical similarities to Iron at 7 cove a) Fe distribution, b) As distribution, c) P distribution, d) Na distribution

Tables 4 -7 display all elements that are behaving similarly to each major element at the study sites. Iron was found to have the largest amount of similarly behaving elements, especially at both Sowden Lake sites. Manganese has the same elements with comparable distributions at most sites. These include barium, lanthanum, cobalt and sulfur. Carbon has the least amount of elements with comparable distribution of the four major elements.

Table 4: Elements with comparable distributions to iron on the contour maps located in Appendix F. Elements in blue represent a trend with iron that is independent to each lake site. Elements in red represent a trend with iron present at the majority of sites.

Site	Similarities to Fe
7 Cove, Lake Charlotte	As, Mo, Na, P, Zr
Bud's Cove, Lake Charlotte	As, P, W
Granite Islands, Lake Charlotte	Ti
Mine Site, Lake Charlotte	none
My Cove, Lake Charlotte	As, Cu, Na
Area 46, Sowden Lake	As, Cr, Cu, La, Mo, Nb, Ni, P, V, Y, Zr
Area 41, Sowden Lake	As, Co, Ni, Li, P
Island Site, Shebandowan	As, La, P
Small Site, Shebandowan	none

Table 5: Elements with comparable distributions to manganese on the contour maps located in Appendix F1. Elements in blue represent a trend with manganese that is independent to each lake site. Elements in red represent a trend with manganese present at the majority of sites.

Site	Similarities to Mn
7 Cove, Lake Charlotte	Ba, La, S, Sr
Bud's Cove, Lake Charlotte	Ba, Co, La, Ni, S
Granite Islands, Lake Charlotte	Ba, Ca, Co, La
Mine Site, Lake Charlotte	Ba, Y
My Cove, Lake Charlotte	Ba, Co, La, V, Y
Area 46, Sowden Lake	Ba, S
Area 41, Sowden Lake	Ba, Co, La, V, Y
Island Site, Shebandowan	Ba, Cd, Mo, Ni, S, Zn
Small Site, Shebandowan	Ba, La, S,

Table 6: Elements with comparable distributions to aluminum on the contour maps located in appendix F1. Elements in blue represent a trend with aluminum that is independent to each lake site. Elements in red represent a trend with aluminum present at the majority of sites.

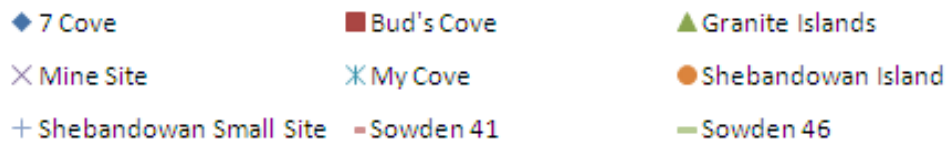
Site	Similarities to Al
7 Cove, Lake Charlotte	Ce, Cu, Sc, Zn
Bud's Cove, Lake Charlotte	K, Mg, Nb
Granite Islands, Lake Charlotte	none
Mine Site, Lake Charlotte	K, Li, Mg, Nb, Sc, Ti, Zr
My Cove, Lake Charlotte	K, Zn
Area 46, Sowden Lake	K, Mg, Sc, Sr
Area 41, Sowden Lake	Mo, Ti, Zr
Island Site, Shebandowan	Cr, K, Mg, Sr, Ti
Small Site, Shebandowan	Cr, Li, Mg, Na

Table 7: Elements with comparable distributions to Carbon on the contour maps located in Appendix F1.

Site	Similarities to C
7 Cove, Lake Charlotte	No similarities
Bud's Cove, Lake Charlotte	No similarities
Granite Islands, Lake Charlotte	Co
Mine Site, Lake Charlotte	No similarities
My Cove, Lake Charlotte	No similarities
Area 46, Sowden Lake	No similarities
Island Site, Shebandowan	Ba, Mn, Mo, Ni, S
Small Site, Shebandowan	Mn, La, S

4. Correlation of Geochemical Results

Elements found concentrating together on the macro-scale in elemental maps were plotted against each other on XY plots to determine the strength of correlation between the two elements. All graphs showing reasonable correlations between two elements are displayed in this section. Any elements which show a positive correlation at a macro-scale in elemental maps, but do not show a correlation graphically can be found in Appendix G. The legend for all correlation plots is:



Positive correlations with iron are observed with the elements arsenic and phosphorous for all sites on lakes studied except those on Shebandowan and the Mine Site of Lake Charlotte. The slopes of the correlation lines for the Lake Charlotte samples are higher than the Sowden Lake samples (Figure 26). Manganese is positively correlated with the elements barium, sulfur and cobalt (Figure 27). A positive correlation between aluminum, potassium, magnesium, and titanium was also present in the data (Figure 28). A positive correlation between aluminum and chromium was present in the data from all sites except Shebandowan Lake. Negative correlations were observed between iron and aluminum (Figure 29). Iron and manganese when plotted against each other displayed both a positive correlation and negative correlation in the Lake Charlotte samples and a negative correlation in both the Shebandowan and Sowden Lake samples (Figure 30). Arsenic and phosphorus, when plotted against one another create an “L” shape suggesting Lake Charlotte is behaving differently than Sowden and Shebandowan Lakes (Figure 31).

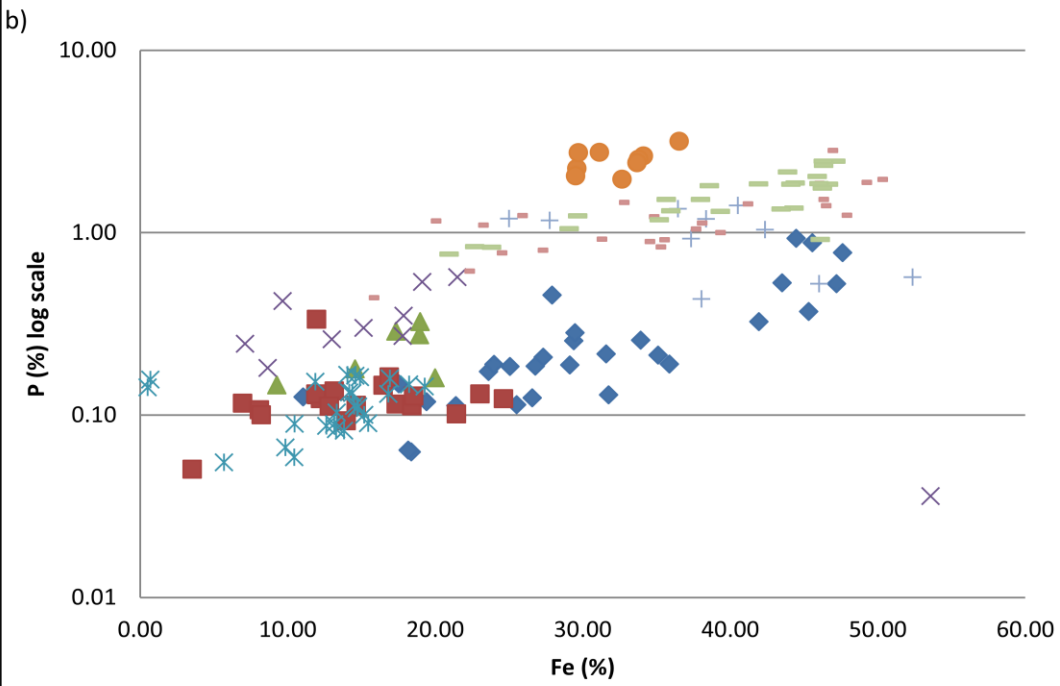
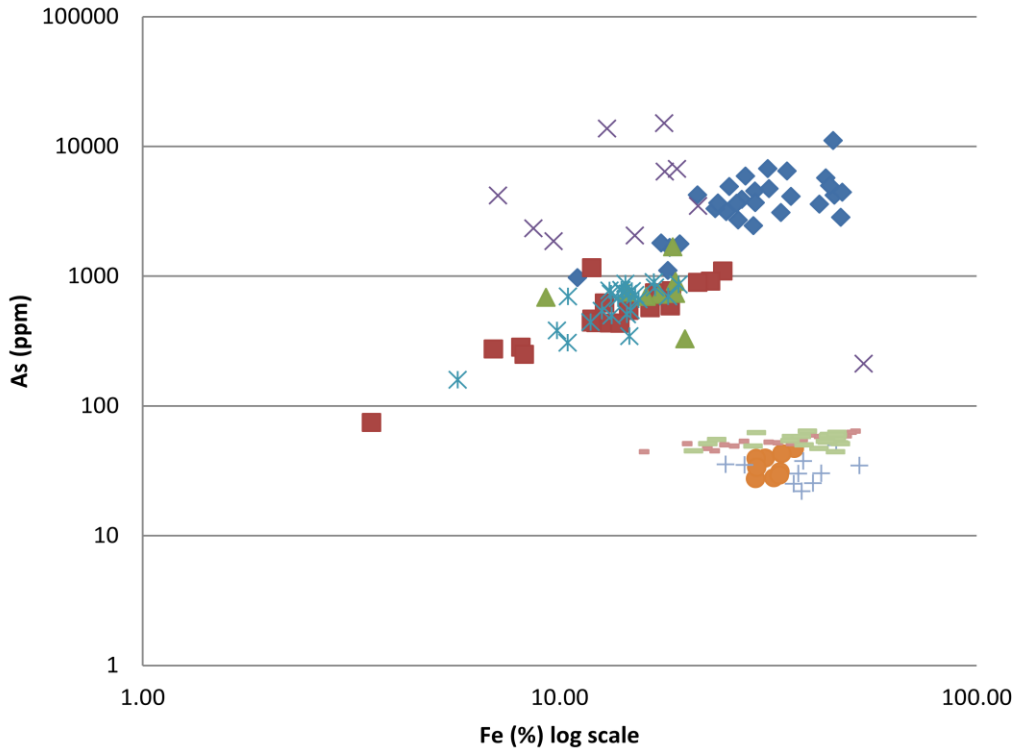


Figure 26: Arsenic vs. iron (a) and phosphorous vs. iron (b) displaying a positive trend

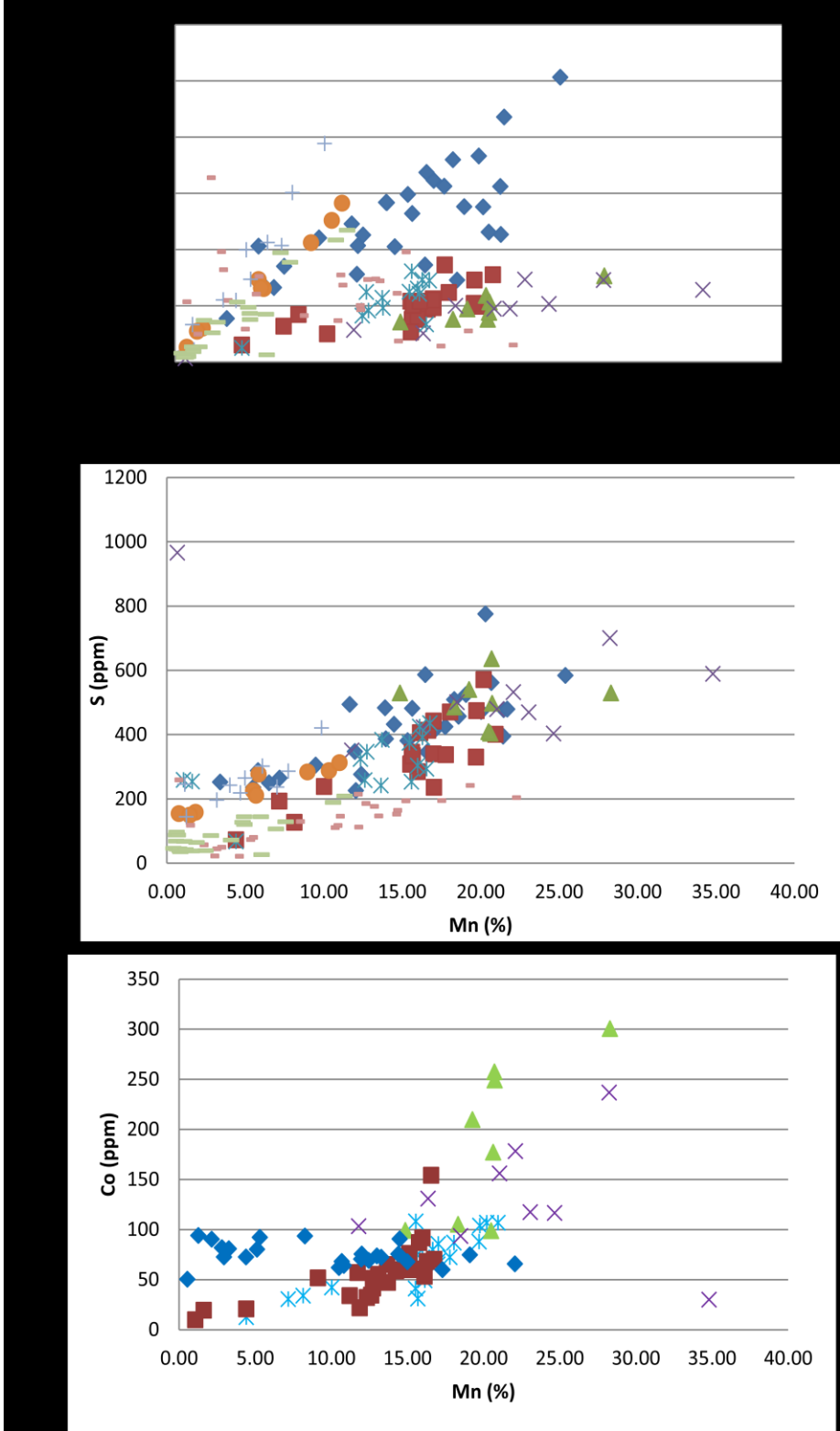


Figure 27: Barium vs. manganese from Lake Charlotte sites (a), and sulphur vs. manganese (b), and cobalt vs. manganese (c) displaying a positive trend towards one another.

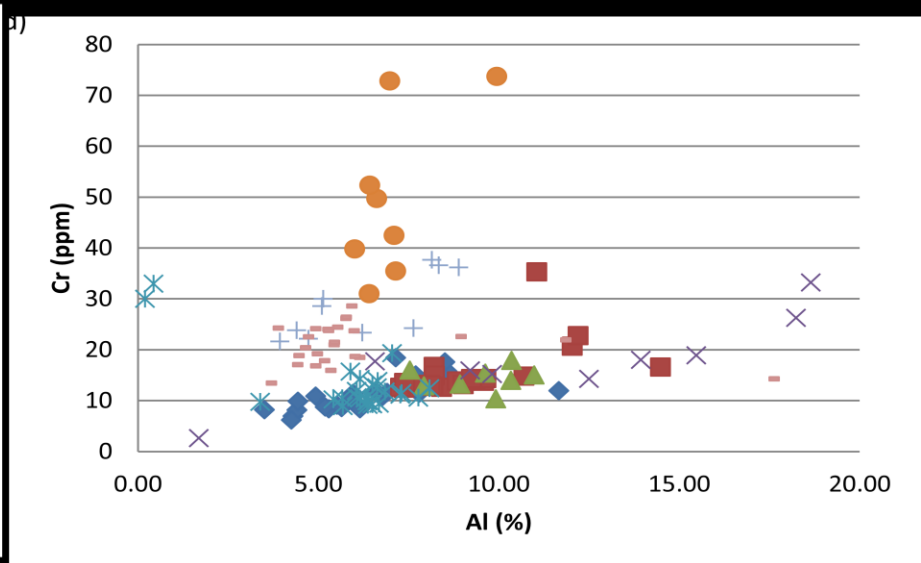
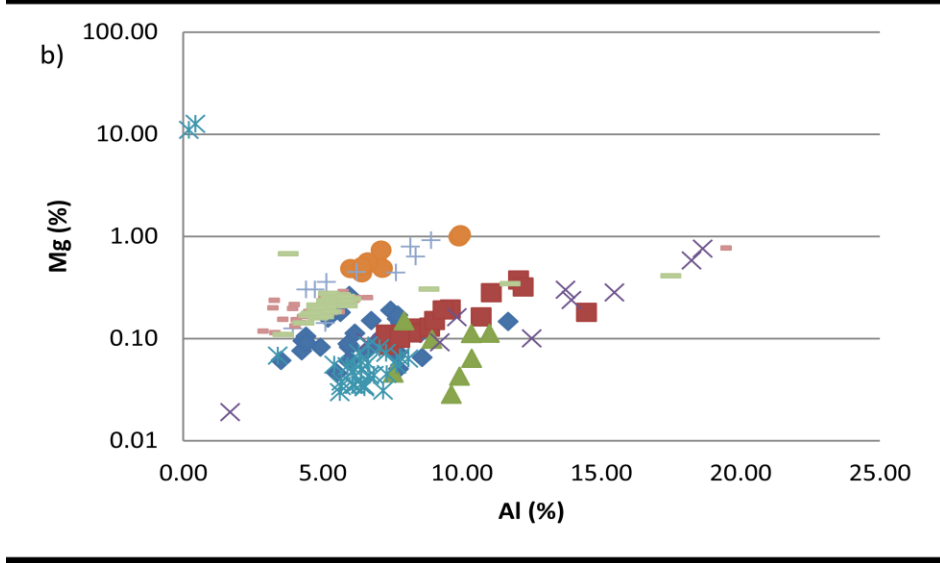
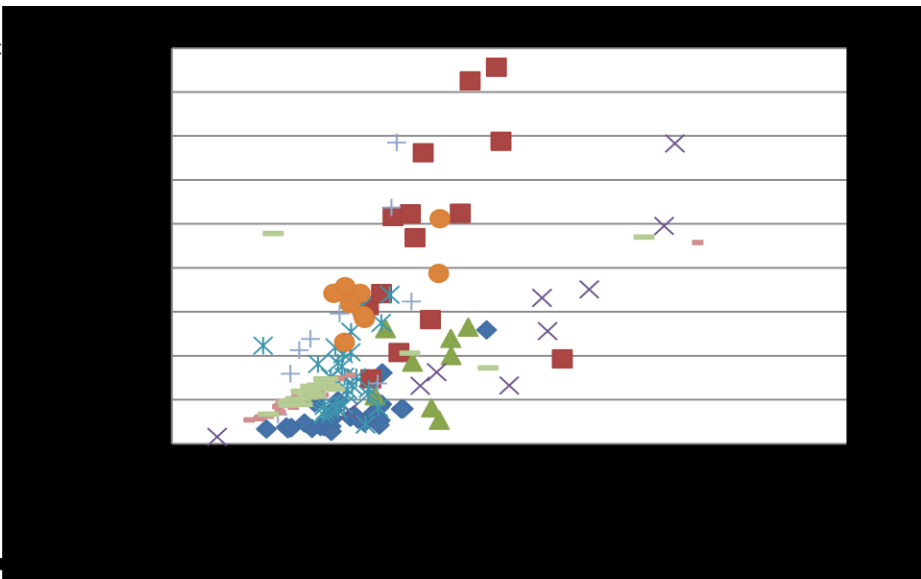
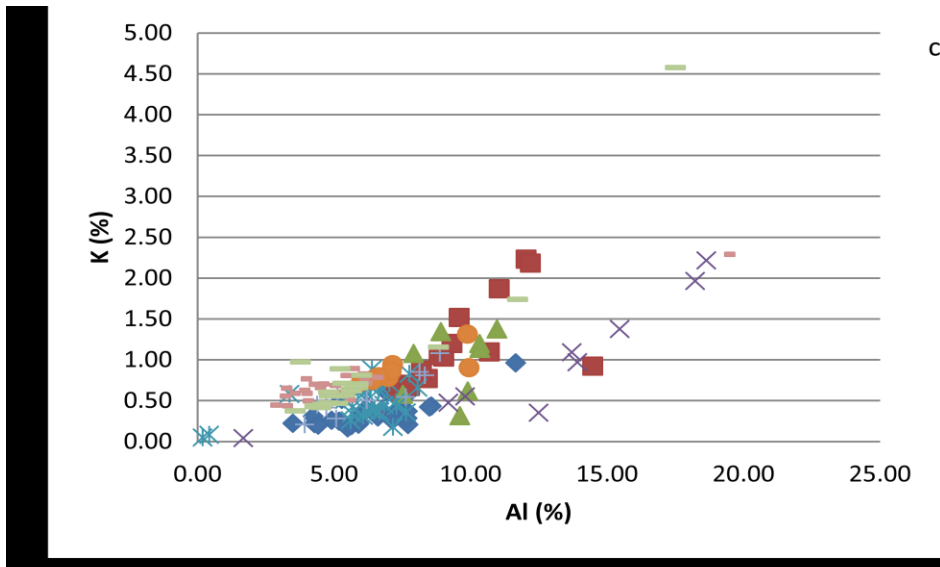


Figure 28: A positive correlation exists between potassium vs. aluminum (a), magnesium vs. aluminum (b), and titanium vs. aluminum (c). There is a positive correlation between aluminum and cr with the exception of the Shebandowan Lake Sites (d).

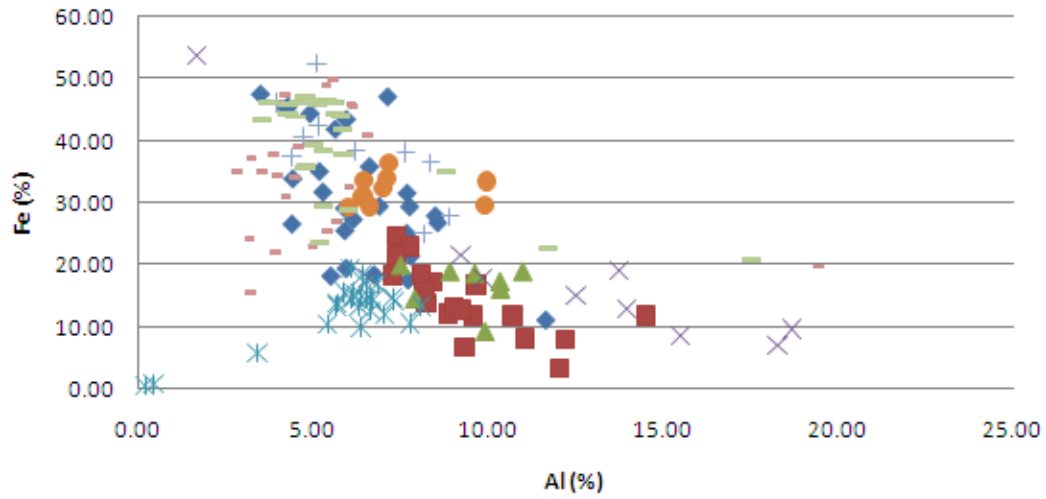


Figure 29: A negative trend exists between iron and aluminum

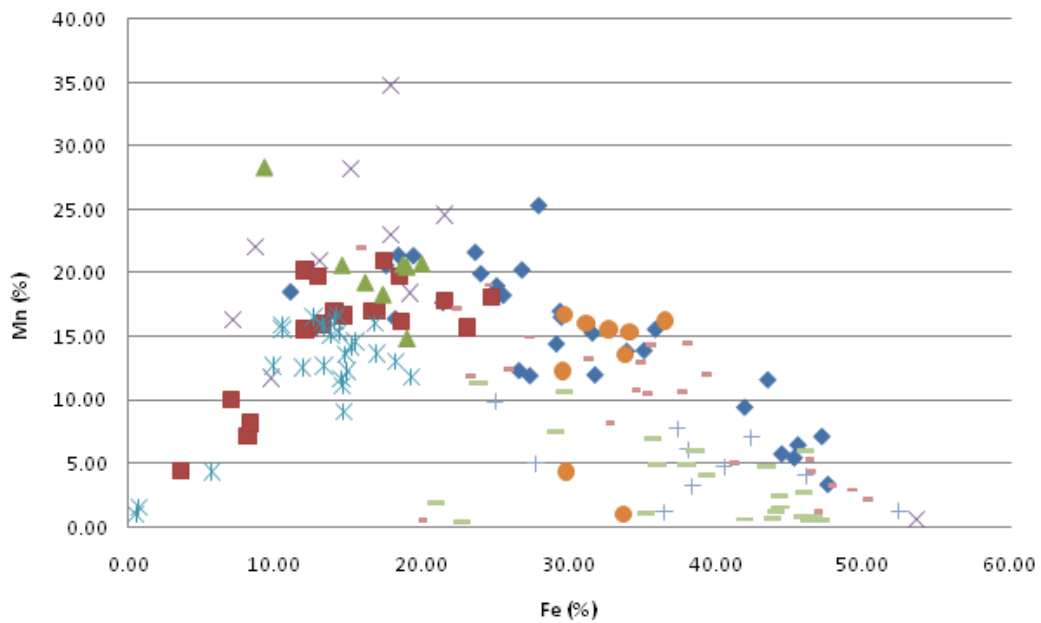


Figure 30: Graph displaying a negative trend between manganese and iron with the exception of the My Cove and Bud's Cove sites showing a positive trend.

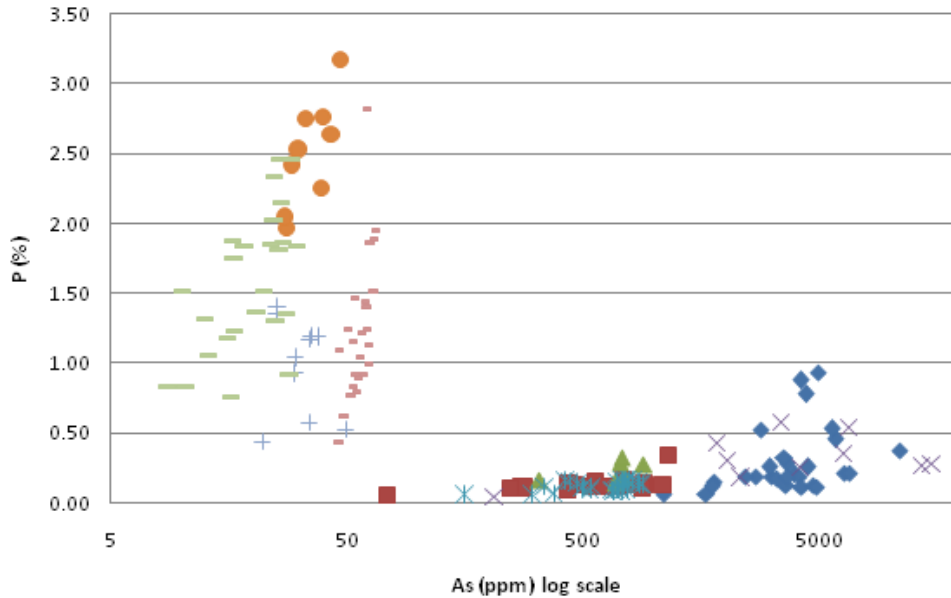


Figure 31: Graph displaying the relationship between As and P

5. Nodule Anatomy, Sediment Geochemistry and Rare Earth Elements

Nodule Anatomy

Three nodules from the Lake Charlotte Sites (7 Cove, My Cove, and Granite Islands) were analyzed for differences in geochemistry between the inner area close to the pebble center and outer portion of the structure. The only minor elements (not including iron and manganese) to show any drastic differences in all three samples were arsenic, boron and barium. The only element which displays a trend is barium which concentrates in a greater amount on the outer portion of the sample. Further analysis is required to conclude that this behaviour is generally applicable. Geochemical data for these samples can be found in Appendix C.

Three nodules from Lake Charlotte's My Cove, and Sowden Lake, Area 46 were analyzed for any differences between the top and bottom of a sample. Geochemical results revealed the only elements

to have differences in all five samples are barium which concentrated on the bottom portion of the precipitate. A conclusion as to whether barium behaves in this manner on a large scale requires further analysis. Full analysis of these samples can be found in Appendix C.

Sediment Geochemistry

The sediment collected from the substrate under nodules at 7 Cove, My Cove, Bud’s Cove and Sowden Lake was analyzed. When the precipitates were compared to data from sediment collected below the precipitate, it was found that iron, manganese, arsenic, barium, cerium, nickel and zinc were considerably enriched in the precipitate (Table 8). Results from comparing sediment collected under precipitates, and beach sand from the My Cove shoreline (which can be assumed to have never been affected by a precipitate) are presented in Table 9. Data analysis of the sediment substrate from all five areas can be found in Appendix D.

Table 8: Percent difference between the precipitate vs. the underlying sediment of a study site showing depletion and enrichment in elements. For example, at site 7 Cove, the average precipitate is enriched 50-100% in Fe, Mo and Zn when compared to the underlying sediment of the precipitate field.

Site	50-100% depletion	100-200% depletion	50-100% enrichment	100-200 % enrichment
7 Cove	Al, Na, P , Cr, Sc	Ca, K, Mg, Ti	Fe, Mo, Zn	Mn, As, Ba, Ce, La, Ni
My Cove	Al	K, Na, Sc	Ca, La, Zn	Fe, Mg, Mn, Ti, As, Ba, Ce, Mo, Ni
Buds	Al	K, Na, Mg		Fe, Mn, As, Ba, Ce, La, Mo, Ni, S , Zn
Sowden 41	Ca, Na	Al, K, Mg, Ti, Cr, La, Y		Mn, As, Li, Mo, Ba
Sowden 46	Li, Al	Ca, K, Mg, Na, Ti, Y	P, Ba, Zn	Mn, Fe

Table 9: Percent difference between the lake sediment found in precipitate fields when compared to the beach sand from My Cove which does not contain any precipitates. For example, at Site 7 Cove, the average sediment found below a precipitate is 150-200% enriched in Fe, Mn, P, As, Ce, Mo and Zn when compared to nearby sand that does not contain precipitate material.

Site	50-100% enrichment	100-150 % enrichment	150-200 % enrichment	200+ % enrichment
7 Cove	Al, Zr, Sr, Li	Ca, Mg, La, Sc, Y	Fe, Mn, P, As, Ce, Mo, Zn	Ba, Ni, S
My Cove	Ca, Na, Ce, Cr, La, Li, Sc, Sr, Y	Fe, Mn, P, As, Mo	Zn	Ba, Ni, S
Buds Cove	Al, Ca, Cr, La, Sr, Y	Fe, Mg Mn, P, Ce, Zn	As, Mo	Ba, Ni, S

Spider Diagrams

ICP-MS analysis of samples from the study areas at Lake Charlotte, Sowden Lake, and Shebandowan Lake, along with material from the top and bottom of nodules, was conducted and the rare earth concentrations normalized to Post Achaean Australian Shale (PAAS). A complete list of geochemical results from each study area can be found in Appendix C. Rare earth data from Bud’s cove, 7 Cove and Shebandowan Lake were taken from Dasti (2008).

Spider graphs of rare earth elements in samples from My Cove, 7 Cove, Buds Cove, Sowden 46 and Shebandowan Lake are normalized to Taylor and McClelland’s PAAS (1985) and displayed in Figure 32. The three study areas found in Lake Charlotte display a positive cerium anomaly. My Cove displays small negative europium, and positive gadolinium anomalies. Positive europium anomalies are observed in 7 Cove data (Figure 32c). Compared to the rare earth data of the Lake Charlotte study areas, Sowden Lake does not display such an extreme positive cerium peak, the negative europium anomaly is more evident, and the positive gadolinium anomaly is present (Figure 32b). Samples from Shebandowan Lake are dissimilar to both Lake Charlotte and Sowden Lake samples, having both positive and small negative cerium anomalies (Figure 32d). A negative europium anomaly is present in the

Shebandowan data; however, it is not as exaggerated as what was observed with Sowden Lake and areas of Lake Charlotte. The top of each of the five samples was compared to the bottom of each nodule to investigate similarities or differences in rare earth chemical concentrations (Figure 33). Although one of the Sowden Lake samples (Figure 33d) displays a greater concentration of cerium and a depleted concentration of europium in the top of the nodule vs. the bottom, this is not seen in both nodule samples from this lake. The top compared to the bottom portion of most samples yields insignificant differences.

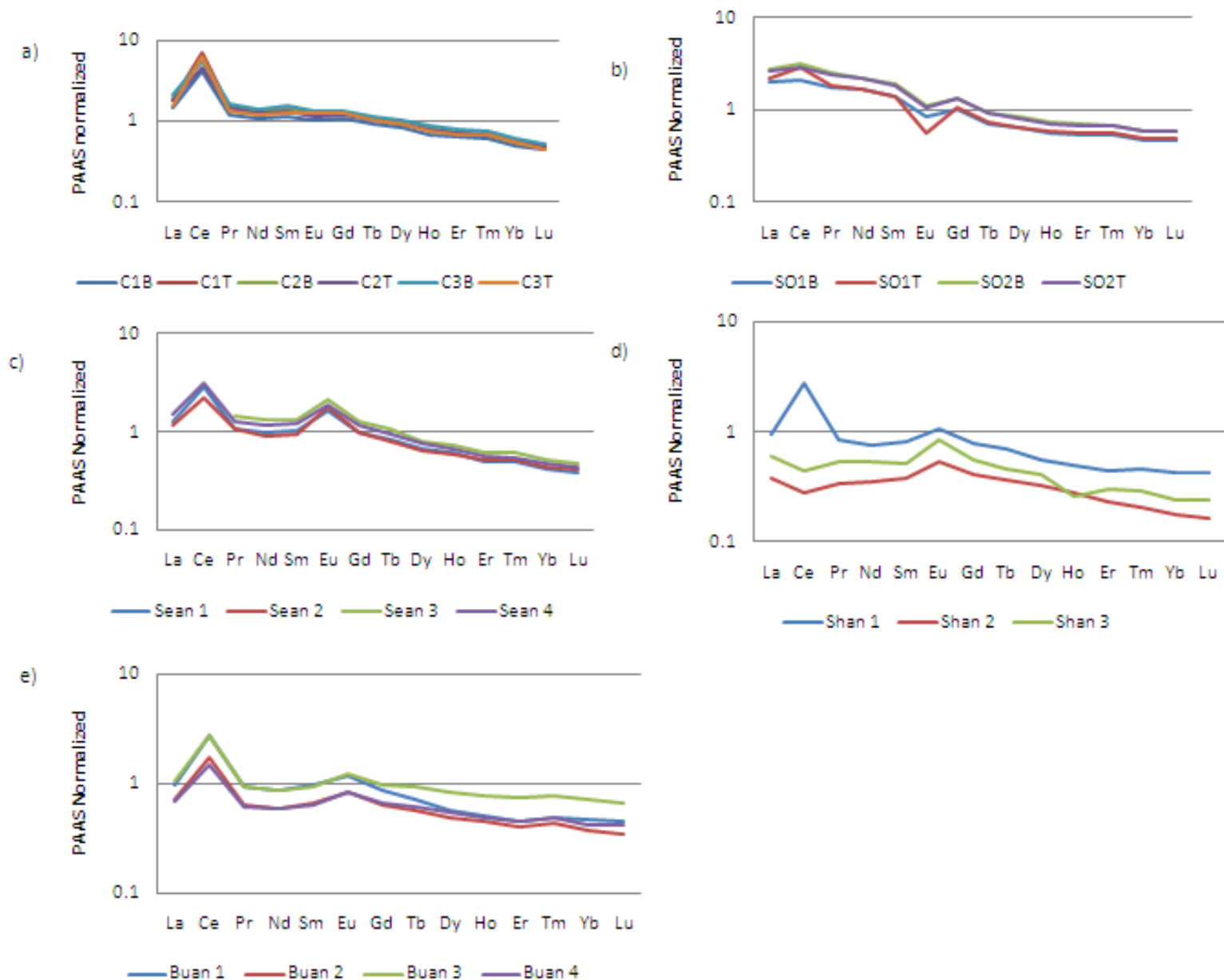


Figure 32: Graphs of Rare earth elements normalized to PAAS (Taylor and Mclenan, 1985) (a) My Cove, Lake Charlotte (b) Area 46, Sowden Lake (c) 7 Cove, Lake Charlotte (d) Lake Shebandowan (Dasti, 2008), (e) Bud's Cove, Lake Charlotte.

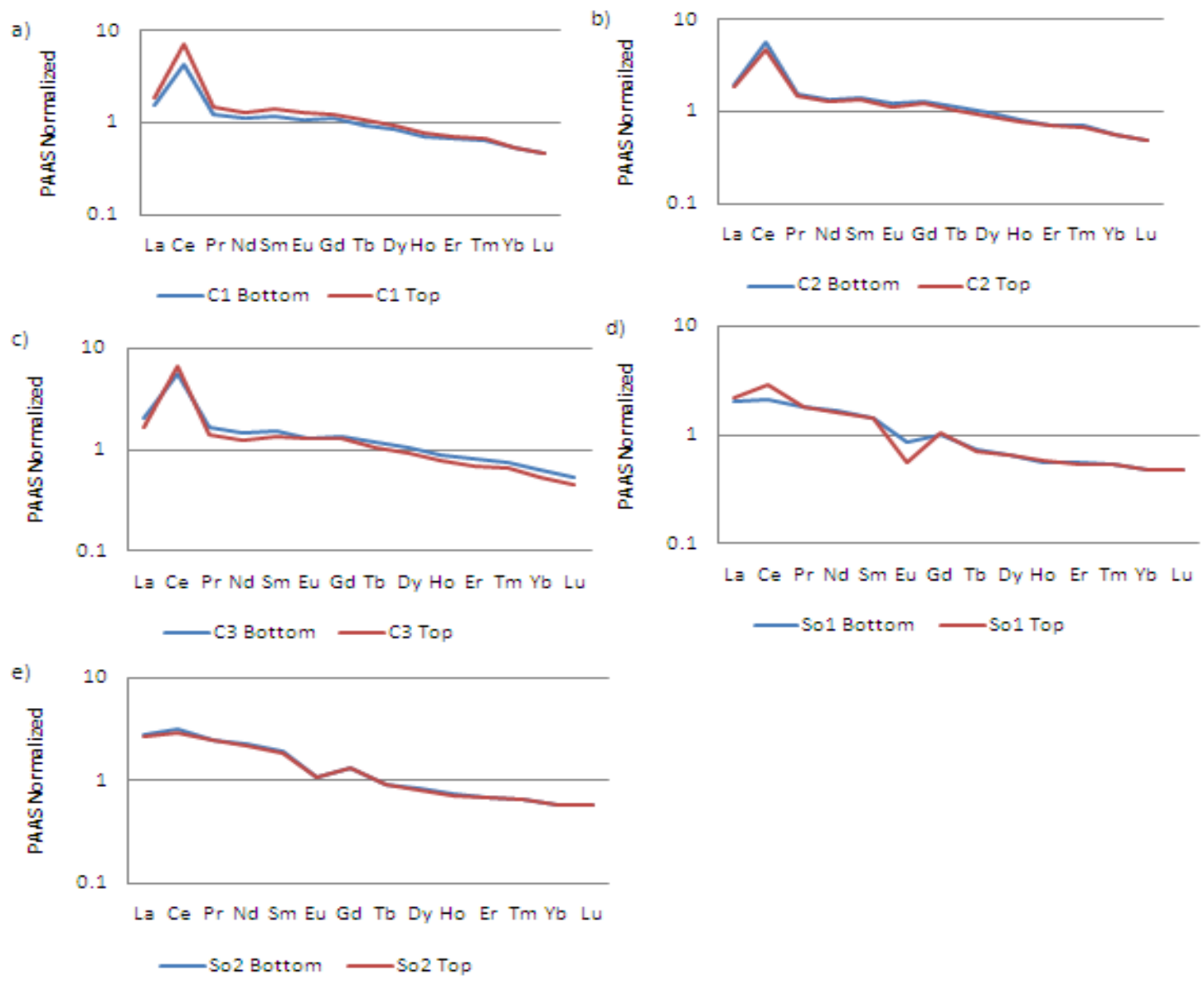


Figure 33: Rare earth element analysis of the top portion compared to the bottom portion of five samples normalized to PAAS. (a-c) Three Lake Charlotte, My Cove samples, displaying analysis from the top portion of the nodule (red) and the bottom portion of the nodule (blue). (d,e) Two Sowden Lake samples analyzed comparing the top portion of the sample (red) to the bottom of the sample (blue).

6. Micro Analysis with a Scanning Electron Microscope (SEM)

Samples from all three study lakes were observed with the SEM. The samples most typical of each site have been used to give an overall representation of findings at the micro scale. Each presented sample has analysis of both its top and bottom portions of each precipitate. It is important to note that the mapping application of Aztec* assigns the the brightness of an element in the mapping image is proportional to the elements abundance.

Results using mapping and linescan analysis cannot be used to accurately estimate the amount of an element in a particular area of a sample. For greater accuracy, results from the mapping and linescan application are compared with point analyse on the sample. The total elemental amounts from the point analysis application do not include the amount of carbon present in the sample and therefore will never equal 100%.

Lake Charlotte SEM Results (My Cove Data):

When a sample of a precipitate from Lake Charlotte was placed under a petrographic microscope, bands of similar size and structure appear concentrically arranged outward from its center (Figure 34, and 35). An FE- SEM-EDS mapping application shows the bands to be dominantly composed of manganese, iron and aluminum (Figure 36 and 37). Iron displays the most evident banding within the structure, with the iron - rich bands separated by high concentrations of manganese. The concentrations of these elements are inversely proportional to one another. If iron is highly concentrated in one area of the precipitate, manganese will appear only as a minor element in that area. If manganese is highly concentrated, iron will appear in a low concentration. Aluminum, although concentrated in both the manganese and iron bands has a greater concentration associated with the manganese. Silica is high in

areas of the sample where sand grains are present. All other elements do not occur in a great enough concentration to properly be mapped in detail.

Similar to the mapping application, a line scan by means of Aztec * was used to observe where the dominate elements which make up precipitates are found. Linescan data present in Figure 38 shows iron to have its highest concentration in areas of low manganese content. A lack of iron allows for a high concentration of manganese and visa versa. Aluminum, although found throughout sample, appears at its greatest concentrations when there is a high amount on manganese present. Silica is again only highly concentrated where sand grains are present in the sample.

Figure 39 is an SEM image depicting areas of a sample that were analyzed using the point analysis application. The point analysis results displayed in Table 10 show the trends observed in all samples analyzed by SEM from 7 Cove. There does not appear to be any trends that differentiate the top vs. the bottom of the precipitate nodules. There appears to be a positive correlation between barium and manganese with the amount of barium increasing as the amount of manganese increases. Higher concentrations of arsenic were present closer to the surface of the precipitate and were rarely above detection near the center of the sample.

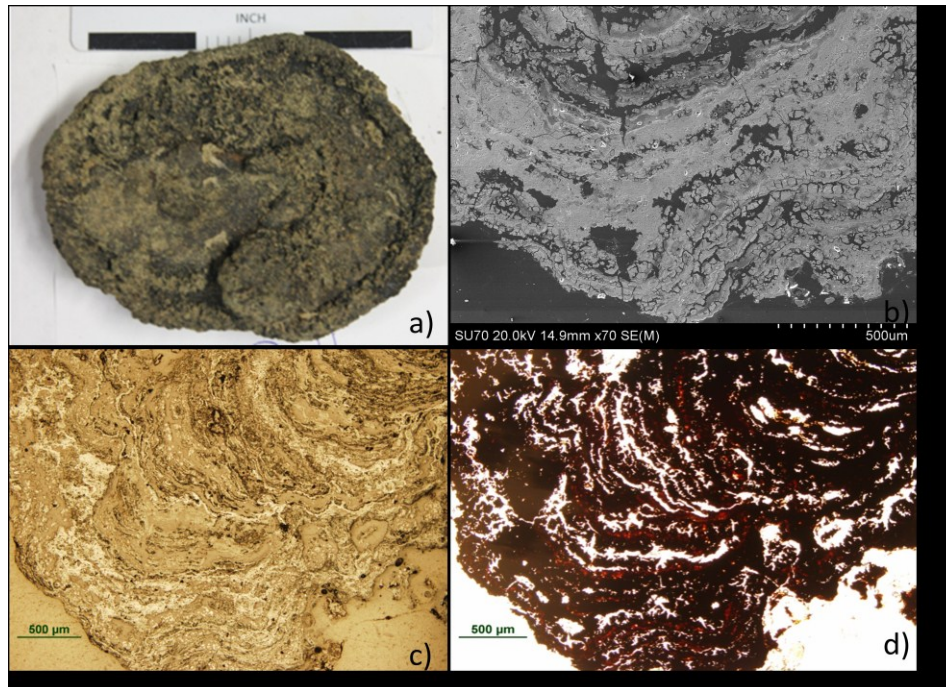


Figure 34: Lake Charlotte, My Cove images of the bottom portion of the nodule. a) photograph of the original nodule before being cut and made into a slide. b) SEM, SE image of a slide created from the nodule in photograph (a). c) A reflected light petrographic image of the bottom portion of nodule (a). d) A cross-polarized petrographic image of the same nodule.

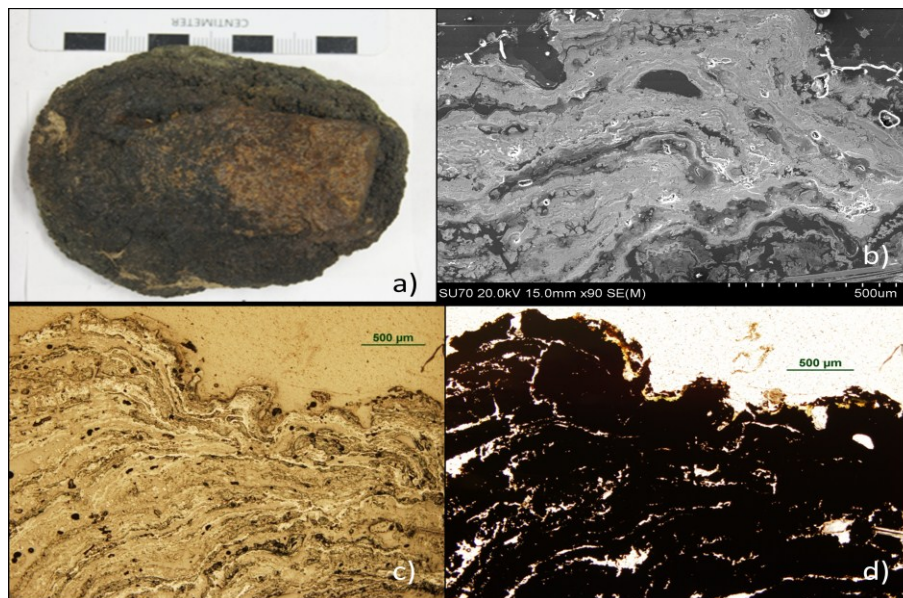


Figure 35: Lake Charlotte, My Cove images of the top portion of the nodule. (a) Photograph of the original nodule before being cut and made into a slide. b) SEM, SE image of a slide created from the nodule in photograph (a). c) A reflected light petrographic image of the bottom portion of nodule (a). d) A cross-polarized petrographic image of the same nodule.

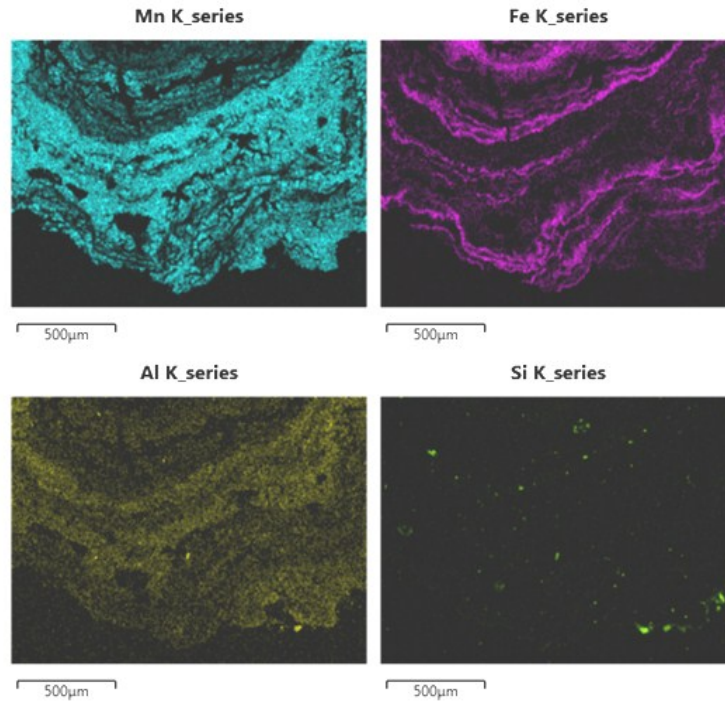


Figure 36: Element distribution images from the bottom portion of a Lake Charlotte sample. This is a visual display of how elements are distributed within a sample.

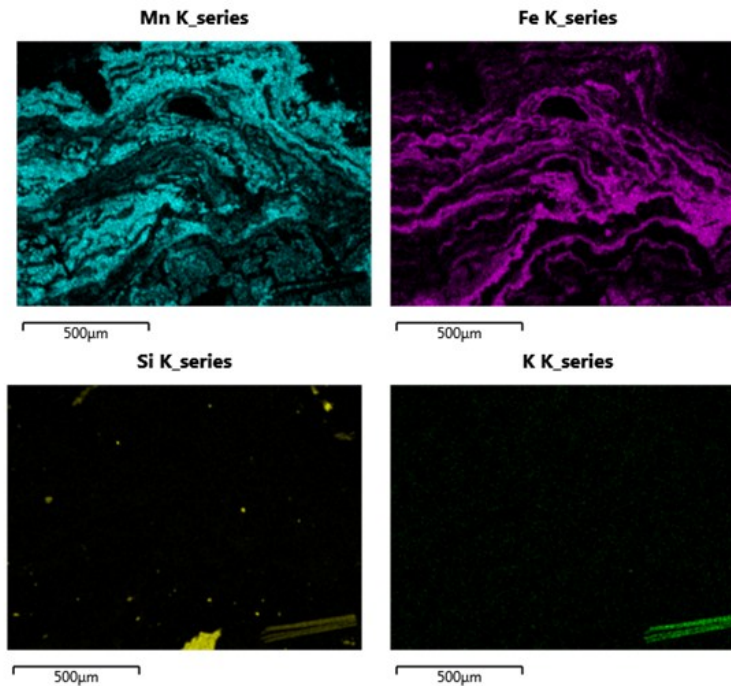


Figure 37: Element distribution images from the top portion of a Lake Charlotte sample. This is a visual display of how elements are distributed within a sample.

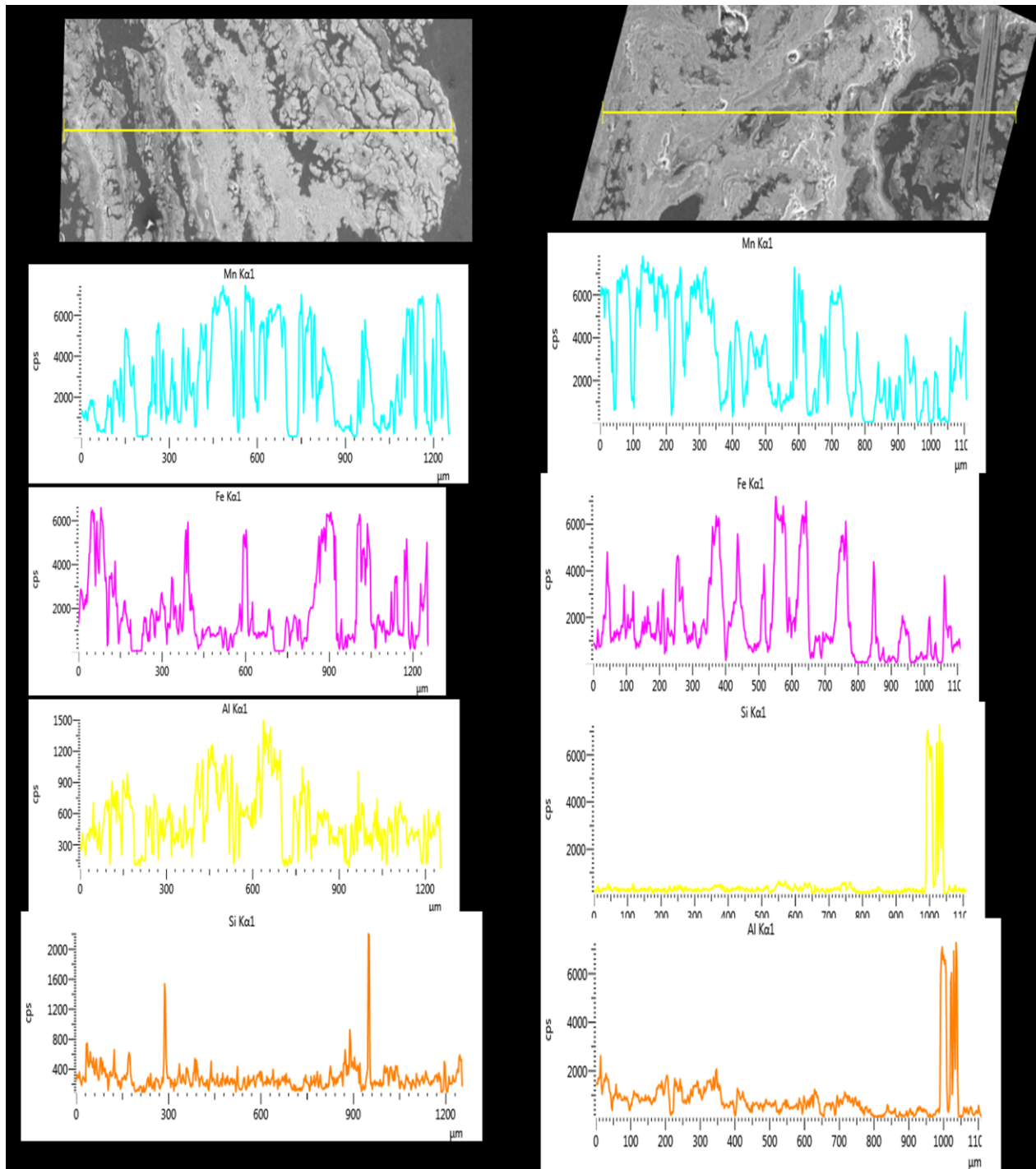


Figure 38: a) A line Scan analysis from the nodule in Figure 33. A linescan offers visual representation of the distribution of elements present within a sample. b) A line Scan analysis from the nodule in Figure 34. A linescan offers visual representation of the distribution of elements present within a sample.

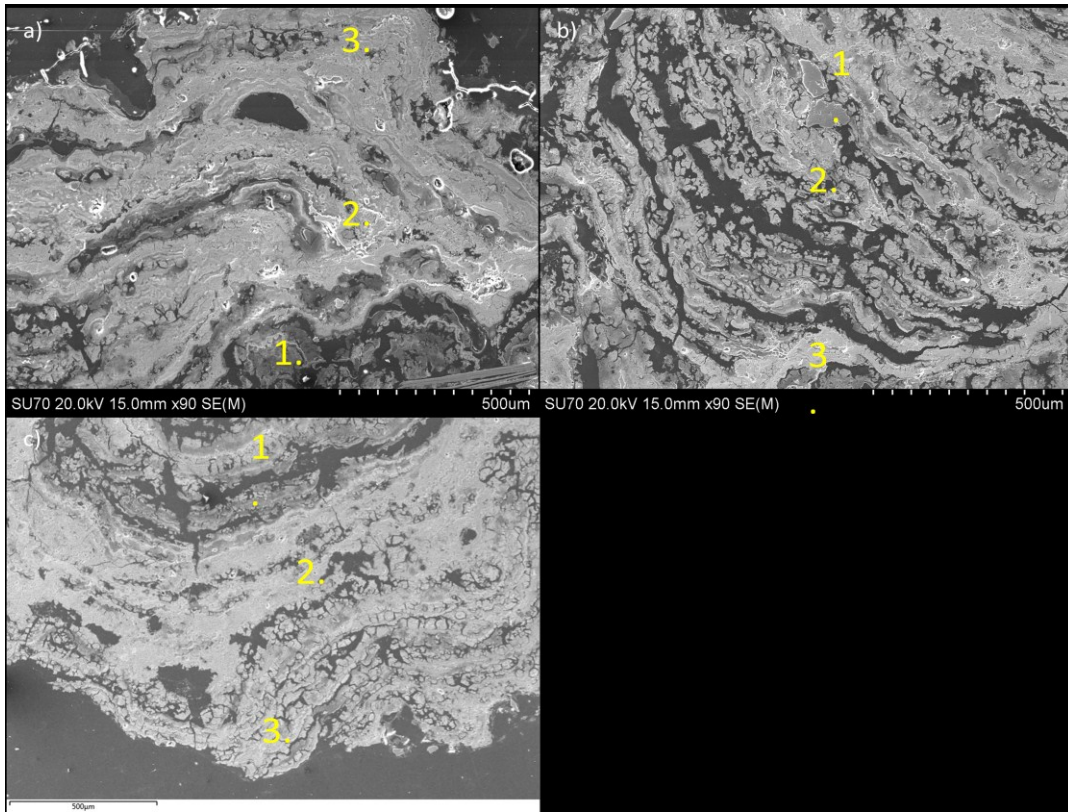


Figure 39: SEM image map of the top of the nodule (a), middle of the nodule (b), and bottom of the nodule (c) of a sample from 7 Cove Lake Charlotte. Analysis of each number is presented on Table 10.

Table 10: Lake Charlotte SEM Point analysis data from Figures 38 (a-c)

Image	Oxide	Oxide %	Image	Oxide	Oxide %	Image	Oxide	Oxide %
Top: 1	Al ₂ O ₃	2.4	Middle: 1	Al ₂ O ₃	2.52	Bottom: 1	Al ₂ O ₃	2.44
	SiO ₂	0.44		SiO ₂	1.42		SiO ₂	1.84
	MnO	31.65		MnO	26.03		MnO	13.46
	FeO	9.54		FeO	50.88		FeO	44.24
	BaO	1.26		BaO	0.72			
			K ₂ O	0.19				
Total oxides for Top (1) = 45.52			Total oxides for Middle (1) = 81.88%			Total oxides for bottom (1) = 61.98%		
Top: 2	Al ₂ O ₃	5.83	Middle: 2	Al ₂ O ₃	3.43	Bottom: 2	Al ₂ O ₃	14.03
	SiO ₂	0.86		SiO ₂	0.87		SiO ₂	0.62
	MnO	34.03		MnO	33.83		SO ₃	0.26
	FeO	26.24		FeO	28.36		MnO	48.03
	AsO ₂	0.2		BaO	0.78		FeO	6.56
	BaO	1.5					ZnO	0.32
							AsO ₂	0.33
				BaO	0.92			
Total oxides for Top (2) =69.01%			Total oxides for Middle (2) = 67.43%			Total oxides bottom for(2) = 71.57 %		
Top 3:	Al ₂ O ₃	3.5	Middle: 3	Al ₂ O ₃	4.37	Bottom: 3	Al ₂ O ₃	1.94
	SiO ₂	0.64		SiO ₂	1.93		SiO ₂	1.88
	MnO	34.26		SO ₃	0.18		SO ₃	0.52
	FeO	10.52		MnO	0.68		MnO	3.13
	BaO	1.34		FeO	64.22		FeO	49.47
							AsO ₂	0.2
Total oxides for Top (2) = 50.26%			Total oxides for middle (3) = 71.38%			Total oxides for bottom(3) = 57.44 %		

Sowden Lake SEM Results:

When samples of precipitates collected from Sowden Lake were observed under a petrographic microscope and SEM, as with those from Lake Charlotte, a banded structure was evident (Figure 40 and 41). However, the grains that make up this banding are more closely compacted together creating a more solid appearance when compared with samples from Lake Charlotte. In polarized light the bright red iron oxides predominantly found in Lake Charlotte samples were rarely seen in any samples from Sowden Lake.

A negative correlation between iron and manganese was observed when samples from Sowden Lake were analyzed using a mapping application (Figure 42 and 43). Calcium has a positive correlation to manganese in the precipitates found in Sowden Lake. Silica was found concentrated in sand grains present in the sample. All other elements mapped had abundances too low to display a meaningful pattern.

Linescan data relays similar results to those concluded by use of the mapping application (Figure 44). A negative correlation appears to exist between the elements iron and manganese. Two positive correlations within the sample occur between manganese, barium and calcium, and aluminum and silica. All other elements analyzed are present in too small a concentration to provide a useful pattern.

Point analysis of the Sowden Lake samples analyzed generally provides the following conclusions (Figure 45, Table 11). When there is an increase in the amount of manganese present, an increase in the amount of barium also occurs. A positive trend is found between phosphorus and iron. As the amount of iron in a sample increases, so to does the amount of phosphorus. The trend between manganese and calcium, as evident in the mapping and linescan methods conducted on Sowden Lake samples, does not appear a good correlation with point analysis. No other correlations with minor and major elements were evident in the Sowden Lake samples. Aluminum, though always present, does not seem to favour iron or manganese concentrations within the sample and is mostly associated with silisiclastic material.

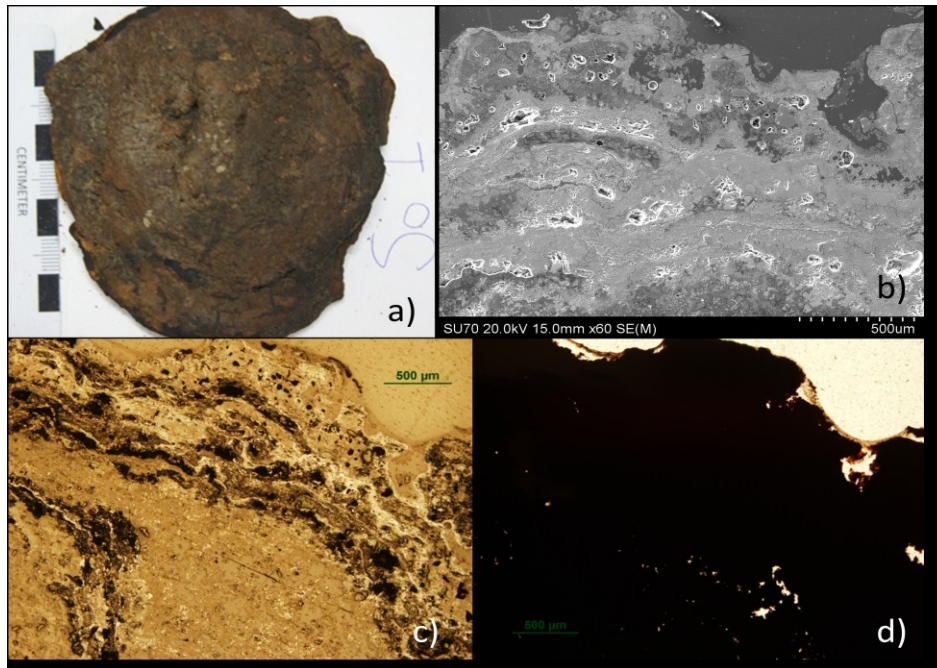


Figure 40: Sowden Lake, Area 46; images of the top portion of the nodule. a) photo of the original nodule before being cut and made into a slide. b) SEM, SE image of a slide created from the nodule found in photo (a). c) A reflected light petrographic image of the bottom portion of a nodule (a). d) A cross-polarized petrographic image of the same nodule.

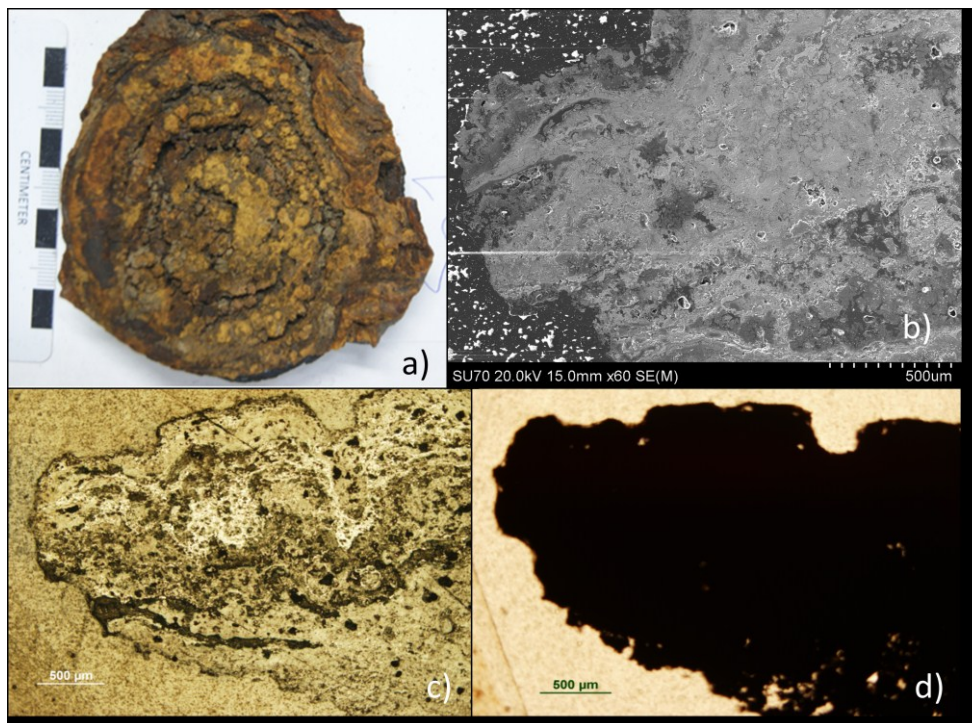


Figure 41: Sowden Lake, Area 46; images of the bottom portion of the nodule. a) photo of the original nodule before being cut and made into a slide. b) SEM, SE image of a slide created from the nodule found in photo (a). c) A reflected light petrographic image of the bottom portion of a nodule (a). d) A cross-polarized petrographic image of the same nodule.

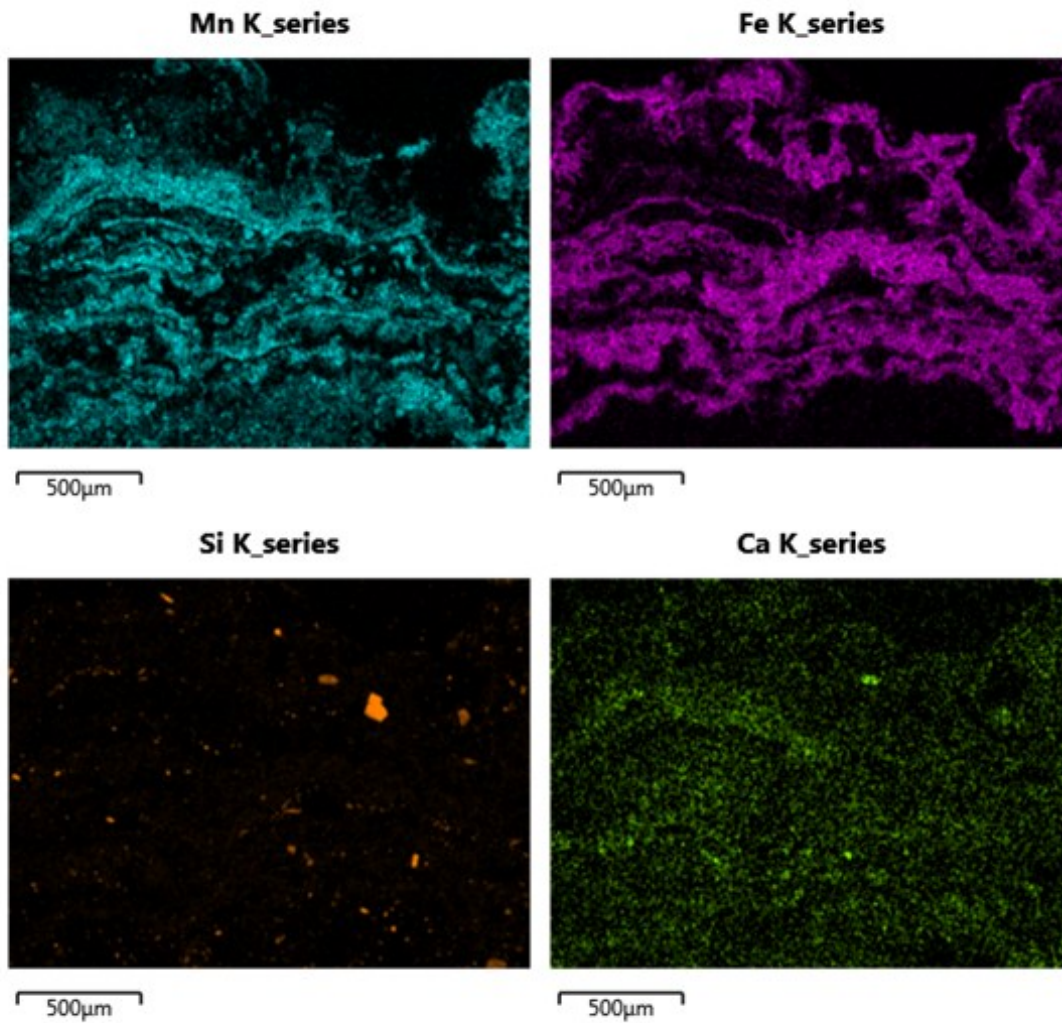


Figure 42: Element distribution images of Figure 39 (top section of Sowden Lake nodule) providing for a visual display of how elements are distributed within a sample.

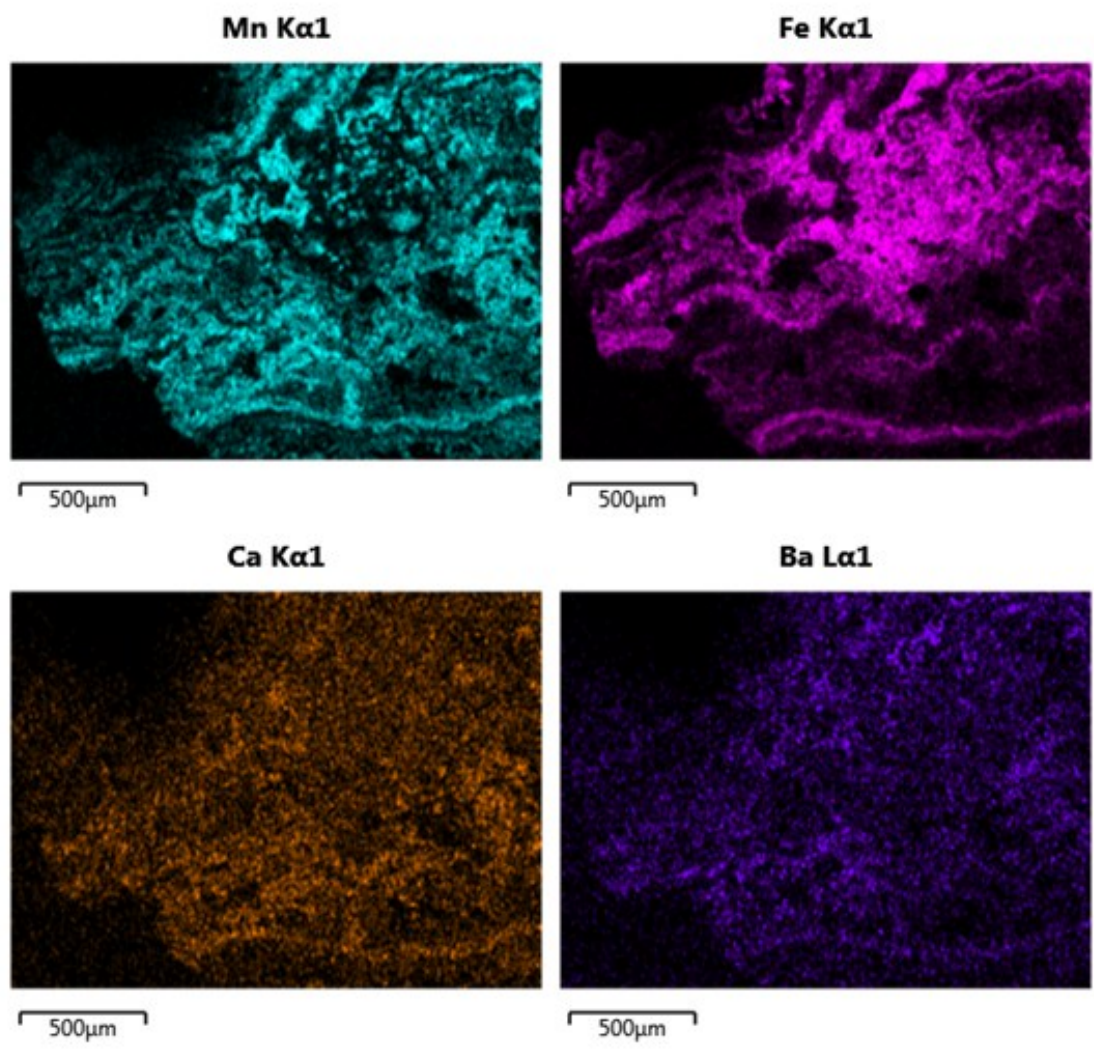


Figure 43: Element distribution images of Figure 39 (bottom section of Sowden Lake nodule) providing for a visual display of how elements are distributed within a sample.

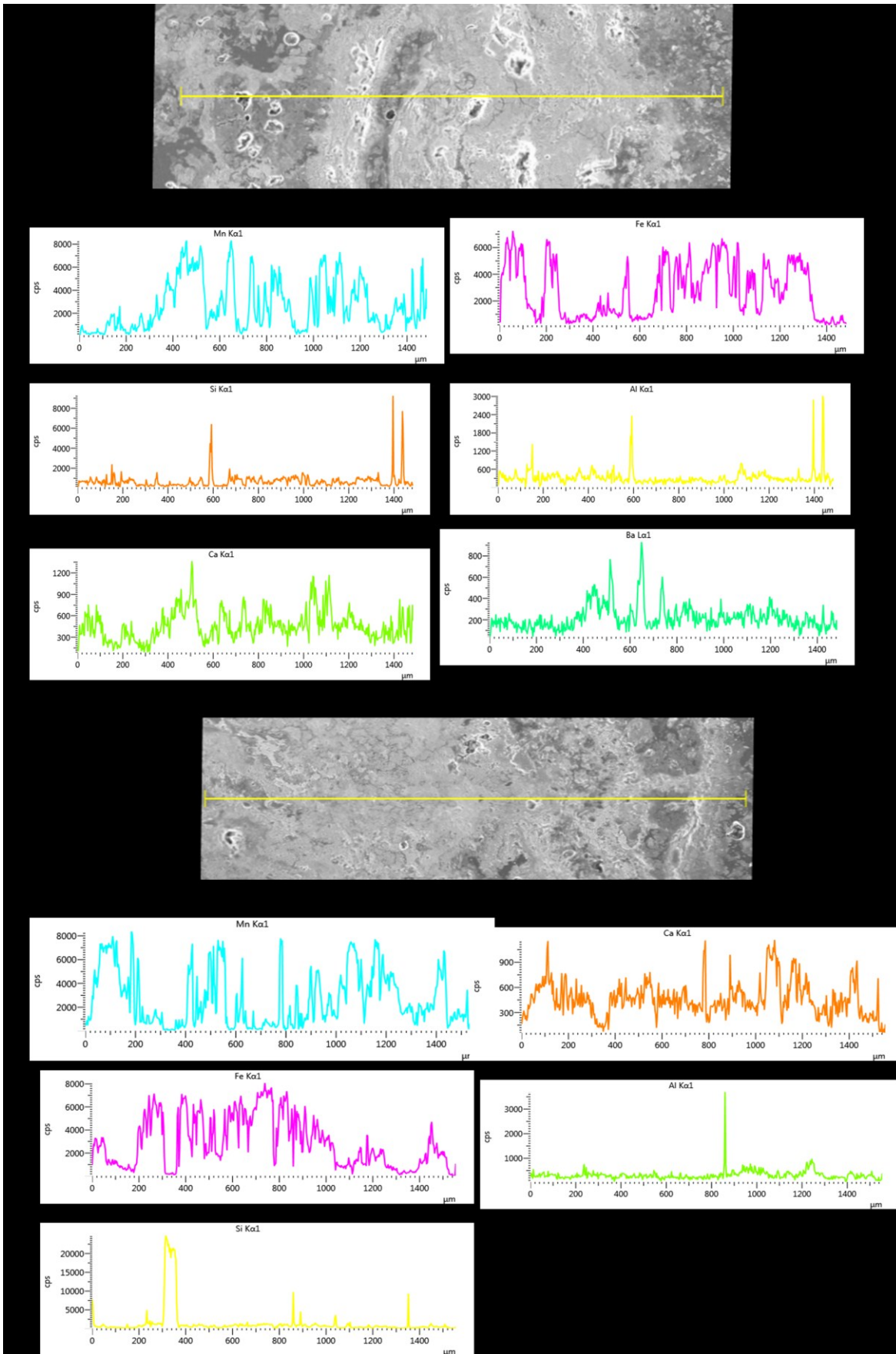


Figure 44: A line Scan analysis from a nodule found in Sowden Lake. A linescan offers visual representation of the distribution of elements present within a sample. a) Represents data from the top of the sample. b) Represents data from the bottom of the sample.

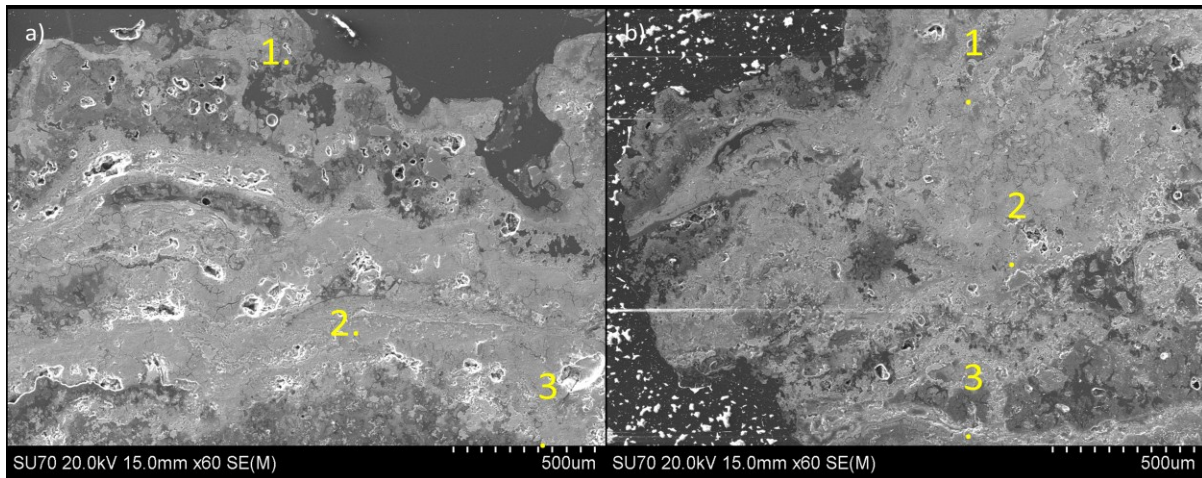


Figure 45: a) SEM image of the top of a sample from Sowden Lake data provided in Table 4 b) Bottom image of a sample from Sowden Lake data provided in Table11.

Table 11: Sowden Lake SEM Point analysis data from Figures 44 (a and b)

Image	Oxide	Oxide %	Image	Oxide	Oxide %
Top: 1	Al ₂ O ₃	0.92	Bottom: 1	Al ₂ O ₃	2.01
	SiO ₂	2.96		SiO ₂	2.54
	P ₂ O ₅	2.16		P ₂ O ₅	0.65
	SO ₃	0.26		CaO	0.94
	CaO	1.61		MnO	37.47
	MnO	0.57		FeO	28.63
	FeO	60.31		BaO	3.49
Total oxides for Top (1) = 68.97%			Total oxides for bottom (1) = 75.85%		
Top: 2	Al ₂ O ₃	1.63	Bottom: 2	Al ₂ O ₃	0.53
	SiO ₂	5.4		SiO ₂	5.14
	P ₂ O ₅	5.4		P ₂ O ₅	1.03
	CaO	1.07		CaO	1.2
	MnO	11.66		MnO	24.28
	FeO	53.98		FeO	47.61
	BaO	0.81		BaO	2.68
Total oxides for Top (2) =75.85%			Total oxides for bottom (2) = 82.47%		
Top: 3	Al ₂ O ₃	0.84	Bottom: 3	MgO	0.67
	SiO ₂	7.9		Al ₂ O ₃	0.47
	P ₂ O ₅	0.88		SiO ₂	0.25
	CaO	0.86		P ₂ O ₅	0.42
	MnO	17.81		CaO	4.02
	FeO	40.27		MnO	63.05
	BaO	0.77		FeO	0.87
				BaO	11.07
Total oxides for top (3) =69.32%			Total oxides for bottom (2) = 81.06%		

Shebandowan Lake SEM results:

Examination of Shebandowan samples under a petrographic microscope revealed differences in the amount of banding between the upper and lower portion of the nodule (Figure 46, 47). The top portion of the nodule is observed to have the greatest amount of banding compared to the rest of the nodule. The red portion found on the image represents iron oxide. The appearance of the nodule under a microscope reveals a very porous structure throughout the specimen.

Mapping analysis reveals the precipitates are iron-rich throughout the entire sample with little manganese present (Figure 48, 49). The small amount of manganese continues to display a negative correlation to that of iron as observed in the previously described research sites. In nodules from Shebandowan, aluminum appears to be concentrating as a silicate and is found with the sand grains present in the sample. Sodium and possibly magnesium are also observed to concentrate with silica. No other elements inspected with the mapping application revealed a trend.

Linescan analysis of the top and bottom portion of a Shebandowan nodule leads to similar conclusions as the mapping analysis. In Figure 50(a), silica, aluminum, sodium and potassium all appear to be concentrated together in the form of sand grains. Iron dominates the majority of the sample. However, manganese is not behaving in an inverse relationship to iron. Cobalt also occurs with the iron and manganese.

Point analysis of the Shebandowan precipitates reveals a greater amount of elements present above detection levels in the sample compared to the previously described sites (Figure 51, Table 12). Iron dominates the sample percentages present in this example with values as high as 64%. The remainder of elements in the sample has similar trends to those found by mapping and linescan analysis. The amount of silica present appears to correlate with the amounts of calcium, magnesium, aluminum and potassium. Unlike the previous sites, correlations between barium and manganese

cannot be identified due to the low abundance of manganese within the sample. Phosphorous is found to concentrate in greater quantities at the outer portions of the sample, just as arsenic did in the Lake Charlotte samples. Unlike the point analysis results of Lake Charlotte and Sowden Lake, cobalt is present in minor amounts throughout the sample.

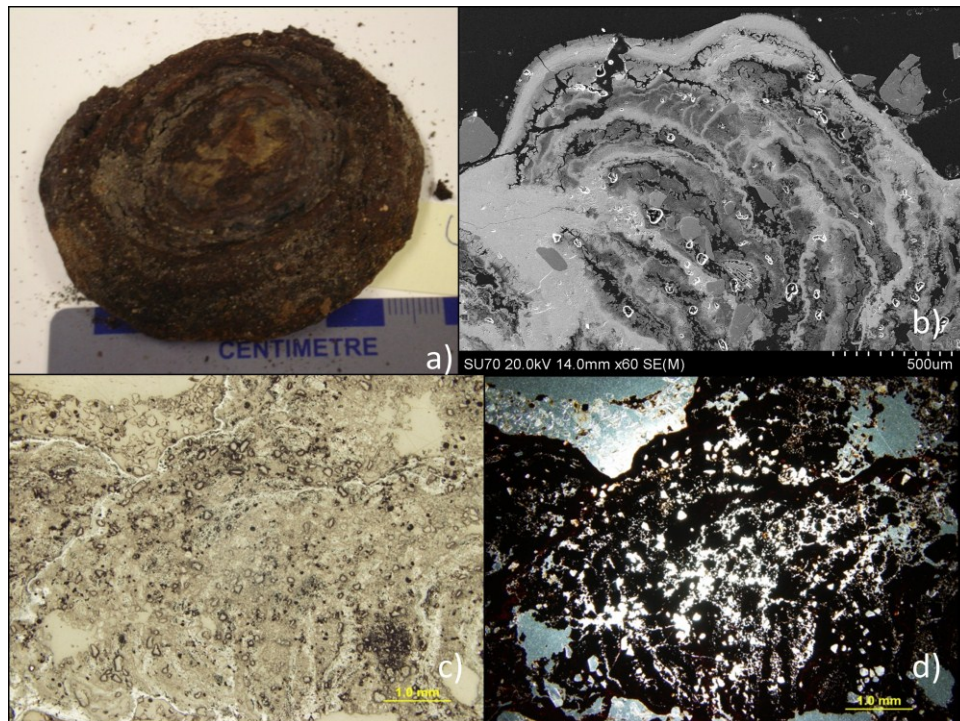


Figure 46: Shebandowan Lake, Island Site images of the top of the nodule. a) Photograph of the original nodule before being cut and made into a slide. b) SEM, SE image of a slide created from the nodule in photograph (a). c) A reflected light petrographic image of the bottom portion of a nodule (a). d) A cross-polarized petrographic image of the same nodule.

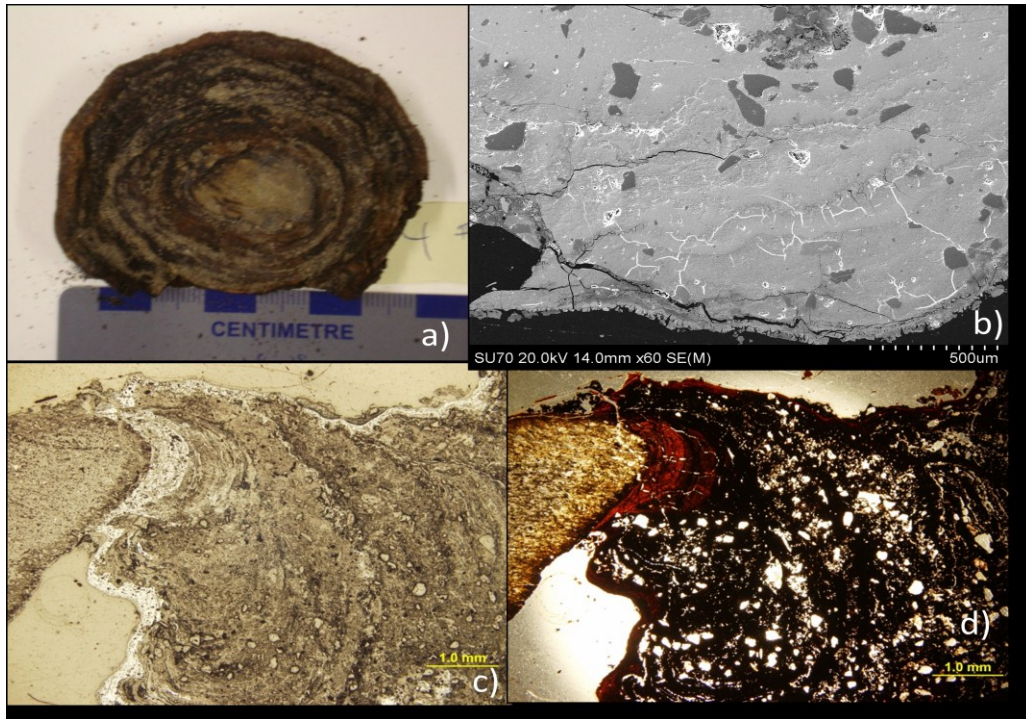


Figure 47: Shebandowan Lake, Island Site images of the bottom portion of the nodule. a) Photograph of the original nodule before being cut and made into a slide b) SEM, SE image of a slide created from the nodule (a) c) A reflected light petrographic image of the bottom portion of a nodule (a) d) A cross-polarized petrographic image of the same nodule

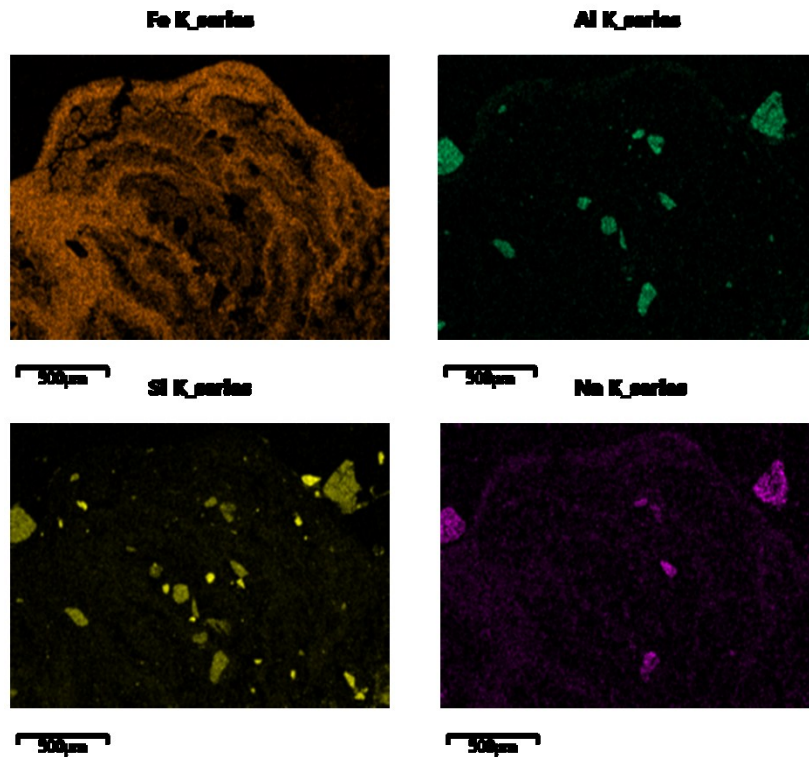


Figure 48: Element distribution images of Figure 45 providing for a visual display of how elements are distributed within a sample

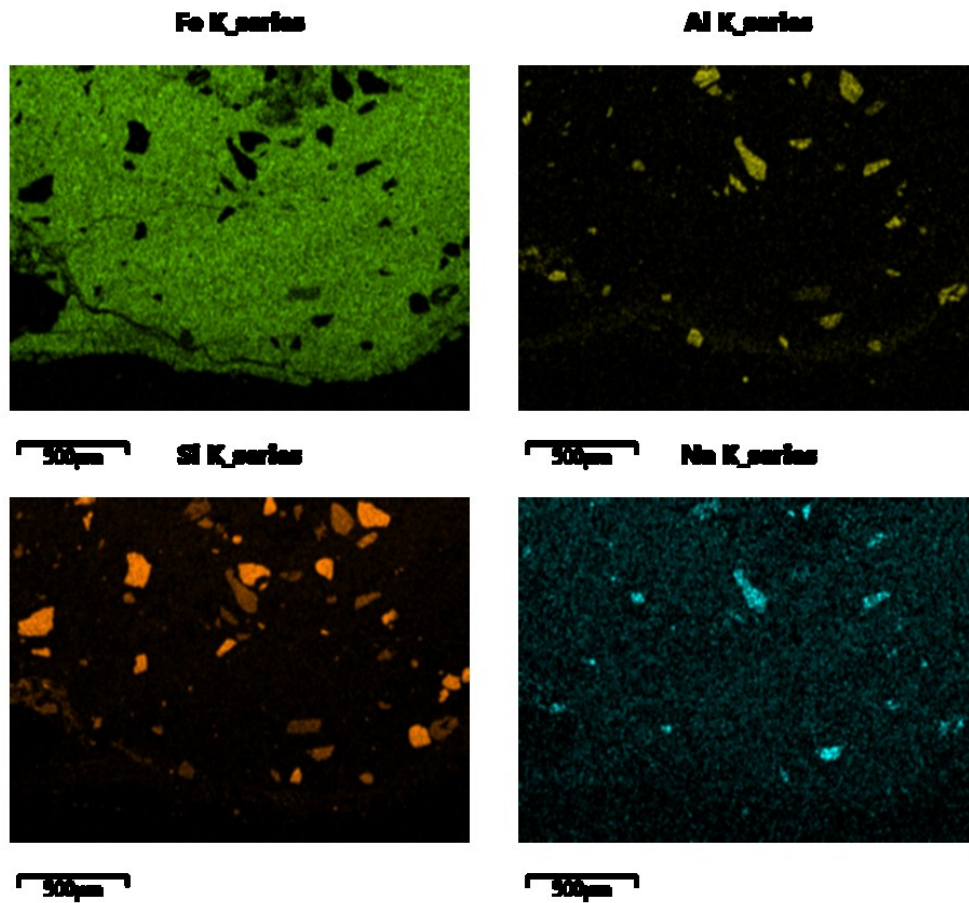
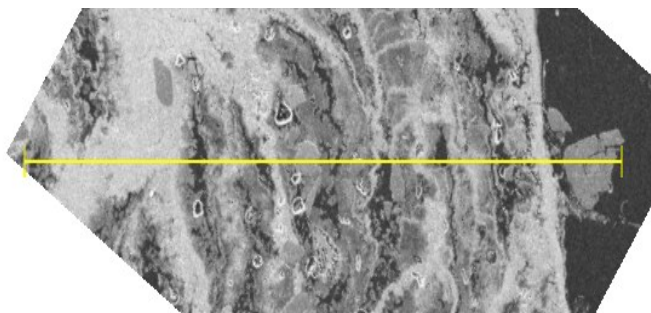


Figure 49: Element distribution images of Figure 46 providing a visual display of how elements are distributed within a sample.

a)



b)

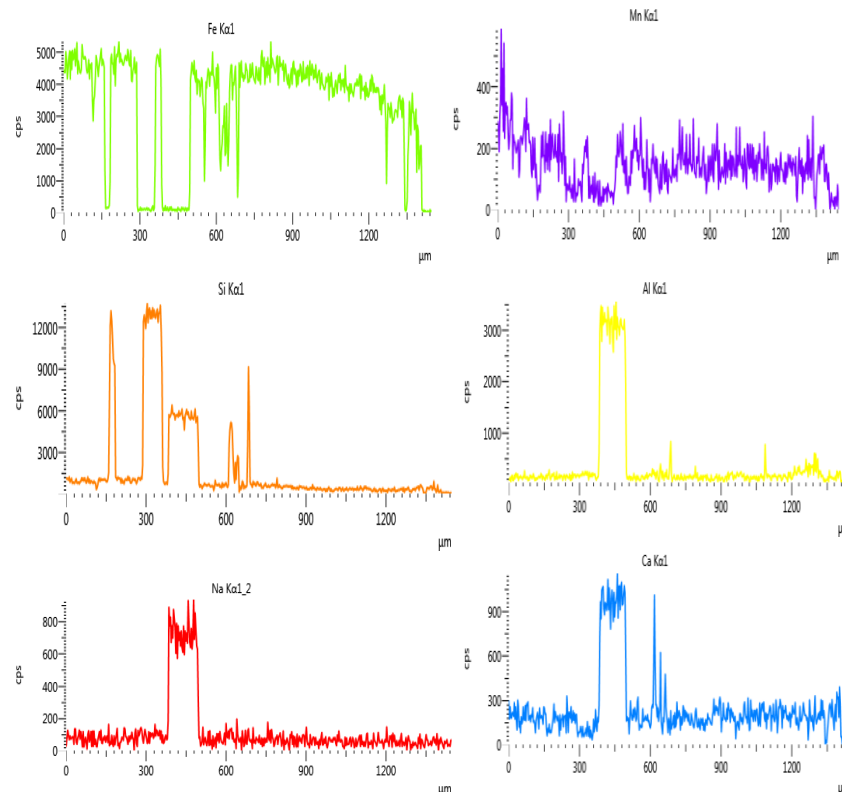
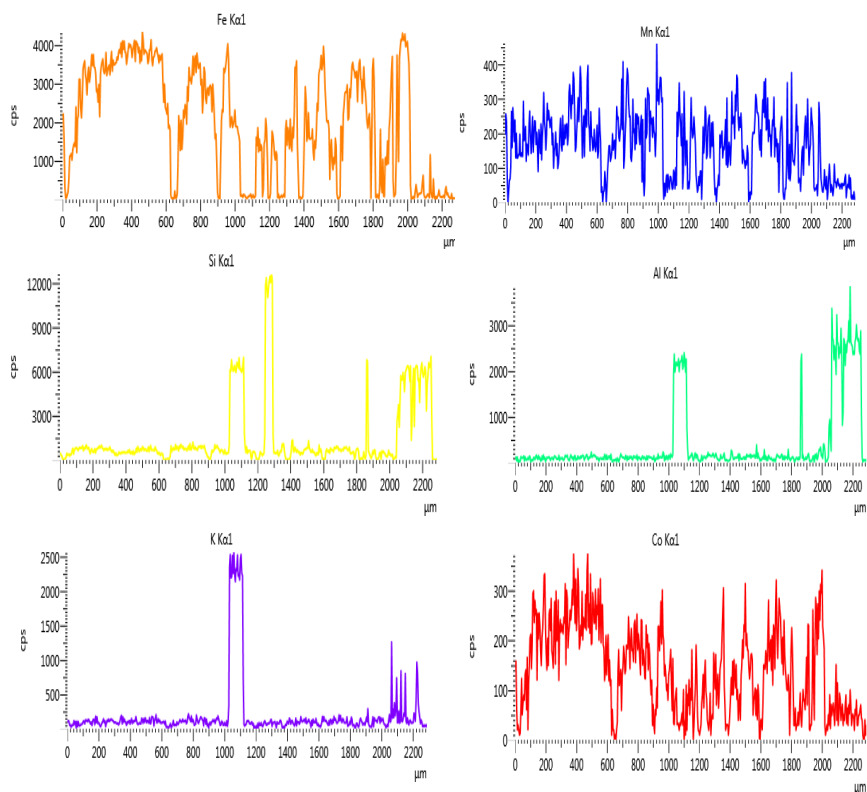
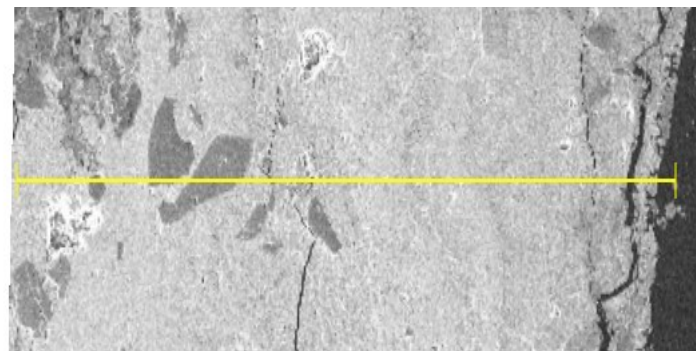


Figure 50: A line Scan analysis from a nodule collected from Shebandown Lake. A linescan offers visual representation of the distribution of elements present within a sample. a) Represents data from the top of the sample. b) Represents data from the bottom of the sample

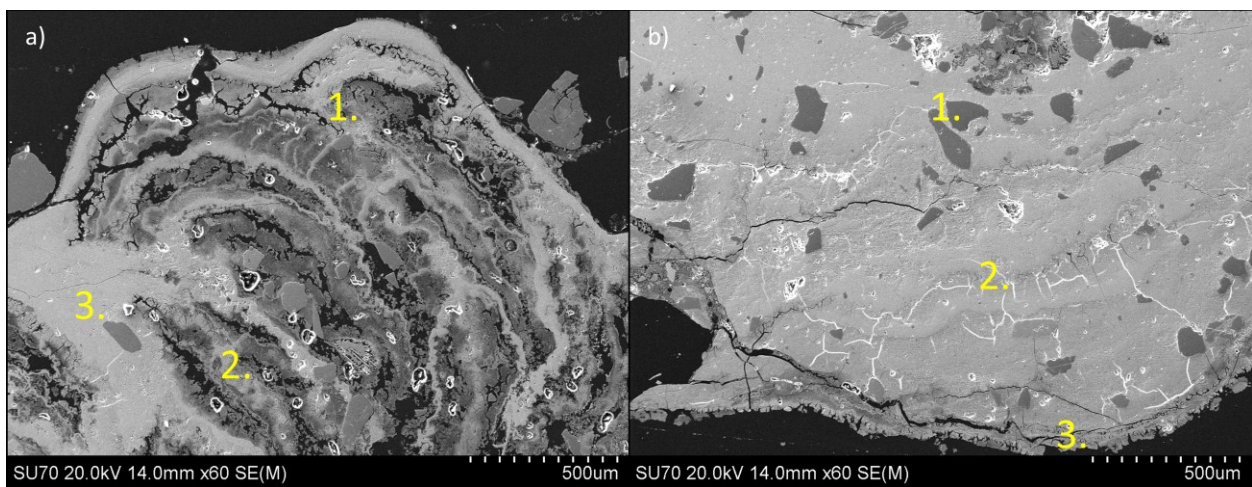


Figure 51: a) SEM image of the top of a sample from Shebandowan Lake. b) SEM bottom image of a sample from Shebandowan Lake. Analyses of labeled areas are presented in Table 12.

Table 12: Shebandowan Lake SEM Point analysis data from Figures 50 (a and b)

Image	Oxide	Oxide %	Image	Oxide	Oxide %
Top: 1	SiO ₂	6.41	Bottom: 1	SiO ₂	9.05
	P ₂ O ₅	2.08		P ₂ O ₅	0.48
	CaO	0.5		MnO	1.2
	MnO	1.85		FeO	63.92
	FeO	62.48		CoO	0.67
	CoO	0.23			
	BaO	0.56			
Total oxides for Top (1) = 74.33%			Total oxides for bottom (1) = 75.54%		
Top: 2	Al ₂ O ₃	0.32	Bottom: 2	SiO ₂	4.37
	SiO ₂	8.37		P ₂ O ₅	1.79
	P ₂ O ₅	0.94		MnO	0.89
	CaO	0.57		FeO	61.7
	MnO	1.53		CoO	0.32
	FeO	48.37			
	CoO	0.25			
Total oxides for Top (2) =60.36%			Total oxides for bottom (2) = 69.18%		
Top: 3	Al ₂ O ₃	0.19	Bottom: 3	MgO	0.41
	SiO ₂	6.09		Al ₂ O ₃	4.05
	P ₂ O ₅	0.68		SiO ₂	3.57
	CaO	0.33		P ₂ O ₅	2.75
	MnO	1.67		CaO	0.76
	FeO	54.35		MnO	0.92
	CoO	0.37		FeO	46.98
		CoO	0.27		
Total oxides for top (3) =63.67%			Total oxides for bottom (2) = 81.06%		

The following table (Table 13) represents the chemical SEM results concluded from all three study areas:

Table 13: Results from SEM data

Precipitate Site	Positive Correlations	Negative Correlations	No correlation, but element is always present	Element is unique to a certain area of precipitate
Lake Charlotte	Mn, Ba and Al	Mn and Fe		As (outer portion) Si (sand grains)
Sowden Lake	Mn, Ba and Ca Fe and P Al and Si	Mn and Fe		Si (sand grains)
Shebandowan Lake	Si, Ca, Mg, Al and K Fe, Mn and Co	none present	P	P (greater concentration on outer portion of sample)

Physical Surface Structure, Lake Charlotte

The physical surfaces of Lake Charlotte samples appear unique when observed with the SEM. Figure 52 displays an image of a raw sample from My Cove where arrays of diatoms are present on the surface. When analyzed with a mapping application (Figure 53), it is interesting to note that the arsenic on the surface of the sample appears to not only be concentrating on the iron- and manganese- rich precipitate, but also on some of the silica- rich diatoms.

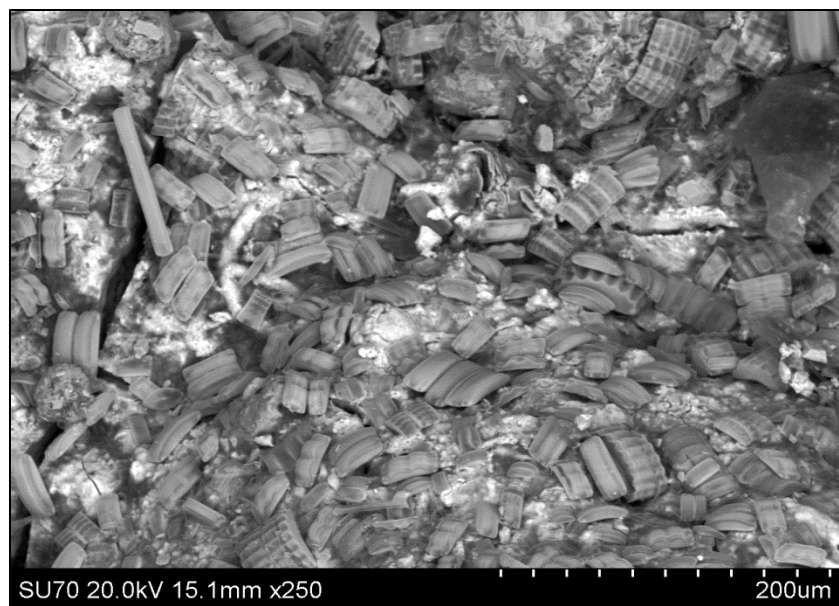


Figure 52: SEM images of the surface of a raw sample from Lake Charlotte. The surface of the sample is covered with various shapes and sizes of diatoms. Organic material can be seen in the right upper portion of the image.

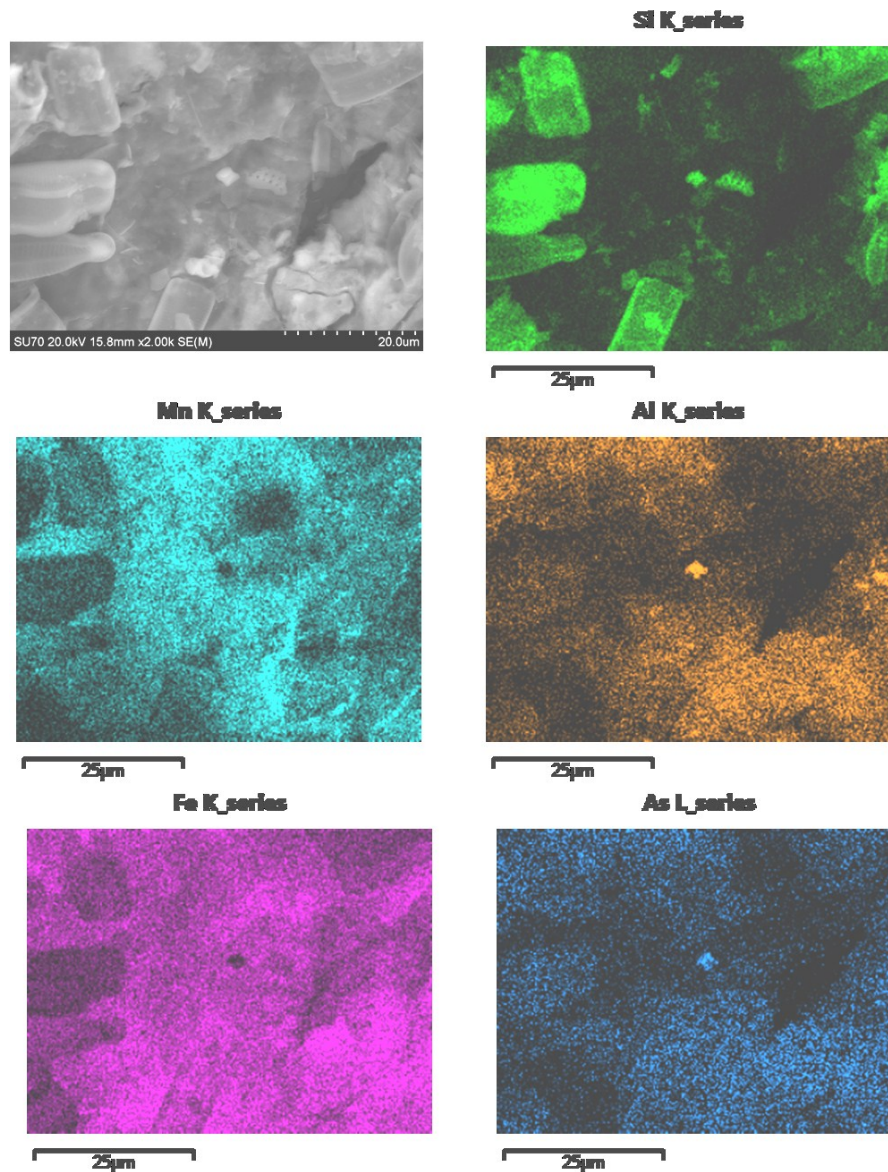


Figure 53: A raw sample SEM image and maps from a Lake Charlotte nodule. Notice the arsenic appears to be concentrating on the diatoms on the center left of the image. The high arsenic in the middle of the image is associated with a siliciclastic grain.

Nanostuctures observed with SEM, Lake Charlotte

Close examination of a Lake Charlotte, My Cove sample at high magnification revealed the presence of nanospherical structures (Figure 54). Extracellular polymeric substances (EPS) may be present around the spheres, however, further examination of precipitates at the nano-structural scale is needed to conclude that EPS is indeed present.

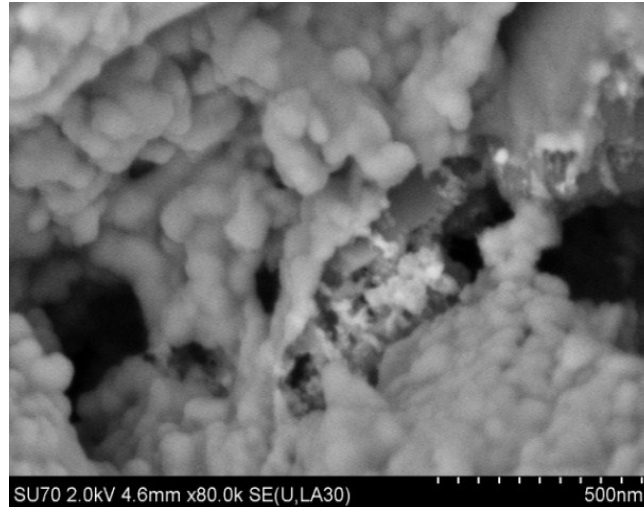


Figure 54: SEM image of potential nanospheres surrounded by possible extracellular polymeric substances (EPS) on the surface of a nodule from Lake Charlotte.

7. My Cove Shoreline Analysis, Lake Charlotte

On the shoreline of site area My Cove, a soil pit 60cm in depth was dug to analyze for grainsize distribution and geochemistry in the sand underlying the bay (Figure 55). The pit was separated into six layers for a detailed analysis. The calculations used to determine the mean grainsize and sorting values as described by Folk and Ward (1957).



Figure 55: Image of the My Cove shoreline pit

Layer A: surface of shoreline

Layer A is composed of a white, dry, rounded sand, which becomes coarser with increasing depth (Figure 56). The coarser material changes its colour slightly due to an increase in the amount of black, white and dark orange sand grains present. In the center of Layer A there is an organic-rich layer, approximately 1cm in width which, is composed largely of decomposing leaves. The total depth of Layer A is 8cm.



Figure 56: Image of layer A

Layer B:

Layer B is composed of rounded sediment grains with a reddish colour and a purple hue (Figure 57). The contact between Layers A and B is wavy and curved. The total thickness of Layer B is approximately 8cm.



Figure 57: Image of layer B

Layer C

Layer C is composed of rounded reddish- orange coloured sediment grains (Figure 58). There is a gradual contact between layer B and C, and again with layer D and C. Layer C is approximately 10cm in thickness.



Figure 58: Image of layer C

Layer C-D

Layer C - D appears as a transition layer and is described as highly compacted reddish yellow sediment (Figure 59a). There is a gradual contact with Layer C and a distinct contact with underlying Layer E. Layer C-D is approximately 9 cm in thickness. The grainsize distribution graph for Layer C-D (Figure 59b) shows a long gradual traction tail, a steep saltation line and a small, shallow suspension tail. The average grainsize is 1.08ϕ or *medium grained sand*. Sorting for Layer C-D is 1.65ϕ meaning poorly sorted sediment.

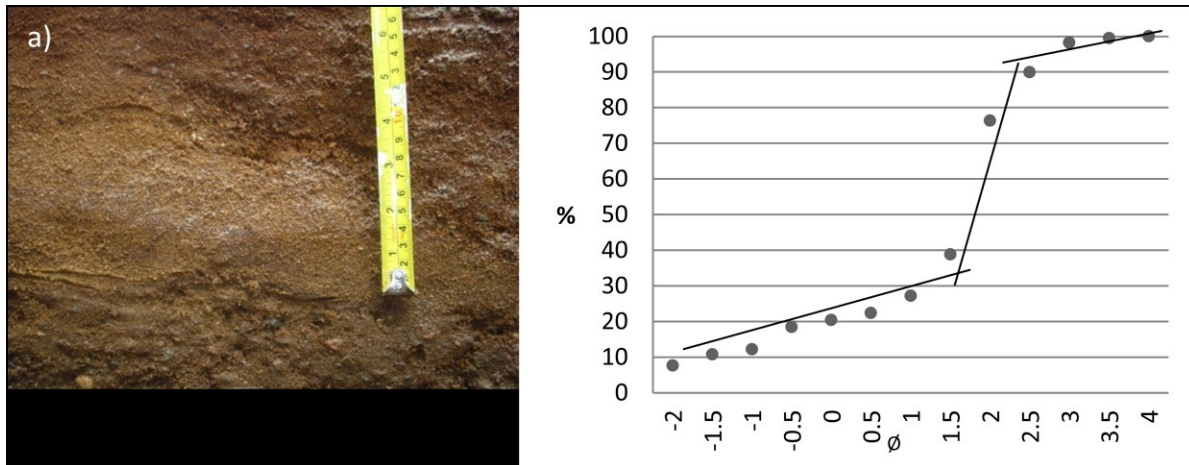


Figure 59: Image of of layer C-D (b) Layer C-D sediment distribution graph

Layer E

Layer E is comprised of brown sediment with pebble sized grains randomly distributed throughout (Figure 60a). There is a distinct contact between the above Layer C-D and a gradual contact with Layer F below. It is approximately 14cm in thickness. The grainsize distribution graph for Layer E reveals a long, steep, traction tail, a short, steep saltation line and a long flat suspension tail (Figure 60b). The mean grainsize is -0.27ϕ or *very coarse grained sand*. The sorting value for layer E is 3.1ϕ meaning very poorly sorted sediment.

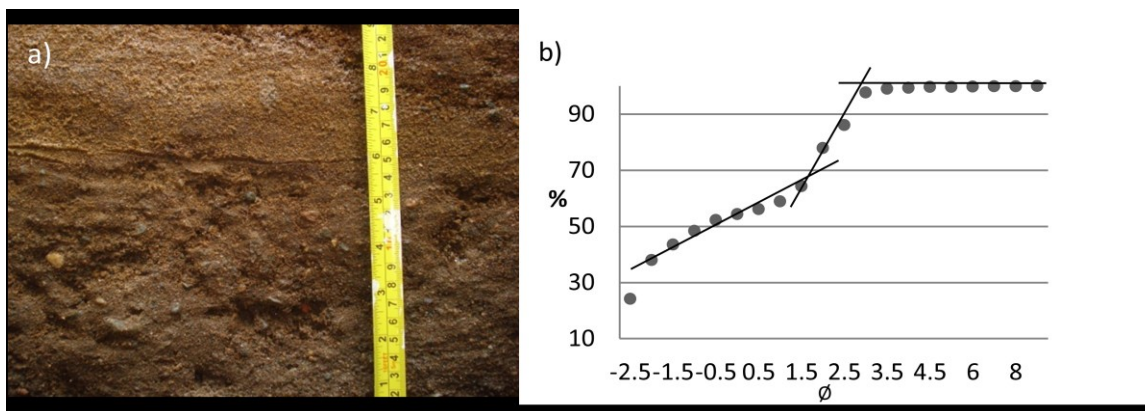


Figure 60: (a) Image of layer E (b) Layer E sediment distribution graph

Layer E-F

Layer E-F appears as a transition zone with both its top and bottom contacts gradually changing to a different layer (Figure 61a). It is composed of brown and grey coloured sediment imbedded with rounded pebbles. The thickness of this layer is approximately 7cm. The grainsize distribution graph reveals a steep traction tail, a long gradual saltation line and a short, flat suspension tail (Figure 61b). The average sediment size of this layer is -1.1ϕ or *granule size*. The sorting value for Layer E-F is 2.46 indicating very poorly sorted sediment.

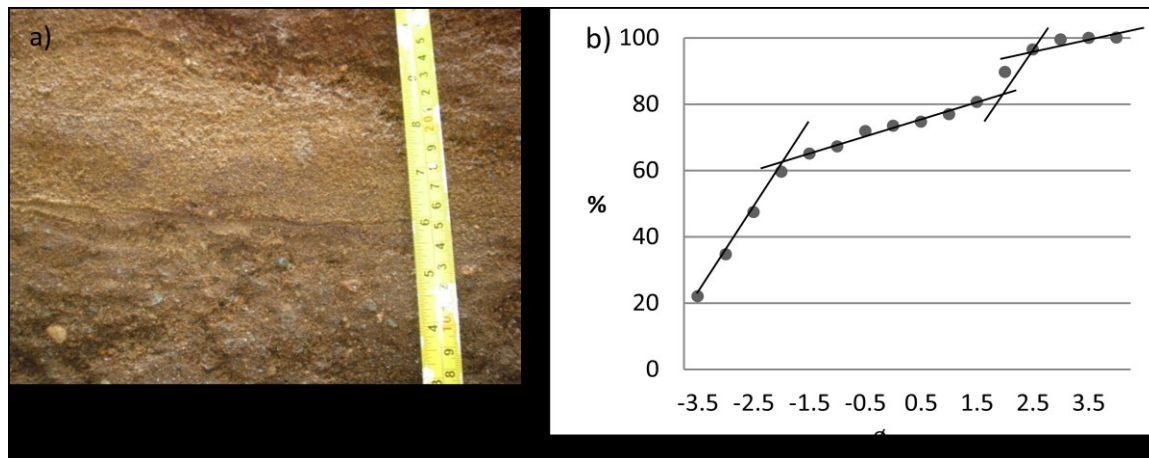


Figure 61: (a) Image of layer E-F (b) Layer E-F sediment distribution graph

Layer F

Layer F consists largely of rounded pebble sized grains with a grey matrix (Figure 62a) and has a thickness of approximately 12 cm. There is a gradual contact between Layer E -F but an obvious contact between layers F and G due to an abrupt change in colour. The grainsize graph for Layer F contains a long gradual saltation line with a long flat suspension line (Figure 62b). There is no traction tail present. The average size of the sediment in Layer F is -0.5ϕ or *very coarse sand*. The sorting size is 2.19, which is very poorly sorted sediment.

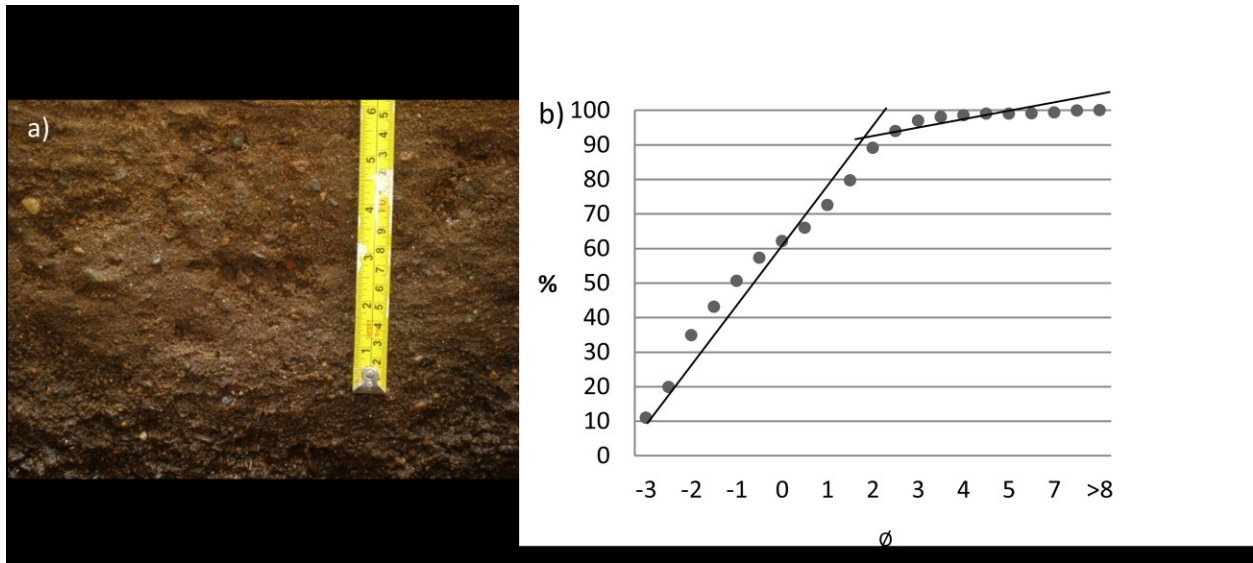


Figure 62: (a) Image of layer F (b) Layer F sediment distribution graph

Layer G

Layer G is found at the bottom of the pit and consists of dark brown coloured sediment with shiny sparkling sediment specs throughout the layer (Figure 63a). The thickness of the layer G is unknown due to the top of the water table making further observation of layering inaccessible. The grainsize distribution graph reveals a long gradual traction tail, a steep saltation line and a long flat suspension tail (Figure 63b). The mean grainsize of layer G is 0.8ϕ or *coarse sand* and its sorting value is 2.56ϕ indicating very poorly sorted sediment.

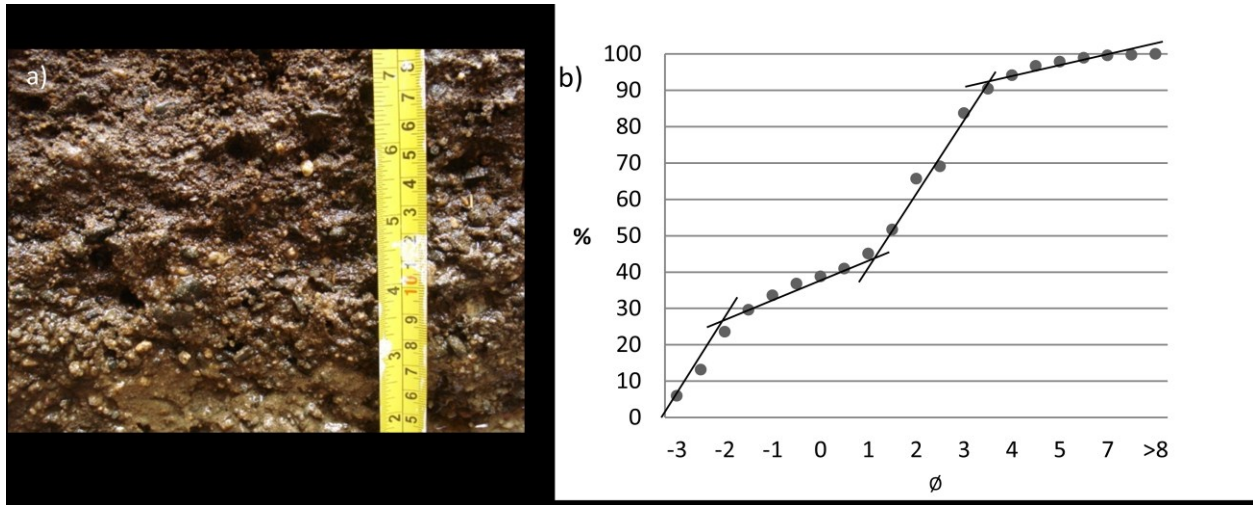


Figure 63: (a) Visual representation of layer G (b) Layer G sediment distribution graph

Geochemical analysis using ICP-AES was completed on all units of the My Cove pit. Elements considered important to this study are displayed as a graph in Figure 64. All other geochemical data is located in Appendix D. Elements showing a downward trend of enrichment include iron, manganese, calcium and magnesium. There are no other obvious trends in the geochemistry.

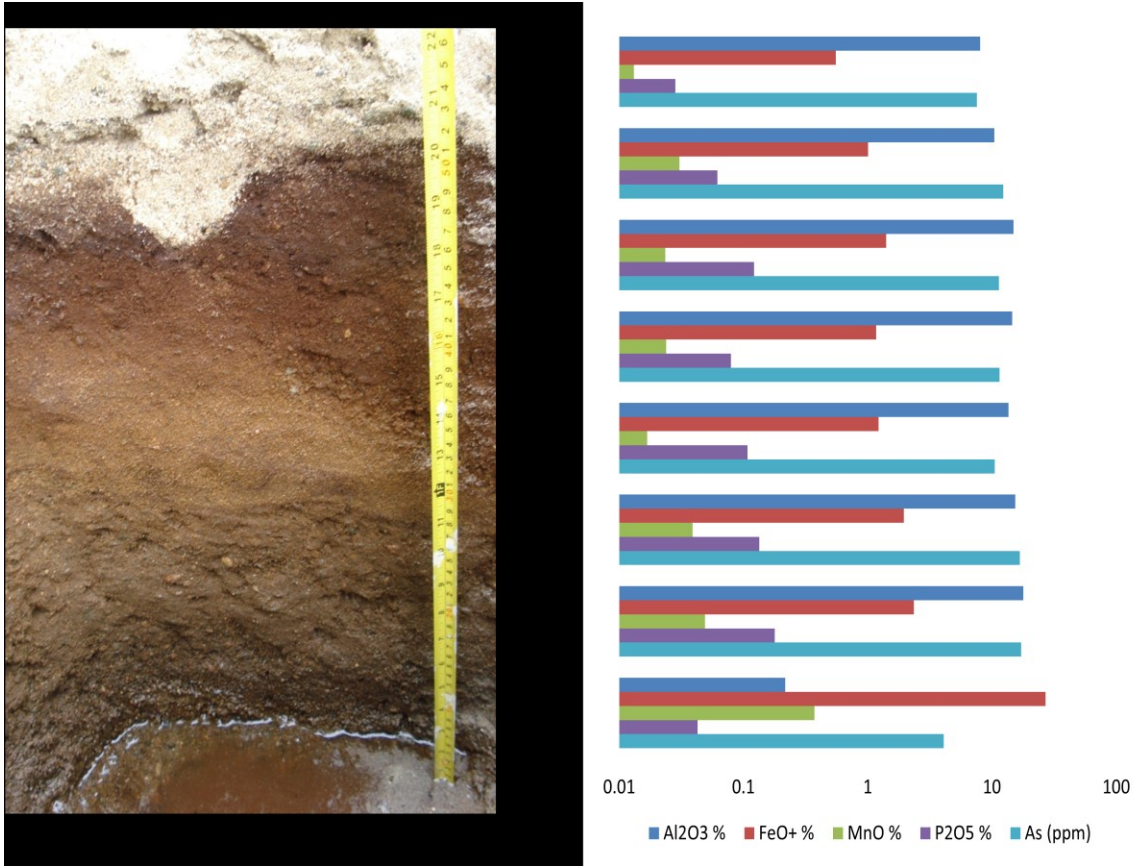


Figure 64: Geochemical data from each layer of the My Cove pit including oxides aluminum, iron, phosphorous and arsenic.

X-Ray Diffraction (XRD) Analysis

Precipitate Analysis

Five samples from each study lake were analyzed by XRD to determine if the precipitates crystalline structures. Example XRD spectrums from each lake are located in Appendix G. Of the three study sites, Sowden Lake had the greatest number of XRD count peaks graphically present suggesting more crystalline structures present then any other site. The minerals identified in Sowden Lake samples included the following: aluminum phosphate (Berlinite, $AlPO_4$), quartz (SiO_2), iron dialuminum oxide ($FeAl_2O_4$), hematite (Fe_2O_3), pyrochroite ($Mn(OH)_2$) and iron (III) hydroxide ($FeO(OH)$). Of the minerals

identified in the Sowden Lake samples, quartz and aluminum phosphate were the only minerals present in all five samples.

The XRD results for the Lake Charlotte samples revealed the following minerals: quartz (SiO_2), aluminum phosphate (Berlinite, AlPO_4), arsenopyrite (FeAsS) and in one instance arsenolite (AsO_2). The majority of Lake Charlotte samples displayed a very small number of peaks when graphed. One sample had only one peak present.

Lake Shebandowan samples displayed the least amount of peaks recorded by XRD. Of the five samples analyzed, two displayed only one peak and one had only noise present on the graph. The minerals determined in the two remaining Lake Shebandowan samples included quartz (SiO_2), and aluminum phosphate (AlPO_4).

My Cove Pit Analysis:

XRD analyses of layers A, F and G from the My Cove shoreline pit were conducted. Sample A, the surface material from the pit, was composed of predominantly quartz (SiO_2). Layer F, taken at a depth of approximately 40cm, was determined to have a composition of quartz (SiO_2), birnessite ($\text{KMnO}_2(\text{H}_2\text{O})$), muscovite ($\text{KAl}_2(\text{Si, Al})_4\text{O}_{10}(\text{OH})_2$) and albite ((Na, Ca) Al, SiO_8). Layer G, taken at a depth of approximately 60cm, is mostly composed of quartz (SiO_2) and albite ((Na, Ca) Al, SiO_8).

Discussion

1. Chemical Correlations

Correlations with iron:

Using elemental mapping data, chemical trends were found to exist on a macro scale between the elements iron, arsenic and phosphorous. These trends were further supported using linear relationship models and SEM-EDX analysis. The chemical similarity between arsenic and phosphorous, as they exist in the environment, as well as their behavior in the presence of iron, explains why these trends exist. Arsenic and phosphorous are very similar in chemical structure. Arsenic is found below phosphorus in the 15th group of the periodic table and can exist in an oxidized electron configuration in a +5 state. Both elements are affected by oxidation and reduction in the environment allowing their valance states to be subject to change (Figure 65 and 66). In a naturally slightly reduced environment such as groundwater (pH between 4 and 6), both elements can be found in the aqueous states of either hydrogen or dihydrogen phosphate (HPO_4^- or H_2PO_4^-), or dihydrogen arsenate and arsenous acid (H_2AsO_4^- and H_3AsO_3) (Lu and Zhu, 2011). Once the reduced environment encounters an oxygenated environment, arsenic and phosphorous prefer to precipitate out of solution (Moore and Reddy, 1994; Lu and Zhu, 2011). Due to the positive trend between iron and these elements, iron hydroxides and oxyhydroxides have the ability to precipitate arsenic and phosphorous.

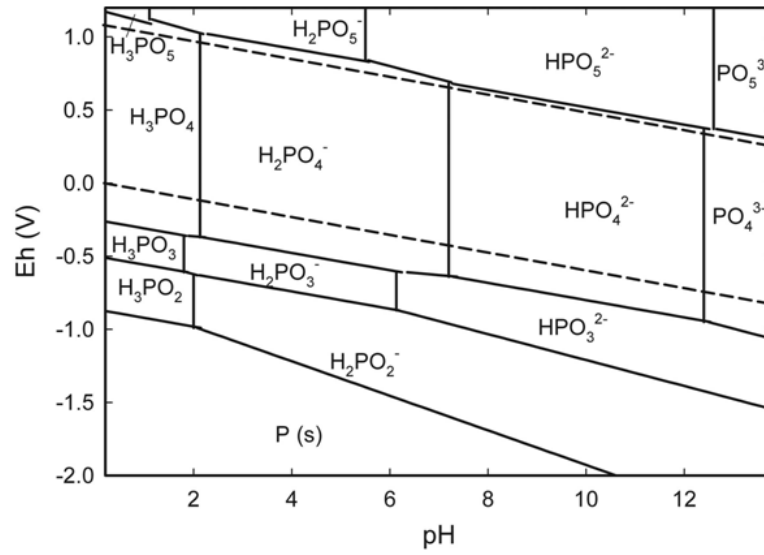


Figure 65: Eh-pH diagram of phosphorous displaying how the element changes valence states depending on the pH and redox potential of the environment (taken from Pasek, 2008).

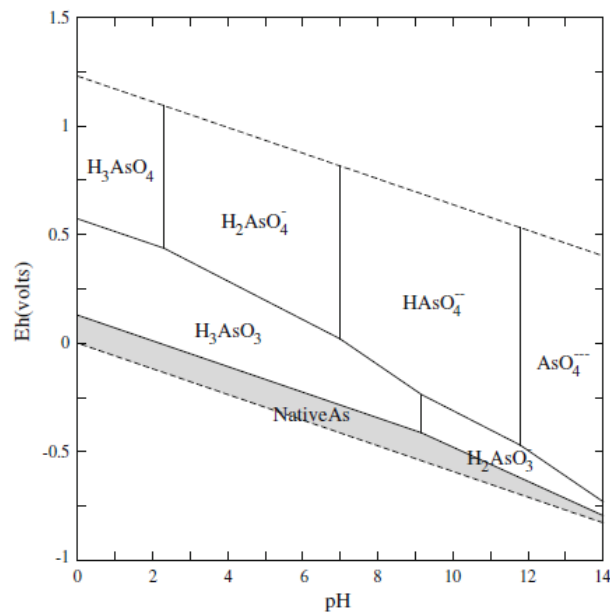
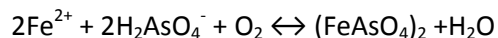
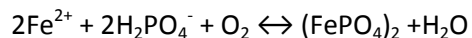


Figure 66: Eh-pH diagram of arsenic displaying how the element changes valence states depending on the pH and redox potential of the environment (taken from Lu and Zhu, 2011)

Iron is greatly influenced by both oxidation and reduction agents found in the environment. If arsenic and iron are found together at a redox boundary the following oxidation reaction can occur (Takamatsu, 1985; Rott et al., 2006): When reduced ferrous iron and dihydrogen arsenate and/or arsenous acid are found in the same aqueous environment, upon oxidation of iron, both iron and arsenic precipitate out of solution, as described in the following equation:



When phosphorous is found in the same reduced, aqueous state with iron, phosphorous can also be precipitated out of solution once an oxygenated boundary is encountered. A chemical equation describing the oxidation of iron in the presence of hydrogen phosphate is as follows:



In the results of this study L shaped trend lines were found between arsenic and phosphorous when plotted together on an XY plot (Figure 67). This graph has been interpreted as follows: If a precipitate contains a high amount of arsenic (e.g. Lake Charlotte), the precipitate will not contain high amounts of phosphorous. This can also work in an inverse manner where precipitates are present with high amounts of phosphorous (e.g. Sowden and Shebandowan Lakes) will not contain high amounts of arsenic. Due to the elemental similarities between arsenic and phosphorous, the ability for arsenic and phosphorous to precipitate out of solution with iron can be interchangeable. Therefore the amounts found in a precipitate are determined by which is in the greatest abundance within the environment and which has the greatest affinity for the iron hydroxide or reduced Fe^{2+} in solution.

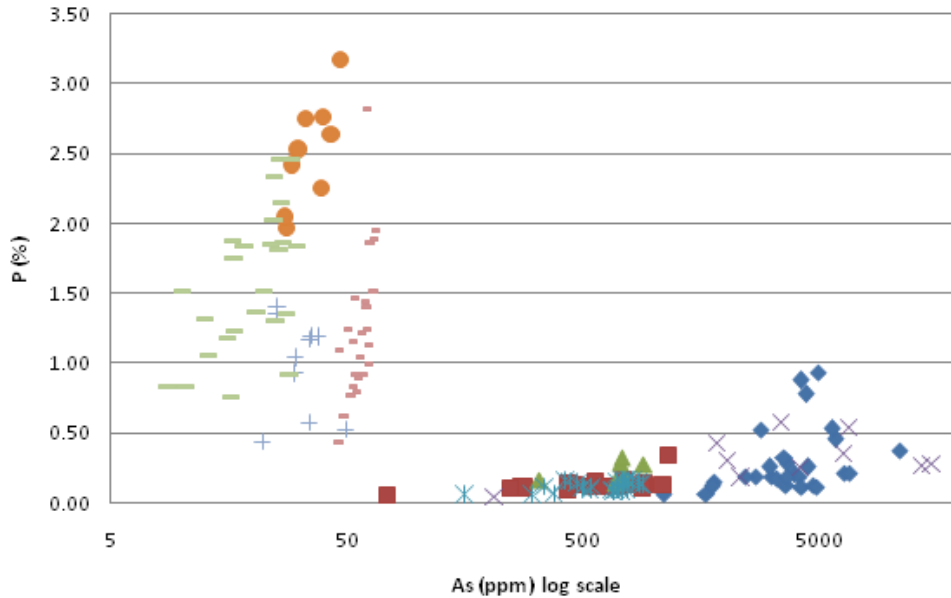


Figure 67: The relationship between phosphorous and arsenic.

Why is it that arsenic and phosphorous prefer to correlate with iron and not with manganese?

The tendency for arsenic and phosphorous to co-precipitate with iron over manganese can be verified by comparing the electrostatic force of each element. The oxidized state of arsenic (As^{5+}) and phosphorous (P^{5+}) have a higher repulsive electrostatic force for oxidized manganese (Mn^{4+}) when compared to ferric iron (Fe^{3+}) (Manceau et al., 2007). This can be proven by use of *Coulomb's law* which states that the magnitude (F) of electrostatic force that is exerted from one point charge (in this case As^{5+} or P^{5+}) onto another point charge (in this case Mn^{4+} or Fe^{3+}) is directly proportional to the magnitude of the charges, and inversely proportional to the square of the distance between (r) the two ions. This as described in the following equation (Cutnell and Johnson, 2004):

$$F = k \frac{(As^{5+} \text{ or } P^{5+})(Mn^{4+} \text{ or } Fe^{3+})}{r^2}$$

where k is a proportionality (electrostatic) constant

It follows from Columb's law that if two charges have the same sign, the force between them is repulsive. If the charges are opposite, the force between the two elements is attractive. Therefore ferric iron (Fe^{3+}) will have a greater attraction to the oxidized arsenic and phosphorous over Mn^{4+} because there is a stronger attraction to the 5+ valance state.

The work of Rott et al. (2006) confirms this relationship by describing how arsenic and iron are found in the natural environment. Reduced ferrous iron (Fe^{2+}) becomes oxidized to ferric iron (Fe^{3+}) and precipitates out of solution by coating a sediment particle. If arsenate (AsO_4)⁻³ is found in the same reduced conditions as ferrous iron (Fe^{2+}), oxidation allows a gain of electrons (As^{5+}). This makes the two elements electrostaticly favourable to one another and they combine to create iron arsenate (AsFeO_4).

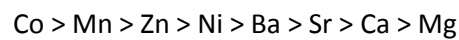
Correlations with Manganese:

Positive correlations were present between manganese, barium, sulfur and cobalt in results from elemental mapping analysis, linear relationship models, and the use of SEM-EDX analysis. By understanding why manganese is attracted to certain elements, an explanation as to how the growth of the manganese-rich layers present in precipitates at Lake Charlotte, Shebandowan Lake and Sowden Lake can be determined.

Precipitate geochemistry of barium showed a greater correlation to manganese then any other element, being as they almost always appear together at both the macro-and micro - scale. Barium, the fifth element in group 2 of the periodic table, is a highly reactive lithophile and is therefore rarely found as a free element in nature (Cox, 1995). Barium is often found in the mineral barite (BaSO_4) where it combines with sulfur, which, coincidentally, is an element that also has a positive correlation with manganese in the precipitates of this study. Sulfur is a redox sensitive element that can occur in its reduced form as a sulfide (S_2^-) and in many positive states of oxidation including sulfate (SO_4^{2-}) (Cox,

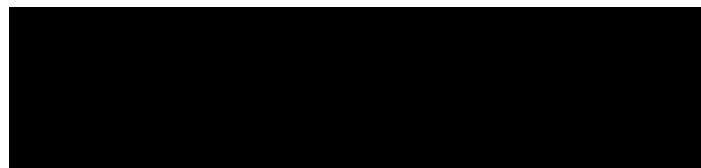
1995). Cobalt occurs mainly with sulfide minerals which have an association with nickel (Cox, 1995). Cobalt is also a redox sensitive element, with common oxidation valance states of 2+ and 3+.

Murray (1975a) describes interactions between metal ions and the adsorption onto hydrous manganese dioxide ($Mn(OH)_2$), which has been shown in experiments to have a slightly positive surface charge. Transition metals were found to adsorb more strongly to the hydrous manganese dioxide surface than alkaline metals in the order as follows (Murray, 1975a):



The amount of metal ions adsorbed onto the hydrous manganese oxide was found to increase with an increase in the pH of the environment.

Murray (1975a) explains that metal ions are able to attach to the surface of hydrous manganese oxide by penetrating the compacted part of the compounds double layer structure. This reaction is able to occur by means of *protonation*, whereby a proton on the surface of the hydrous manganese oxide is replaced by a divalent ion, thus releasing a proton into solution. This chemical reaction is given in the following equation (Murray 1975a):



This idea was again described by Takamatsu et al. (1985) who states that the protons (H^+) released into solution are able to change the surface charge of the hydrous manganese oxide to become more positive. The positive surface allows for greater amounts of divalent cations to become adsorbed onto the surface of the structure or for the possibility of connecting additional hydrous manganese oxides to form a larger structure. 01211

Cobalt would be more susceptible to protonation in its reduced 2+ state; however, in a redox environment cobalt oxidizes. Murray (1975b) states both hydrous manganese dioxide and ferric oxyhydroxide (FeOOH) have the ability to catalyze the oxidation of cobalt to Co^{3+} . According to Burns and Burns (1977) the ionic radius of Co^{3+} is close to the radius of Mn^{4+} suggesting that both ions may be interchangeable in the octahedral shape of a manganese oxide. Murray (1975b) suggests that both cobalt states can be found on hydrous manganese oxide at an oxidation interface. Cobalt could be so strongly attracted to the surface of the hydrous manganese oxide that it will attach to its surface by protonation in the form of Co^{2+} :



An alternative to protonation is oxidization of cobalt to Co^{3+} which allows the element to become interchangeable with Mn^{4+} in the octahedral structure of a manganese oxide.

Manceau (2007) describes adsorption of divalent cations onto an octahedral shaped manganese oxide in the form of the minerals birnessite $(\text{Na, Ca, K})(\text{Mn}^{3+}, \text{Mn}^{4+})_2\text{O}_4 \cdot 1.5\text{H}_2\text{O}$ and hollandite $(\text{Ba}(\text{Mn}^{4+} \text{Mn}^{2+})_8\text{O}_{16})$ (Figure 68). Barium and calcium cations had been found attracted to the structural bonding of the eight oxygen bonds of manganese at both the center and side of the compounds structure (Figure 68). Manceau (2007) relates the attraction between the elements barium and manganese as a means of understanding reactions between radium and manganese oxide in the environment.

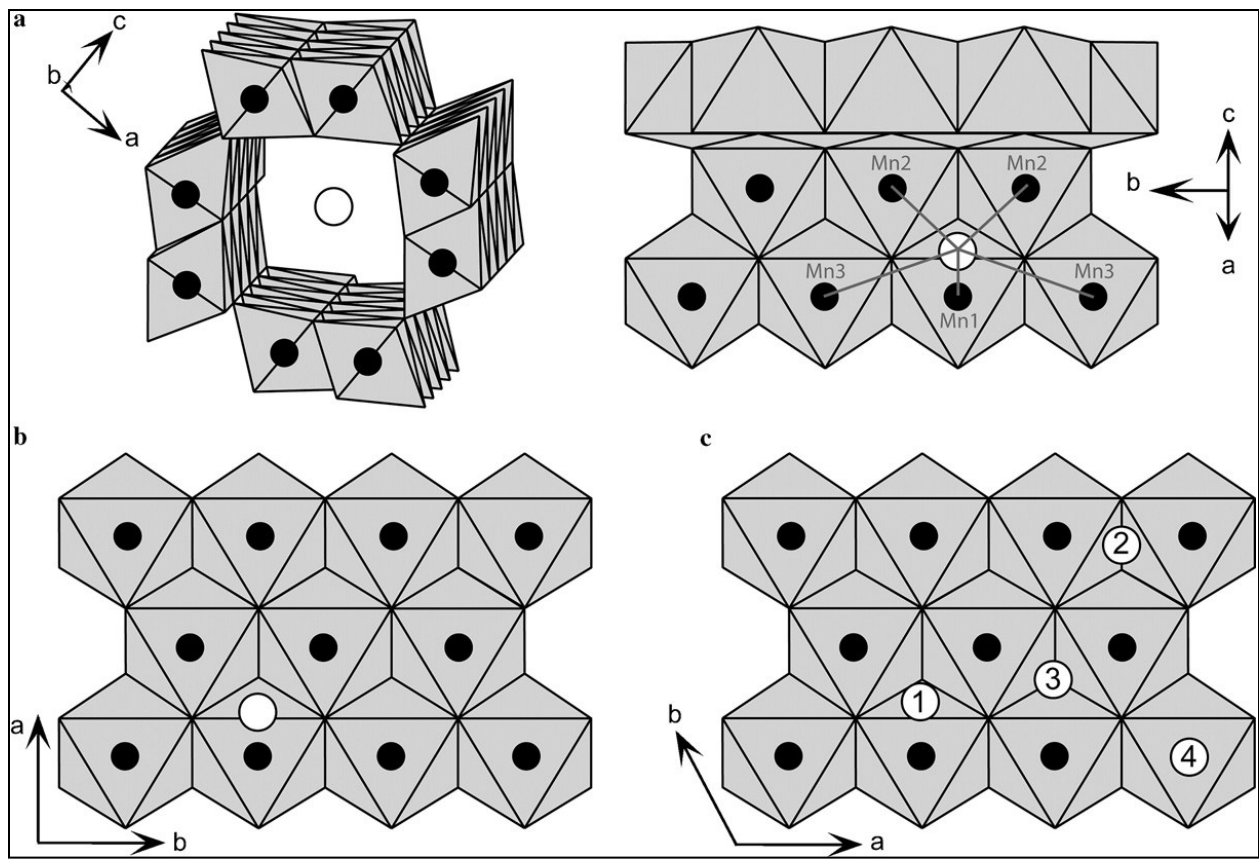


Figure 68: A visual representation of how barium is able to attach to a manganese oxide taken from Manceau (2007). Oxygen is represented as a grey hexagonal shape, manganese a black dot and barium a white dot. Figure (a) displays binding of barium at the hollow center of hollandite by its attraction to the oxygen found on the inside of the tunnel. Figures (b) and (c) represent the binding of barium to the interlayer of the mineral birnessite. In figure (c) barium 1 describes the adsorption of barium onto a tetrahedral cavity. Barium 2, 3 and 4 are hypothetical interlayer sites in which barium may become attracted onto a birnessite.

The manganese layers in the lacustrine precipitates of Lake Charlotte, Sowden Lake and Shebandowan Lake appear to follow the laboratory concepts of Murray (1975a) and Takamatsu et al. (1985) during the attraction of barium and cobalt (II) to hydrous manganese dioxide. Murray (1975a) suggests that cobalt has the greatest attraction of all transition metals tested, and barium the strongest attraction of all the alkaline metals tested. Barium and cobalt are able to penetrate manganese hydroxide by means of protonation. Cobalt may either oxidize and become interchangeable with Mn^{4+} in the octahedral structure of a manganese oxide (Burns and Burns, 1977), or be attracted to the oxygen atoms found in the center structure of a manganese oxide (Manceau, 2007).

Correlations with Aluminum

Using mapping comparisons from GIS software and graphical analysis of geochemistry, correlations between aluminum, potassium and magnesium in nodule samples. A correspondence was also found between aluminum, titanium and chromium (with the exception of Shebandowan Lake). Aluminum was considered in this study to be dominant in the silicate-rich areas of the precipitates collected due to its low correspondence with manganese, iron or carbon. Aluminum is a strong lithophile and a highly electropositive element found in feldspars (plagioclase: $(\text{Na,Ca})[(\text{Al,Si})_4\text{O}_8]$) and $(\text{KAlSi}_3\text{O}_8]$), clay minerals (kaolinite: $\text{Al}_4[\text{Si}_4\text{O}_{10}](\text{OH})_8$) and other silicates (Cox, 1995). The correlation between potassium, magnesium and aluminum may be due to their occurrence in the metavolcanics and granitic rocks of the underlying geology of Shebandowan and Sowden Lake. The meta-sandstone and granite bedrock present at Lake Charlotte is also rich in these elements and is most probably the source of elements typically found in silicate minerals (Aubut and Campbell, 2012, Proctor and Redfern, 1981, Patrie, 1995). Titanium and chromium are also prevalent in silicate minerals, therefore the trend between these elements and aluminum in the precipitates in Lake Charlotte, Lake Shebandowan and Sowden Lake is not surprising (Cox, 1995).

Although a correlation between aluminum and silicate minerals has been observed, analysis of precipitates using SEM-EDX and XRD also suggest an aluminum presence in the precipitated material suggesting aluminum to be abundant in both materials. Results from the SEM-EDX proved aluminum to be present in the majority of precipitates analyzed. XRD confirmed the presence of the mineral aluminum phosphate in precipitates collected at all lakes studied. SEM-EDX line scans of Lake Charlotte samples also showed a correlation between higher values of manganese and aluminum.

2. Geochemistry

Precipitate Anatomy:

Geochemistry results comparing the inner section of precipitates in a nodule to the outer section reveals that arsenic and boron concentrate to higher levels in the center of the precipitate and barium concentrates in the outer section. However, these findings do not agree with results from SEM data, which reveal a greater concentration of arsenic in the outer portion of the nodules analyzed. This is due to the limited data sets that consisted of different nodules for the whole rock geochemistry compared to the SEM analysis.

Rare Earth Elements:

Rare earth element data was normalized to Post Achaean Australian Shale and graphed. Data collected from this study has large positive cerium and small gadolinium anomalies present in samples collected from all study lakes with the exception of Sowden Lake. Europium was slightly enriched at the Lake Charlotte and Shebandowan Lake study sites, but was slightly depleted in Sowden Lake. To explain these results, freshwater precipitates described in this study can be compared to deep sea manganese nodules due to their similarities in structure and geochemistry (Figure 69). By comparing rare earth element data from deep sea manganese nodules, ocean water and fresh water precipitates, a general understanding of why cerium anomalies are present can be determined.

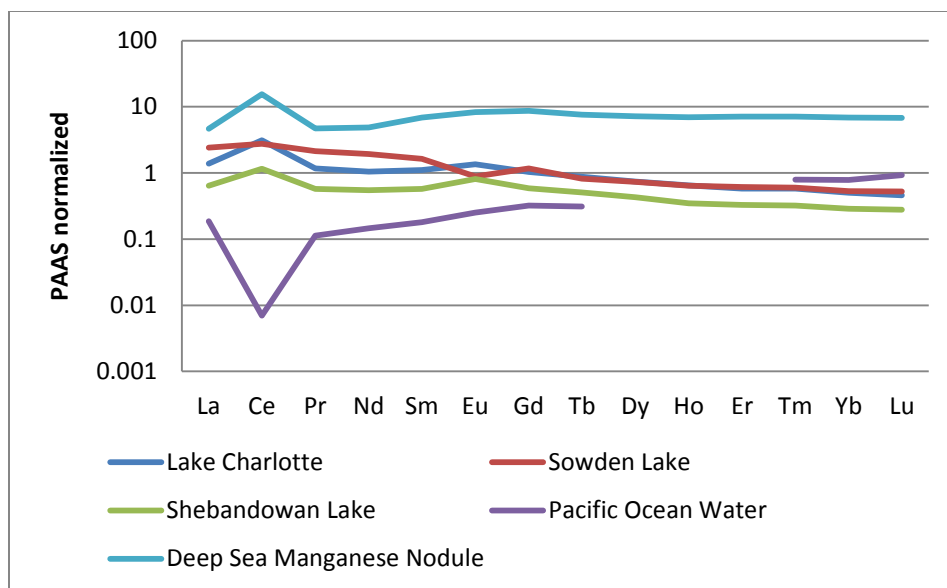


Figure 69: Average rare earth concentrations normalized to PAAS. Data from Lake Charlotte and Sowden Lake taken from this study, Shebandowan Lake data from Dasti (2008), Pacific Ocean Water from Klinkhammer et al., (1983), and deep sea manganese nodule data from Takahashi et al., (2000). All data normalized as ppm units with the exception of Pacific Ocean water which was normalized as ppt units to allow for the data to be more comparable on a graph.

Deep sea manganese nodules are consistently observed on the ocean floors of the Atlantic, Pacific and Indian Oceans. These nodules can be located at any depth from 3m in the shallow ocean to the abyssal plains, which reach kilometers below the water’s surface (Crerar and Barnes, 1974). Mn nodules generally appear with a surface structure of closely spaced spherical protrusions called botryoids which give the nodules a ‘grapelike’ appearance. Some nodules show a complex system of layered rings within the structure (Margolis and Burns, 1976).

Mn deposits are found unattached to the sediment of the ocean floor. They are created by a variety of factors which all contribute to the precipitation of heavy metals from ocean water. Nodules that are found in pelagic (open sea water) away from shallow waters and shorelines are considered to be of hydrogenous origin as they are precipitated from the seawater in contact with the ocean bottom (Reyss et al., 1982). Nodules found along coastlines are considered to be of diagenetic origin, in which heavy metals are precipitated from the sediment pore space on the ocean bottom due to a redox boundary between the sediment and the seawater (Reyss et al., 1982).

When rare earth analysis from deep sea manganese nodules (Takahashi et al., 2000) are compared with Pacific Ocean water (Kinkhammer et al., 1983) cerium is found to be enriched in the nodule and depleted in the ocean water. An enrichment of cerium in a nodule will occur when the oxidation of the element changes its valance state from Ce(III) to Ce(IV) (Takahashi et al., 2000). The oxidation of a deep sea nodule can be affected by bacteria such as benthic epifauna (Crerar and Barnes, 1974) or the presence of reduced water found in sediment pores coming into contact with the oxidized ocean water (Yoshikawa 1991, Ostwald and Frazer, 1973, Burns and Burns, 1977, Reyss et al., 1982). The enrichment of cerium in deep sea nodules compared to the depletion of Pacific Ocean water, as is observed in Figure 69, suggests that the origin of the cerium found in the nodules comes from the surrounding ocean water (Takahashi et al., 2000).

Rare earth analysis of precipitates from Lake Charlotte and Shebandowan Lake appear to follow the same cerium enrichment trend as was described with deep sea manganese nodules (Figure 69). An environment which allows growth of freshwater precipitates must be associated with a redox boundary, this will enable redox sensitive elements (such as cerium) to precipitate out of the somewhat reduced groundwaters.

The slight enrichment of europium in the precipitates of Lake Charlotte and Shebandowan Lake may reflect the source enrichment of the element in the host rock of the area. Obviously the rocks in the Shebandowan and Lake Charlotte watersheds contain more units formed early in the crystallization history of parent melts. They may also have the erosive products of these rocks, and thus contain more plagioclase producing positive europium anomalies compared to rocks in the Sowden Lake watershed.

3. Microbiology

Micro-stromatolitic structures

Although the presence of microorganisms was not investigated during this study, evidence to support microorganisms playing a role in the growth of iron- and- manganese-rich precipitates is evident. The presence of stromatolitic structures was found to occur on both the top and bottom of most nodule structures. The presence of stromatolites growing towards the lake bottom suggests there are microorganisms present during precipitate growth which do not rely on photosynthesis for energy. It is suggested that microbial growth of a precipitate- rich nodule could be due to iron/manganese reducing bacteria. Further research with focus on microbiology is needed to accurately suggest which iron/manganese reducing microorganisms assist in the growth of precipitates found in Lake Charlotte, Lake Shebandowan and Sowden Lake. Further research with a focus on cyanobacteria is also needed to determine if any of these microorganisms have an affect on the formation of precipitates in the three study lakes.

Arsenic precipitation related to photosynthesis:

SEM-EDX analysis of Lake Charlotte specimens have concluded arsenic concentrates on not only on the surface of iron hydroxides and oxyhydroxides (the majority) and manganese oxides (minimal concentration) but also in places on diatoms that are found on the outer sections of the nodule. The ability for arsenic to concentrate on biogenic silica (a diatom) has been recently described in the freshwater system of the Gangetic Delta of West Begal where high incidences of arsenic and iron have become a public health concern due to water contamination (De and Bhattacharyya, 2010). The ability of arsenic and iron to adsorb onto diatoms has become a means of precipitation for water sources in this area.

De and Bhattacharyya (2010) have described the ability for the EPS surrounding biogenic silica (diatoms) to precipitate iron and arsenic from a groundwater source onto the diatom as a precipitate coating. The chemical process of this precipitation is as follows: Polysaccharides and proteins found as EPS form as algae over diatoms which are found in biomats on the surface of the sediment. The EPS, which was excreted from microorganisms, can carry a negative charge allowing for the formation of a highly reactive diffusion barrier between water found on the top of the biofilm, and water found on the bottom (De and Bhattacharyya, 2010, Czaczyk and Myszka, 2007). As water passes through the biofilm, cations such as ferrous iron are attracted to the negative charge of the EPS. If sunlight is available the biofilm is able to photosynthesize, creating an oxidizing condition for cations such as ferrous iron to precipitate as a coating onto the diatom (De and Bhattacharyya, 2010). Due to the attraction of arsenic to iron in an aqueous environment, arsenic will precipitate onto the surface of the diatom (Figure 70). The chemical process described by De and Bhattacharyya (2010), explains why arsenic appears on diatoms in SEM imagery from the surface of a Lake Charlotte nodule.

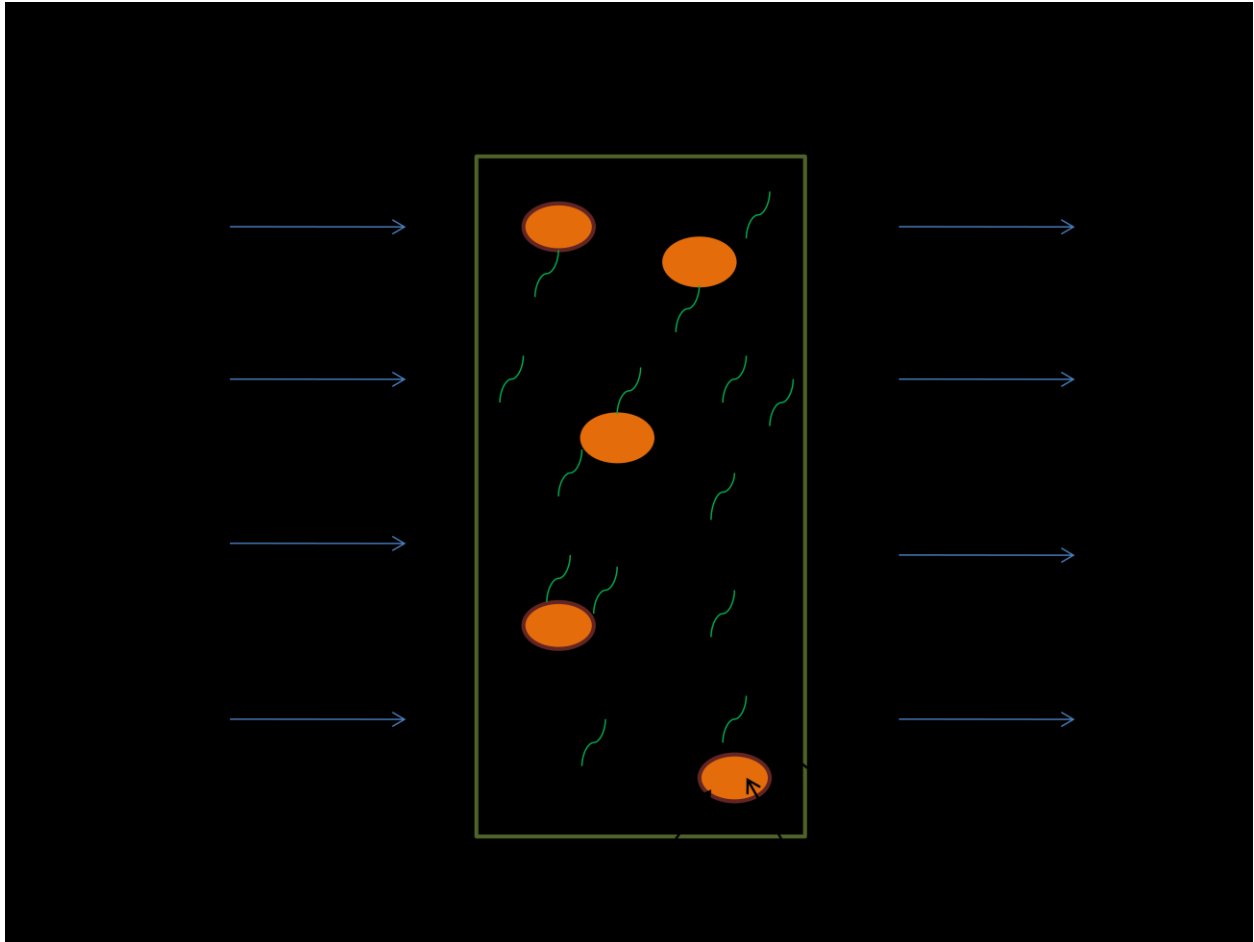


Figure 70: A visual representation of how EPS and diatoms found in a biofilm are able to naturally remove iron and arsenic from contaminated water. Groundwater containing reduced iron and oxidized arsenic passes through a biofilm created from EPS that has been discharged from microorganisms such as diatoms. EPS has a negative charge which attracts iron and arsenic to the biofilm. Photosynthesis from diatoms creates an oxidized environment allowing for precipitation of iron and arsenic onto the surface of the diatom. The water that has moved through the biofilm will now be without the oxidized iron and arsenic (De and Bhattacharyya, 2010).

4. Water Chemistry

Water Depth and Sediment Temperature:

The temperature of the pore water 5cm below the lake bottom was measured from Lake Charlotte at My Cove, Bud's Cove and 7 Cove. Findings revealed the average lake water temperature to be warmer by 0.94-1.35°C when compared to the sediment temperature. The difference between the

two temperatures becomes greater for samples taken further from the shoreline. The difference is also depth dependent, showing similar temperature values at the end of a precipitate field where there is a sudden increase in the depth of the lake. Thus, the temperature differential only exists in the sandy substrate below the precipitate fields.

The idea of precipitate growth by means of a redox boundary occurring between lake water and groundwater has been previously proposed (Sozanski and Cornan, 1976, Dean et al., 1981, Sommers et al., 2002, Stevens, 2007). At the Lake Charlotte site, the following model, representing nodule growth by means of a redox boundary created by diffuse groundwater flow into the lake, can be put forward using data collected in this study.

When groundwater comes into contact with the lake water it is colder, and therefore has a greater density than the lake water, causing it to remain near the lake bottom. This creates a boundary between the more reduced groundwater and the more oxidized lake water allowing for redox sensitive elements such as iron, manganese and arsenic to precipitate out of the groundwater creating a nodule. In the shallow water where the lake bottom is sandy and therefore porous and permeable due to the presence of a reworked esker, a redox boundary exists. Further offshore in deeper waters the bottom is more clay-rich and impermeable so groundwater does not have a means to infiltrate through the lake bottom and create a redox boundary. In deeper waters precipitate growth cannot exist via this mechanism, and, in fact, no precipitates were found.

The lack of nodules near the shoreline of most study sites (with the exception of Sowden Lake where nodules were collected next to a sheltered island shoreline) could be due to the presence of wave activity. As an area with nodules becomes shallow, waves have an ability to disturb the lake bottom hindering the ability for a redox boundary between the lake bottom water and groundwater to exist.

With continual disturbance from waves iron –manganese precipitates are not able to grow in the shallow waters.

Dissolved Oxygen and pH Water Chemistry:

When the average Eh and pH from each lake was plotted on an Eh/pH diagram for iron, all data points were found to sit along the $\text{Fe}^{2+}/\text{Fe}(\text{OH})_3$ boundary (Figure 71a). This suggests that any change in the Eh of each lake studied has the potential to favour either iron precipitation, resulting from a high Eh, or, with a lower Eh, the iron remaining in solution. On an Eh/pH diagram for manganese, data from all three study lakes plotted in the Mn^{2+} area (Figure 71b). This suggests that either the pH or Eh at all three study lakes must rise for a significant amount of Mn^{2+} in solution to precipitate. An alternative method for precipitation of manganese out of solution is if its cation (Mn^{2+}) attaches to another element which is able to precipitate out of solution (such as iron). Data plotted on the aluminum Eh/pH diagram suggests that aluminum is able to precipitate from solution at all of the environmental conditions where data was collected (Figure 71c).

Lake Charlotte, Lake Shebandowan and Sowden Lake were all analyzed, in this study, for pH and Eh of the lake water that could be related to the growth of nodules by precipitation. The average pH and Eh at each study area was used to examine the ability of elements of interest to precipitate. Lake Charlotte was found to have the lowest average pH, at approximately 5.85, whereas the average pH at Shabandowan and Sowden Lake was approximately 7.0-7.5. Eh values, as with dissolved oxygen values, declined in Shabandowan Lake over a monthly period from early June to late July from approximately 90mV to 55mV. Lake Charlotte Eh values from all five site areas ranged from an average of 93mV at Mine Site to 145mV at My Cove.

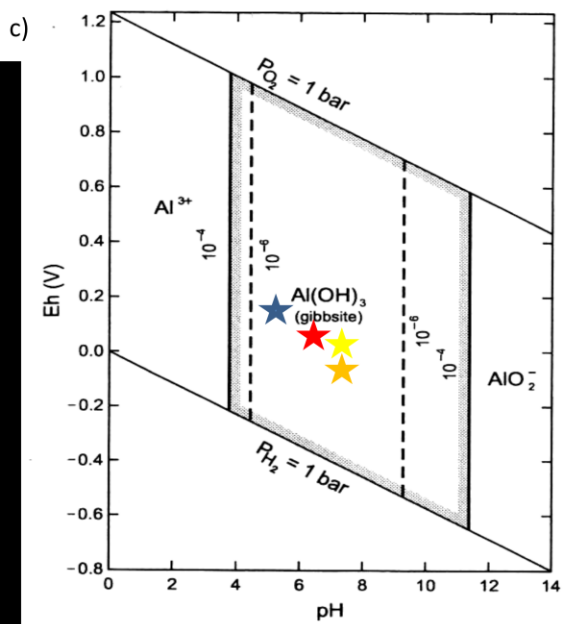
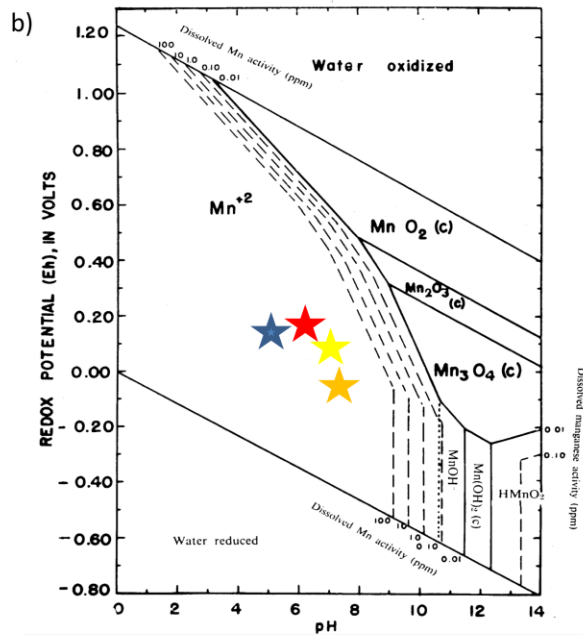
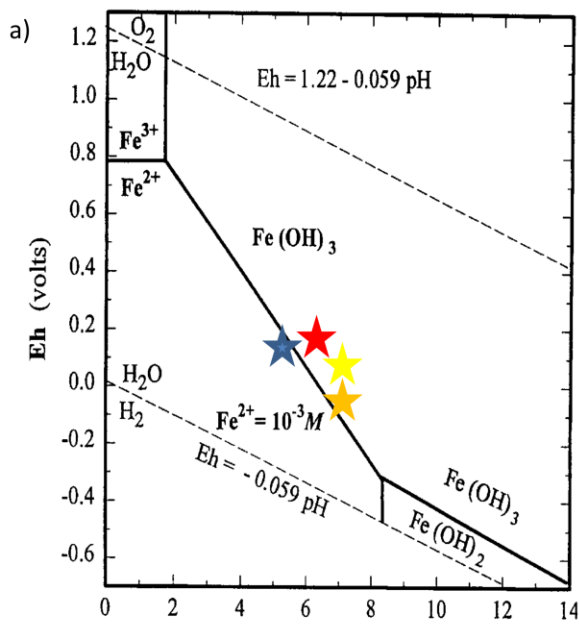


Figure 71: Eh/pH diagrams displaying averages from each lake (Hitchon et al., 1999) (a) Iron Eh/pH diagram (b) manganese Eh/pH diagram, (Hem, 1963) (c) aluminum Eh/pH diagram (Hitchon et al., 1999). All averages from each lake were collected from lake water temperatures between 18.5-23°C

The amount of oxygen found in the lake water around the precipitate fields of Lake Charlotte, Lake Shebandowan, and Sowden Lake was highly concentrated in the months of June and early July when the majority of water sampling was completed. Data collected from Shebandowan Lake in late July, when compared with the earlier readings from June, displayed a decrease in the amount of oxygen in the lake water by approximately 30%. The difference in the amount of dissolved oxygen found in the lake between spring and summer suggest seasonal variations of the amount of dissolved oxygen in the lake throughout the year.

The amount of oxygen present, and therefore redox potential, in a mesotrophic, dimictic lake such as Shebandowan is a factor of thermal stratification and biological activity within the lake. In the spring and summer months the lake will be stratified below the thermocline. An increase in solar radiation will cause a decrease in the amount of oxygen found in a lake. However, plants and microorganisms found in the water will continue to be a means of creating oxygen (Wetzel, 1983). In the winter the presence of ice over the lake also creates thermal stratification with the warmest water being below the thermocline.

Seasonal variation in the amount of oxygen found in a lake is dependent on the water turnovers of a dimictic lake throughout the year (Figure 72). During summer months, most lakes in the mid latitudes become stratified with an epilimnion (the upper wind mixed portion of the lake above the lakes thermocline), and hypolimnion (the bottom, cold, dense portion of a lake remaining below the thermocline). This allows for very little dispersion in oxygenated water throughout the winter and summer months. In fall, as the surface water cools a mixing created by the change in the water temperature and surface wind causes the epilimnion and the hypolimnion to shift and mingle with one another. Water overturn happens again in the spring when the warmer water cycles to the surface of

the lake creating an isothermal environment where oxygen is dispersed throughout the water column (Wetzel, 1983).

The amount of oxygen present in the lake water surrounding a nodule field could be a factor in the time and rate a precipitate can grow throughout the year. In the spring and fall when oxygen is prevalent throughout the lake, the increase in dissolved oxygen may increase the Eh of the lake water allowing for a preferred environment for iron and manganese precipitation. In the winter and summer when the lake remains stratified, the amount of oxygen surrounding the precipitate field will decline, altering the Eh of the environment and potentially inhibiting precipitate growth or causing dissolution.

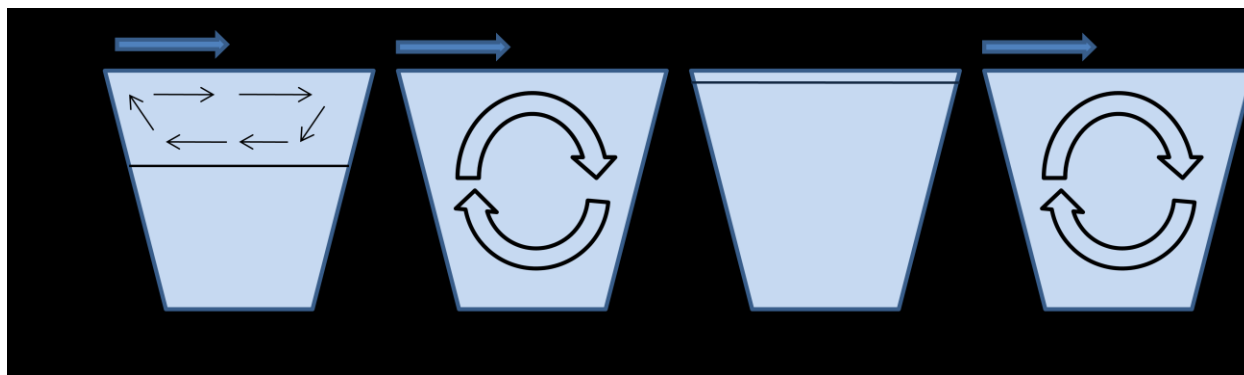


Figure 72: An illustration of overturn in a dimictic lake adapted from Wetzel (1983). In the summer months surface wind allows for the warm lake water of the epilimnion to cycle above the thermocline. The remainder of the lake becomes stratified and is not affected by water cycling, minimizing the amount of oxygen found in the hypolimnion. In the fall and spring dimictic lakes overturn their epilimnion and the hypolimnion due to the warming and cooling of surface water allowing for oxygen to become dispersed throughout the lake. In the winter when the lake becomes covered with ice, wind is not able to affect water circulation and the warmer water is found below the thermocline. With no water movement, there is little addition of new oxygen into the lake.

Seasonal variation effecting iron precipitation will also affect the amount of arsenic and phosphorous that is precipitated from solution. Penn et al. (2000) describes seasonal change with respect to iron and phosphorous precipitation in a dimictic lake and finds the precipitation of iron hydroxides that contain adsorbed phosphorous are prevalent during the spring turnover between the months of March and June. During the winter months of lake stratification, phosphorus no longer adsorbs onto the iron but instead is found in solution (Penn et al., 2000). In the case of arsenic and

phosphorus adsorption onto iron- and manganese- rich precipitates, seasonal variation within a dimictic lake must be considered a factor.

5. The growth of a nodule: A review of past theories

Iron- and manganese - rich precipitates found in near neutral pH, dimictic lakes in mid – latitudinal climates have been previously described and their growth speculated upon. Microbiology (Dean et al., 1981, Sommers et al., 2002, Konhouser, 2007) and the existence of a redox boundary (Sosanski and Coran, 1978, Kepkay, 1985, Boudreau, 1988, Stevens, 2007) are both considered factors for precipitate growth. Previous literature suggests there is some dispute whether the existence of microorganisms at an oxidation-reduction boundary is the primary mechanism for the growth of an iron-manganese precipitate.

Emphasizing the importance of microbiology, Sommers et al. (2002) described a theory of biogenesis as the primary mechanism of precipitate growth, with bacterial catalysts such as EPS and cyanobacteria as a means of initiating deposition. Sommers et al. (2002) suggested limiting factors for the growth of a precipitate to be: lack of a suitable substrate such as sand, competition between microorganisms, and the amount of sunlight able to penetrate to the lake bottom.

Dean et al. (1981) and Konhouser (2007) also described the importance of cyanobacteria, suggesting a manganese cycle initiated by cyanobacteria within lakes. They propose bacteria initiate a cycle where metals such as iron and manganese are oxidized from the lake water and precipitated in a nodule on the lake bottom. As the nodules become eroded and moved offshore, the metals will reduce back into solution with a change in their environment from oxygenated shallow waters to the more reduced deeper lake waters.

Kepkay (1985) and Boudreau (1988) suggested that a nodule plays the role of a strong sink for heavy metals when compared to its underlying lake bottom sediment. As the lake water passes over the nodules, gradients in metal concentrations develop in the water adjacent to its surface. This allows the lake water coming into contact with the nodule to diffuse elements onto the nodule surface. Therefore, the concentration of iron and manganese in the precipitate would be dependent on the concentration of these elements within the lake water. Kepkay (1985) investigated the amounts of iron and manganese present in the pore waters of sediment underlying the nodules of Lake Charlotte, Nova Scotia. It is suggested that the oxidation of heavy metals onto the sediment had a strong affiliation with the existence of microorganisms in the environment.

The importance of a redox boundary outlook has been previously theorized for both Lake Shebandowan and Lake Charlotte. Sozanski and Cornan (1978) described a theory for Lake Shebandowan where diagenesis below the nodule-rich substrate allows for an upward remobilization of iron and manganese into the lake bottom substrate. Sozanski and Cornan (1978) suggested that initial precipitation of $\text{Fe}(\text{OH})_3$ results in the adsorption of Mn^{2+} , which oxidizes to MnO_2 as the Eh-pH of the lake water changes with the seasons. Stevens (2007) using the Lake Charlotte site as an example, suggested that a reduced groundwater environment coming into contact with oxidized lake water can cause a redox boundary, which can effect redox elements such as iron and manganese. Groundwater also has the ability to leach ions into solution from a large area and transport them for long distances. This can create a precipitate highly concentrated in elements such as arsenic, which are not normally found in high concentrations. Stevens (2007) also noted the presence of iron oxidizing bacteria and suggested the possible ability of these organisms to scavenge arsenic from solution.

6. Nodule Growth Models

Nodule Growth at Lake Charlotte's 7 Cove, Bud's Cove, My Cove

Site areas 7 Cove, Bud's Cove and My Cove, all have similar characteristics in their geography and precipitate descriptions. Their nodule fields were approximately the same size (50m²) and found at depths of 1-2m after which a sudden increase in depth and a related transition to a clay rich bottom marked the non-existence of nodules. The lake bottom of the precipitate field consisted of a sandy substrate. However, an increase in depth and termination of nodule development coincided with a change in the substrate, which became finer grained and organic- rich. The nodules at all three sites were similar in appearance and followed the trend of nodules increasing in size with an increase in depth.

The results from this study regarding precipitate geochemistry, chemical correlations, and water chemistry, indicated the following method for precipitate growth at these three sites can be proposed. Firstly, a redox gradient must be established. The existence of diffuse groundwater flow has been confirmed to exist in 7 Cove, Bud's Cove and My Cove due to the temperature decrease from the bottom lake water to the pore-water underlying the nodule fields. Springs are also common on the land near the My Cove bay (Stevens, 2007). As the groundwater comes into contact with the lake water, a redox sensitive boundary is produced. Since the groundwater is colder and denser than the lake water, the groundwater will have negative buoyancy and increased residing time in the near bottom waters. Once the lake bottom sediment becomes less porous and permeable in deeper waters, groundwater is no longer able to infiltrate upward into the lake and the redox boundary becomes non-existent (Figure 73).

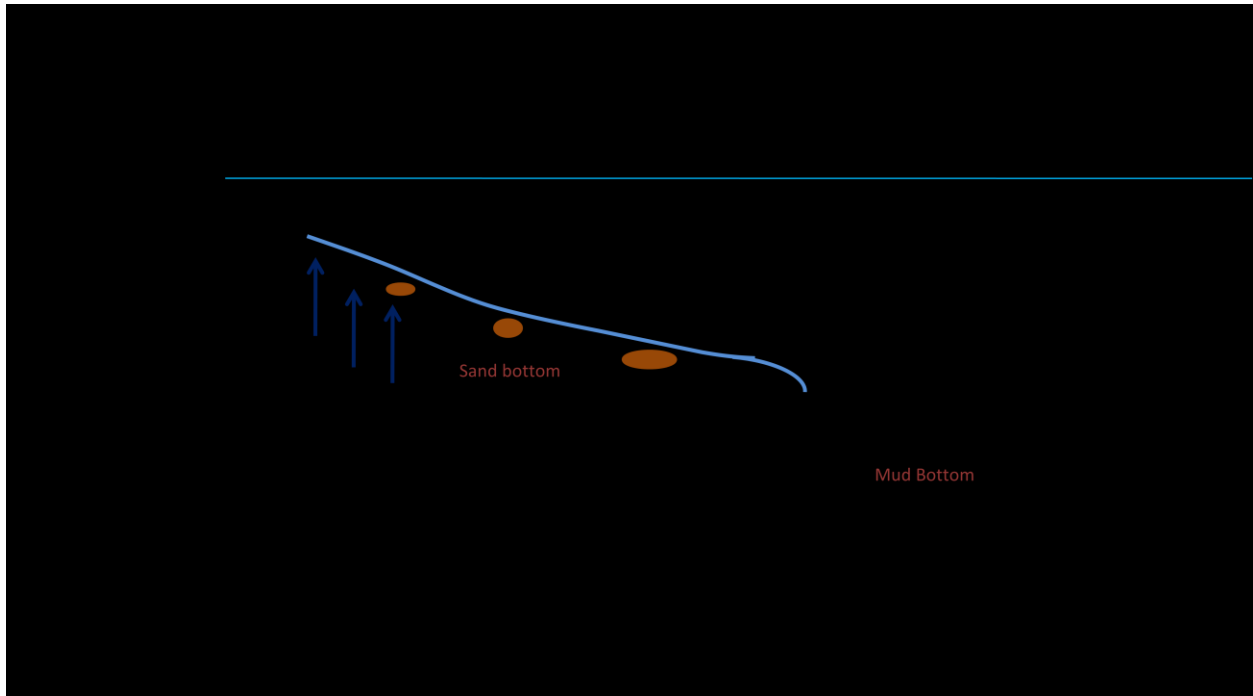


Figure 73: A diagram of how a potential redox boundary can be created when ground water comes into contact with lake water. When groundwater infiltrates into a lake an oxidation-reduction boundary is created. When the lake bottom becomes less porous in deeper waters, groundwater is no longer able to flow through the lake sediment and the redox environment is terminated.

The deposition of precipitates near the redox boundary would be sensitive to fluctuations in the Eh and pH of lake water, and therefore the rate at which the precipitate grows is affected seasonally. In the spring and fall seasons of a dimictic lake such as Lake Charlotte, the mixing of the lake causes an increase in the Eh and pH of the lake water, allowing for the potential of iron and manganese to precipitate in a redox environment. As suggested by Sozanski and Cornan (1978) the initial growth of the precipitate should begin with an oxidized iron banding due to the ability of iron to precipitate at an Eh that is less than that of manganese. The ability for iron to precipitate at a lower Eh suggests a longer duration of precipitation during a year than manganese, possibly the spring, early summer, fall and early winter. Once the iron precipitates, Mn^{2+} is able to adsorb onto the iron oxide. If the Eh of the lake water becomes high enough to allow the oxidation of manganese (over approximately 0.8V at a pH of 7 (Hem,

1963)) then the manganese ions adsorbed onto the iron oxide can also oxidize as MnO_2 , thus creating a manganese rich layer.

As either iron or manganese continues to oxidize the elements found to correspond with either element will also come out of solution. Iron is more electrostatically favourable to arsenic and phosphorous as opposed to manganese in its oxidized state (Manceau et al., 2007). Therefore, arsenic and phosphorous will concentrate with iron in the precipitate. Manganese adsorbs barium, cobalt and sulfur, and will therefore take these elements out of solution during oxidation. For elements such as arsenic and barium to be so highly concentrated in precipitates at these three sites lends credence to the theory proposed by Stevens (2007) regarding the ability for groundwater to collect elements over a large area and deposit them at the redox boundary.

Lake Charlotte samples from My Cove, 7 Cove, and Bud's Cove appear to be influenced by two types of microorganisms during growth. Diatoms were found on the surface of the precipitates examined with SEM imagery suggesting assistance in growth from photosynthetic bacteria. However, there is no evidence to suggest the diatoms on the surface were effecting nodule growth and could have been simply been living on the lake bottom. The stromatolitic structures found growing downward into the lake substrate suggest iron and manganese - oxidizing bacteria as a means of microbiological growth.

The size of the nodules increasing with depth may be due to wave activity of the cove. As wind and waves come into the cove, the shallow lake bottom found towards the shoreline will become disturbed and therefore inhibit precipitate growth. As the lake increases in depth, less disturbance from wind and waves will allow the nodules to increase in size throughout time. Some nodules found in Bud's cove appear as smaller nodules covered by larger nodules until a pavement-like structure is created on the tops of pebbles and cobbles. A possible reason for this growth could again be due to wave or storm

disturbance. As waves come into the cove during a storm event they deposit a layer of sand and/or pebbles. This may cover the existing nodules on the lake bottom creating a new surface for nodule growth.

Nodule Growth at Mine Site and Granite Islands

Lake Charlotte's Mine Site is different in appearance to 7 Cove, Bud's Cove and My Cove due to its drop in depth close to the shoreline, and its rocky vegetated beach with minimal protection from wind and waves. The nodules from this site were not well developed and were only found on the lake bottom at the top of the slope before the drop off to deep water. Although differences in appearance exist, the same principles of precipitate growth in My Cove, Bud's Cove and 7 Cove may still be used at the Mine Site. The high arsenic values at this site indicate local groundwater from the arsenopyrite – bearing rocks of the mine site was important in formation of the nodule. The only difference at the Mine Site is the lack of a gradual decline in water depth making the area with a redox boundary at this site narrower, present only along the top of the drop off slope. The area is also more susceptible to wave action and storms than the other Lake Charlotte sites so the growth of precipitates could often have been disturbed.

The Granite Island site is anomalous compared to the other sites investigated on Lake Charlotte. Why are there so many nodules at a site where the granite bedrock found underneath the nodule field should have a much lower permeability than the sand and cobbles present at other sites? Why are the nodules found so evenly distributed on the lake bottom? Why are there nodules at the Granite Islands at depths as great as 18m? Perhaps in the instance of this site the proposal from Kepkay (1985) and Boudreau (1988) where nodules act as a sink for heavy metals during mass transport of lake water over the structure may be considered. In this instance nodules would be able to grow due to lake water diffusing elements onto the surface of a pebble or cobble (Kepkay (1985), Boudreau (1988)). Another

possibility could be that there are fractures within the granite lake bottom which allow for groundwater seepage into the lake.

Nodule Growth at Shebandowan Areas Island Site and Small Site

The growth of precipitates at the Shebandowan Lake sites can be explained in a similar manner as Lake Charlotte's 7 Cove, Bud's Cove and My Cove sites due to the similarities of the lake environments. All nodule fields were found slightly off the shoreline and were underlain by a sandy substrate. The nodules of both lakes were morphologically similar, however, the nodules at Shebandowan Lake were often smaller. Differences between the sites include the depths of the nodule fields at Shebandowan Lake being greater (up to approx. 6m) than those of the Lake Charlotte sites. Rational for this difference could be due the depth at which groundwater infiltrates into the lake possibly controlled by where appropriate diffusive substrates are found in the lake.

The substrate on the deeper side of the Shebandowan Lake nodule site areas consisted of reddish coloured clay with precipitates embedded within the clay and on the surface of the clay bottom. It is not fully understood why nodules would grow on an impermeable clay layer or beneath the surface of a clay layer. A possible explanation as to why precipitates exist in this environment could be the deposition of clay sediment burying existing nodules on the former surface layers (Figure 74). The reddish colour of the clay indicates that iron is oxidized in this environment.

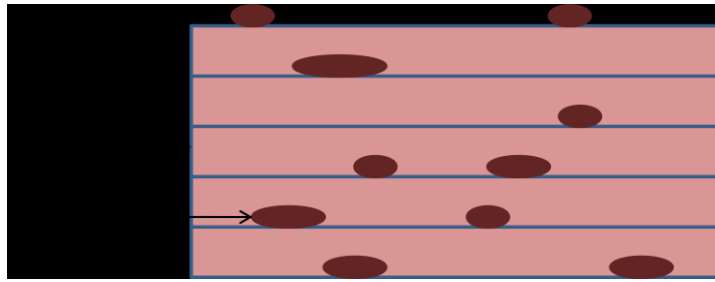


Figure 74: A possible explanation as to why precipitates were found embedded in clay at Shebandowan and Sowden Lakes. The lake bottom at these areas may be so undisturbed that overtime clay from the lake water is able to settle on top of existing precipitates burying and entombing them.

Initial growth of the nodules on the surface of the clay could have been due to microbial activity. Iron and manganese –oxidizing bacteria require ferrous iron and/or reduced manganese to create energy and therefore cannot thrive in a highly oxygenated environment where they must compete with instantaneous abiotic oxidation of metals (Emerson and Moyer, 1997). Hedrich et al. (2011) suggested that at an oxic/anoxic interface, which in Shebandowan Lake could be considered as the reddish coloured clay, could be an environment where microaerophiles would thrive. These bacteria require an environment of little present oxygen and some concentration of carbon dioxide to survive. Some iron and manganese –oxidizing bacteria such as the *Gallionella ferruginea sp.* are microaerophiles and could thrive in the clay allowing for microbial oxidation of the iron and manganese into a nodule.

Nodule Growth at Sowden Lake Areas Sowden 41 and Sowden 46

The nodule-rich areas at Sowden Lake remain difficult to interpret. The nodules found in this lake are different then those found at all other sites:

- Sowden lake samples are more oval in shape.
- There is a lack of iron –manganese-rich banding in most of the precipitates.
- Very few precipitates are found with a pebble or any material at their center.
- Sowden Lake nodules are stronger and difficult to break without the use of a tool.

- The precipitates lack a positive cerium anomaly when compared to PAAS.

The nodule size vs. water depth is also different than what was found in Lake Charlotte. Sowden Lake precipitates are larger when formed closer to the water's surface and become smaller with an increase in depth. Sowden Lake, as with Lake Shebandowan was observed to have reddish clay below the deeper portions of the nodule field where small precipitates were found on top of and embedded within the clay.

Broken fragments of nodules were found along the slope of the nodule field; however it is difficult to determine if these were all naturally fragmented or were broken during collection. If these fragments were indeed naturally fragmented along a slope, there is potential for the theory of Dean et al. (1981) to be used. The theory of Dean et al. (1981) can be related to the study site in Sowden Lake if the majority of oxidation of redox sensitive elements in this lake is affected more importantly by algae and photosynthetic bacteria than a reducing groundwater source (Figure 75). In this case, manganese and iron found in the lake water are oxidized by algae and precipitated onto the lake bottom forming a nodule. Movement by animals or wind and waves then carry the nodules down slope where they become fragmented. The nodules then travel to deeper waters are reduced compared to those present in the water found closer to the surface of the lake. This causes the reduction of iron and manganese back into the lake water, which can be used to continue the cycle of oxidation and reduction within the lake. Konhouser (2007) expanded on this theory suggesting that the algae on the lake bottom were buried in the sediment allowing for elements to become remobilized in this reducing environment.

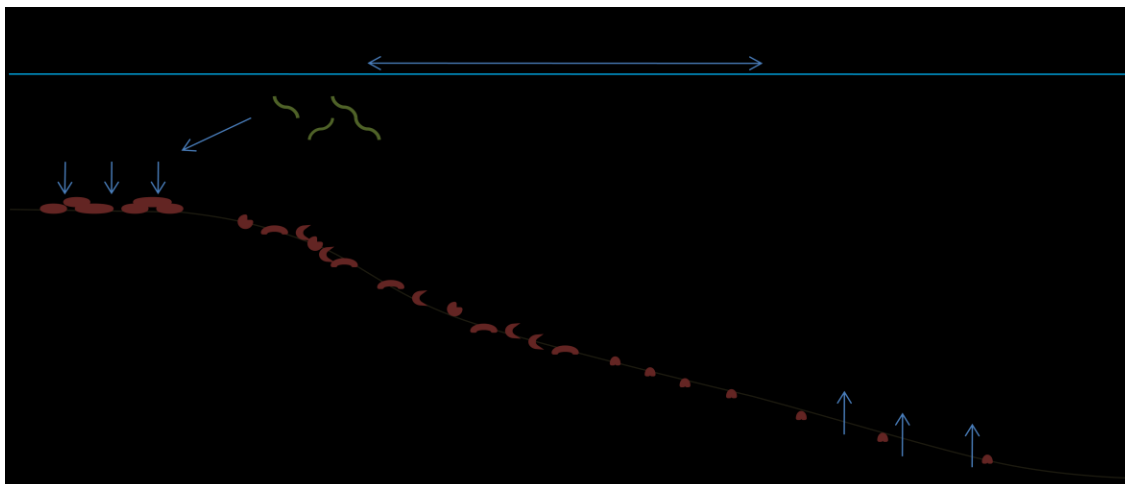


Figure 75: Visual representation, adapted from Dean et al (1981), of a potential redox cycle within a lake. Mixing of water by wind allows for oxygen created by algae and other photosynthetic bacteria in the lake waters (1) to circulate throughout the lake. The Mn^{2+} and/or Fe^{2+} ions found in the lake waters become oxidized by the algae and precipitate out of the water. Death of the algae concentrates the metals and forms nodules on the shallow lake bottom (2). Movement by animals or storm events cause the precipitates to travel down slope where they become broken into fragments (3). In deeper waters where less oxygen is present, the iron and manganese are reduced and released back into the lake water (4) allowing for the cycle to continue.

7. Potential Environmental Implications of Iron-Manganese Precipitate

Research:

Research regarding the growth of iron-and manganese-rich nodules holds environmental significance in a number of study areas involving water contamination. In this study arsenic concentrations as high as 11 000ppm (7 Cove site) were observed in the iron- rich banding of the precipitates of Lake Charlotte. Water sampling of the lake indicated no significant amounts of arsenic are present, suggesting the precipitates have created a natural arsenic adsorption system by means of a redox boundary. Results from this study may aid in design of natural arsenic adsorption systems that could potentially be used for clean up of contaminated drinking water, waste water, agricultural runoff (phosphorous), and mine waste disposal sites.

Another conclusion of this study involves the interaction between arsenic and phosphorous. Results suggest that if a large amount of arsenic is present in a nodule, there will be low amounts of

phosphorous and vice-versa. This implies competition between these two elements over precipitation onto iron during oxidation. An understating of this relationship can be of value in cases such as water contamination clean up in agricultural areas. Farmland may produce an excess amount of phosphorous in the water runoff. If the area is also being treated for arsenic contamination, the existence of both elements could cause competition during adsorption onto iron hydroxides allowing high concentrations of phosphorous to pass through an oxidation barrier. Arsenic and phosphorous contents must be taken into account when assessing the areas ability for water remediation using an oxidative barrier. In an agricultural environment with a high amount of phosphorous present, arsenic may not be effectively removed from solution.

Results acquired from this study have the possibility of contributing to potential research involving the removal of radium from contaminated water bodies. Manceau (2007) suggested that research involving the removal of barium from solution can be extended to radium due to their behavioural similarities in nature. Radium, a radioactive product of uranium or thorium, can be an environmental factor in water surrounding and/or leaching from uranium mining areas. Past research by Herczeg et al. (1988) and Qureshi and Nelson (2003) found the oxidation of manganese to be an efficient means of extracting barium (and potentially radium) out of solution. Research with iron-manganese - rich precipitates could be used to further understand the relationship between manganese and barium, while comparing these findings with those for radium found in uranium mining waste.

Conclusions

Iron-and-manganese- rich precipitates were collected from the lake bottoms of Lake Charlotte, (Nova Scotia), Lake Shebandowan (Ontario) and Sowden Lake (Ontario). Lake Charlotte precipitates were highly enriched in arsenic and the Lake Shebandowan and Sowden Lake samples to be highly enriched in phosphorous. Research of redox sensitive elements in lacustrine environments was used to postulate how precipitates are able to grow, and concentrate elements such as arsenic and phosphorous, which are not normally found in abundance in the environment. Analysis of study areas at the macro-, meso -and micro- scale was conducted to attempt to understand growth of the iron-manganese rich precipitates in their natural environment.

Positive correlations between iron, arsenic and phosphorous were determined. This suggests that as iron is oxidized arsenic and phosphorous will adsorb from solution into the iron hydroxides. Positive correlations between manganese, barium and cobalt were also present suggesting the ability of barium and cobalt to adsorb onto manganese during oxidation and precipitation.

The existence of a redox boundary at the sediment/lake water interface was indicated by the following results and observations: An enrichment of cerium in the nodules (with the exception of Sowden Lake) gives evidence that the element has been oxidized to its 4^+ state, suggesting the presence of a redox boundary. The redox potential data results suggest that nodule growth is dependent on seasonality, the greatest precipitate growth being during the spring and fall when the amount of oxygen dispersed throughout the lake increases. Finally, the difference in temperature between the lake water and sediment water revealed a groundwater source below the lake bottom at sites 7 Cove, Bud's Cove and My Cove.

It appears that not one model for nodule formation can be applied to all study sites; instead each site must be analyzed individually to determine dominant processes that take place and are considered a means for nodule growth. After environmental analysis of all nodule fields in this study, the following models for nodule growth have been acknowledged as potentially viable.

It was determined that nodule growth at the study sites My Cove, 7 Cove, Bud's Cove and Mine Site occur due to the diffuse upward flow of groundwater coming into contact with lake water. This creates a redox boundary due to the infiltration of reduced groundwater coming into contact with the oxidized lake water. This process is probably further enhanced by means of photosynthetic and iron/manganese oxidizing microorganisms. At this redox boundary, iron, manganese and their associated elements, precipitate from the groundwater creating a nodule.

The Shebandowan Lake study sites appear to be affected by the diffusion of groundwater to the lake bottom creating a redox boundary. This is supported by the work of Sozanski and Cornan (1978) who suggested the flow of groundwater in Shebandowan Lake was a significant factor. It is postulated that the nodules found within the clay at both the Shebandowan and Sowden Lakes sites may be present due to the presence of microaerophile bacteria precipitating iron and manganese in an environment with little oxygen present and the burial of nodules by clay overtime.

The growth of precipitates found at Sowden Lake is probably affected more by bacteria found in the lake water than a groundwater redox boundary (c.f. Dean et al., 1981). In this case, manganese and iron in the lake water are oxidized by algae and precipitated onto the lake bottom forming a nodule. The breakdown of the nodule by animals, wind and waves allows precipitate fragments to travel to deeper reduced waters allowing redox sensitive elements to cycle back into the lake water. This results in a continuous cycle of precipitate growth. In order to prove this theory is applicable to the Sowden Lake site, further research is required.

Acknowledgments

I would like to thank Dr. P. Fralick for the opportunity to participate in this study. Along with sharing his knowledge and skills he has also brought patience, reassurance and a sense of humour. Thank you to Allan Makenzie and Dr. W. Woo for their assistance with the SEM, Ain Raitsaka for his assistance with the ICP-AES geochemistry, and Anne Hammond for making my microscope slides and SEM discs. A big thank you also goes out to Adrian Arts for sharing his knowledge and great attitude in the field during the summer months. Finally, thank you to all my family and friends for their support in this endeavour, particularly the Drewman Ezack.

References

- Aloisi, G., Gloter, A., Kruger, M., Wallmann, K., Guyot, F., Zuddas, P. 2006. Nucleation of calcium carbonate on bacterial nanoglobules. *Geology*. 34(12). 1017-1020.
- Aubut, A., Campbell, D. 2012. Shebandowan mine area. *Proceedings of the 58th institute of lake superior geology annual meeting-part 2*. 67-73.
- Benzerara K., Miot J., Morin, G., Ona-Nguema G., Skouri-Panet, F., Fèrard, C. 2011. Significance, mechanisms, and environmental implications of microbial biomineralization. *Comptes Rendus Geoscience*. 343. 160-167.
- Bontognali, T., Vasconcelos, C., Warthmann, R., Dupraz, C., Berasconi, S., McKenzie, J., 2008. Microbes produce nanobacteria-like structures, avoiding cell entombment. *Geology*. 36(8) 663-666.
- Boudreau, B. 1988. Mass transport constraints on the growth of discoidal ferromanganese nodules. *Journal of American Science*. 288. 777-797.
- Burns, R., Burns V. 1977. The mineralogy and crystal chemistry of deep-sea manganese nodules, a polymetallic resource for the twenty-first century. *Philosophical Transactions of the Royal Society of London*. A. 286, 283-301.
- Chan, C., De Stasio, G., Weich, S., Girasole, M., Frazer, B., Nesterova, M., Fakra, S., Banfield, J. 2004. Microbial polysaccharides template assembly of nanocrystal fibers. *Science*. 202. 5664. 1656-1658.
- Card K.D. 1990. A review of the superior province of the Canadian shield, a product of archaic accretion. *Precambrian Research*. 48. 99-156.
- Casanova, J., Bodéan, F., Nègre, P., Azaroual M. 1999. Microbial control on the precipitation of modern ferrihydrite and carbonate deposits for the Cézallier hydrothermal springs (Massif Central, France). *Sedimentary Geology*. 126, 125-145.
- Chen, Z., Kim, K., Zhu, Y., McLaren, R., Liu, F., He, J. 2006. Adsorption (As III, V) and oxidation (AsIII) of arsenic by pedogenic Fe-Mn nodules. *Geoderma*. 136 (566-572).

- Cox, P. A. 1995. The elements on Earth: inorganic chemistry in the environment. Oxford University Press. Oxford.
- Crerar, D., Barnes, H. 1974. Deposition of deep-sea manganese oxides. *Geochimica et Cosmochimica Acta*. 38. 279-300.
- Cudmore S., Losee, W., McDowell, R. 1945. Chronological record of Canadian mining events from 1604-1943 and historical tables of the mining production of Canada. Minister of Trade and Commerce. Ottawa.
- Cutnell, J., Johnson, K. 2004. Physics. 6th ed. John Wiley and Sons Inc. New Jersey
- Czaczyk, K., Myszka, K. 2007. Biosynthesis of extracellular polymeric substances (EPS) and its role in microbial biofilm formation. *Polish Journal of Environmental Studies*. 16 (6)799-806.
- Dasti. I. 2008. Geochemical Constraints on Formation of Lactustrine Fe-Mn Nodules from Nova Scotia and Northwestern Ontario. *Unpublished B.Sc. thesis, Lakehead University*. 61pp.
- De, C., Bhattacharyya, S. 2010. Biogeochemical role of surficial diatomaceous biomats in groundwater purification: A key revelation from the Gangetic Alluvial Floodplain, South 24 Parganas, India. *Geomicrobiology Journal*. 27, 355-379.
- Dean, W.E, Moore W.S., Nealson, K.H. 1981. Manganese cycles and the origins of manganese nodules, Oneida Lake, New York. USA. *Chemical Geology*. 34. 53-64.
- Duquesne, K., Lebrun, S., Casiot, C., Bruneel, O., Personné J., Leblanc, M., Poulichet, F., Morin, G., and Bonnefoy, V. 2003. Immobilization of arsenite and ferric iron by *Acidithiobacillus ferrooxidans* and its Relevance to acid mine drainage. *Applied and Environmental Microbiology*. 69(10). 6165-6173.
- Egal, M., Casiot, C., Morin, G., Parentier, M., Bruneel, O., Lebrun, S., Elbaz-Poulichet, F. 2009. Kinetic control on the formation of tooeleite, schwertmannite and jorosite by *Acidithiobacillus ferrooxidans* in an As(III)-rich acid mine water. *Chemical Geology*. 265, 432-441.
- Emerson, D., and Moyer, C. 1997. Isolation and characterization of novel iron-oxidizing bacteria that grow at circumneutral pH. *Applied and Environmental Microbiology*. 63(12). 4784-4792.

- Environmental Protection Agency. 2007. National primary drinking water regulations. Retrieved November 14th from www.epa.gov/drink/contaminants/upload/mcl-2.pdf
- Enst, Trent. 2009. Northwestern Ontario backroad mapbook outdoor recreation guide, 2nd ed. Mussio Ventures Ltd.
- Esri. 2012. ArcGIS Resources: ArcGIS Arcmap Help 10.1. Retrieved November 13th from <http://resources.arcgis.com>
- Folk, R. L., Ward W. C. 1957. Brazos river bar (Texas); a study of the significance of grainsize parameters. *Journal of Sedimentary Petrology*. 27 (1) 3-26.
- Fralick, P. 1980. A model for the concentration processes of arsenic in well waters of Nova Scotia, Canada. *Institute for resources and environmental studies, Dalhousie University*. 39pp.
- Ghiorse, W.C. 1984. Biology of iron and manganese depositing bacteria. *Annual Review of Microbiology*. 38. 515-550.
- Golder Associates Ltd. 2011. Coldstream mine site 2010 surface water and groundwater monitoring report.; unpublished report. *Ministry of Northern Development and Mines, Thunder Bay Mines and Minerals Office*. 51pp.
- Gorham, E. 1957. The chemical composition of lake waters in Halifax County, Nova Scotia. *Limnology and Oceanography*. 2(1). 12-21.
- Gupta, K., Maity, A., Ghosh, U. 2010. Manganese associated nanoparticles agglomerate in iron (III) oxide: Synthesis, characterization and arsenic (III) adsorption behaviours. *Journal of Hazardous Materials*. 184. 832-842.
- Han, X., Li, Y., Gu, J. 2011. Oxidation of As(III) by MnO₂ in the absence and presence of Fe(II) under acidic conditions. *Geochimica et Cosmochimica Acta*. 75, 368-379.
- Hallbeck, L., Peterson, K. 1991. Autotrophic and mixotrophic growth of *Gallionella ferruginea*. *Journal of Microbiology*. 137. 2657-2661.
- Hammarstorm, J., Seal, R., Meier, A., Kornfeld, J. 2005. Secondary sulphate minerals associated with acid mine drainage in the eastern US: recycling of metals and acidity in surficial environments. *Chemical Geology*. 215. 407-431.

- Harris, R., Troup, A. 1969. Freshwater ferromanganese concretions: Chemistry and internal structures. *Science*. 166(3905).604-606.
- Harrison A. 1984. The Acidophilic thiobacilli and other acidophilic bacteria that share their habitat. *Annual Review of Microbiology*. 38. 265-92.
- He. Y., Hering, J. 2009. Enhancement of arsenic (III) sequestration by manganese oxides in the presence of iron (II). *Water Air Soil Pollution*. 203, 359-368.
- Hedrich, S., Schloman, M., Johnson, B. 2011. The iron-oxidizing proteobacteria. *Microbiology*. 157. 1551-1564.
- Hem, J. 1963. Chemical equilibria and rates of manganese oxidation. *U.S Geological Survey Water Supply Paper*. 1667-A.
- Herczeg, A., Simpson, H., Anderson, R., Trier, R., Mathieu, G., Deck, B. 1988. Uranium and radium mobility in groundwaters and brines within the Delaware basin, Southeastern New Mexico U.S.A. *Chemical Geology*. 72. 181-196.
- Hitchon, B., E. H. Perkins, *et al.* (1999). Introduction to Ground Water Geochemistry. Sherwood Park, Alberta, Canada, Geoscience Publishing Ltd.
- Inco Limited Ontario Division. 2001. Shebandowan mine closer plan part I of II: unpublished report. *Ministry of Northern Development and Mines Thunder Bay Mines and Minerals Division Office*, 84p.
- Jackson, J. 2003. Ignace High density regional lake sediment geochemical survey, operation treasure hunt. *Ontario Geological Survey, Open File Report 6106*. 190pp.
- James, R.E., Ferris, F.G. 2004. Evidence for Microbial-Mediation iron oxidation at a neutrophilic groundwater spring. *Chemical Geology*. 212. 301-311.
- Jürgensen, A., Widmeyer, J., Gordon, R., Bendell, Y., Moore, M., Crozier, E. 2004. The structure of manganese oxide on the sheath of bacterium *Lepothrixdiscophoria*: and XAFS study. *American Mineralogist*. 89. 1110-1118.

- Katsoyiannis, I., Zouboulis, A. 2006. Use of iron and manganese reducing bacteria for the combined removal of iron, manganese and arsenic from contaminated groundwater. *Water Quality Research Journal of Canada*. 41. 117-129.
- Kepkay, P. 1985. Kinetics of microbial manganese oxidation and trace metal binding in sediments: results from an in situ dialysis technique. *Limnology and Oceanography*. 30. 713-726.
- Keim, C., 2011. Arsenic in biogenic iron minerals from a contaminated environment. *Geomicrobiology Journal*. 28. 242-251.
- Kindle E.M. 1932. Lacustrine concretions of manganese. *American Journal of Science*. 24. 496-504.
- Klinkhammer G., Elderfield H., Hudson A. 1983 Rare earth elements in seawater near hydrothermal vents. *Nature*. 305, 185–188.
- Konhauser, K. 2007. Introduction to geomicrobiology. Blackwell publishing. Malden MA.
- Larson, D., and Mann, R. 2005. Origin of high manganese concretions in coal mine drainage, eastern Tennessee. *Journal of Geochemical Exploration*. 86. 143-163.
- Leblanc, M., Achard, B., Othman, D.B., Luck, J.M. Bertrand-Sarfati, J., Personne, J, Ch. 1996. Accumulation of arsenic from acid mine waters by ferrous bacterial accretions (stromatolites). *Applied Geochemistry*. 11. 541-554.
- Leduc, D., Leduc, L.G., Ferroni, G.D. 2002. Quantification of bacterial populations indigenous to acidic drainage streams. *Water, Air and Soil Pollution*. 135. 1-21.
- Lu, P., and Zhu, C. 2011. Arsenic Eh-pH at 25°C and 1 bar. *Environmental Earth Science*. 62. 1673-1683.
- Malcolm, W., 1976. Gold fields of Nova Scotia. *Geological Survey of Canada Memoir*. 156, 19-29.
- Manceau A., Lanson, M., Geoffroy, N. 2007. Natural speciation of Ni, Zn, Ba, and As in ferromanganese coatings on quartz using X-ray fluorescence, adsorption and diffraction. *Geochimica et Cosmochimica Acta*. 71. 95–128
- Miot, J., Benzerara, K., Obst, M., Kappler, A., Hegler, F., Schadler, S., Bouchea, C., Guyot, F., Morin, G. 2009. Extracellular iron biomineralization by photoautotrophic iron-oxidizing bacteria. *Applied and Environmental Microbiology*. 75(17) 5586-5591

- Moore, P., Reddy, K. 1994. Role of Eh and pH on phosphorous geochemistry in sediments of Lake Okeechobee, Florida. *Journal of Environmental Quality*. 23. 955-964.
- Mongolis, S., Burns, R., 1976. Pacific deep-sea manganese nodules: Their distribution, composition and origin. *Annual Review of Earth and Planetary Sciences*. 4. 229-259.
- Morin, J. 1973. The geology of lower Shebandowan Lake area district of Thunder Bay. *Ontario Division of Mines. Geological Report 110*. 68 pp.
- Morin, G., Juillot, F., Casiot, C., Bruneel O., Personné, J., Elbaz-Poulichet F., Leblanc, M., Ildefonse P., Calas, G. 2003. Bacterial formation of tooeleite and mixed arsenic (III) or arsenic (V)-iron (III) gels in the Carnoulès Acid Mine Drainage, France, A Xanes, XRD, and SEM Study. *Environmental Science and Technology*. 37(9).1705-1712.
- Murray, J. W. 1975a. The interaction of metal ions at the manganese dioxide- solution interface. *Geochemica et Cosmochimica Acta*. 39. 505-519.
- Murray, J. W. 1975b. The interaction of cobalt with hydrous manganese dioxide. *Geochemica et Cosmochimica Acta*. 39. 635-647.
- Natural Resources Canada. 2012. National Topographic Database. Maps Retrieved September 2012 at www.geogratis.cgdi.gc.ca
- Nova Scotia Department of Natural Resources. 2004. Geological map of Nova Scotia. Government of Nova Scotia.
- Ontario Geologic Survey. 1991. Map 2542: Bedrock Geology of Ontario, West Central Sheet. *Ministry of Northern Development and Mines*
- Osmani, I. 1996. Geology and mineral potential of the Upper and middle Shebandowan Lake area, west central shebandowan greenstone belt. *Ontario Geologic Survey*. Open file report 5938. 105pp.
- Ostwald J., Fraser F.W. 1973. Chemical and mineralogical investigations in deep sea manganese nodules from the southern oceans. *Mineralium Deposita*. 8(4) 303-311.
- Pacton, M., Gorin, G., Vasconelos, C., Gautschi, H., Barbarand, J. 2010. Structural arrangement of sedimentary organic matter: Nanaometer-scale spheroids as evidence of microbial signature in early diogenic processes. *Journal of Sedimentary Research*. 80. 919-932.

- Partie, D. 1995. Physics report on the Lake Charlotte gold property Halifax County, Nova Scotia. Ellsin Resources Ltd.
- Pasec, M. 2008. Rethinking early earth phosphorus geochemistry. *Proceedings of the National Academy of Sciences of the United States of America*. 105. 854-858.
- Penn, M., Aurer, M., Doerr S., Driscoll, C., Brooks, C., Effler, S. 2000. Seasonality in phosphorous release rates from the sediments of a hypereutrophic lake under a matrix of pH and redox conditions. *Canadian Journal of Fish and Aquatic Science*. 57. 1033-1041.
- Perera E. Jinno K. 2009. Mathematical modeling of the formation of reduced environments in a coastal aquifer under the bacterial mediation. *18th World International Association of Mathematics and Computers in Stimulation Congress, Cairns, Australia*. 13-17
- Proctor and Redfern Group Ltd. 1984. Peat and Peatland Evaluation of the Ignace area. *Ontario Geologic Survey. Open file report 5487*. vol. 1. 332pp.
- Qureshi, N., Nelson, S., 2003. Radium removal by HMO and manganese greensand. *Journal of American Water Works Association*. 95, 101–108.
- Reyss, J., Marchig, V., Ku, T. 1982. Rapid growth in deep sea manganese deposits. *Nature*. 295(4). 401-403.
- Ridgeway, H., Means E., Olsen B. 1981. Iron bacteria in drinking water distribution systems: Elemental analysis of *Gallionella* stalks, using X-ray, energy dispersive microanalysis. *Applied and Environmental Microbiology*. 41(1). 288-297.
- Rott, U., Meyer, C., Friedle, M. 2002. Residue-free removal of arsenic, iron, manganese and ammonia from groundwater. *Water Science and Technology: Water Supply*. 2. 17-24.
- Sanchez-Roman, M., Vasconcelos, C., Schmid, T., Dittrich, M., McKenzie, J., Zenobi, R., Rivadeneyra, M., 2008. Aerobic microbial dolomite at the nanometer scale: Implications for the geologic record. *Geology* 36. 879-882.
- Shaver, K. 2011. Adaptive phase management initial screening-the cooperation of the township of Ignace. *Golder Associates Ltd*. 12pp.

- Sommers M., Dollhopf, M., Douglas, S. 2002. Freshwater ferromanganese stromatolites from Lake Vermilion, Minnesota: Microbial culturing of environmental scanning electron microscopy investigations. *Geomicrobiology Journal*. 19. 207-427.
- Sozanski . A., Cornan, D., 1976. Environmental differentiation of morphology of ferromanganese oxide concentration in Shebandowan Lakes, Ontario. *Limnology and Oceanography*.21. 894-898.
- Sozanski, A., Cornan, D. 1978. Ferromanganese concretions in Shebandowan Lakes, Ontario. *Canadian Journal of Earth Sciences*.16. 126-140
- Smith, A., Smith, M. 2004. Arsenic drinking water regulations in developing countries with extensive exposure. *Toxicology*. 198. 39-44
- Stevens, L.B. 2007. Investigation of ferromanganese nodule precipitation and arsenic uptake in modern biochemical sediments: Lake Charlotte, Nova Scotia. *Unpub. B.Sc. thesis, Lakehead University*, 70pp.
- Straskraba, V., Moran, R. 2006. Environmental occurrence and impacts of arsenic at gold mining sites in the western United States. *Mine Water and the Environment: International Mine Water Association*. 11pp.
- Takahashi, Y., Shimizu, H., Usui, A., Kagi, H., Nomura, M. 2000. Direct observation of tetravalent cerium in ferromanganese nodules and crusts by X-Ray adsorption near-edge structure (XANES). *Geochimica et Cosmochimica Acta*. 64 (17) 2929-2935
- Takamatsu, T., Kaswashima, M., and Koyama, M., 1985. The role of Mn²⁺- rich hydrous manganese oxide in the accumulation of arsenic in lake sediments. *Water Resource*. 19 (8). 1029-1032.
- Taylor and McClennan. 1985. *The Continental Crust. Its Composition and Evolution*. Blackwell Scientific. Oxford.
- Thomas, D., Styblo, M., Lin, S. 2001. Review: The cellular metabolism and systemic toxicity of arsenic. *Toxicology and Applied Pharmacology*. 176. 127-144.
- Toner, B., Fakra, S., Villalibod, M., Warwick, T., 2005. Spatially resolved characterization of biogenic manganese oxide production within a bacterial biofilm. *Applied Environmental Microbiology*. 71(3). 1300-1310.

- Vali, H., McKee M., Ciftcioglu, N., Sears, S. K., Plows, F.L., Chevet, E., Ghiabi, P., Plavsic, M., Kajander, E., Zare, R. 2001. Nanoforms: A new type of protein-associated mineralization. *Geochimica et Cosmochimica. Acta.* 65(1) 63-74.
- Vander Wal, J., Stedwill, R. 1973. Aquatic macrophyte report of the Shebandowan lake system. *Ministry of the Environment of Ontario. Water Quality Branch and Resource Division.* 34pp.
- Villalobos, M., Bargar, J., Sposito, G. 2005. Trace metal retention on biogenic manganese oxide nanoparticles. *Elements.* 1. 223-226.
- Wang S, Mulligan C N, 2005. Occurrence of arsenic contamination in Canada: Sources, behavior and distribution. *Science of the Total Environment.* 366. 701–721.
- Wetzel, R.G. 1975. *Limnology.* W.B. Saunders Company
- World Health Organization. 2012. Arsenic in drinking-water. Background document for development of WHO guidelines for drinking-water quality. 55p.
- Yoshikawa, K., 1991. The relationship between manganese minerals and metallic elements in deep-sea manganese nodules. *Marine Geology.* 101. 267-286.
- Zhang, G., Huijun, L., Qu, J., Jefferson, W. 2012. Arsenate uptake and arsenite simultaneous sorption and oxidation by Fe-Mn binary oxides: Influence of Mn/Fe ratio, pH, Ca²⁺ and humic acid. *Journal of Colloid Interface Science.* 366(1) 141-146.

Appendix

Appendix A: Accuracy and Precision values.....	2
Appendix B: Transect point precipitate geochemistry data and water data values.....	3
Appendix C: Precipitate geochemistry dissection values.....	31
1. Data values from specific areas of a precipitate	
2. Top and bottom precipitate values including rare earth elements	
Appendix D: Geochemistry of silisioclasitc sediment.....	34
1. Study Site sediment chemistry	
2. My Cove pit geochemistry	
Appendix E: Water analysis Data.....	38
1. Water elemental chemistry data	
2. Water analysis maps	
Appendix F: Environmental distribution elemental maps.....	54
1. Maps of the three most comparable elements to iron, manganese, aluminum and carbon	
2. Remaining elemental maps	
Appendix G: XRD spectrums.....	117










Appendix A: Accuracy and Precision values

	Al	As	B	Ba	Ca	Ce	Co	Fe	K	La	Li	Mg
Precision %	10.26	5.72	10.08	3.18	8.27	21.37	5.02	0.46	10.60	5.43	8.10	4.09
Accuaracy %	8.41	8.06		16.34	16.02	21.97	14.58	8.73	3.19	13.69	58.43	2.61
	Mn	Mo	Na	Ni	P	S	Sc	Sr	Ti	Y	Zn	Zr
Precision %	11.04	16.02	8.55	13.39	0.66	30.05	13.85	9.93	9.72	12.01	1.43	12.10
Accuaracy %	1.02	15.81	24.58	5.80	4.70			11.26	7.85	20.51	1.59	45.92





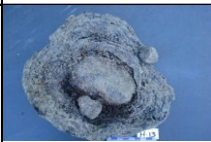




Appendix B: Transect point precipitate geochemistry data and water data values

B1: 7 Cove	4
B2: Bud's Cove	8
B3: Granite Islands	11
B4: Mine Site	13
B5: My Cove.....	15
B6: Shebandowan Island Site.....	20
B7: Shebandowan Small Site.....	22
B8: Sowden 41.....	24
B9: Sowden 46.....	28










B: 7 Cove Coordinates, Bottom Water chemistry and Precipitate chemistry

7 Cove	Sample Picture	Easting	Northing	Depth (m)	Sediment temp (°C)	DO ppm	pH	Temp (°C)	millibar	µs/cm	TDS	Eh	DO (%)	Al ₂ O ₃ (%)	CO ₂ (%)	CaO (%)	FeO+ (%)	K ₂ O (%)	MgO (%)	MnO (%)	Na ₂ O (%)	P ₂ O ₅ (%)	TiO ₂ (%)	As (ppm)	B (ppm)	Ba (ppm)	Ce (ppm)	Cr (ppm)	La (ppm)	Li (ppm)	Mo (ppm)	Ni (ppm)	S (ppm)	Sc (ppm)	Sr (ppm)	Y (ppm)	Zn (ppm)	Zr (ppm)		
F1		503844	4957500	0.2	21.6	8.02	5.98	21.46	992.8	22	11	111.6	82.4																											
F2		503844	4957505	0.28	21	7.73	5.98	21.48	999.3	22	11	123.8	87.1																											
F3		503844	4957510	0.31	21.1	7.88	5.96	21.42	993.4	22	11	128.8	92.8																											
F4		503844	4957515	0.47	20.8	8.06	5.96	21.36	993.5	22	11	131.5	91.6	4.30	5.46	0.40	45.58	0.22	0.09	6.52	1.55	0.88	0.02	4194	4568	2646	79.31	6.94	25.51	43.02	6.76	170.86	250.2	0.77	51.2	12.60	432	59.28		
F5		503844	4957520	0.7	19.7	8.11	5.94	21.32	99.36	22	11	134	90.5	6.16	2.82	0.56	27.34	0.40	0.11	11.98	1.41	0.21	0.05	3908	2974	3112	150.31	8.36	32.26	94.54	6.9	194.2	347.6	0.97	66.5	10.54	718.2	40.08		
F6		503844	4957525	0.82	20.3	8.21	5.94	21.12	993.7	22	11	140.4	99.2	6.75	4.25	0.78	18.39	0.38	0.15	21.47	0.92	0.06	0.03	1664.6	1969.2	4530	202.51	10.64	43.57	84.08	5.82	223.2	477.6	0.89	101.32	11.26	997	22.86		
F7		503844	4957530	0.87	19	8.02	5.91	20.87	993.7	22	11	143	88.6																											
F8		503844	4957535	0.99	19.9	8	5.91	20.87	993.7	22	11	145.3	90.6	6.62	3.01	0.31	35.88	0.30	0.08	15.64	1.54	0.19	0.03	4122	4090	5278	148.29	11.64	38.14	40.26	7.86	201.6	482	1.09	127.36	11.37	695	83.48		
F9		503844	4957540	1.19	20.1	7.53	5.84	20.15	993.8	22	11	147.4	88.7	7.77	3.23	0.59	29.40	0.60	0.13	17.05	1.64	0.26	0.04	4514	3766	6456	126.91	13.5	42.97	50.32	7.92	197	413.6	1.31	127.78	12.91	621.4	48.26		
F10		503844	4957545	1.2	20.4	7.62	5.9	20.19	993.6	22	11	146.5	78.7																											
F11		503844	4957550	1.38	20	7.77	5.79	19.9	993.5	22	11	150.1	88.1	7.73	4.58	0.22	17.54	0.21	0.05	20.68	0.82	0.15	0.03	1802.6	2290	4610	257.03	11.8	43.20	70.08	7	237.6	561.6	1.23	48.98	11.14	1059.4	25.02		
F12		503844	4957555	1.52	20	7.9	5.79	19.53	993.5	22	11	151.6	85.1																											
F13		503844	4957560	2.68		8.11	5.73	19.03	993.6	22	11	156.1	86.3	8.57	5.10	0.22	26.80	0.43	0.07	20.32	1.28	0.19	0.04	2712	3564	5514	221.51	15.76	42.49	61.16	7.74	228.6	775.4	1.46	94.04	12.54	956.8	37.76		
G1		503829	4957500	0.34	20.2	8.08	6.18	21.03	989.9	21	11	72.1	91.3																											
G2		503829	4957505	0.42	20.2	7.97	5.97	20.98	990.2	22	11	82.5	91.5																											
G3		503829	4957510	0.42	20.1	7.43	5.93	20.9	990.5	22	11	89.1		11.66	4.25	0.34	11.05	0.96	0.15	18.59	1.72	0.13	0.13	972.4	1298.6	2910	221.74	11.94	35.91	101.26	5.94	197.26	457.2	1.86	56.34	10.89	971.6	33.3		
G4		503829	4957515	0.47	19.9	7.8	5.91	20.93	990.8	22	11	95.3	88.7																											
G5		503829	4957520	0.59	19.8	7.77	5.89	20.89	991.1	22	11	99.2	88.9	7.80	4.58	0.52	21.42	0.63	0.14	17.74	1.27	0.11	0.08	4224	1537.6	6250	154.86	11.46	43.97	77.76	4.22	211.8	424.6	1.31	145.28	12.23	910.6	42.32		
G6		503829	4957525	0.7	19.7	7.83	5.89	20.89	991.5	22	11	103.5	88.3																											
G7		503829	4957530	0.84	20.1	7.82	5.88	20.87	991.7	22	11	109.7	86.9																											


B1: 7 Cove Coordinates, Bottom Water chemistry and Precipitate chemistry

7 Cove	Sample Picture	Easting	Northing	Depth (m)	Sediment temp (°C)	DO ppm	pH	Temp (°C)	millibar	µs/cm	TDS	Eh	DO (%)	Al ₂ O ₃ (%)	CO ₂ (%)	CaO (%)	FeO+ (%)	K ₂ O (%)	MgO (%)	MnO (%)	Na ₂ O (%)	P ₂ O ₅ (%)	TiO ₂ (%)	As (ppm)	B (ppm)	Ba (ppm)	Ce (ppm)	Cr (ppm)	La (ppm)	Li (ppm)	Mo (ppm)	Ni (ppm)	S (ppm)	Sc (ppm)	Sr (ppm)	Y (ppm)	Zn (ppm)	Zr (ppm)	
G8		503829	4957535	0.98	19.8	7.61	5.86	20.81	992.2	22	11	116.6	87.7	4.41	2.38	0.53	26.59	0.23	0.11	12.39	1.12	0.12	0.02	3634	3398	4510	92.09	8.16	29.20	47.18	8.28	161.72	276.4	0.77	135.06	9.00	551.6	42.94	
G9		503829	4957540	1.13	19.9	7.3	5.87	20.81	992.5	22	11	122.1	85.6	6.91	3.37	0.42	29.47	0.61	0.09	16.59	1.32	0.28	0.03	3680	3314	6738	136.31	11.56	48.37	54.02	7.9	185.98	345.2	1.43	133.24	14.03	656.2	53.26	
G10		503829	4957545	1.34	19.6	7.62	5.86	20.77	993	22	11	128.3	81																										
G11		503829	4957550	1.52	19.8	7.61	5.84	20.74	993.3	22	11	133.3	84.3	5.52	6.01	0.25	18.17	0.17	0.05	16.47	0.81	0.06	0.02	1107.4	2162	3440	157.40	9.1	34.83	39.44	0.36	162.96	586.2	0.71	41.74	8.69	748	23.32	
G12		503829	4957555	1.8	19.1	7.83	5.9	20.72	992.9	21	11	135.7	86.7																										
G13		503829	4957560	2.8		6.22	5.86	20.42	995.4	22	11	140.7	68.4	8.51	4.62	0.60	27.93	0.42	0.11	25.40	1.47	0.46	0.04	5894	4288	10122	289.14	17.58	87.91	76.76	14.74	289.8	583.8	1.83	177.02	22.11	981.6	99.58	
H14		503814	4957560	3.3		5.83	6.12	19.85	993.6	26	13	107.9	64.2																										
H13		503814	4957555											5.96	3.04	0.25	43.52	0.32	0.08	11.66	1.28	0.53	0.03	5728	3518	4904	63.29	10.84	32.51	21	7.58	160.06	494.4	1.06	289.6	11.97	352	74.38	
H12		503814	4957550	1.49	19.5	8.2	5.85	20.8	993.7	22	11	119.9	88.8	7.69	3.78	0.32	25.08	0.29	0.07	19.07	0.64	0.18	0.02	3134	2108	5522	209.66	13.54	47.51	69.42	5.5	230.8	524.4	1.40	84.82	13.60	959.6	27.44	
H10		503814	4957545	1.32	19.1	7.29	5.86	20.87	993.8	22	11	131.8	91	5.96	3.89	0.90	19.41	0.68	0.26	21.44	0.86	0.12	0.04	1772.2	1129	6240	110.31	11.4	34.54	75.04	5.74	157.44	395.4	1.03	334	10.57	565	16.6	
H9		503814	4957540	1.24	19.5	7.68	5.85	20.9	993.9	22	11	138.3	84																										
H8		503814	4957535	1.1	19.6	8.16	5.92	21.03	994.2	22	11	139.6	92.1	7.67	3.92	0.57	23.62	0.57	0.16	21.71	1.09	0.17	0.05	3306	2184	8706	158.06	13.94	41.94	71.58	8.84	224.4	479.4	1.54	324.4	12.71	893	28.06	
H7		503814	4957530	0.92	19.5	7.45	6.02	21.13	994.8	22	11	134.8	90.6	5.29	2.64	0.74	31.76	0.52	0.18	12.05	1.19	0.13	0.05	4712	2210	4128	62.11	8.36	27.43	51.02	9.88	156.84	226.2	0.94	220	9.03	377.8	38.42	
H6		503814	4957525	0.82	19.9	8.08	5.86	21.24	995.7	22	11	143.4	91.4																										
H5	?	503814	4957520	0.69	20.1	7.62	5.9	21.28	996.2	22	11	144.2	86.7	3.51		0.25	47.61	0.22	0.06	3.41	1.36	0.78	0.02	4440	4020	1536.4	44.23	8.18	20.03	18.28	9.94	146.1	252.4	0.74	25.6	9.71	414.4	61.88	
H4		503814	4957515	0.78	20.2	8.03	5.86	21.32	996.6	22	11	146.7	93.5																										
H3		503814	4957500	0.42	20.5	8.2	5.88	21.54	997.9	22	11	148.9	149.3																										
H2		503814	4957495	0.37	20.3	8.21	5.88	21.65	998.2	22	11	149.4	93.1																										
H1		503814	4957490	0.3	21	8.27	5.95	22.34	998.3	22	11	147.8	93																										
I1		503799	4957505	0.39	20.6	8.25	6.08	22.17	1001	22	11	82.3	95.5																										
I2		503799	4957510	0.46	20.4	8.34	6.03	22.1	1000.9	22	11	93.1	93.3																										
I3		503799	4957515	0.64	20.2	8.21	6.01	22.11	1000.8	22	11	102.1	96.6																										





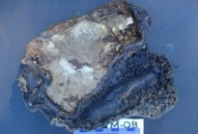


B1: 7 Cove Coordinates, Bottom Water chemistry and Precipitate chemistry

7 Cove	Sample Picture	Easting	Northing	Depth (m)	Sediment temp (°C)	DO ppm	pH	Temp (°C)	millibar	µs/cm	TDS	Eh	DO (%)	Al ₂ O ₃ (%)	CO ₂ (%)	CaO (%)	FeO+ (%)	K ₂ O (%)	MgO (%)	MnO (%)	Na ₂ O (%)	P ₂ O ₅ (%)	TiO ₂ (%)	As (ppm)	B (ppm)	Ba (ppm)	Ce (ppm)	Cr (ppm)	La (ppm)	Li (ppm)	Mo (ppm)	Ni (ppm)	S (ppm)	Sc (ppm)	Sr (ppm)	Y (ppm)	Zn (ppm)	Zr (ppm)							
I4		503799	4957520	0.82	19.9	8.17	5.96	21.92	1000.7	22	11	108.8	95.4	7.14	4.58	0.41	47.20	0.26	0.11	7.19	1.79	0.52	0.02	2834	5302	3400	120.94	18.42	37.97	51.9	16.64	205	264.8	1.40	56.96	13.94	723.4	58.02							
I5		503799	4957525	0.96	20	8.01	5.95	21.86	1000.4	22	11	118.5	91.5																																
I6		503799	4957530	1.08	19.6	8.1	5.92	21.72	999.9	22	11	125	94.9	5.64	3.70	0.76	41.95	0.19	0.18	9.49	1.85	0.33	0.02	3580	6192	4402	69.06	8.64	39.03	55.3	31.5	185.62	305	1.00	82.28	14.20	578.6	64.6							
I7		503799	4957535	1.22		8.04	5.89	21.68	999.1	22	11	129.5	90.5																																
I8		503799	4957540	1.3	20	7.98	5.9	21.66	998.6	22	11	133.5	92.5																																
I9		503799	4957545	1.41	19.6	7.91	5.88	21.67	998.2	22	11	137.2	91.3	7.45	4.69	0.87	23.99	0.41	0.19	20.03	1.15	0.19	0.03	3670	2828	7324	150.66	12.48	63.49	90.54	9.52	202.2	471.4	1.34	148.44	14.31	788.4	37.74							
I10		503799	4957550	1.56	19.8	8.07	5.89	21.66	997.1	16	11	142.1	93.7																																
I11		503799	4957555	1.92		7.16	6.02	21.66	996.4	23	11	136.1	86.5	5.91	6.75	0.43	29.14	0.21	0.09	14.49	1.08	0.19	0.02	2442	3444	4098	102.40	10.88	31.74	36.4	4.74	155.16	432.2	1.11	83.7	10.86	542.4	42.62							
I12		503799	4957560	3.8		7.88	5.8	20.4	996.8	22	11	150.2	88.2																																
I13		503784	4957560			7.37	5.95	21.48	996.9	22	11	112.5	86.4																																
J11		503784	4957550	1.48		7.94	5.86	21.62	995.8	22	11	140.9	93.4	5.92	4.00	0.28	25.52	0.22	0.06	18.32	0.61	0.11	0.01	4906	1841.2	7188	170.11	10.7	37.83	62.92	8.22	225.2	508.6	0.91	125.28	10.34	886.2	16.8							
J10		503784	4957545	1.42		8.04	5.88	21.78	994.7	22	11	144.7	92.7																																
J9		503784	4957540	1.34	20	8.02	5.91	21.77	994.7	22	11	146.1	93.5																																
J8		503784	4957535	1.28	19.9	8.12	5.89	21.86	995	22	11	148	90.9	5.19	5.10	0.73	35.11	0.25	0.16	13.97	1.41	0.21	0.02	6442	4486	5662	107.94	8.76	38.14	57.82	9.56	197.3	386.8	0.86	154.88	11.71	568.8	41.3							
J7		503784	4957530	1.13	19.7	7.83	5.93	22.07	994.7	22	11	148.2	85.9	7.70	3.41	0.51	31.58	0.37	0.17	15.34	1.61	0.22	0.04	6752	4146	5954	149.29	15.02	38.20	49.62	12.52	234.8	381.2	1.57	150.24	12.43	862.4	34.04							
J6		503784	4957525	0.9	20.6	8.22	5.96	22.29	994.5	22	11	147.9	93.8																																
J5		503784	4957520	0.77	20.7	8.21	5.95	22.26	994.6	22	11	148.9	94.1	4.25	3.74	0.36	45.32	0.31	0.08	5.51	1.59	0.37	0.02	11056	4252	4112	46.46	6.16	25.03	15.66	9.7	191.28	235.6	0.77	61.62	9.69	362.4	59.2							
J4		503784	4957515	0.6	21	8.1	5.93	22.64	994.9	22	11	148	94.2																																
J3		503784	4957510	0.42	20.2	8.37	5.94	22.67	995.1	22	11	149.1	98.9																																
J2		503784	4957505	0.39	20.9	8.44	5.98	23	995.1	22	11	149	99																																
K1		503769	4957525	0.43	21.7	8.55	6.05	24.04	995.8	22	11	125.6	104.9																																
K2		503769	4957530	0.46	21	8.54	6.05	23.6	995.7	22	11	128.1	102.1																																
K3		503769	4957535	0.52	21	8.42	6.05	23.37	996.4	22	11	133.2		4.92	4.51	0.32	44.47	0.26	0.08	5.82	1.62	0.93	0.02	4984	4788	2740	85.17	10.86	28.97	28.4	11.72	178.98	287.6	1.00	42.2	13.43	489.4	85.12							



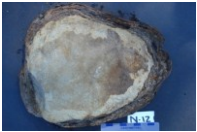






B1: 7 Cove Coordinates, Bottom Water chemistry and Precipitate chemistry

7 Cove	Sample Picture	Easting	Northing	Depth (m)	Sediment temp (°C)	DO ppm	pH	Temp (°C)	millibar	µs/cm	TDS	Eh	DO (%)	Al ₂ O ₃ (%)	CO ₂ (%)	CaO (%)	FeO+ (%)	K ₂ O (%)	MgO (%)	MnO (%)	Na ₂ O (%)	P ₂ O ₅ (%)	TiO ₂ (%)	As (ppm)	B (ppm)	Ba (ppm)	Ce (ppm)	Cr (ppm)	La (ppm)	Li (ppm)	Mo (ppm)	Ni (ppm)	S (ppm)	Sc (ppm)	Sr (ppm)	Y (ppm)	Zn (ppm)	Zr (ppm)			
K4		503769	4957540	0.82	20.8	8.36	6	23.7	996.7	22	11	134.9	98.1																												
K5		503769	4957545	0.99	20.4	8.49	5.98	22.49	996.9	22	11	138.7	98.2																												
K6		503769	4957550			8.07	5.93	22.43	996.6	22	11	144.6	96.4																												
K7		503769	4957555	1.72		8.17	5.92	21.92	996.2	22	11	145.1	95.1	4.43	3.92	0.22	33.93	0.20	0.09	13.91	1.30	0.26	0.02	3096	4382	5666	68.40	9.88	31.31	15.06	9.08	148.16	483.6	0.77	118.22	10.69	432.2	44.4			
K8		503769	4957560	3.3		7.92	5.92	21.63	99.64	22	11	101.5	89.8																												
K9		503769	4957660	5.18		7.6	5.42	18.99	997.8	23	11	126.2	87.3																												
J14		503784	4957700	6.1		7.26	5.66	17.89	998.1	23	11	121.2	77.1																												
I13		503799	4957700	5.49		7.3	5.68	19.15	998.4	22	11	121.6	82.3																												
H15		503814	4957700	6.71		7.3	5.67	18.56	998.6	23	11	126	77.7																												
F14		503844	4957700	5.49		7.55	5.83	20.84	998.7	22	11	115.8	86.4																												
J15		503784	4957800	7.62		7.55	5.58	16.67	998.7	23	11	134.8	76.2																												
H16		503814	4951800	7.92		7.48	5.58	16.53	998.6	23	11	136.9	77.7																												
G14		503829	4957800	7.92		7.31	5.59	16.58	998.8	23	11	137.2	74.6																												
F15		503844	4957800	9.14		6.89	5.59	16.04	998.9	23	12	139.2	70.7																												
I14		503799	4957900	8.53		7.27	5.58	16.44	998.8	23	12	138.3	68.7																												
K10		503769	4957860	10.67		7.45	5.57	16.04	999.2	23	12	139.9	76.6																												
G15		503829	4957760	15.24		7.01	5.56	16.86	999.4	23	11	139.5	79.8																												

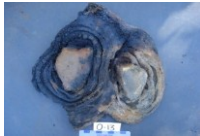








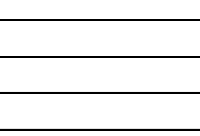
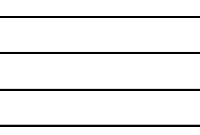
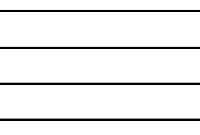
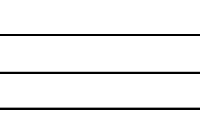
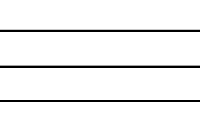
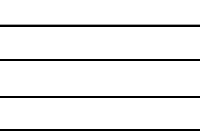
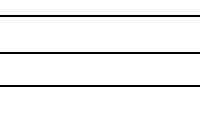
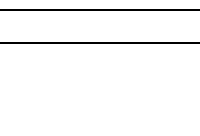





B 1: Bud's Cove Coordinates, Bottom Water chemistry and Precipitate chemistry

Bud's Cove Bottom	Sample Pictures	UTM Easting	UTM Northing	Depth (m)	Sediment Temp (°C)	DO ppm	pH	Temp (°C)	millibar	µs/cm	TDS	Eh (mV)	DO (%)	Al ₂ O ₃ (%)	CO ₂ (%)	CaO (%)	FeO+ (%)	K ₂ O (%)	MgO (%)	MnO (%)	Na ₂ O (%)	P ₂ O ₅ (%)	TiO ₂ (%)	As (ppm)	B (ppm)	Ba (ppm)	Cd (ppm)	Ce (ppm)	Co (ppm)	Cr (ppm)	Ce (ppm)	Li (ppm)	Mo (ppm)	Ni (ppm)	S (ppm)	Sr (ppm)	W (ppm)	Y (ppm)	Zn (ppm)	Zr (ppm)																		
XX1		503761	4958671	27.4		5.64	5.76	13.43		23	15	91.1	65.9																																													
XX2		503761	4958686	32		5.24	5.95	12.86	1001.4	31	15	118.5	55.7																																													
XX3		503761	4958701	30.5		4.68	5.71	12.08	1001.1	29	15	126.1	47.6																																													
XX4		503761	4958716	30.5		5.41	5.9	22.71	1000.8	29	15	76.9	41.2																																													
WW4		503721	4958716	24.4		5.94	5.76	14.31	1001.3	28	14	54	47.9																																													
WW3		503721	4958701	18.29		5.26	5.64	15.41	1001.2	28	14	114.4	52.3																																													
WW2		503721	4958686	19.81		6.66	5.64	13.58	1001.1	28	14	124.1	62.8																																													
WW1		503721	4958671	22.25		3.4	5.84	13.36	1000.2	39	19	108.5	32.8																																													
L1		503626	4958671	0.64		22.9	7.47	5.95	21.38	1003.1	19	10	97.1	85.7																																												
L2		503631	4958671	0.77		22.9	7.56	5.86	21.43	1003.2	20	10	110.2	86.2																																												
L3		503636	4958671	0.92		22.7	7.61	5.82	21.36	1003.5	21	10	121.1	86.2																																												
L4		503641	4958671	1.02		23.4	7.76	5.83	21.34	1003.7	21	10	124.9	88.2	7.37	5.43	0.26	24.64	0.61	0.09	18.06	0.86	0.12	0.07	1094.4	1079.6	2458	14.68	66.4	86.84	12.4	94.86	15.94	4.9	135.7	470.4	66.08	5.76	9.20	499.2	25.76																	
L5		503646	4958671	1.14		22.8	7.82	5.82	21.04	1003.9	20	10	127.1																																													
L6		503651	4958671	1.23		22.6	7.75	5.84	21.13	1004.2	21	10	129.6	88.2	8.42	2.93	0.47	17.38	0.77	0.13	20.95	1.10	0.11	0.10	711.2	677.4	3096	13.4	97.34	106.64	12.58	139.06	32.26	4.16	163.16	400.8	71.34	6.58	9.80	670.6	30.12																	
L7		503656	4958671	1.33		22.5	7.86	5.83	20.95	1004.2	20	10	131.7	88.1																																												
L8		503661	4958671	1.35			7.92	5.82	20.92	1003.9	20	10	133.4	90																																												
M1		503601	4958686	0.42		23	77.4	5.85	22.89	1005.4	21	11	121.9	86.6																																												
M2		503606	4958686	0.53		23.1	7.93	5.84	22.62	1006.2	21	11	127	90.5																																												
M3		503611	4958686	0.72		23	7.89	5.84	22.24	1006.4	21	11	128.9	90																																												
M4		503616	4958686	0.9		22.9	7.72	5.82	21.85	1006.5	21	11	130.7		9.58	3.45	0.37	11.97	1.52	0.19	15.53	1.60	0.13	0.14	466.4	203.4	2150	8.86	62.64	41.02	13.78	89.49	23.06	3.72	99.16	307.4	124.66	2.62	9.26	415.2	35.34																	
M5		503621	4958686	1.04		22.8	7.78	5.81	21.71	1006.4	21	11	132.6	90																																												
M6		503626	4958686	1.17		22.7	7.15	5.84	21.47	1005.9	21	11	132	82.8	12.03	0.66	0.40	3.54	2.23	0.37	4.41	2.88	0.05	0.43	74.34	125.3	598.6	3.08	21.74	12.36	20.68	31.06	22.38	0.68	28.3	72.14	98.56	2.46	8.91	262.8	71.6																	
M7		503631	4958686	1.22		22.3	7.82	5.82	21.48	1005.8	21	11	131.9	88.7																																												
M8		503636	4958686	1.29		22.6	7.7	5.84	21.4	1005.7	21	11	134	88.8	14.48	7.88	0.18	11.96	0.92	0.18	20.20	1.01	0.33	0.10	1159	461.4	1974	26.3	296.8	106.62	16.6	424.00	56.28	11.46	267.2	570.4	38.26	5.6	9.46	935	14.86																	
M9		503641	4958686	1.34		22.5	7.86	5.81	21.57	1005.8	21	11	136	91.2	8.21		0.21	14.66	0.87	0.11	16.65	1.26	0.11	0.26	541.8	254.8	1865.8	10.56	68.2	79.94	16.7	97.43	20.64	2.14	113.06	413.6	55.54	1.78	7.37	456.8	46.3																	
M10		503646	4958686	1.39		22.3	7.8	5.82	21.34	1005.9	21	11	136.2	88																																												
M11		503651	4958686	1.44		22.1	7.71	5.82	21.32	1005.8	21	11	136.7	86.7	7.28	2.68	0.34	18.42	0.70	0.11	19.71	1.00	0.11	0.16	586.6	366.6	2074	11.02	63.72	87.92	12.6	91.03	18.84	2.48	107.92	329.8	75.52	3.66	7.66	366.6	24.26																	





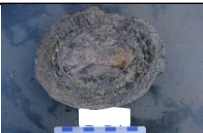
B2: Bud's Cove Coordinates, Bottom Water chemistry and Precipitate chemistry

Bud's Cove Bottom	Sample Pictures	UTM Easting	UTM Northing	Depth (m)	Sediment Temp (C)	DO ppm	pH	Temp (C)	millibar	µs/cm	TDS	Eh (mV)	DO (%)	Al ₂ O ₃ (%)	CO ₂ (%)	CaO (%)	FeO+ (%)	K ₂ O (%)	MgO (%)	MnO (%)	Na ₂ O (%)	P ₂ O ₅ (%)	TiO ₂ (%)	As (ppm)	B (ppm)	Ba (ppm)	Cd (ppm)	Ce (ppm)	Co (ppm)	Cr (ppm)	Ce (ppm)	Li (ppm)	Mo (ppm)	Ni (ppm)	S (ppm)	Sr (ppm)	W (ppm)	Y (ppm)	Zn (ppm)	Zr (ppm)							
M12		503656	4958686	1.53		7.89	5.81	21.27	1005.8	21	11	138.3	89.9	8.85		0.22	12.24	1.05	0.13	15.63	1.41	0.12	0.26	436.2	158.8	1512	10.36	65.56	74.74	13.82	93.66	21.08	0.32	107.36	344.4	63.26	2.86	7.49	407.4	46.6							
M13		503661	4958686	1.63		7.62	5.87	21.26	1005.6	22	11	138.2	88	9.02	2.93	0.34	13.17	1.03	0.15	15.99	1.48	0.14	0.23	434.6	80.8	1511.8	8.82	61.7	72.08	13.12	88.14	22.08	2.42	103.46	284.2	62.86	3.96	7.80	386	46.72							
N13		503661	4958701	1.57		7.69	6.13	21.22	1005.5	19	10	100.7	85.6																																		
N12		503656	4958701	1.5		7.74	5.84	21.21	1005.7	21	11	115.8	87	10.70	3.92	0.26	11.92	1.10	0.16	15.55	1.62	0.13	0.26	440.8	325	1056.4	11.42	102.74	107.9	14.78	146.77	20.3	2.68	129.56	309.4	54.86	4.2	8.49	456.8	39.22							
N11		503651	4958701	1.42		7.57	5.97	21.23	1005.5	23	12	122.4	80.1	9.33	1.61	0.31	6.95	1.20	0.19	10.03	1.68	0.12	0.33	274.4	71.76	989.4	8.2	51.56	42.06	13.94	73.66	26.28	1.94	79.36	238.6	61.38	2.06	7.80	314.2	44.38							
N10		503646	4958701	1.37		7.71	5.88	21.29	1005.5	22	11	128.5	86.4		0.00																																
N9		503641	4958701	1.27		7.78	5.82	21.32	1005.7	21	11	131	91.5	7.78	3.12	0.27	23.03	0.67	0.10	15.68	1.30	0.13	0.17	912.8	1670.2	1998.6	12.08	60.48	31.02	13.18	86.40	21.84	3.1	117.82	334.2	68.36	6.86	7.71	418.2	58.5							
N8		503636	4958701	1.17		7.74	5.87	21.41	1005.8	21	11	132.5	87																																		
N7		503631	4958701	1.07		7.92	5.85	21.42	1005.8	21	11	133.8	91	12.20	1.36	0.28	8.08	2.18	0.32	7.17	2.30	0.11	0.34	283.4	337.2	1263.6	6.26	42.4	30.54	22.72	60.57	28.96	2.96	63.34	192.88	72.14		9.83	241.6	46.56							
N6		503626	4958701	0.99		7.9	5.85	21.52	1005.9	21	11	134.6	89.5	11.06	0.88	0.38	8.23	1.87	0.28	8.14	2.20	0.10	0.41	248.8	130.66	1683.2	6.32	37.88	33.88	35.28	54.11	33.24	3.94	75.56	126.94	83.82	1.44	11.74	232.8	48.62							
N5		503621	4958701	22.3		7.75	5.8	21.59	1006	21	11	134.9	89.1																																		
N4		503616	4958701	0.75		7.23	5.9	21.68	1006.2	21	11	133.3	78.4																																		
N3		503611	4958701	0.58		7.92	5.92	21.96	1006.2	21	11	129.3	90.6																																		
N2		503606	4958701	0.5		7.8	5.86	22.46	1006.3	21	11	131.7	91.3																																		
O1		503601	4958716	0.37		7.94	5.84	22.57	1006.2	21	11	135.6	92																																		
O2		503606	4958716	0.46		8.7	5.83	22.13	1006.2	21	11	136.8	91.3																																		
O3		503611	4958716	0.58		7.88	5.84	22.08	1006.2	21	11	137	89.7																																		
O4		503616	4958716	0.68		7.77	5.83	21.96	1006.1	21	11	137.5	89.9																																		
O5		503621	4958716	0.81		7.6	5.87	21.81	1005.8	21	11	136.7	88.7																																		
O6		503626	4958716	1		7.67	5.86	21.77	1005.6	21	11	135.1	88																																		
O7		503631	4958716	1.13		7.98	5.82	21.51	1005.5	21	11	137.8	90	8.22	2.35	0.44	13.96	1.09	0.18	17.03	1.38	0.09	0.28	432.4	248.2	1926	9.18	57.36	85.52	14.94	81.94	20.1	1.96	97.82	235.8	78.44	3.5	7.83	332.2	46.86							
O8		503636	4958716	1.23		7.58	5.86	21.5	1005.3	21	11	137.2	85.5		0.00																																
O9		503641	4958716	1.31		7.81	5.82	21.52	1005	21	11	131.3	89.2	8.18	2.79	0.34	16.48	0.86	0.15	17.00	1.21	0.15	0.16	569.6	145.8	2234	10.68	66.62	65.06	12.78	95.17	31.22	2.2	106.5	340	80.26	3.5	7.94	441	23.82							
O10		503646	4958716	1.33		7.81	5.84	21.46	1004.9	21	11	132.5	89.6																																		
O11		503651	4958716	1.34		7.81	5.81	21.41	1005	21	11	136.7	90.9																																		



B2: Bud's Cove Coordinates, Bottom Water chemistry and Precipitate chemistry

Bud's Cove Bottom	Sample Pictures	UTM Easting	UTM Northing	Depth (m)	Sediment Temp (C)	DO ppm	pH	Temp (C)	millibar	µs/cm	TDS	Eh (mV)	DO (%)	Al ₂ O ₃ (%)	CO ₂ (%)	CaO (%)	FeO+ (%)	K ₂ O (%)	MgO (%)	MnO (%)	Na ₂ O (%)	P ₂ O ₅ (%)	TiO ₂ (%)	As (ppm)	B (ppm)	Ba (ppm)	Cd (ppm)	Ce (ppm)	Co (ppm)	Cr (ppm)	Ce (ppm)	Li (ppm)	Mo (ppm)	Ni (ppm)	S (ppm)	Sr (ppm)	W (ppm)	V (ppm)	Zn (ppm)	Zr (ppm)													
O12		503656	4958716	1.35	22	7.92	5.81	21.38	1005	22	11	137.5	89.3																																								
O13		503661	4958716	1.4	22.5	7.9	5.8	21.29	1004.8	21	11	138.8	91.2	9.64	3.01	0.33	16.90	0.85	0.14	17.00	1.22	0.16	0.18	742.6	229	2194	11.42	85.22	67.98	14.34	121.74	35.8	2.96	133.06	442.2	63.98	6.34	9.09	529	24.6													
P10		503661	4958731	1.47		7.15	5.93	21.46	1004.9	22	11	133.9	83.6		0.00																																						
P9		503661	4958731	1.4		7.85	5.83	21.44	1005	21	11	136.5	88	8.09	2.90	0.20	18.54	0.71	0.10	16.15	0.85	0.13	0.13	770.6	59.96	2150	11.6	82.8	49.28	13.06	118.29	25.4	2.48	126	405.6	51.62	5.42	7.11	507.6	14.2													
P8		503661	4958731	1.29		7.82	5.85	21.72	1004.6	21	11	135.7	88.6																																								
P7		503661	4958731	1.23		7.88	5.87	21.51	1004.4	21	11	135.4	87.3																																								
P6		503661	4958731	1.16		7.67	5.85	21.62	1004.4	21	11	136.1	87.7	9.24	4.95	0.28	12.83	0.95	0.15	19.75	1.22	0.11	0.17	619.6	36.2	2904	15.38	111.64	103.86	14.34	159.49	34.14	2.22	162.52	474.4	63.68	4.26	8.23	719.6	24													
P5		503661	4958731	1.17		7.61	5.92	21.73	1004.4	22	11	132.6	87																																								
P4		503661	4958731	0.99		7.99	5.84	21.76	1004.3	21	11	136.9	91.4	7.39	3.81	0.43	21.44	0.93	0.16	17.79	1.02	0.10	0.11	893.6	223.2	3440	11.12	52.34	72.28	13.54	74.77	29.76	3.84	114.66	337.4	175.76	5.08	9.29	451	16.58													
P3		503661	4958731	0.72		7.78	5.88	21.91	1004.4	21	11	135.3	89.5																																								
P2		503661	4958731	0.64		7.88	5.87	21.93	1004.4	21	11	137.5	90.2																																								
P1		503661	4958731	0.54		7.87	5.89	22.14	1004.2	20	11	134.8																																									
UU1		503681	4958671	4.88		7.67	6.03	21.06	1005.9	22	11	77.5	86.6																																								
UU2		503681	4958686	5.18		7.41	5.92	21.06	1006.2	22	11	98.4	83.5																																								
UU3		503681	4958701	5.18		7.46	5.92	21.06	1006.6	22	11	106.4	85.2																																								
UU4		503681	4958716	4.88		7.41	5.89	21.2	1007.3	22	11	1110	83.8																																								
UU5		503681	4958731	4.88		7.31	5.9	21.44	1007.9	22	11	112	83.8																																								
VV5		503701	4958731	5.48		7.41	5.9	21.36	1008.4	22	11	112.8	84.3																																								
VV4		503701	4958716	8.53		7.01	5.86	21.3	1009.2	23	11	115.5	80.3																																								
VV3		503701	4958701	8.53		6.78	5.88	21.24	1010	23	11	119.4	77.6																																								
VV2		503701	4958686	9.75		7.21	5.89	21.36	1009.9	22	11	118.3	81.2																																								
VV1		503701	4958671	22.86		4.24	5.79	16.69	1009.5	27	14	99.1																																									






B 2: Granite Islands Coordinates, Bottom Water Chemistry and Precipitate Chemistry

Granite Islands	Sample Pictures	UTM Easting	UTM Northing	Depth (m)	DO ppm	pH	Temp (C)	millibar	µs/cm	TDS	Eh (mV)	DO (%)	Al ₂ O ₃ (%)	CaO (%)	FeO+ (%)	K ₂ O (%)	MgO (%)	MnO (%)	Na ₂ O (%)	P ₂ O ₅ (%)	TiO ₂ (%)	As (ppm)	B (ppm)	Ba (ppm)	Cd (ppm)	Ce (ppm)	Co (ppm)	Cr (ppm)	La (ppm)	Li (ppm)	Mo (ppm)	Ni (ppm)	S (ppm)	Sb (ppm)	Sr (ppm)	W (ppm)	Y (ppm)	Zn (ppm)	Zr (ppm)							
S1		501662	4962151	0.59	7.5	5.79	22.13	1005.3	21	11	103.9		9.91	0.21	9.28	0.62	0.04	28.30	0.46	0.15	0.03	686.2	86.48	3060	26.3		300.4	10.34	36.51	18.08	6.18	114.76	529.4	45.44	792.4	0.82	6.86	302.8	24.3							
S2		501667	4962151	0.78	7.62	5.77	22.09	1005.9	21	11	103.4	80																																		
S3		501672	4962151	0.91	7.69	5.77	21.57	1006.6	21	11	104.2	84.5																																		
S4		501677	4962151	2.06	7.64	5.76	21.16	1008.1	21	11	105.8	83.6																																		
Q1		501707	4962111	0.5	8.24	5.77	21.51	1010.4	21	11	13.5	91	7.93	0.23	14.57	1.08	0.15	20.62	1.36	0.18	0.13	749.6	681.8	1513.8	11.56	82.43	177.18	12.88	19.29	15.28	5.24	109.52	403.8	1.08	57.12	5.52	6.89	382.8	30.26							
Q2		501717	4962111	1.75	7.73	5.76	21.17	1010.8	22	11	117.5	87.7	8.93	0.21	18.95	1.34	0.10	20.50	1.25	0.28	0.09	906.8	742.8	2362	13.5	99.31	98.66	13.26	22.23	28.54	6.5	117.16	409	1.52	90.26	4.64	7.83	401.6	26.86							
Q3		501727	4962111	4.25	7.82	5.75	21.28	1011.3	22	11	120.6	72	10.34	0.12	17.34	1.20	0.11	18.33	1.15	0.29	0.12	723.4	176.2	1510.8	12.64	121.37	105.08	13.96	19.97	22.04	3.92	123.42	485.6		32.5	4	7.54	363	21.66							
Q7		501737	4962111	12.19	5.48	5.63	20.48	1008.9	26	13	126.5	62.5	10.98	0.14	18.98	1.38	0.11	14.87	1.50	0.33	0.13	736.2	332	1411.6	11.74	102.69	98.94	15.04	16.31	18.08	6.18	114.76	529.4		45.44	0.82	6.86	302.8	24.3							
Q8		501747	4962111	12.8	5.65	5.64	19.4	1007.4	24	12	128	62.8																																		
Q9		501767	4962111	15.24	4.72	6.15	18.11	1007.7	38	19	100.1	46.4																																		
Q10		501787	4962111	16.76	7.87	5.78	21.37	1007.9	22	11	117.1	86.3																																		
R10		501787	4962131	18.28	7.3	5.76	21.48	100.78	22	11	123	82.7																																		
R9		501767	4962131		2.7	5.88	17.96	1007.7	27	13	110.1	20.7																																		
R8		501747	4962131	21.3	7.64	5.74	21.46	1007.7	22	11	123.7	87.9																																		
R7		501737	4962131	15.24	7.78	5.75	21.48	1007.5	23	11	125.1	88																																		
R6		501727	4962131		4.55	5.58	18.58	1007.3	27	13	129.9	43.5																																		
R5		501717	4962131	7.62	7.4	5.76	21.46	1006.4	22	11	126	84.6																																		
R4		501707	4962131	4.27	6.84	5.68	18.83	1006.8	23	12	123.7	75.1																																		
R3		501697	4962131	3.35	6.79	5.98	19.43	1006.6	22	11	136.4	73	7.53	0.22	19.99	0.58	0.05	20.73	0.50	0.16	0.05	327.8	123.18	2126	14.36	117.54	249.2	15.98	28.11	16.9		129.54	497.2	0.86	44.62	2.22	7.83	420.2	6.36							
R2		501687	4962131	2.44	7.3	5.72	21.03	1007	22	11	128.9	82.5																																		
R1		501677	4962131	1.23	7.63	5.74	21.19	1008	21	11	130	85.6																																		
S5		501687	4962151	4.87	6.52	5.72	20.99	1011.1	21	11	128.4	73.7																																		
S6		501697	4962151	6.1	7.1	5.62	19.91	1011.5	22	11	133	74.9																																		
S7		501707	4962151	7.62	4.55	5.93	18.84	1001.6	24	12	130.7	45.3																																		
S8		501717	4962151	10.67	2.25	6.34	18.01	1011.3																																						
S9		501737	4962151	12.19	3.5	6.17	17.98	1010.5	34	17	51.4	32																																		
T9		501787	4962171	22.86	4.5	5.85	16.36	1009.7	30	15	93.3	47																																		
T8		501767	4962171	15.24	4.76	5.93	18.69	1009.4	28	14	89.7	45.9																																		
T7		501747	4962171	12.19	4.8	6.01	17.41	1008.9	33	17	82.4	47.4																																		
T6		501737	4962171		4.34	5.89	18.03	1008.3	27	14	100.1	38.3																																		
T5		501727	4962171	10.67	5.4	5.81	16.92	1008.7	29	14	103.7	41.1																																		
T4		501717	4962171		6.25	5.68	19.97	1008.5	23	11	124.7	64.5																																		
T3		501707	4962171	9.14	5.75	5.75	18.24	1008.2	26	13	110.5	62.9																																		
T2		501697	4962171	6.1	6.04	5.98	20.57	1007.3	21	11	128.7	66.8																																		
T1		501687	4962171	1.22	6.44	5.76	21.54	1007.1	20	10	127.9	72.5																																		



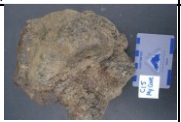





B3: Granite Islands Coordinates, Bottom Water Chemistry and Precipitate Chemistry

Granite Islands	Sample Pictures	UTM Easting	UTM Northing	Depth (m)	DO ppm	pH	Temp (C)	millibar	µs/cm	TDS	Eh (mV)	DO (%)	Al ₂ O ₃ (%)	CaO (%)	FeO+ (%)	K ₂ O (%)	MgO (%)	MnO (%)	Na ₂ O (%)	P ₂ O ₅ (%)	TiO ₂ (%)	As (ppm)	B (ppm)	Ba (ppm)	Cd (ppm)	Ce (ppm)	Co (ppm)	Cr (ppm)	La (ppm)	Li (ppm)	Mo (ppm)	Ni (ppm)	S (ppm)	Sb (ppm)	Sr (ppm)	W (ppm)	Y (ppm)	Zn (ppm)	Zr (ppm)			
U1		501707	4962191	1.22	6.28	5.77	21.87	1007.1	20	10	28.4	75.7	9.63	0.13	18.70	0.31	0.03	20.71	0.27		0.04	1683.6	144.68	1752.8	18.4	250.03	257.4	15.4	31.11	36.92	7.96	192.72	636	0.42	20.28	5.58	7.60	824.8	5.12			
U2		501717	4962191	2.44	6.12	5.71	21.17	1007.3	21	10	129.6	68																														
U3		501727	4962191	7.32	6.24	5.64	18.81	1007.5	21	11	133.1	67																														
U4		501737	4962191		5.12	5.73	17.13	1007.4	26	13	112.4	44.3																														
U5		501747	4962191	15.24	4.58	5.88	18	1007.3	25	13	131	45																														
U6		501767	4962191	19.81	4.44	5.94	17.79	1007.9	33	17	100.3	43.7	10.35	0.14	16.14	1.14	0.06	19.26	1.47		0.10	697.2	1866.2	1880.2	12.58	137.46	209.6	17.9	25.57	23.3	4.82	141.74	540.4	#VALUE!	33.76	2.38	7.51	435.4	32.82			
U7		501787	4962191		5.62	5.62	18.22	1007.1	24	12	123.5	60.1																														

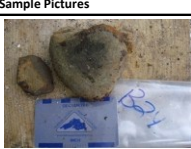





B 4: Mine Site Coordinates, Bottom Water Chemistry and Precipitate Chemistry

Sample	Sample Pictures	UTM Easting	UTM Northing	Depth (m)	DO ppm	pH	Temp (C)	millibar	µs/cm	TDS	Eh (mV)	DO (%)	Al ₂ O ₃ (%)	CO ₂ (%)	CaO (%)	FeO+ (%)	K ₂ O (%)	MgO (%)	MnO (%)	Na ₂ O (%)	P ₂ O ₅ (%)	TiO ₂ (%)	As (ppm)	B (ppm)	Ba (ppm)	Cd (ppm)	Ce (ppm)	Co (ppm)	Cr (ppm)	La (ppm)	Li (ppm)	Mo (ppm)	Nb (ppm)	Ni (ppm)	S (ppm)	Sc (ppm)	Sr (ppm)	Y (ppm)	Zn (ppm)	Zr (ppm)
ZQ		500576	4966709										18.24	5.13	0.43	7.12	1.96	0.58	16.36	2.35	0.25	0.25	4188	2214	1010		422.57	130.8	26.28	31.57	79.34	6.62	5.12	281.8	422.6	4.14	80.52	8.11	743.6	56.98
ZK		500586	4966743										6.57	4.25	0.39	17.88	0.43	0.09	34.81	0.44	0.35	0.04	6388	843.4	2556		136.31	29.84	17.7	28.57	17.28	4.8	0.68	209.4	589	1.40	132.48	8.94	502.8	11.62
ZI1		500586	4966760										9.82	7.48	0.25	17.81	0.55	0.16	23.07	1.03	0.27	0.08	15104	2086	2924		258.89	117.36	15.22	28.23	31.22	8.46	1.86	309.2	469.2	1.80	62.42	8.49	715.2	31.46
ZJ		500627	4966775										13.72	4.14	0.39	19.12	1.09	0.30	18.49	1.69	0.54	0.17	6716	1904.4	1987.2		216.63	93.52	934.8	24.26	35.98	133.4	3.08	887.6	500.8	3.14	58.36	8.20	6106	46.32
ZR		500586	4966575										18.65	4.44	0.54	9.67	2.21	0.76	11.79	2.56	0.42	0.34	1854.6	1577	1132		183.86	103.18	33.22	19.51	50.14	3.56	6	121.74	350.6	4.63	95.98	6.86	364.6	53.66








B 5: My Cove Coordinates, Bottom Water Chemistry and Precipitate Chemistry

My Cove	Sample Pictures	UTM Easting	UTM Northing	Depth (m)	Sediment Temp (°C)	DO ppm	pH	Temp (°C)	millibar	µs/cm	TDS	Eh (mV)	DO (%)	Al ₂ O ₃ (%)	CO ₂ (%)	CaO (%)	FeO+ (%)	K ₂ O (%)	MgO (%)	MnO (%)	Na ₂ O (%)	P ₂ O ₅ (%)	TiO ₂ (%)	As (ppm)	Ba (ppm)	Ce (ppm)	Co (ppm)	Cr (ppm)	La (ppm)	Li (ppm)	Mn (ppm)	Mo (ppm)	Ni (ppm)	Pb (ppm)	S (ppm)	Sr (ppm)	W (ppm)	Y (ppm)	Zn (ppm)	Zr (ppm)								
C1		503581	4958965	0.12	19.7	8.38	5.87	19.97	997.4	22	11	142.7	97.6																																			
C3		503585	4958965	0.12	19.7	8.48	5.87	20.22	997.3	22	11	146.8	94.8																																			
C4		503589	4958965	0.2	19.6	8.28	5.88	20.18	997.4	22	11	150.5	92																																			
C5		503593	4958965	0.27	19.6	8.22	5.87	20.03	997.2	22	11	154.8	90.6																																			
C6		503597	4958965	0.33	19.6	8.04	5.84	19.93	997.1	21	11	159.2	91																																			
C7		503601	4958965	0.4	19.6	8.2	5.87	19.76	997.1	21	11	160	91.1																																			
C8		503605	4958965	0.48	19.6	8.06	5.87	19.78	997.2	21	11	160.9	91.5																																			
C9		503609	4958965	0.63	19.6	8.24	5.85	19.69	997.1	21	11	161.7	90.4																																			
C10		503613	4958965	0.77	19.6	8.24	5.85	19.59	997	21	11	160.4	88.9																																			
C11		503617	4958965	0.9	19.5	8.15	5.9	19.59	997.2	22	11	151.8	91.2	7.77	2.20	0.36	10.48	0.83	0.07	15.60	1.21	0.09	0.14	697.40	3218.00	142.34	60.42	10.56	27.06	39.68	604.10	3.26	132.90	45.62	253.20	85.04	4.84	7.63	625.80	44.66								
C12		503621	4958965	0.99	19.5	7.82	6.18	19.66	997.8	22	11	118.1	87	6.50	2.79	0.16	16.82	0.39	0.03	16.11	0.88	0.13	0.06	900.20	2412.00	119.77	53.12	13.14	24.29	25.42	624.00	2.94	129.14	61.84	424.40	57.02	3.30	7.00	521.60	45.06								
C13		503625	4958965	1.04	19.5	8.11	5.95	19.71	997.9	22	11	135	91.5																																			
C14	?	503629	4958965	1.06	19.4	8.41	5.95	19.77	998.5	22	11	138.9	93.5	7.31	2.86	0.29	14.07	0.43	0.04	16.29	0.58	0.17	0.06	784.00	2918.00	163.43	67.94	11.46	30.03	44.28	630.90	3.82	152.32	55.68	391.00	50.54	3.62	8.66	716.00	34.34								
C15		503633	4958965	1.1	19.6	8.61	5.86	19.82		21	11	151	95.8	6.50	3.59	0.18	14.38	0.38	0.03	15.46	0.57	0.13	0.06	875.00	2492.00	137.97	59.96	9.24	24.66	26.34	598.50	3.56	130.28	56.70	374.40	37.68		7.17	546.20	39.66								
C16		503637	4958965	1.16	19.7	8.57	5.87	19.87	998.5	21	10	154.8	95.2																																			
C17		503641	4958965	1.2	19.6	8.61	5.81	19.95	998.4	20	10	160.4	95.4	6.68	2.97	0.33	14.19	0.37	0.04	16.76	0.44	0.13	0.07	752.20	2886.00	155.80	70.18	9.40	29.11	38.42	649.10	1.96	152.98	54.92	435.40	61.18	5.18	8.14	711.20	34.76								
C18		503645	4958965	1.23	19.6	8.34	6	20.01	998.8	22	11	132.7	93.7																																			
C19		503649	4958965	1.4	19.6	7.31	6.21	20	999.1	23	12	126.3	86.8	6.37	2.68	0.18	14.90	0.38	0.04	12.34	0.71	0.16	0.04	766.20	1643.00	95.71	32.14	9.12	19.57	19.32	477.90	3.50	102.56	48.12	324.40	32.40	3.08	6.29	424.60	41.06								
C20		503653	4958965	1.52	19.6	8.43	5.88	20.05	999.3	21	11	148.6	90.3	3.39	1.87	0.11	5.70	0.58	0.07	4.41	0.56	0.05	0.11	158.64	494.00	25.14	20.68	9.74	6.49	7.92	170.90	0.70	36.10	13.20	67.38	26.30		2.83	123.24	24.54								
C21		503657	4958965	1.59	19.5	8.42	5.85	20.01	1000.3	21	11	155.4	94	6.63	1.94	0.24	14.79	0.70	0.06	13.66	1.24	0.11	0.10	545.80	2274.00	83.34	64.88	12.60	20.46	24.64	528.90		101.26	39.82	241.40	92.92	5.10	6.49	888.20	47.40								
C22		503661	4958965	1.75	19.5	8.38	5.92	20.09	1000.2	21	10	152.8	93.2	0.20	1.65	14.66	0.52	0.05	11.03	1.06	0.12	0.14	16.38	474.80	176.51	9.68	29.98	15.37	69.12		3942.00	262.00	329.80	259.20	45.68	4.32	6.20	319.20	31.72									
C23		503665	4958965	1.84		8.29	5.88	21.53	999.5	22	11	155.2	91.6	0.44	0.00	11.88	0.71	0.08	12.62	1.62	0.15	0.16	21.06	422.20	0.94	143.60	19.28	32.96	22.09	194.78	0.18	6002.00	342.20	282.60	253.80	72.38	5.40	7.74	414.80	65.56								

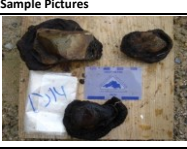




B6: My Cove Coordinates, Bottom Water Chemistry and Precipitate Chemistry

My Cove	Sample Pictures	UTM Easting	UTM Northing	Depth (m)	Sediment Temp (°C)	DO ppm	pH	Temp (°C)	millibar	µs/cm	TDS	Eh (mV)	DO (%)	Al ₂ O ₃ (%)	CO ₂ (%)	CaO (%)	FeO+ (%)	K ₂ O (%)	MgO (%)	MnO (%)	Na ₂ O (%)	P ₂ O ₅ (%)	TiO ₂ (%)	As (ppm)	Ba (ppm)	Ce (ppm)	Co (ppm)	Cr (ppm)	La (ppm)	Li (ppm)	Mn (ppm)	Mo (ppm)	Ni (ppm)	Pb (ppm)	S (ppm)	Sr (ppm)	W (ppm)	Y (ppm)	Zn (ppm)	Zr (ppm)									
B24		503661	4958975	1.62	19.5	8.25	5.86	20.18	999.5	21	11	160	94.6	6.64	3.48	0.21	12.63	0.63	0.09	16.56	1.11	0.09	0.13	541.60	1328.60	77.91	154.20	13.86	16.63	10.84	641.30	2.28	102.68	65.06	293.40	45.32	4.26	5.83	482.80	46.96									
B23		503657	4958975	1.53		8.45	5.86	20.21	999.2	21	11	160.9	94.2	7.04	1.80	0.44	11.88	0.71	0.08	12.62	1.62	0.15	0.16	442.60	2480.00	102.40	34.48	19.28	22.60	31.18	488.60	0.18	100.70	47.86	258.00	79.02	2.40	7.71	412.80	83.54									
B22		503653	4958975	1.46		8.23	5.91	20.39	999.1	21	11	151.4	93.1																																				
B21		503649	4958975	1.33		8.3	5.82	20.42	999.4	21	11	160.5	95.4	6.84	3.52	0.16	16.93	0.45	0.04	13.72	1.06	0.16	0.08	818.40	1912.40	99.74	47.02	11.76	20.80	18.16	531.30	3.02	103.28	58.06	383.40	47.36	4.34	7.06	401.20	50.12									
B20		503645	4958975	1.24		19.8	8.1	5.89	20.71	1000.3	21	11	132.7	89.7	8.08	1.94	0.25	13.33	0.66	0.06	12.75	0.99	0.10	0.17	497.00	1818.60	113.83	41.46	12.44	21.31	28.62	493.60		108.42	41.54	346.40	56.90		7.43	446.60	50.76								
B19		503641	4958975	1.18		19.7	8.55	5.94	20.94	1000	21	11	144.3	93.8																																			
B18		503637	4958975	1.15		19.8	8.58	5.88	21.13	1000.8	21	11	150.2	97.2																																			
B17		503633	4958975	0.98		19.7	8.43	6.01	21.27	1001.1	21	11	139.3	97.1	5.42	2.64	0.40	10.45	0.51	0.06	15.99	1.02	0.06	0.09	306.00	2608.00	100.17	91.56	10.22	23.86	22.14	619.00		109.16	41.32	303.60	66.84	2.64	6.74	511.60	42.58								
B16		503629	4958975	0.92		19.9	8.42	5.95	21.28	1001.4	21	11	145.6	96.8																																			
B15		503625	4958975	0.91		19.8	8.19	6.03	21.59	1001.2	21	11	138.1	96.8																																			
B14		503621	4958975	0.81		20	8.42	5.92	21.57	1001.2	21	11	148.8	96.2																																			
B13		503617	4958975	0.62		20	8.5	5.95	21.98	1001.2	21	11	150.43	99.7																																			
B12		503613	4958975	0.5		20	8.77	5.94	22.61	1001.1	21	11	153.7	100.9																																			
B11		503609	4958975	0.45		20.2	8.6	5.95	22.82	1001.3	21	11	154.2	101.9																																			
B10		503605	4958975	0.39		20.2	8.67	5.97	22.89	1001.5	21	11	154.6	100.8																																			
B9		503601	4958975	0.32		20.3	8.71	5.96	23.23	1001.7	21	11	155	101.2																																			
B8		503597	4958975	0.27		20.2	5.58	5.97	23.8	1001.9	21	11	154.7	101.5																																			
B7		503593	4958975	0.2		20.5	8.4	5.97	24.77	1002.3	21	11	154.6	102																																			
B6		503589	4958975	0.19		21.4	8.31	5.98	25.6	1002.8	21	11	154.5	101.8																																			
B5		503585	4958975	0.15		20.8	8.14	5.99	25.77	1002.9	21	11	154.2	102.9																																			
A1		503573	4958985	0.1		24.6	7.78	6.03	27.89	1003.3	22	11	119.8	97.8																																			
A2		503577	4958985	0.12		22.9	7.74	6.02	27.1	1003.3	23	11	126.2	99.1																																			
A3		503581	4958985	0.17		21.5	7.8	6	27.73	1003.4	23	11	129	98.2																																			
A4		503585	4958985	0.19		22.1	7.84	5.98	27.38	1003.3	22	11	131.6	98.6																																			
A5		503589	4958985	0.26		22.4	8.1	5.98	26.41	1003	22	11	134.2	101.8																																			
A6		503593	4958985	0.27		21.5	8.23	5.97	26.76	1003.4	22	11	131.7	101.7																																			
A7		503597	4958985	0.4		21.2	8.29	5.97	24.83	1003.4	22	11	138.8	101.1																																			
A8		503601	4958985	0.58		20.5	8.45	5.94	23.4	1002.7	22	11	142.1	98.7																																			
A9		503605	4958985	0.75		20.1	8.54	5.96	22.94	1002.4	22	11	140.3	99.7																																			
A10		503609	4958985	0.79		20.3	8.72	5.91	23.36	1002.3	23	11	143.8	99.1	5.89	2.82	0.39	15.47	0.60	0.05	14.66	0.68	0.09	0.08	661.80	2536.00		59.74	15.68		20.20	567.60	2.62	107.28	47.82	292.00	105.90	2.82		522.80	32.08								
A11		503613	4958985	0.82		20.3	8.34	5.94	22.85	1001.7	22	11	144.6	92.6																																			

B6: My Cove Coordinates, Bottom Water Chemistry and Precipitate Chemistry

A12		503617	4958985	0.82	20.2	8.6	5.98	22.16	1001.7	23	11	140.6	99.7	7.27	3.85	0.29	14.60	0.48	0.07	11.21	0.58	0.16	0.06	732.20	2400.00		33.82	11.14		38.78	433.90	4.22	109.56	45.20	376.60	85.76	3.00		516.00	26.24								
A13		503621	4958985	0.85	20.4	8.6	5.9	22.51	1001.8	22	11	147	100.4																																			
A14		503625	4958985	0.96		7.87	5.92	22.56	1001.6	22	11	137.6	94.2	6.36	2.49	0.26	9.86	0.68	0.06	12.75	0.92	0.07	0.10	380.60	1924.60		51.02	9.88		22.40	493.90	#VALUE!	92.86	34.92	284.40	56.56	2.82		417.20	36.22								
A15		503629	4958985	1.01	20.3	8.62	5.87	21.93	1001	22	11	149.8	97.3																																			
A16		503633	4958985	1.06	20.2	8.3	5.86	21.84	1001.1	22	11	151.9	93.9																																			
A17		503637	4958985	1.17	20.4	8.51	5.84	21.43	1001.3	22	11	153.9	97.6	6.30	2.71	0.16	13.17	0.35	0.03	16.07	0.28	0.09	0.04	775.00	2318.00		60.00	10.42		32.94	622.30	2.68	155.88	52.06	393.40	31.70	2.98		665.20	28.00								
A18		503641	4958985	1.28	20.3	8.55	5.83	21.33	1001.9	22	11	155.6	97.8	6.16	4.99	0.22	15.19	0.38	0.04	14.25	0.35	0.10	0.04	713.80	2280.00		58.40	14.26		27.60	551.70	3.44	125.36	54.68	383.60	49.18	3.96		591.40	26.58								
A19		503645	4958985	1.28	20.3	7.81	5.84	21.31	1001.9	22	11	153.5	89.7		0.00																																	
A20	?	503649	4958985	1.48	20.3	8.55	5.84	21.45	1001.3	22	11	154.5	95.9	6.07	3.08	0.31	19.29	0.31	0.04	11.87	1.14	0.14	0.04	861.00	1990.40		21.84	10.64		16.60	459.60	0.52	93.98	47.08	299.20	68.84	0.86		353.80	51.00								
A21		503653	4958985	1.75	19.9	8.04	5.94	21.56	1000.6	29	11	153	93.6	6.06	1.87	0.21	14.51	0.65	0.05	11.72	1.14	0.11	0.11	505.60	1750.60		56.86	11.86		16.70	454.00	0.26	77.46	37.02	273.20	73.06	1.84		286.60	49.24								
A22		503657	4958985	1.6	19.7	7.91	6.15	21.55	1000	22	11	144	86.8	6.15	2.09	0.14	14.69	0.60	0.05	9.13	1.40	0.11	0.09	345.00	1118.60		51.74	10.40		14.10	353.50	#VALUE!	68.06	36.98	241.20	51.58	1.06		256.40	46.00								
A23		503661	4958985	1.65	19.8	8	5.92	21.68	999.7	2	11	138.7	94																																			
D24		503661	4958955	1.82	20.3	8.46	5.81	21.75	1000.4	21	11	155.9	97.1																																			
D23		503657	4958955	1.74	20.2	6.7	5.9	21.34	1001.2	22	11	153.6	74.6																																			
D22		503653	4958955	1.62	20	8.2	5.87	21.57	1001.8	22	11	149.4	90.2	6.40	2.57	0.22	18.23	0.88	0.05	13.08	1.10	0.15	0.08	696.60	1675.20		55.10	9.94		14.94	506.40	2.94	83.60	50.64	299.40	93.08	2.70		276.40	40.10								
D21		503649	4958955	1.54	19.9	8.1	5.88	21.6	1001.8	22	11	150	86.5																																			
D20		503645	4958955	1.3	20.5	8.33	5.86	21.88	1001.3	22	11	149.3	86.9																																			
D19		503641	4958955	1.27	20.3	8.11	5.85	21.83	1000.8	22	11	153.7	92.8																																			
D18		503637	4958955	1.3	20.4	7.54	5.88	21.73	1000.3	22	11	151.9	87.8																																			
D17		503633	4958955	0.91	20.4	7.58	5.85	21.71	999.9	22	11	153.6	91.7																																			
D16		503629	4958955	1.04	20.5	8.45	5.84	21.74	999.5	22	11	154.7	94.2	5.68	4.07	0.20	13.82	0.42	0.04	15.12	0.40	0.08	0.04	675.20	1931.80		76.08	8.92		17.60	585.60	#VALUE!	125.14	53.94	358.60	42.16	#VALUE!		520.20	28.28								
D15		503625	4958955	1	20.9	8.2	5.85	21.93	999.3	22	11	153.9	95.6																																			








B6: My Cove Coordinates, Bottom Water Chemistry and Precipitate Chemistry

My Cove	Sample Pictures	UTM Easting	UTM Northing	Depth (m)	Sediment Temp (C)	DO ppm	pH	Temp (C)	millibar	µs/cm	TDS	Eh (mV)	DO (%)	Al ₂ O ₃ (%)	CO ₂ (%)	CaO (%)	FeO+ (%)	K ₂ O (%)	MgO (%)	MnO (%)	Na ₂ O (%)	P ₂ O ₅ (%)	TiO ₂ (%)	As (ppm)	Ba (ppm)	Ce (ppm)	Co (ppm)	Cr (ppm)	La (ppm)	Li (ppm)	Mn (ppm)	Mo (ppm)	Ni (ppm)	Pb (ppm)	S (ppm)	Sr (ppm)	W (ppm)	Y (ppm)	Zn (ppm)	Zr (ppm)			
D14		503621	4958955	0.92	20.6	8.22	5.88	22.19	999.3	22	11	152.7	94.7	5.66	3.37	0.27	13.29	0.35	0.03	15.76	0.44	0.08	0.04	731.40	2320.00		86.74	10.44		25.00	610.30	3.38	135.10	55.64	390.20	42.10	3.18		621.20	34.08			
D13		503617	4958955	0.92	21	8.23	5.88	22.17	999.3	21	10	152.4	94																														
D12		503613	4958955	0.9	20.8	8.24	5.88	22.33	999.2	22	11	153	96.4																														
D11		503609	4958955	0.84	20.7	8.21	5.94	22.67		22	11	150.2	95.3																														
D10		503605	4958955	0.77	21.1	8.39	5.91	22.67	999.1	22	11	150.1	94.8																														
D9		503601	4958955	0.65	20.9	8.18	5.93	22.57	998.8	22	11	151.3	97.2																														
D8		503597	4958955	0.4	21.8	8.21	5.97	23.52	998.4	22	11	148.7	98.2																														
D7		503593	4958955	0.3	22.6	8.22	5.97	24.56	998.4	22	11	148.6	100.5																														
D6		503589	4958955	0.26	22.8	8.11	5.98	25.02	998.3	22	11	148.7	100.2																														
D5		503585	4958955	0.2	23	8	5.98	25.25	998.2	22	11	148.6	99.3																														
D4		503581	4958955	0.15	23.8	8.6	5.98	24.51	999.8	22	11	148.7	102.6																														
D3		503577	4958955	0.11	24.3	8.07	5.97	25.51		22	11	148.9	98.5																														
E2		503577	4958945	0.11	23	8.11	6.01	27.06	1000.6	22	11	146.8	99.9																														
E3		503581	4958945	0.16	23.4	7.46	6	26.93	1001	22	11	147	93.1																														
E4		503585	4958945	0.23	23.2	7.74	5.98	25.41	1001.1	22	11	148.7	91.3																														
E5		503589	4958945	0.29	22.6	8.25	6.02	24.64	1001.4	21	11	149.1	99.7																														
E6		503593	4958945	0.43	21.9	8.65	6.06	23.62	1001.6	21	10	143	100.3																														
E7		503597	4958945	0.48	21.3	8.4	5.98	23.38	1001.7	22	11	142.6	100.4																														
E8		503601	4958945	0.63	21.6	8.34	5.9	22.29	1002	22	11	151.4	93.9																														
E9		503605	4958945	0.77	21.4	8.14	5.9	22.32	1002.4	22	11	151.4	93																														
E10		503609	4958945	0.85	20.6	7.87	5.84	22.12	1002.4	22	11	154.2	92.5																														
E11		503613	4958945	0.82	21.4	8.06	5.81	22.21	1002	22	11	153	91.5	6.31	3.37	0.42	11.15	0.68	0.07	12.34	0.98	0.07	0.09	358.20	2526.00		69.30	9.84		29.20	477.70	#VALUE!	106.14	36.36	304.80	105.38	3.26		553.20	45.28			
E12		503617	4958945	0.87	21.2	7.85	5.86	21.99	1001.7	22	11	148.5	82																														
E13		503621	4958945	0.85	21.5	8.01	5.83	22.26	1001.2	22	11	153.2	89.2	7.66	4.51	0.41	12.52	0.36	0.06	16.49	0.58	0.12	0.04	685.40	2422.00		93.26	10.96		44.76	638.70	5.64	183.26	52.76	430.80	47.26	5.84		880.40	40.14			
E14		503625	4958945	0.85	21.8	8.13	5.83	22.07	1000.5	22	11	154.6	87.6																														
E15		503629	4958945	0.87	21.1	7.84	5.83	22.16	999.9	22	11	154.6	84																														
E16		503633	4958945	0.94	22.1	7.75	5.83	22.26	999.3	22	11	154.4	91	5.62	3.23	0.23	11.39	0.26	0.03	15.67	0.37	0.06	0.03	672.20	2532.00		77.00	10.78		36.82	606.60	3.14	151.20	50.48	#NAME?	30.52	4.46		735.20	32.30			
E17		503637	4958945	0.94	21.4	7.77	5.86	22.04	999.3	22	11	149.3	88.3																														
E18		503641	4958945	0.95	21.5	8.14	5.81	22.02	999.5	22	11	154.2	94.2	7.18	3.52	0.21	12.67	0.18	0.03	17.39	0.12	0.11	0.02	1431.20	#NAME?		35.50	10.94		84.62	673.40	8.16	235.40	51.64	#NAME?	46.54	6.18		1098.00	27.90			
E19		503645	4958945	1.05		8.01	5.82	21.97	999.6	22	11	154.7	94.4																														
E20		503649	4958945	1.07	20.9	8.45	5.81	21.91	999.3	22	11	155	96.5																														
E21		503653	4958945	1.18	20.9	8.25	5.81	22.13	999.1	21	11	154.6	96.4																														
E22		503657	4958945	1.67	20.6	8.16	5.85	21.83	998.9	22	11	148.5	83.6																														
AA1		503677	4958945	6.7		7.26	5.91	21.1	1009.7	22	11	119.4	81.5																														
AA2		503677	4958955	7.62		7.38	5.96	20.91	1010	22	11	121.9	82.2																														
AA3		503677	4958965	6.7		7.15	5.91	20.99	1010.6	22	11	121.8	81.7																														


B6: My Cove Coordinates, Bottom Water Chemistry and Precipitate Chemistry

My Cove	Sample Pictures	UTM Easting	UTM Northing	Depth (m)	Sediment Temp (C)	DO ppm	pH	Temp (C)	millibar	µs/cm	TDS	Eh (mV)	DO (%)	Al ₂ O ₃ (%)	CO ₂ (%)	CaO (%)	FeO+ (%)	K ₂ O (%)	MgO (%)	MnO (%)	Na ₂ O (%)	P ₂ O ₅ (%)	TiO ₂ (%)	As (ppm)	Ba (ppm)	Ce (ppm)	Co (ppm)	Cr (ppm)	La (ppm)	Li (ppm)	Mn (ppm)	Mo (ppm)	Ni (ppm)	Pb (ppm)	S (ppm)	Sr (ppm)	W (ppm)	Y (ppm)	Zn (ppm)	Zr (ppm)												
AA3		503677	4958965	6.7		7.15	5.91	20.99	1010.6	22	11	121.8	81.7																																							
AA4		503677	4958975	6.7		7.5	5.9	21.07	1011.4	22	11	122.7	84.3																																							
AA5		503677	4958985	7.62		7.19	5.89	20.95	1011.5	22	11	122.7	80.5																																							
BB5		503697	4958985	8.23		7.23	5.84	21	1011.4	22	11	123.9	87.8																																							
BB4		503697	4958975	8.23		6.88	5.88	21.38	1010.6	22	11	123.8	77.7																																							
BB3		503697	4958965	6.87		6.87	5.9	21.01	1010.2	22	11	122.8	78.6																																							
BB2		503697	4958955	6.1		7.08	5.89	21.2	1010.4	22	11	124.8	81.5																																							
BB1		503697	4958945	9.14		6.65	5.94	21.29	1010.7	22	11	122.1	80.9																																							
CC1		503717	4958945	12.91		6.92	5.88	20.97	1011.4	22	11	123.9	78.1																																							
CC2		503717	4958955	12.91		6.72	5.8	20.58	1011.8	22	11	125	75.8																																							
CC3		503717	4958965	12.91		6.44	5.65	21.08	1010.8	22	11	126.6	66.7																																							
CC4		503717	4958975	11.58		7.15	5.83	21.17	1011.2	21	11	124.2	79.3																																							
CC5		503717	4958985	15.24		6.86	5.75	20.46	1011.9	22	11	125.6	75.5																																							









B 6 Shebandowan Island: Coordinates, Bottom Water Chemistry and Precipitate Chemistry

Sample	Sample Picture	Easting	Northing	DO_ppm	pH	Temp	Mbar	ms_cm	TDS	ORP	DO	Depth	Al ₂ O ₃ (%)	CO ₂ (%)	CaO (%)	FeO+ (%)	K ₂ O (%)	MgO (%)	MnO (%)	Na ₂ O (%)	P ₂ O ₅ (%)	TiO ₂ (%)	As (ppm)	B (ppm)	Ba (ppm)	Cd (ppm)	Ce (ppm)	Cr (ppm)	La (ppm)	Li (ppm)	Mo (ppm)	Ni (ppm)	S (ppm)	Sr (ppm)	W (ppm)	Y (ppm)	Zn (ppm)	Zr (ppm)				
SE1		702108	5386272	6.49	8	22.61	969.3	58	29	-55.7	76	2.74																														
SE2		702118	5386272	7	8.12	22.64	969.4	55	28	-55.9	76.9	2.74																														
SE3		702128	5386272	6.79	8.11	22.67	969.4	59	30	-55.1	80.5	1.82																														
SE4		702138	5386272	6.74	8.11	22.67	969.4	59	30	-55.1	80.5	1.82																														
SE5		702148	5386272	6.91	8.26	22.72	969.5	59	30	-54.8	81.1	1.22																														
SF1		702158	5386282	6.51	7.99	22.52	969.5	58	29	-55.8	78.2	4.6																														
SF2		702168	5386282	6.25	8.01	22.48	969.7	60	30	-55.8	74.8	4.6																														
SF3		702178	5386282	6.4	7.99	22.51	970.1	60	30	-56.6	75.5	5.18																														
SF4		702188	5386282	6.79	8.09	23.21	970.6	59	30	-53.3	84.2	4.88																														
SF5		702198	5386282	6.33	7.98	22.33	970.7	60		-55	77.9	5.79																														
SF6		702208	5386282	6.47	8	22.43	970.6	60	30	-54.2	77.1	4.88																														
SG1		702158	5386302	4.73	7.71	19.95	970.2	60	30	-53	49.4	8.23	6.99	7.26	1.50	32.67	0.78	0.53	10.34	1.89	1.97	0.17	27.92	906.00	5026.00		45.32	72.80	27.98	2.64	17.62	186.30	287.40	108.42				10.56	194.34	45.18		
SG2		702168	5386302	4.14	7.42	19.93	971.9	65	33	-53.2	44.2	7.92																														
SG3		702178	5386302	3.82	7.54	19.96	971.7	64	32	-51.5	34.6	7.92																														
SG4		702188	5386302	4.86	7.7	20.14	972.4	59	30	-53.7	51.1	7.62	6.41	7.48	1.20	31.13	0.75	0.44	5.84	2.16	2.76	0.12	39.56	2584.00	2606.00	13.24	27.60	31.00	20.83	2.82	12.96	136.78	277.20	89.28	3.72	7.51	156.24	54.90				
SG5		702198	5386302	3.72	5.49	20.35	972.6	65	32	-54.6	39.4	7.62																														
SG6		702208	5386302	5.29	5.17	22.34	972.9	56	29	-56.2	62.7	6.71																														
SH1		702208	5386312	2.52	7.05	16.41	973.2	66	33	-39.8	22.3	9.14	7.15	6.49	1.28	36.54	0.94	0.49	0.78	2.30	3.17	0.14	46.92	2506.00	520.80	12.70	27.37	35.46	24.06	2.82	7.56	88.22	153.86	83.60	0.44	9.06	104.62	54.14				
SH2		702198	5386312	4.85	7.58	18.14	973.7	60	30	-51.5	49	9.14	7.10	7.15	1.34	34.12	0.86	0.73	5.50	2.14	2.64	0.15	42.94	1802.60	2924.00	12.22	26.83	42.44	22.54	2.76	13.22	129.72	225.00	104.40	2.86	8.43	169.30	44.68				
SH3		702188	5386312	2.31	7.32	16.57	975.7	111	56	-53.4	18.5	10.06																														
SH4		702178	5386312	13	7.24	16.51	975.8	88	44	-49	25.7	9.75																														
SH5		702168	5386312	3.11	7.28	16.11	976.5	85	43	-44.7	27	9.75																														
SH6		702158	5386312	3.74	7.38	15.91	976.8	86	43	-56	30.2	10.06																														
SI1		702168	5386292	4.51	7.61	18.71	975.8	60	30	-54.3	47	7.92	6.62	7.99	1.38	29.61	0.79	0.56	8.97	1.86	2.25	0.16	39.32	1558.80	4240.00	14.72	27.34	49.72	21.60	2.54	15.70	152.18	283.40	97.20	2.06	7.86	191.14	31.24				
SI2		702178	5386292	6.2	8.09	22.39	975	60	30	-55.6	71.5	8.23	6.01	7.59	1.50	29.53	0.73	0.48	11.00	1.46	2.05	0.17	27.50	432.80	5642.00		42.08	39.82	26.86	2.34	18.16	152.02	312.60	102.76	0.64	10.12	179.92	40.44				
SI3		702188	5386292	3.09	7.27	16.2	973.8	74	37	-47.3	31.1	8.84	9.89	5.72	1.69	29.72	1.31	0.99	1.83	2.67	2.75	0.19	33.64	1125.00	1197.60	10.68	21.14	137.50	18.66	3.94	7.98	93.16	157.86	122.42	2.76	7.77	133.64	42.44				
SI4		702198	5386292	5.91	8.04	22.42	966.2	60	30	-55.7	69.2	7.62																														



B7: Shebandowan Island: Coordinates, Bottom Water Chemistry and Precipitate Chemistry

Sample	Sample Picture	Easting	Northing	DO_ppm	pH	Temp	Mbar	ms_cm	TDS	ORP	DO	Depth	Al ₂ O ₃ (%)	CO ₂ (%)	CaO (%)	FeO+ (%)	K ₂ O (%)	MgO (%)	MnO (%)	Na ₂ O (%)	P ₂ O ₅ (%)	TiO ₂ (%)	As (ppm)	B (ppm)	Ba (ppm)	Cd (ppm)	Ce (ppm)	Cr (ppm)	La (ppm)	Li (ppm)	Mo (ppm)	Ni (ppm)	S (ppm)	Sr (ppm)	W (ppm)	Y (ppm)	Zn (ppm)	Zr (ppm)			
SI5		702208	5386292	4.53	7.8	19.59	966.2	61	30	-54.7	47.2	7.62	6.42	7.26	1.32	33.78	0.75	0.51	5.68	1.73	2.53	0.18	31.10	1064.20	2620.00	13.22	20.63	52.34	16.94	2.38	12.68	134.78	211.40	89.18	1.64	7.09	125.26	60.22			
SI6		702208	5386292	5.42	8.03	22.43	966.1	60	30	-54.5	67.1	6.71																													
SJ1		702018	5386440	2.52	7.24	15.14	967.1	105	53	-46.2	23.1	10.97																													
SJ2		702028	5386440	1.92	6.98	14.96	964.3	91	45	-56.5	16.5	10.67																													
SJ3		702038	5386440	2.5	7.31	15.32	962.7	103	51	-46.7	24.1	10.97																													
SJ4		702048	5386440	2.41	7.36	16.41	961.6	83	42	-51.9	23.3	10.67	9.95	5.79	1.89	33.68	0.90	1.03	1.46	2.33	2.42	0.26	29.30	1370.60	1088.00	11.86	19.46	73.72	16.00	6.04	8.94	98.02	148.78	104.74	1.68	8.51	110.30	50.54			
SJ5		702058	5386440	2.48	7.34	15.4	960.6	86	43	-51.4	23.5	10.97																													
SJ6		702068	5386440	3.2	7.26	16.28	959.6	68	31	-51.8	28.7	10.37																													









B 7: Shebandowan Small Site: Coordinates, Bottom Water Chemistry and Precipitate Chemistry

Shebandowan Small Site	Sample Picture	Easting	Northing	DO_ppm	pH	Temp	Mbar	mscm	TDS	ORP	DO	Depth	Al ₂ O ₃ (%)	CO ₂ (%)	CaO (%)	FeO+ (%)	K ₂ O (%)	MgO (%)	MnO (%)	Na ₂ O (%)	P ₂ O ₅ (%)	TiO ₂ (%)	As (ppm)	B (ppm)	Ba (ppm)	Cd (ppm)	Ce (ppm)	Cr (ppm)	La (ppm)	Li (ppm)	Mo (ppm)	Ni (ppm)	S (ppm)	Sr (ppm)	W (ppm)	Y (ppm)	Zn (ppm)	Zr (ppm)			
SAA		696195	5391881	6.19	7.53	22.36	996.2	53	27		77.4	2.7																													
SAB		696195	5391891	7.08	7.43	22.38		53	27		78.6	5.49																													
SAC		696195	5391901	3.01	7.24	19.71	960	58	29		13.4	6.1	4.40	7.44	1.10	37.35	0.45	0.30	7.74	1.60	0.93	0.08	30.04	2408.00	6018.00		40.66	23.84	33.22	2.76	11.36	101.92	285.80	95.00	5.14	12.80	136.24	42.38			
SAD		696195	5391911	1.33	6.97	16.86	960	65	33		13.4	7.62	5.14	6.49	1.04	42.37	0.55	0.36	7.03	1.64	1.04	0.12	30.18	1939.40	4132.00		49.42	30.00	36.94	3.22	14.36	112.08	236.60	85.30	3.68	14.52	160.56	47.02			
SAE		696195	5391921	2.2	7.1	15.28	960.2	89	44	-58.8	19.3	9.45																													
SAF		696195	5391931	1.46	7.19	15.52	961.1	86	43	-57	13.4	10.06	8.34	8.91	1.58	36.45	0.81	0.63	1.15	2.48	1.35	0.34	25.08	1751.60	1322.40		45.00	36.56	28.28	3.16	10.12	78.72	246.00	100.74	3.48	12.94	133.40	41.08			
SAG		696195	5391941	2.76	7.26	15.13	961.7	79	39	-65.4	23.6	9.44																													
SAH		696195	5391951	1.63	7.33	15.1	962.1	93	47	-64.5	11.1	10.06																													
SA1		696205	5391801	1.56	7.25	14.97		66		-64.8	12.3	10.36																													
SA2		696205	5391811	1.1	7.19	15.02	962.1	80	40	-65.4	10.3	10.36																													
SA3		696205	5391821	0.96	7.3	14.77	962.1	87	43	-61.8	9.2	10.67																													
SA4		696205	5391831	1.17	7.26	14.94	962.3	84	40	-65.2	10.1	10.67																													
SA5		696205	5391841	1.02	7.24	15.14	962.6	83	42	-64.1	8.2	10.36																													
SA6		696205	5391851	0.83	7.14	16.5	962.4	70	35	-63.5	8.2	7.62	8.89	7.37	1.58	27.76	1.08	0.92	4.99	2.26	1.17	0.16	35.06	992.40	2938.00	10.86	42.43	36.20	26.57	4.32	10.72	87.18	264.60	102.02	2.16	10.40	136.82	26.82			
SA7		696205	5391861	5.38	7.36	19.3	962.3	58	29	-64.3	45.2	6.4	6.21	7.04	1.35	38.36	0.50	0.45	3.18	1.92	1.19	0.15	37.64	1667.80	2198.00		38.98	23.34	30.46	2.22	8.10	90.48	196.44	94.90	5.14	12.44	145.70	40.00			
SA8		696205	5391871	7.6	7.75	22.42	969.2	53	27	-63.4	90.5	5.45																													
SA9		696205	5391881	7.2	7.81	22.38	962.3	53	26	-63	81.6	3.04																													
SB1		696215	5391881	7.41	7.8	22.47	962.1	54	27	-63.5	82.6	3.04																													
SB2		696215	5391901	6.36	7.79	22.39	961.8	54	27	-64.4	82.5	5.18	3.94	7.74	0.51	46.03	0.21	0.13	4.02	1.47	0.52	0.03	49.70	1728.80	2180.00	18.00	29.86	21.64	22.83	1.02	17.96	119.26	242.60	40.14	3.38	9.74	225.40	25.18			
SB3		696215	5391921	1.2	7.24	14.88	961.9	85	42	-63.9	9.4	10.36																													
SB4		696215	5391941	0.92	7.28	14.86	962	86	43	-63.3	7.7	10.67																													
SC1		696225	5391951	0.47	7.37	15.28	956.1	96	48	-58.5	4.5	9.75																													
SC2		696225	5391941	2.27	7.32	15.26	956.4	90	45	-59.3	15.3	10.36																													
SC3		696225	5391931	1.48	7.3	14.77	956.5	86	43	-64	12.2	10.67																													
SC4		696225	5391921	0.84	7.25	14.83	956.9	84	42	-63.4	7.5	8.23	8.15	10.41	1.76	25.00	0.85	0.79	9.87	2.14	1.19	0.27	35.48	1586.20	7766.00	11.54	85.71	37.64	41.00	3.66	17.70	131.98	420.80	115.06	4.02	14.46	213.40	38.48			
SC5		696225	5391911	0.45	7.04	15.63	964.3	78	39	-37	4.4	7.62																													
SC6		696225	5391901	6.43	7.75	22.46	962.3	47	23	-63	75.5	5.18	7.64	6.56	0.90	38.05	0.54	0.44	6.10	2.46	0.43	0.07	21.96	2012.00	4246.00		60.08	24.22	29.38	4.58	14.96	121.66	302.20	129.80		11.88	190.10	59.80			


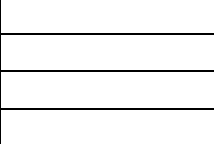



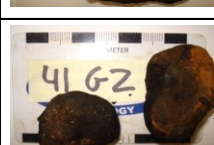
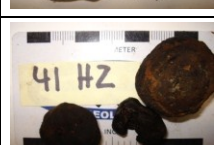



B8: Shebandowan Small Site: Coordinates, Bottom Water Chemistry and Precipitate Chemistry

Shebandowan Small Site	Sample Picture	Easting	Northing	DO_ppm	pH	Temp	Mbar	mscm	TDS	ORP	DO	Depth	Al ₂ O ₃ (%)	CO ₂ (%)	CaO (%)	FeO+ (%)	K ₂ O (%)	MgO (%)	MnO (%)	Na ₂ O (%)	P ₂ O ₅ (%)	TiO ₂ (%)	As (ppm)	B (ppm)	Ba (ppm)	Cd (ppm)	Ce (ppm)	Cr (ppm)	La (ppm)	Li (ppm)	Mo (ppm)	Ni (ppm)	S (ppm)	Sr (ppm)	W (ppm)	Y (ppm)	Zn (ppm)	Zr (ppm)		
SC7		696225	5391891	6.12	7.7	22.49	964.6	53	27	-60.3	76.9	4.56																												
SC8		696225	5391881	6.62	7.81	22.55	958.2	54	27	-60.9	70	4.27																												
SD1		696235	5391881	6.1	7.77	22.44	963.3	53	27	-66.4	74.6	5.18																												
																																								
SD2		696235	5391891	6.07	7.76	22.42	965.8	55	27	-60.9	71.9	5.18	5.10	6.01	0.36	52.35	0.28	0.14	1.25	1.55	0.57	0.05	34.66	1466.80	414.40		19.10	28.56	12.04	1.94	23.92	124.12	144.56	43.34	3.18	10.44	270.80	23.46		
SD3		696235	5391901	6.07	7.76	22.42	965.8	55	27	-60.9	71.9	6.1																												
																																								
SD4		696235	5391911	3.61	7.45	18.58	958.6	59	29	-57.4	30.5	7.31	4.73	8.73	0.87	40.52	0.42	0.30	4.69	1.55	1.41	0.11	25.40	2058.00	3982.00	17.64	40.89	22.14	27.66	1.82	15.46	105.20	218.20	69.40	3.04	10.20	206.20	38.30		
SD5		696235	5391921	6.02	7.67	22.38	959.3	35	18	-59.1	68.7	7.01																												
SD6		696235	5391931	1.2	7.3	17.2	959.8	63	33	-57.7	10.5	8.23																												
SD7		696235	5391941	7.06	7.8	22.66	961	52	26	-59.8	74.2	2.44																												






B 8: Sowden 41 Site: Coordinates, Bottom Water Chemistry and Precipitate Chemistry

Sowden 41 Bottom	Sample Pictures	UTM Easting	UTM Northing	DO ppm	pH	Temp (C)	millibar	µs/cm	TDS	Eh (mV)	DO (%)	Depth (m)	AlO ₂ (%)	CO ₂ (%)	CaO (%)	FeO+ (%)	K ₂ O (%)	MgO (%)	MnO (%)	Na ₂ O (%)	P ₂ O ₅ (%)	TiO ₂ (%)	As (ppm)	B (ppm)	Ba (ppm)	Cd (ppm)	Ce (ppm)	Co (ppm)	La (ppm)	Li (ppm)	Mo (ppm)	Ni (ppm)	S (ppm)	Sr (ppm)	Y (ppm)	Zn (ppm)	Zr (ppm)			
A		630107	5486202	7.48	7.16	19.16	972	24	12	81.9	85.7	5.5	5.91	6.60	0.97	32.52	0.83	0.24	8.28	1.71	1.46	0.06	51.98	1719.90	1643.91		113.57	93.41	14.43	48.23	2.67	76.08	129.42	250.22	13.74	102.67	35.79			
B		630107	5486192	7.45	7.19	19.22	971.5	24	12	85.3	85.7	5.5	4.06	6.05	0.58	47.63	0.44	0.14	3.27	1.28	1.24	0.04	58.69	2343.10	2184.11		110.43	80.85	8.63	44.09	3.23	93.10	49.32	55.88	12.43	115.53	51.21			
C		630107	5486182	7.68	7.18	18.83	962	24	12	91.8	82.9	5.5																												
D		630107	5486172	7.31	7.04	18.35	966.3	24	12	84.3	80.6	7.62																												
E		630107	5486162	7.44	7.13	18.31	961	24	12	156.8	84.3	8.5																												
F		630107	5486152	6.7	7.33	17.84	960	24	12	155.3	74.8	8.5																												
G		630107	5486212	6.83	7.14	18.71	957.6	24	12	68.8	79.8	8.5	19.32		2.18	19.77	2.29	0.77	0.55	4.78	1.16	0.23	51.03	2231.10	2128.11		50.33	11.97	23.47	8.67	53.18	258.60	191.72	13.69	141.27	113.45				
H		630107	5482622	7.5	7.13	18.68	957	23	12	183.3	82.9	7.9																												
I		630107	5482632	7.26	7.27	18.82	957.1	22	11	133.9	83.1	7.32	5.27	6.34	1.30	25.63	0.81	0.25	12.46	1.95	1.24	0.06	48.96	3677.80	2926.11		72.14	69.07	12.20	34.45	4.57	68.90	185.20	209.22	10.31	77.67	52.97			
J		630107	5482642	7.24	7.17	18.88	956.5	23	12		85.2	6.7																												
K		630107	5482652	7.61	7.15	18.97	956.6	23	12	192	85.6	6.1																												
L		630107	5482662	7.47	7.14	19.14	957.2	23	12	194.4	85.3	5.49	4.10	4.55	0.69	31.01	0.70	0.16	13.28	1.62	0.92	0.05	52.52	6291.80	2882.11	0.08	65.28	72.39	8.94	38.05	2.11	78.52	146.58	377.42	10.29	97.53	46.21			
M		630107	5482672	7.74	7.16	19.12	956.6	23	12	192.9	84.1	5.18																												
A1		630097	5482662	6.7	7.32	18.83	958.2	24	12	156.9	74.3	7.01																												
B1		630097	5482652	7.45	7.25	18.92	958.7	24	12	162.8	80.2	5.79	2.69	4.07	0.64	35.02	0.45	0.12	10.50	0.86	0.83	0.03	51.14	4411.80	1464.11		73.57	62.03	6.26	34.41	1.65	77.66	110.32	207.62	9.49	89.39	23.63			
C1		630097	5482642	7.47	7.18	19.16	959.1	23	12	173.8	83.8	5.49																												
D1		630097	5482632	7.03	7.16	19.12	959.9	23	12	177.8	80.3	5.49	3.40	4.84	0.83	35.25	0.59	0.15	14.41	1.28	0.91	0.03	56.86	5885.80	2432.11		90.71	75.49	7.80	39.31	1.63	84.60	152.40	302.82	10.66	112.75	30.79			
E1		630097	5482622	7.42	7.19	19.11		24	12	184.8	77.5	5.18																												
F1		630097	5486212	7.24	7.2	18.7	961.7	24	12	193.9	79.4	5.18	3.05	4.77	1.29	24.25	0.56	0.20	19.11	0.79	0.77	0.03	50.04	6293.80	1095.31	0.10	85.86	74.69	12.89	35.51	2.13	79.66	242.00	203.02	9.69	144.45	18.05			
G1		630097	5486202	7.13	7.2	18.7	962.5	24	12	189.9	70.7	5.18																												
H1		630097	5486192	7.15	7.19	18.64	962.7	24	12	198.7	77.6	5.79	6.03	4.69	0.60	45.75	0.71	0.25	2.82	2.01	1.86	0.07	60.10	1131.80	3914.11		106.14	81.73	13.86	48.05	6.27	104.28	21.82	58.08	16.20	133.17	82.95			











B9: Sowden 41 Site: Coordinates, Bottom Water Chemistry and Precipitate Chemistry

Sowden 41 Bottom	Sample Pictures	UTM Easting	UTM Northing	DO ppm	pH	Temp (C)	millibar	µs/cm	TDS	Eh (mV)	DO (%)	Depth (m)	AlO ₂ (%)	CO ₂ (%)	CaO (%)	FeO+ (%)	K ₂ O (%)	MgO (%)	MnO (%)	Na ₂ O (%)	P ₂ O ₅ (%)	TiO ₂ (%)	As (ppm)	B (ppm)	Ba (ppm)	Cd (ppm)	Ce (ppm)	Co (ppm)	La (ppm)	Li (ppm)	Mo (ppm)	Ni (ppm)	S (ppm)	Sr (ppm)	Y (ppm)	Zn (ppm)	Zr (ppm)		
I1		630097	5486182	7.2	7.18	18.46	962.8	24	12	195.9	80.2	6.1																											
J1		630097	5486172	7.27	7.1	17.97	963.6	24	12	216.5	72.4	6.71	4.87	8.58	1.40	22.99	0.68	0.25	11.97	1.62	1.10	0.06	44.95	3505.80	2002.11		45.29	70.47	15.77	33.19	2.91	73.28	214.20	125.72	10.74	175.05	61.89		
K1		630097	5486162	5.6	7.1	17.5	964	21	12	192.2	60.1	8.53																											
L1		630097	5486152	6	6.91	16.3	965.1	24	12	194.2	64.5	8.84																											
M1		630097	5486142	6.33	6.88	17.43	965.9	24	12	204.2	67.3	9.14																											
A2		630077	5482647	7.52	7.06	18.01	967.2	23	12	212.7	81.1	6.1																											
B2		630067	5482647	6.81	6.91	15.92	968.1	24	12	224.8	70.5	8.53																											
C2		630057	5482647	5.51	6.85	15.63	969.6	24	12	222.4	59.6	9.14																											
D2		630107	5482647	7.41	7.11	18.62	969.9	23	11	207.9	79.4	5.79	3.89	3.34	0.50	46.21	0.50	0.15	4.40	1.00	1.40	0.05	58.10	1171.90	1164.91		82.14	72.49	7.31	44.03	1.71	99.40	20.96	74.42	12.80	171.09	28.51		
E2		630207	5482647	7.07	7.17	18.71	970.4	23	12	222.6	78.6	5.18	3.84	6.60	0.67	34.56	0.59	0.13	12.99	1.59	1.22	0.04	55.64	5517.80	2940.11		81.00	73.65	9.00	36.39	1.89	80.22	176.26	279.02	10.46	98.45	56.43		
F2		630307	5482647	7.53	7.08	17.99	971.3	23	12	215.8	82.3	6.7	3.82	4.58	1.13	22.06	0.77	0.21	17.30	0.89	0.61	0.04	46.83	4573.80	555.51		64.14	59.73	8.37	27.99	1.97	65.10	194.70	238.22	7.63	109.39	19.07		
G2		630183	5486438	7.45	7.15	18.19	971.3	24	12	213.4	81.3	6.4	3.12	4.88	0.59	37.39	0.44	0.11	10.68	1.49	1.05	0.03	54.90	4217.80	3084.11		75.57	67.97	8.17	35.85	1.45	88.50	117.40	200.82	10.14	94.83	47.23		
H2		630203	5486438	7.39	7.15	18.08	971	24	12	219.8	73.1	6.71	6.44	5.54	0.85	40.91	0.79	0.25	5.11	1.99	1.43	0.08	57.85	1740.60	2404.11		90.14	80.27	9.20	44.31	2.37	95.76	72.94	111.10	14.29	112.77	41.57		
I2		630243	5486438	6.76	6.89	15.8	971.4	24	12	229.3	66.4	8.53																											
J2		630233	5486438	6.91	7	15.71	971.3	24	12	211.5	74.7	7.01																											
K2		630077	5482587	7.73	7.23	18.56	971.3	23	12	199.8	79.4	5.75	3.10	4.07	1.56	15.57	0.65	0.24	22.05	0.73	0.44	0.03	44.36	6473.80	597.91		72.43	65.75	19.54	29.33	2.29	68.08	268.00	204.02	7.69	173.59	8.49		
M2		630077	5482607	6.71	7.21	17.83	972.2	24	12	208.9	72.5	6.75																											
A3		630077	5482602	6.91	7.28	17.79	972.9	24	12	210.5	77.3	6.75																											
B3		630077	5482592	6.83	7.11	17.71	972.1	24	12	216.3	70.3	7	5.43	6.20	0.68	50.05	0.51	0.18	2.15	2.84	1.95	0.06	63.84	6581.10	6550.11		114.71	90.41	8.57	45.21	7.67	109.26	39.54	56.50	17.40	137.17	108.57		
C3		630077	5482582	7.94	7.18	19.13	972	23	11	205.3	85.4	7	5.57	7.04	1.38	27.02	0.89	0.29	15.00	2.27	0.80	0.06	53.28	2955.80	3908.11		72.14	67.75	7.37	33.59	3.37	69.08	193.52	217.62	10.54	87.89	62.43		



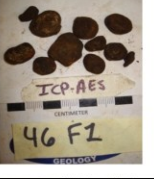





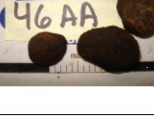

B9: Sowden 41 Site: Coordinates, Bottom Water Chemistry and Precipitate Chemistry

Sowden 41 Bottom	Sample Pictures	UTM Easting	UTM Northing	DO ppm	pH	Temp (°C)	millibar	µs/cm	TDS	Eh (mV)	DO (%)	Depth (m)	AlO ₂ (%)	CO ₂ (%)	CaO (%)	FeO+ (%)	K ₂ O (%)	MgO (%)	MnO (%)	Na ₂ O (%)	P ₂ O ₅ (%)	TiO ₂ (%)	As (ppm)	B (ppm)	Ba (ppm)	Cd (ppm)	Ce (ppm)	Co (ppm)	La (ppm)	Li (ppm)	Mo (ppm)	Ni (ppm)	S (ppm)	Sr (ppm)	Y (ppm)	Zn (ppm)	Zr (ppm)			
D3		630077	5482612	7.21	7.18	18.64	971.6	23	12	197.3	75.3	5.5																												
E3		630077	5482622	6.92	7.26	18.53	972.2	23	12	210.8	73.1	5																												
F3		630077	5482632	7.61	7.19	18.68	971.8	23	12	174.3	78.1	4.75	4.45	4.03	0.82	39.06	0.70	0.20	12.00	1.26	1.00	0.05	59.55	4743.80	1852.91		82.71	75.43	9.11	40.19	2.41	89.34	111.90	235.82	11.46	100.81	36.95			
G3		630077	5482642	7.51	7.19	18.79	971.9	23	12	198.8	85	5																												
H3		630077	5482652	6.65	7.18	18.89	971.6	23	12	208.4	74.5	5.3																												
I3		630077	5482662	7.66	7.18	18.78	971.5	23	11	186.5	83.9	4.5	5.96	5.79	0.64	46.06	0.75	0.24	5.30	1.70	1.52	0.07	62.23	3493.10	3036.11		122.71	92.07	8.57	45.21	5.93	102.22	79.54	144.50	15.20	135.39	61.35			
J3		630077	5482672	7.19	7.1	17.91	971.6	23	11	223.4	73.9	6.5	5.25	4.88	0.68	48.96	0.59	0.18	2.96	1.91	1.88	0.06	62.49	3705.10	3278.11		86.14	72.49	8.49	37.59	4.07	108.64	44.28	60.86	14.46	145.17	62.57			
K3		630077	5482682	7.21	6.92	16.28	972.1	24	12	236.2	73.1	8.4																												
M4		630087	5482692	7.22	6.94	16.01	972	24	12	232.6	76	8.75																												
N4		630087	5482692	6.82	6.96	16.51	971.3	24	12	239.3	71.6	8.25	5.18	9.24	0.89	46.67	0.60	0.18	1.28	1.37	2.82	0.05	59.05	1008.10	982.71		110.14	93.87	9.94	52.25	1.51	97.70	118.18	66.56	20.77	117.09	38.95			
O4		630087	5482642	7.86	7.16	18.64	971.5	23	11	211.8	82.1	5.5																												
P4		630087	5482632	7.97	7.16	18.97	97.4	23	11	213.1	89.6	5.25	3.75	4.55	1.01	37.80	0.62	0.20	14.48	0.81	1.13	0.04	59.84	756.50	738.51		103.86	90.51	11.91	46.23	1.75	95.26	164.44	207.62	12.63	122.09	22.05			
Q4		630087	5482622	7.86	7.18	19.13	971.1	23	11	205.8	88	4.5																												
R4		630087	5482612	8.15	7.18	19.12	970.1	23	11	196.8	88.2	4																												
S4		630087	5482602	8.15	7.18	19.12	970.1	23	11	196.8	88.2	4																												
T4		630087	5482592	8.01	7.16	18.48	969.8	23	12	198.9	87.3	5.5																												
U4		630087	5482582	7.88	7.16	18.44	969.3	24	12	208.8	86.3	5.75	4.34	7.15	0.95	34.27	0.66	0.18	10.83	1.70	0.89	0.04	53.86	2941.10	2726.11		71.86	64.13	11.26	32.57	2.11	81.58	146.16	195.40	9.43	168.09	33.83			
V4		630087	5482572	7.43	7.11	17.89	969.3	24	12	210.9	77.1	7																												
W4		630087	5482562	7.56	6.95	16.32	969.2	24	12	216.5	75.9	8																												

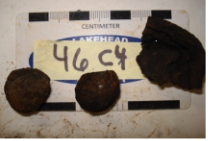





B 9: Sowden 46 Site: Coordinates, Bottom Water Chemistry and Precipitate Chemistry

Sample	Sample Pictures	UTM Easting	UTM Northing	DO ppm	pH	Temp (C)	millibar	µs/cm	TDS	Eh (mV)	DO (%)	Depth (m)	Al ₂ O ₃ (%)	CO ₂ (%)	CaO (%)	FeO+ (%)	K ₂ O (%)	MgO (%)	MnO (%)	Na ₂ O (%)	P ₂ O ₅ (%)	TiO ₂ (%)	As (ppm)	B (ppm)	Ba (ppm)	Cd (ppm)	Ce (ppm)	Co (ppm)	Cr (ppm)	La (ppm)	Li (ppm)	Mo (ppm)	Ni (ppm)	S (ppm)	Sc (ppm)	Sr (ppm)	Y (ppm)	Zn (ppm)	Zr (ppm)						
A1		626661	5486699	8.2	7.15	19.35	972	24	12	151.6	91.3	3.05																																	
B1		626661	5486689	7.96	7.05	19.2	972.7	24	12	170.2	89.1	4.88																																	
C1		626661	5486679	7.41	6.96	18.97	973.3	24	12	188.3	84	6.09	5.40	5.68	0.48	46.67	0.57	0.22	0.87	1.47	1.84	0.07	30.88	3196.00	191.22		108.86		24.44	57.43	5.60	16.50	93.42	35.38	1.89	34.12	17.57	172.64	62.50						
D1		626661	5486669	7.19	6.9	18.76	973.6	25	12	191.9	78.5	5.5																																	
E1		626661	5486659	7.15	6.87	18.39	974.7	24	12	182.3	84.2	6.7	5.14	7.48	0.39	46.26	0.47	0.20	0.82	1.28	1.75	0.06	16.66	3206.00	177.84		108.63		24.00	56.34	5.94	15.82	87.74	39.10	1.77	25.98	17.11	180.10	96.44						
F1		626661	5486649	7.23	6.88	18.43	974.1	24	12	192.9	74.3	7.01	4.80	6.78	0.54	47.16	0.47	0.21	0.59	1.61	2.47	0.06	26.12	3536.00	153.76		95.77		24.12	54.94	3.02	16.66	87.78	87.68	1.74	35.22	18.11	200.60	63.42						
G1		626661	5486639	7.04	6.81	18.38	973.7	24	12	201.1	77.1	6.7	6.02	7.19	0.85	29.10	0.81	0.24	7.58	1.92	1.05	0.06	12.94	3174.00	3542.00	0.44	96.69		18.50	43.37	4.76	12.12	71.48	128.54	1.71	143.66	9.40	244.60	60.80						
H1		626661	5486629	7.13	6.81	18.28	973.2	24	12	206.2	77.7	7.32	4.51	7.55	0.60	43.89	0.41	0.17	0.70	1.64	2.15	0.05	26.62	3666.00	151.24		116.97		20.36	62.54	4.16	16.66	80.92	87.18	1.51	39.72	18.86	173.66	71.46						
I1		626661	5486619	7.24	6.81	18.22	973.1	24	12	204.6	78.3	7.32	11.73	7.48	1.32	22.69	1.74	0.34	0.43	3.42	0.84	0.09	10.36	1717.20	298.20		49.17		21.90	27.06	3.26	8.72	42.66	45.98	2.23	129.44	7.11	253.00	53.52						
J1		626661	5486609	7.33	6.9	18.92	969.6	24	12	204.2	78.7	6.7	4.30	7.48	0.48	44.33	0.44	0.14	2.47	1.45	1.36	0.05	20.76	2686.00	1031.60		112.43		17.02	60.29	1.78	11.54	82.42	38.96	1.40	50.44	12.89	237.60	50.34						
K1		626661	5486599	7.21	6.84	18.96	964.2	24	12	202.8	84.5	6.7	5.31	6.75	0.72	38.59	0.57	0.18	5.99	2.09	1.81	0.05	25.86	4826.00	1688.40		101.31		20.94	50.94	4.32	14.72	87.44	144.56	1.66	71.28	13.83	299.00	91.24						
AA		626641	5486599	7.44	6.84	18.37	963.1	24	12	206.78	82.8	9.14	5.64	6.56	0.52	44.40	0.64	0.27	1.60	1.40	1.87	0.07	16.54	2792.00	527.20		98.09		26.12	50.09	9.14	14.60	88.48	37.72	2.03	41.12	16.20	223.20	62.82						
BB		626621	5486599		6.53	7.04	964.1	28	14	225.4		12.12																																	
CC		626601	5486599	5.75	6.72	15.55	959.9	26	13	79.9	59.9	11.28																																	
DD		626581	5486599	5.84	6.7	15.56	958	26	13	85.1	59.1	11.58																																	
EE		626641	5486699	7.03	6.84	17.36	967.3	24	12	164.9	75.5	8.23	17.50	6.97	1.29	20.94	4.58	0.41	1.91	4.88	0.76	0.23	16.22	1989.20	1467.60		104.86		14.26	44.66	7.72	4.76	42.64	64.34	1.51	325.40	8.71	185.82	134.30						

B10: Sowden 46 Site: Coordinates, Bottom Water Chemistry and Precipitate Chemistry

Sample	Sample Pictures	UTM Easting	UTM Northing	DO ppm	pH	Temp [C]	milibar	µs/cm	TDS	Eh (mV)	DO (%)	Depth (m)	Al ₂ O ₃ (%)	CO ₂ (%)	CaO (%)	FeO + (%)	K ₂ O (%)	MgO (%)	MnO (%)	Na ₂ O (%)	P ₂ O ₅ (%)	TiO ₂ (%)	As (ppm)	B (ppm)	Ba (ppm)	Cd (ppm)	Ce (ppm)	Co (ppm)	Cr (ppm)	La (ppm)	Li (ppm)	Mo (ppm)	Ni (ppm)	S (ppm)	Sc (ppm)	Sr (ppm)	Y (ppm)	Zn (ppm)	Zr (ppm)								
A1		626661	5486699	8.2	7.15	19.35	972	24	12	151.6	91.3	3.05																																			
B1		626661	5486689	7.96	7.05	19.2	972.7	24	12	170.2	89.1	4.88																																			
C1		626661	5486679	7.41	6.96	18.97	973.3	24	12	188.3	84	6.09	5.40	5.68	0.48	46.67	0.57	0.22	0.87	1.47	1.84	0.07	30.88	3196.00	191.22		108.86		24.44	57.43	5.60	16.50	93.42	35.38	1.89	34.12	17.57	172.64	62.50								
D1		626661	5486669	7.19	6.9	18.76	973.6	25	12	191.9	78.5	5.5																																			
E1		626661	5486659	7.15	6.87	18.39	974.7	24	12	182.3	84.2	6.7	5.14	7.48	0.39	46.26	0.47	0.20	0.82	1.28	1.75	0.06	16.66	3206.00	177.84		108.63		24.00	56.34	5.94	15.82	87.74	39.10	1.77	25.98	17.11	180.10	96.44								
F1		626661	5486649	7.23	6.88	18.43	974.1	24	12	192.9	74.3	7.01	4.80	6.78	0.54	47.16	0.47	0.21	0.59	1.61	2.47	0.06	26.12	3536.00	153.76		95.77		24.12	54.94	3.02	16.66	87.78	87.68	1.74	35.22	18.11	200.60	63.42								
G1		626661	5486639	7.04	6.81	18.38	973.7	24	12	201.1	77.1	6.7	6.02	7.19	0.85	29.10	0.81	0.24	7.58	1.92	1.05	0.06	12.94	3174.00	3542.00	0.44	96.69		18.50	43.37	4.76	12.12	71.48	128.54	1.71	143.66	9.40	244.60	60.80								
H1		626661	5486629	7.13	6.81	18.28	973.2	24	12	206.2	77.7	7.32	4.51	7.55	0.60	43.89	0.41	0.17	0.70	1.64	2.15	0.05	26.62	3666.00	151.24		116.97		20.36	62.54	4.16	16.66	80.92	87.18	1.51	39.72	18.86	173.66	71.46								
I1		626661	5486619	7.24	6.81	18.22	973.1	24	12	204.6	78.3	7.32	11.73	7.48	1.32	22.69	1.74	0.34	0.43	3.42	0.84	0.09	10.36	1717.20	298.20		49.17		21.90	27.06	3.26	8.72	42.66	45.98	2.23	129.44	7.11	253.00	53.52								
J1		626661	5486609	7.33	6.9	18.92	969.6	24	12	204.2	78.7	6.7	4.30	7.48	0.48	44.33	0.44	0.14	2.47	1.45	1.36	0.05	20.76	2686.00	1031.60		112.43		17.02	60.29	1.78	11.54	82.42	38.96	1.40	50.44	12.89	237.60	50.34								
K1		626661	5486599	7.21	6.84	18.96	964.2	24	12	202.8	84.5	6.7	5.31	6.75	0.72	38.59	0.57	0.18	5.99	2.09	1.81	0.05	25.86	4826.00	1688.40		101.31		20.94	50.94	4.32	14.72	87.44	144.56	1.66	71.28	13.83	299.00	91.24								
AA		626641	5486599	7.44	6.84	18.37	963.1	24	12	206.78	82.8	9.14	5.64	6.56	0.52	44.40	0.64	0.27	1.60	1.40	1.87	0.07	16.54	2792.00	527.20		98.09		26.12	50.09	9.14	14.60	88.48	37.72	2.03	41.12	16.20	223.20	62.82								
BB		626621	5486599		6.53	7.04	964.1	28	14	225.4		12.12																																			
CC		626601	5486599		5.75	6.72	15.55	959.9	26	13	79.9	59.9	11.28																																		
DD		626581	5486599		5.84	6.7	15.56	958	26	13	85.1	59.1	11.58																																		
EE		626641	5486699	7.03	6.84	17.36	967.3	24	12	164.9	75.5	8.23	17.50	6.97	1.29	20.94	4.58	0.41	1.91	4.88	0.76	0.23	16.22	1989.20	1467.60		104.86		14.26	44.66	7.72	4.76	42.64	64.34	1.51	325.40	8.71	185.82	134.30								

B10: Sowden 46 Site: Coordinates, Bottom Water Chemistry and Precipitate Chemistry

Sowden 46 Bottom	Sample Pictures	UTM Easting	UTM Northing	DO ppm	pH	Temp (C)	millibar	µs/cm	TDS	Eh (mV)	DO (%)	Depth (m)	Al ₂ O ₃ (%)	CO ₂ (%)	CaO (%)	FeO+ (%)	K ₂ O (%)	MgO (%)	MnO (%)	Mg ₂ O (%)	P ₂ O ₅ (%)	TiO ₂ (%)	As (ppm)	B (ppm)	Ba (ppm)	Cd (ppm)	Ce (ppm)	Co (ppm)	Cr (ppm)	La (ppm)	Li (ppm)	Mn (ppm)	Ni (ppm)	S (ppm)	Sc (ppm)	Sr (ppm)	Y (ppm)	Zn (ppm)	Zr (ppm)		
C4		626691	5486729	7.37	6.83	18.22	974	24	12	172.3	81	4.88	5.31	4.66	1.15	29.66	0.71	0.25	10.60	1.74	1.23	0.06	16.84	2868.00	4332.00	1.70	124.03		21.46	56.83	4.36	12.16	89.74	188.96		138.44	11.91	228.20	62.90		
D4		626691	5486739	7.41	6.79	17.91	972.1	24	12	176.7	80.9	5.49	5.64	5.46	0.61	46.31	0.62	0.26	0.63	1.74	2.46	0.07	29.06	3404.00	172.78		99.54		26.40	54.66	3.64	17.50	85.96	96.66		44.06	18.40	213.60	99.26		
E4		626691	5486749	7.27	6.82	17.74	972.4	24	12	177.7	78.6	5.79																													
F4		626691	5486759	7.16	6.83	17.56	970.9	24	12	178.5	78.4	6.1																													
G4		626691	5486769	7.52	6.85	17.66	970	24	12	181.4	83.2	6.4	5.80	4.91	0.56	44.12	0.68	0.26	1.20	1.29	1.84	0.07	18.38	1959.40	362.20		104.49		28.56	55.49	3.50	16.20	88.76	41.72		42.82	16.94	341.40	49.00		
H4		626691	5486779	7.37	6.81	17.18	969.7	25	12	185.2	80.1	7.32	3.76	6.64	2.88	46.11	0.97	0.68	6.04	2.26	0.92	0.24	28.56	3234.11	250.06		121.50		24.23	61.44	3.45	16.17	100.76	26.04		39.40	18.34	110.95	54.29		
I4		626691	5486789	6.2	6.92	16.79	969	24	13	148.9	74.7	10.06																													
A5		626671	5486709	8.31	7.08	20.15	967	24	12	156.3	95.8	2.74	4.80	7.48	0.94	35.68	0.60	0.20	6.96	1.71	1.52	0.05	10.08	2910.00	3882.00	0.24	90.74		16.78	47.20	2.24	17.54	81.70	106.44		146.34	11.29	179.32	43.94		
B5		626671	5486719	7.93	7.09	20.3	968.4	24	12	159.2	91.5	2.44	8.83	4.11	1.13	35.19	1.16	0.30	1.12	2.89	1.17	0.10	15.68	3228.00	524.80		77.71		22.56	42.54	4.42	11.12	66.12	67.32		101.38	11.51	193.32	85.12		
C5		626671	5486729	8.26	7.12	20.4	969.4	24	12	160	95.9	3.35																													
D5		626671	5486739	7.97	7.13	20.55	970.5	24	12	157.7	93.1	1.52																													

Appendix C: Precipitate geochemistry dissection values

- C1.** Data values from specific areas of a precipitate.....32
- C2.** Top and bottom precipitate values including rare earth elements.....33

C 1: Data values from specific areas of a precipitate

7 Cove Dissection	Al ₂ O ₃ (%)	CaO (%)	FeO+ (%)	K ₂ O (%)	MgO (%)	MnO (%)	Na ₂ O (%)	P ₂ O ₅ (%)	TiO ₂ (%)	As (ppm)	B (ppm)	Ba (ppm)	Cd (ppm)	Ce (ppm)	Co (ppm)	Cr (ppm)	La (ppm)	Li (ppm)	Mo (ppm)	Ni (ppm)	S (ppm)	Sc (ppm)	Sr (ppm)	Y (ppm)	Zn (ppm)	Zr (ppm)
H-13-Inside	7.35	0.13	39.02	0.26	0.06	8.33	1.85	0.55	0.04	8614.00	6248.00	6064.00		74.63		12.44	39.91	8.10	7.74	166.70	427.20	1.34	109.86	13.54	376.40	84.52
H-13-Outside	6.74	0.40	29.89	0.29	0.13	19.53	1.25	0.30	0.02	2250.00	3758.00	7792.00		117.09		12.20	40.26	69.20	9.94	168.18	769.80	1.29	224.00	13.57	544.40	54.42
My Cove Dissection	Al ₂ O ₃ (%)	CaO (%)	FeO+ (%)	K ₂ O (%)	MgO (%)	MnO (%)	Na ₂ O (%)	P ₂ O ₅ (%)	TiO ₂ (%)	As (ppm)	B (ppm)	Ba (ppm)	Cd (ppm)	Ce (ppm)	Co (ppm)	Cr (ppm)	La (ppm)	Li (ppm)	Mo (ppm)	Ni (ppm)	S (ppm)	Sc (ppm)	Sr (ppm)	Y (ppm)	Zn (ppm)	Zr (ppm)
B-20-Inside	9.85	0.30	13.36	1.02	0.08	12.28	1.96	0.15	0.22	1035.60	2138.00	2084.00	10.04	137.06	24.04	15.30	25.69	35.60	4.02	117.84	346.80	1.69	89.84	7.97	487.60	80.40
B-20- Outside	5.82	0.24	17.77	0.38	0.04	14.83	0.42	0.06	0.08	577.40	36.20	1649.00	10.94	85.43	77.40	15.90	24.74	14.02	2.90	106.04	370.00	0.91	48.42	6.66	395.40	30.36
Q-06-Inside	11.43	0.21	19.51	1.64	0.17	16.42	1.51	0.38	0.17	1264.20	875.20	2428.00	11.42	87.40	13.68	21.30	26.31	44.40	6.28	102.30	476.60		83.40	10.29	259.00	32.82
Q-06-Outside	9.11	0.16	21.19	0.91	0.10	20.35	0.97	0.33	0.10	863.00	459.40	2296.00	13.42	106.00	100.12	14.58	22.29	23.92	5.06	125.80	503.40		56.44	8.14	384.20	17.76
My Cove	Al ₂ O ₃ (%)	CaO (%)	FeO+ (%)	K ₂ O (%)	MgO (%)	MnO (%)	Na ₂ O (%)	P ₂ O ₅ (%)	TiO ₂ (%)	As (ppm)	B (ppm)	Ba (ppm)	Cd (ppm)	Ce (ppm)	Co (ppm)	Cr (ppm)	La (ppm)	Li (ppm)	Mo (ppm)	Ni (ppm)	S (ppm)	Sc (ppm)	Sr (ppm)	Y (ppm)	Zn (ppm)	Zr (ppm)
C1 -Top	12.87	0.43	17.00	0.67	0.09	18.63	1.23	0.10	0.04	1805.60	3174.00	4012.00	28.60	414.00	166.08	17.22	46.86	89.52	11.22	350.60	828.60	66.16		11.78		17.00
C2- Top	10.45	0.42	21.00	0.48	0.09	18.18	1.18	0.11	0.05	1451.00	3302.00	5800.00	19.52	272.00	103.78	17.22	46.86	90.08	9.26	284.20	590.00	69.02		12.46		34.66
C3- Top	13.40	0.54	23.85	0.36	0.08	18.76	0.75	0.17	0.04	1551.80	2910.00	3108.00	29.30	377.60	180.52	20.90	42.32	47.46	12.12	329.80	808.40	48.86		12.38		24.82
C1- Bottom	10.97	0.36	20.38	0.63	0.10	17.20	1.36	0.12	0.07	1288.20	2914.00	4662.00	16.20	239.00	123.12	16.60	35.82	67.50	8.72	237.00	609.00	78.12		10.68		31.32
C2- Bottom	11.71	0.48	21.50	0.72	0.11	18.77	1.04	0.11	0.06	1711.80	2592.00	5996.00	26.30	337.00	106.38	18.02	51.66	109.84	12.76	331.40	740.00	82.28		13.34		21.46
C3- Bottom	11.19	0.34	22.25	0.54	0.09	17.54	0.87	0.14	0.04	1795.20	1713.20	5910.00	20.64	282.40	81.02	20.12	46.88	84.86	11.84	287.20	734.00	84.82		12.76		16.36
Ave My Cove Top	12.24	0.46	20.62	0.50	0.09	18.52	1.05	0.13	0.04	1602.80	3128.67	4306.67	25.81	354.53	150.13	18.45	45.35	75.69	10.87	321.53	742.33	61.35		12.21		25.49
Ave My Cove bottom	11.29	0.39	21.38	0.63	0.10	17.84	1.09	0.12	0.06	1598.40	2406.40	5522.67	21.05	286.13	103.51	18.25	44.79	87.40	11.11	285.20	694.33	81.74		12.26		23.05
Sowden 46	Al ₂ O ₃ (%)	CaO (%)	FeO+ (%)	K ₂ O (%)	MgO (%)	MnO (%)	Na ₂ O (%)	P ₂ O ₅ (%)	TiO ₂ (%)	As (ppm)	B (ppm)	Ba (ppm)	Cd (ppm)	Ce (ppm)	Co (ppm)	Cr (ppm)	La (ppm)	Li (ppm)	Mo (ppm)	Ni (ppm)	S (ppm)	Sc (ppm)	Sr (ppm)	Y (ppm)	Zn (ppm)	Zr (ppm)
So1 -Bottom	3.43	0.86	45.08	0.55	0.16	8.58	1.09	1.87	0.03	54.82	3932.00	4504.00	9.30	117.98		18.44	52.02	4.12	15.40	102.46	230.40	168.06		10.40		39.82
So2 - Bottom	4.84	1.02	41.50	0.63	0.22	10.09	1.99	1.40	0.04	42.78	6434.00	4704.00	9.04	157.36		22.34	61.08	5.52	18.46	101.56	266.40	220.00		11.44		70.76
So1- Top	4.43	1.48	32.71	0.82	0.27	16.39	1.51	1.08	0.04	28.64	3944.00	8950.00	8.58	127.66		23.94	49.96	4.84	19.30	114.98	337.60	383.20		9.50		61.82
So2- Top	5.06	1.12	39.73	0.86	0.24	11.11	1.83	1.36	0.04	37.50	4594.00	5550.00	8.60	149.88		21.12	59.98	6.00	19.04	97.24	258.60	307.20		11.42		92.34
Ave. Sowden 46 Top	4.14	0.94	43.29	0.59	0.19	9.33	1.54	1.63	0.04	48.80	5183.00	4604.00	9.17	137.67		20.39	56.55	4.82	16.93	102.01	248.40	194.03		10.92		55.29
Ave. Sowden 46 Bottom	4.75	1.30	36.22	0.84	0.26	13.75	1.67	1.22	0.04	33.07	4269.00	7250.00	8.59	138.77		22.53	54.97	5.42	19.17	106.11	298.10	345.20		10.46		77.08

Appendix D: Geochemistry of siliclastic sediment

D1: Study Site Siliclastic Chemistry.....35

D2: My Cove pit geochemistry.....37

D1: Study Site Siliciclastic Chemistry

7 Cove Sediment	Al ₂ O ₃ (%)	CaO (%)	FeO+ (%)	K ₂ O (%)	MgO (%)	MnO (%)	Na ₂ O (%)	P ₂ O ₅ (%)	TiO ₂ (%)	As (ppm)	B (ppm)	Ba (ppm)	Ce (ppm)	Cr (ppm)	La (ppm)	Li (ppm)	Mo (ppm)	Ni (ppm)	S(ppm)	Sc (ppm)	Sr (ppm)	Y (ppm)	Zn(ppm)	Zr (ppm)
SK-03	16.81	0.71	8.58	3.33	0.66	0.41	3.77	0.37	0.28	414.00	1658.20	447.60	33.77	31.42	16.86	30.90	2.00	33.14	93.90	4.17	92.62	16.89	153.72	65.62
SK-08	15.22	0.39	10.31	1.73	0.33	0.31	2.18	0.51	0.23	440.00	1133.60	185.20	35.49	22.18	17.94	20.30	4.22	38.74	1529.80	3.11	58.22	11.43	191.48	54.16
SH-08	14.15	0.64	18.19	2.29	0.37	3.71	3.31	0.17	0.18	2352.00	2158.00	1652.40	53.60	19.20	22.23	51.96	6.16	96.50	157.40	2.43	104.10	8.91	429.40	44.58
Average in Sediment (1)	15.39	0.58	12.36	2.45	0.45	1.48	3.09	0.35	0.23	1068.67	1649.93	761.73	40.95	24.27	19.01	34.39	4.13	56.13	593.70	3.24	84.98	12.41	258.20	54.79
Ave. Precipitates, 7 Cove (2)	6.46	0.47	30.51	0.37	0.11	14.97	1.29	0.29	0.03	3975.28	3312.06	5093.05	136.40	11.26	38.76	55.51	9.04	195.24	417.60	1.14	124.42	12.02	692.94	46.28
Average of (1) and (2)	10.93	0.52	21.44	1.41	0.28	8.22	2.19	0.32	0.13	2521.97	2480.99	2927.39	88.67	17.76	28.88	44.95	6.58	125.68	505.65	2.19	104.70	12.21	475.57	50.53
Difference between (1) and (2)	8.93	0.11	-18.15	2.08	0.34	-13.50	1.80	0.06	0.19	-2906.62	-1662.12	-4331.31	-95.44	13.01	-19.75	-21.13	-4.91	-139.11	176.10	2.10	-39.44	0.39	-434.74	8.51
% Difference (+ or-) (1) and (2)	81.75	20.39	-84.68	147.09	119.01	-164.11	82.40	19.75	148.28	-115.25	-66.99	-147.96	-107.63	73.23	-68.38	-47.00	-74.62	-110.69	34.83	95.79	-37.67	3.21	-91.42	16.84
Beach Sand from My Cove (3)	8.05	0.13	0.55	2.27	0.11	0.01	2.03	0.03	0.18	7.57	42.48	-70.69	5.26	7.72	4.12	12.50	0.00	-3.15	-50.14	0.78	35.12	2.26	15.03	26.24
Average of (1) and (3)	11.72	0.36	6.46	2.36	0.28	0.74	2.56	0.19	0.20	538.12	846.21	345.52	23.11	15.99	11.56	23.44	2.06	26.49	271.78	2.01	60.05	7.33	136.62	40.51
Difference between (1) and (3)	7.34	0.44	11.81	0.18	0.34	1.46	1.06	0.32	0.05	1061.09	1607.45	832.42	35.69	16.55	14.89	21.89	4.13	59.27	643.84	2.46	49.86	10.15	243.17	28.55
% Difference (+ or-) (1) and (3)	62.65	125.02	182.82	7.43	119.83	196.47	41.44	170.08	25.15	197.19	189.96	240.92	154.47	103.46	128.75	93.36	200.00	223.76	236.90	122.35	83.03	138.38	177.99	70.46
My Cove Sediment	Al ₂ O ₃ (%)	CaO (%)	FeO+ (%)	K ₂ O (%)	MgO (%)	MnO (%)	Na ₂ O (%)	P ₂ O ₅ (%)	TiO ₂ (%)	As (ppm)	B (ppm)	Ba (ppm)	Ce (ppm)	Cr (ppm)	La (ppm)	Li (ppm)	Mo (ppm)	Ni (ppm)	S(ppm)	Sc (ppm)	Sr (ppm)	Y (ppm)	Zn(ppm)	Zr (ppm)
SC-22	14.19	0.33	5.19	2.41	0.21	0.36	3.94	0.14	0.24	169.76	1062.20	215.80	15.26	21.92	7.89	18.34	1.16	22.86	159.86	2.29	76.30	5.37	219.80	46.54
SA-10	13.53	0.38	3.24	2.45	0.22	0.33	4.13	0.16	0.24	93.22	1064.00	206.60	16.37	21.34	8.74	21.12	1.06	18.92	286.80	2.26	75.30	5.46	352.40	48.10
SC-19	13.85	0.38	2.37	2.48	0.20	0.25	4.21	0.12	0.27	74.70	425.00	229.80	16.57	16.38	8.34	19.98	0.54	13.90	211.00	2.26	82.88	5.46	60.34	41.88
SB-19	10.10	0.31	4.00	2.41	0.19	0.15	2.95	0.12	0.24	78.88	373.80	175.76	12.20	21.96	6.60	15.82	0.94	18.52	110.84	1.97	68.12	4.46	118.08	34.86
SA-10	15.23	0.37	1.72	3.69	0.18	0.19	4.54		0.21	44.16	1204.80	203.00	12.09	15.24	6.23	52.10	0.74	10.96	101.14	1.97	65.68	4.26	152.06	47.30
SC-13	12.30	0.34	1.93	2.32	0.20	0.22	3.79	0.11	0.25	52.76	1103.00	187.78	16.83	13.44	8.17	22.56	0.36	10.96	240.20	2.09	69.16	5.23	77.82	50.70
SC-18	13.51	0.37	2.70	2.39	0.21	0.30	3.91	0.14	0.29	88.68	382.80	201.40	16.89	18.34	8.60	19.44	0.26	15.46	333.80	2.31	78.00	5.80	75.10	51.64
SB-14	10.97	0.30	1.17	2.09	0.15	0.13	3.67	0.07	0.24	25.42	637.20	180.88	11.66	13.80	5.86	14.68	0.38	10.22	146.70	1.69	70.74	3.97	71.08	39.52
Average in Sediment (1)	12.96	0.35	2.79	2.53	0.20	0.24	3.89	0.12	0.25	78.45	781.60	200.13	14.73	17.80	7.55	23.01	0.68	15.23	198.79	2.10	73.27	5.00	140.84	45.07
Ave. Precipitates, My Cove (2)	6.02	1.13	12.72	0.48	0.84	13.08	0.76	0.11	1.32	640.24		2078.96	115.85	12.73	21.62	34.77	435.05	130.54	319.17		59.54	6.86	527.99	40.87
Average of (1) and (2)	9.49	0.74	7.76	1.50	0.52	6.66	2.33	0.12	0.78	359.34	781.60	1139.54	65.29	15.27	14.59	28.89	217.87	72.88	258.98	2.10	66.41	5.93	334.41	42.97
Difference (1) and (2)	6.94	-0.78	-9.93	2.05	-0.64	-12.84	3.14	0.01	-1.07	-561.79	781.60	-1878.83	-101.11	5.07	-14.07	-11.77	-434.37	-115.32	-120.38	2.10	13.73	-1.86	-387.16	4.20
% Difference (+ or-) (1) and (2)	73.14	-105.76	-128.05	136.52	-124.03	-192.76	134.84	8.09	-136.91	-156.34	100.00	-164.88	-154.87	33.24	-96.44	-40.73	-199.38	-158.22	-46.48	100.00	20.68	-31.38	-115.77	9.76
Beach Sand (3)	8.05	0.13	0.55	2.27	0.11	0.01	2.03	0.03	0.18	7.57	42.48	-70.69	5.26	7.72	4.12	12.50		-3.15	-50.14	0.78	35.12	2.26	15.03	26.24
Average of (1) and (3)	10.50	0.24	1.67	2.40	0.15	0.13	2.96	0.08	0.21	43.01	412.04	64.72	10.00	12.76	5.84	17.75	0.68	6.04	74.33	1.44	54.20	3.63	77.93	35.65
Difference between (1) and (3)	4.91	0.21	2.24	0.26	0.08	0.23	1.86	0.09	0.07	70.87	739.12	270.81	9.47	10.08	3.43	10.51	0.68	18.37	248.93	1.32	38.15	2.74	125.80	18.83
% Difference (+ or-) (1) and (3)	46.74	88.92	133.68	10.75	53.31	179.35	62.98	124.96	33.37	164.78	179.38	418.44	94.76	79.01	58.83	59.17	100.00	304.21	334.92	91.80	70.40	75.48	161.42	52.81
Bud's Cove Sediment	Al ₂ O ₃ (%)	CaO (%)	FeO+ (%)	K ₂ O (%)	MgO (%)	MnO (%)	Na ₂ O (%)	P ₂ O ₅ (%)	TiO ₂ (%)	As (ppm)	B (ppm)	Ba (ppm)	Ce (ppm)	Cr (ppm)	La (ppm)	Li (ppm)	Mo (ppm)	Ni (ppm)	S(ppm)	Sc (ppm)	Sr (ppm)	Y (ppm)	Zn(ppm)	Zr (ppm)
SN-12	13.81	0.35	3.23	2.50	0.33	0.18	3.20	0.13	0.25	90.82	332.60	217.20	16.37	20.36	8.51	17.84	0.46	16.26	95.94		75.04	5.06	66.16	45.70
SO-07	15.49	0.42	3.45	3.16	0.48	0.30	3.54	0.11	0.31	71.58	163.28	281.80	16.89	20.04	8.00	24.46	0.40	15.94	34.80		81.52	5.97	60.86	44.14
Average in Sediment (1)	14.65	0.39	3.34	2.83	0.41	0.24	3.37	0.12	0.28	81.20	247.94	249.50	16.63	20.20	8.26	21.15	0.43	16.10	65.37		78.28	5.51	63.51	44.92
Ave. Precipitates, Bud's Cove (2)	9.35	0.31	14.32	1.11	0.17	15.42	1.43	0.13	0.22	584.66	344.26	1953.97	77.76	15.76	111.08	26.98	3.13	116.58	331.53		75.52	8.60	452.18	36.45
Average of (1) and (2)	12.00	0.35	8.83	1.97	0.29	7.83	2.40	0.13	0.25	332.93	296.10	1101.74	47.19	17.98	59.67	24.07	1.78	66.34	198.45		76.90	7.06	257.85	40.68
Difference (1) and (2)	5.30	0.07	-10.97	1.72	0.24	-15.18	1.94	-0.01	0.06	-503.46	-96.32	-1704.47	-61.13	4.44	-102.82	-5.83	-2.70	-100.48	-266.16		2.76	-3.09	-388.67	8.47
% Difference (+ or-) (1) and (2)	44.14	20.64	-124.27	87.65	81.89	-193.86	80.91	-4.01	26.23	-151.22	-32.53	-154.71	-129.53	24.70	-172.32	-24.23	-151.66	-151.46	-134.12		3.59	-43.72	-150.74	20.83
Beach Sand (3)	8.05	0.13	0.55	2.27	0.11	0.01	2.03	0.03	0.18	7.57	42.48	-70.69	5.26	7.72	4.12	12.50	0.00	-3.15	-50.14		35.12	2.26	15.03	26.24
Average of (1) and (3)	11.35	0.26	1.95	2.55	0.26	0.13	2.70	0.08	0.23	44.39	145.21	89.41	10.94	13.96	6.19	16.83	0.22	6.48	7.62		56.70	3.89	39.27	35.58
Difference (1) and (3)	6.60	0.25	2.79	0.56	0.29	0.23	1.34	0.09	0.10	73.63	205.46	320.19	11.37	12.48	4.14	8.65	0.43	19.25	115.51		43.16	3.25	48.48	18.68
% Difference (+ or-) (1) and (3)	58.16	97.58	143.10	21.82	112.52	179.27	49.77	125.10	45.38	165.88	141.49	358.12	103.88	89.40	66.85	51.41	200.00	297.17	1516.87		76.12	83.72	123.44	52.50

D1: Study Site Siliciclastic Chemistry

Sowden 41 Sediment	Al ₂ O ₃ (%)	CaO (%)	FeO+ (%)	K ₂ O (%)	MgO (%)	MnO (%)	Na ₂ O (%)	P ₂ O ₅ (%)	TiO ₂ (%)	As (ppm)	B (ppm)	Ba (ppm)	Ce (ppm)	Cr (ppm)	La (ppm)	Li (ppm)	Mo (ppm)	Ni (ppm)	S(ppm)	Sr (ppm)	V(ppm)	Y (ppm)	Zn(ppm)	Zr (ppm)	
SI-00	25.72	4.21	5.73	4.00	2.50	0.19	6.65	0.32	0.38	8.14	2888.11	507.46	50.64	56.47	24.24	22.43	5.71	35.38	273.40	256.62		84.88	121.19	121.19	
SD-01	18.05	2.21	19.40	2.42	0.73	0.50	4.69	1.42	0.20	12.50	1006.31	379.66	82.10	46.03	43.70	7.59	5.29	53.30	224.60	201.62	10.49	121.65	70.93	70.93	
SI-02	15.91	1.66	26.84	1.95	0.46	0.55	4.27	1.34	0.14	13.90	2120.11	325.06	74.55	35.75	37.52	6.19	9.57	57.66	110.84	184.16	17.09	150.08	76.95	76.95	
SC-03	13.01	1.51	36.38	1.83	0.93	1.19	3.51	1.61	0.17	26.20	4360.11	379.86	97.24	40.71	48.72	12.65	18.27	91.26	98.46	110.18	31.11	247.48	111.47	111.47	
SF-04	12.17	1.20	35.56	2.25	0.21	1.69	3.39	2.06	0.07	22.16	1454.11	585.06	94.38	20.49	44.67	3.29	12.31	72.98	106.88	129.86	50.93	173.90	47.81	47.81	
Average in Sediment (1)	16.97	2.16	24.78	2.49	0.96	0.82	4.50	1.35	0.19	16.58	2365.75	435.42	79.78	39.89	39.77	10.43	10.23	62.12	162.84	176.49	27.40	155.60	85.67	85.67	
Ave. Precipitates, Sowden 41 (2)	5.12	0.95	35.27	0.71	0.22	9.72	1.64	1.24	0.06	54.92	18.98	2353.81	86.64		10.40	38.73	3.18	84.98	135.74	178.09	35.23	12.17	123.47	47.71	
Average of (1) and (2)	11.04	1.55	30.02	1.60	0.59	5.27	3.07	1.29	0.12	35.75	1192.37	1394.62	83.21	39.89	25.08	24.58	6.71	73.55	149.29	177.29	31.32	83.88	104.57	66.69	
Difference (1) and (2)	11.85	1.21	-10.48	1.78	0.74	-8.89	2.86	0.11	0.13	-38.34	2346.77	-1918.39	-6.86	39.89	29.37	-28.30	7.06	-22.86	27.10	-1.60	-7.83	143.42	-37.80	37.96	
% Difference (+ or -) (1) and (2)	107.31	77.60	-34.92	110.98	125.59	-168.70	93.06	8.88	108.70	-107.25	196.82	-137.56	-8.24	100.00	117.09	-115.15	105.23	-31.08	18.15	-0.90	-25.00	170.98	-36.15	56.93	
Beach Sand (3)	8.05	0.13	0.55	2.27	0.11	0.01	2.03	0.03	0.18	7.57	42.48	-70.69	5.26	7.72	4.12	12.50	0.00	-3.15	-50.14	0.78	35.12	2.26	15.03	26.24	
Average of (1) and (3)	12.51	1.15	12.67	2.38	0.54	0.42	3.27	0.69	0.18	12.08	1204.12	182.37	42.52	23.81	21.94	11.46	5.12	29.48	56.35	88.63	31.26	78.93	50.35	55.96	
Difference (1) and (3)	8.92	2.02	24.23	0.22	0.85	0.81	2.47	1.32	0.01	9.01	2323.27	506.11	74.52	32.17	35.65	-2.07	10.23	65.26	212.98	175.71	-7.72	153.34	70.64	59.43	
% Difference (+ or -) (1) and (3)	71.31	176.71	191.24	9.08	157.90	193.73	75.76	191.78	7.92	74.58	192.94	277.52	175.26	135.14	162.45	-18.09	200.00	221.34	377.97	198.24	-24.69	194.27	140.29	106.21	
Sowden 46 Sediment	Al ₂ O ₃ (%)	CaO (%)	FeO+ (%)	K ₂ O (%)	MgO (%)	MnO (%)	Na ₂ O (%)	P ₂ O ₅ (%)	TiO ₂ (%)	As (ppm)	B (ppm)	Ba (ppm)	Ce (ppm)	Cr (ppm)	La (ppm)	Li (ppm)	Mo (ppm)	Ni (ppm)	S(ppm)	Sr (ppm)	V(ppm)	Y (ppm)	Zn(ppm)	Zr (ppm)	
C1	14.56	10.27	12.21	6.62	1.66	1.36	8.63	0.30	0.36	18.12	1988.11	422.26	35.70	23.93	17.04	5.05	3.91	31.86	62.46	229.02		90.36	71.25	71.25	
CC	15.36	12.44	9.77	5.04	4.45	1.56	6.81	0.25	1.09	10.92	2072.11	487.46	70.21	49.85	34.98	17.69	0.79	33.82	560.00	199.46		159.79	86.25	86.25	
FF	5.67	4.95	44.33	1.46	0.88	3.82	3.49	1.24	0.27	36.06	3932.11	186.20	115.81	28.33	61.52	5.37	16.59	91.66	92.54	75.08	114.35	169.62	98.01	98.01	
HH	13.27	9.06	21.32	6.82	1.72	10.06	7.07	0.41	0.31	14.68	1262.11	1039.26	70.78	27.97	32.70	5.33	9.79	50.34	50.24	201.62		124.02	53.85	53.85	
D2	10.71	8.01	28.15	4.39	1.77	4.40	5.77	0.70	0.45	14.10	2212.11	516.26	85.84	32.27	42.50	6.29	9.41	68.82	282.40	145.64	5.23	170.13	53.43	53.43	
G2	7.26	5.11	44.26	2.19	2.16	4.41	4.61	0.94	0.47	24.60	6110.11	249.06	106.10	39.31	56.90	9.51	15.01	105.36	59.30	71.76	38.77	213.53	108.19	108.19	
H2	6.92	6.33	35.43	2.01	1.43	3.42	4.23	0.96	0.38	20.76	3138.11	226.46	87.21	25.57	44.95	4.31	16.65	86.78	83.94	101.52	54.93	185.65	64.51	64.51	
D3	11.28	9.25	21.75	3.87	1.59	1.93	6.91	0.65	0.45	12.02	2786.11	322.86	51.30	37.63	26.75	4.79	6.61	51.02	63.76	195.12		128.33	75.31	75.31	
G3	13.46	11.80	15.98	4.34	2.31	1.44	8.06	0.51	0.56	15.56	2200.11	359.46	49.72	32.27	24.61	7.19	3.29	37.70	92.44	234.62		87.85	77.13	77.13	
A4	11.09	7.72	26.50	4.61	1.28	1.96	6.02	0.50	0.40	21.08	779.11	293.46	44.24	24.71	22.58	3.85	8.23	56.40	38.28	166.04		124.39	49.09	49.09	
F4	4.32	3.00	51.59	0.99	0.82	5.31	2.23	1.03	0.24	25.64	3022.11	206.06	115.30	31.11	62.47	5.85	18.73	115.74	44.48	39.30	82.59	222.25	64.73	64.73	
I4	15.26	13.04	7.98	4.92	4.00	1.27	7.00	0.20	1.08	6.88	768.31	421.26	60.04	43.09	28.87	14.07	0.31	27.76	433.40	224.62		113.68	85.23	85.23	
A5	7.16	7.07	33.63	2.25	1.53	17.20	3.73	0.92	0.43	22.78	1951.31	1073.66	127.87	26.05	73.72	5.63	14.39	75.90	212.40	126.62	32.93	166.48	69.89	69.89	
Average in Sediment (1)	10.49	8.31	27.15	3.81	1.97	4.47	5.74	0.66	0.50	18.71	2478.61	446.44	78.47	32.47	40.74	7.30	9.52	64.09	159.66	154.65	54.80	150.47	73.61	73.61	
Ave. Precipitates, Sowden 46 (2)	5.96	0.82	39.28	0.82	0.24	3.38	1.90	1.58	0.07	20.72	3013.96	1307.94	102.88	21.01	52.59	3.90	14.12	80.24	85.99	85.93	39.40	14.00	211.41	65.02	
Average of (1) and (2)	8.22	4.57	33.21	2.32	1.11	3.93	3.82	1.12	0.29	19.71	2746.29	877.19	90.67	26.74	46.67	5.60	11.82	72.17	122.83	120.29	47.10	82.23	142.51	69.31	
Difference (1) and (2)	4.53	7.49	-12.13	2.98	1.73	1.09	3.84	-0.92	0.42	-2.01	-535.36	-861.50	-24.41	11.46	-11.86	3.40	-4.60	-16.15	73.68	68.72	15.39	136.47	-137.81	8.58	
% Difference (+ or -) (1) and (2)	55.04	163.91	-36.52	128.84	156.30	27.77	100.56	-81.70	148.17	-10.18	-19.49	-98.21	-26.92	42.84	-25.41	60.77	-38.94	-22.38	59.99	57.13	32.68	165.95	-96.70	12.38	
Beach Sand (3)	8.05	0.13	0.55	2.27	0.11	0.01	2.03	0.03	0.18	7.57	42.48	-70.69	5.26	7.72	4.12	12.50	0.00	-3.15	-50.14	0.78	35.12	2.26	15.03	26.24	
Average of (1) and (3)	9.27	4.22	13.85	3.04	1.04	2.24	3.88	0.35	0.34	13.14	1260.54	187.88	41.86	20.10	22.43	9.90	4.76	30.47	54.76	77.71	44.96	76.36	44.32	49.92	
Difference (1) and (3)	2.44	8.18	26.59	1.53	1.86	4.46	3.71	0.63	0.32	11.13	2436.13	517.13	73.21	24.75	36.62	-5.20	9.52	67.24	209.80	153.87	19.68	148.21	58.57	47.37	
% Difference (+ or -) (1) and (3)	26.30	193.68	191.99	50.47	178.23	198.83	95.48	183.60	95.51	84.73	193.26	275.25	174.87	123.17	163.26	-52.54	200.00	220.65	383.12	197.99	43.77	194.08	132.16	94.88	

D 2: My Cove pit geochemistry

Sample Labels	Al ₂ O ₃	CaO	FeO+	K ₂ O	MgO	MnO	Na ₂ O	P ₂ O ₅	TiO ₂	As	B	Ce
A	8.05	0.13	0.55	2.27	0.11	0.01	2.03	0.03	0.18	7.57	42.48	5.26
AB	10.47	0.17	1.01	3.08	0.21	0.03	2.47	0.06	0.25	12.35	49.90	9.46
C	14.91	0.35	1.41	3.25	0.40	0.02	3.20	0.12	0.28	11.35	432.44	19.50
CD	14.55	0.29	1.17	2.92	0.33	0.02	3.24	0.08	0.25	11.53	916.84	
D	13.58	0.26	1.22	3.23	0.33	0.02	3.08	0.11	0.23	10.55	337.64	14.96
E	15.41	0.40	1.95	3.50	0.58	0.04	3.58	0.13	0.34	16.75	457.04	20.00
F	17.91	0.59	2.36	3.99	0.78	0.05	3.99	0.18	0.39	17.15	432.04	24.74
G	0.22	2.63	26.97	0.04	2.21	0.37	0.24	0.04	0.01	4.09	662.64	-0.22

Sample Labels	Cr	La	Li	Mo	Ni	Sc	Sr	Y	Zn	Zr
A	7.72	4.12	12.50	0.00		0.78	35.12	2.26	15.03	26.24
AB	15.88	5.34	18.46	0.54		1.38	47.16	3.08	17.95	37.72
C	19.10	11.08	23.88		8.79	2.68	71.14	9.26	24.45	71.86
CD	14.54	9.18	22.00		16.85	2.26	64.52	9.26	21.49	59.78
D	13.48	8.94	20.62	0.44	23.35	2.08	59.28	7.36	20.15	62.94
E	18.98	11.56	38.92	0.40	8.59	3.44	76.52	8.28	33.17	65.80
F	23.52	13.00	42.30	0.00	9.49	4.54	87.54	9.80	41.23	77.00
G	3.54	4.20	4.04	2.66	46.33	0.48	14.84	4.76	42.59	17.54

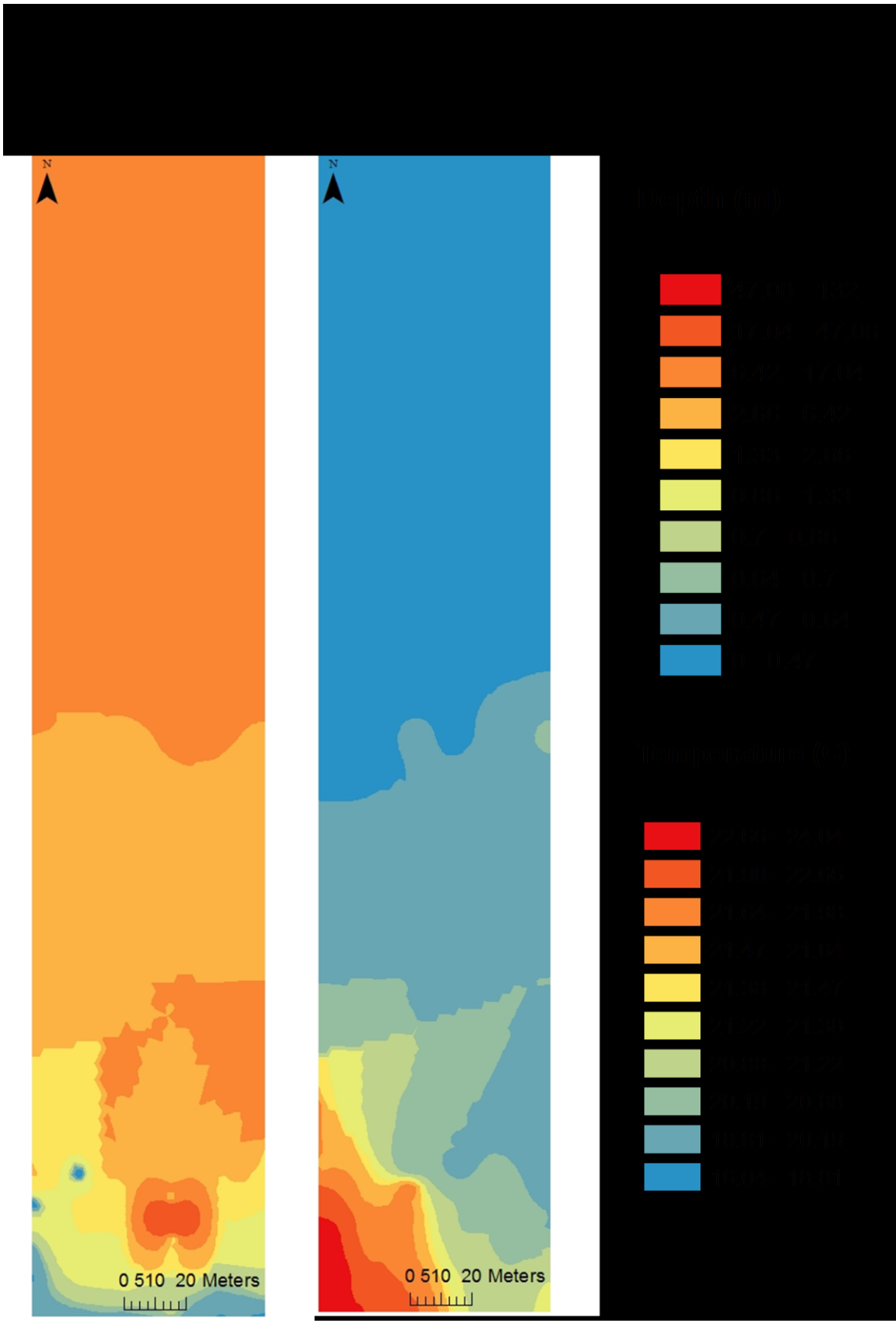
Appendix E: Water analysis Data

E1: Water elemental chemistry data.....	39
E2: Water analysis maps	
E2.1: Depth, Temperature and Dissolved Oxygen.....	40
E2.2: Eh and pH Maps. Sowden 41 Site and Shebandowan Small Site not included.....	47

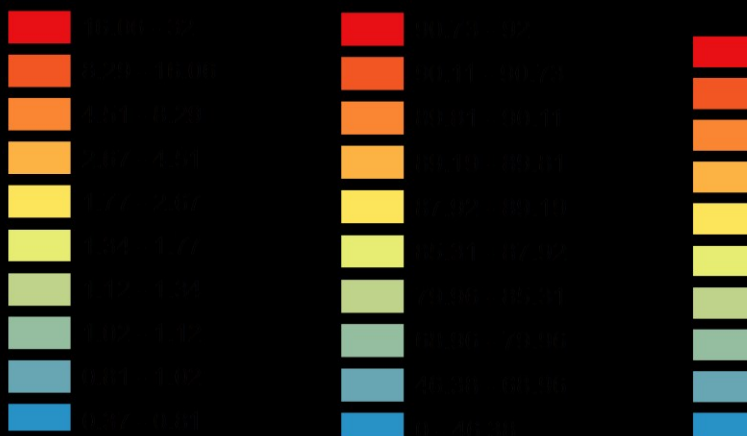
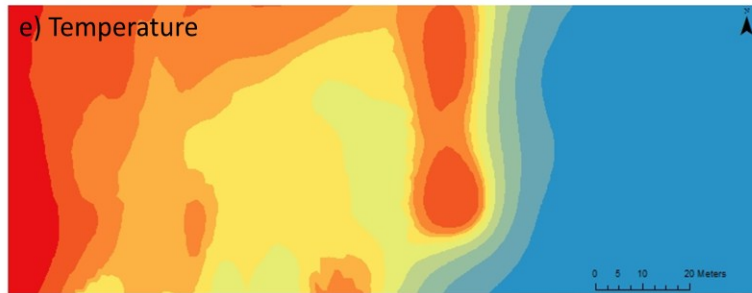
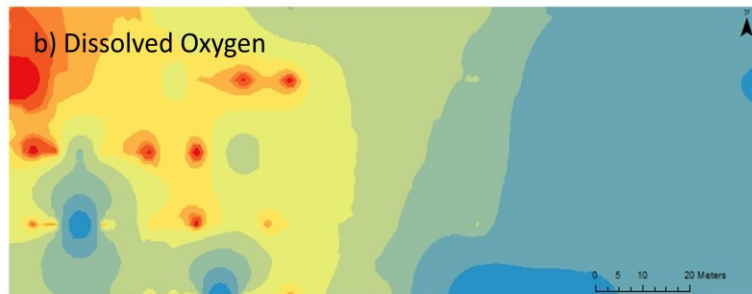
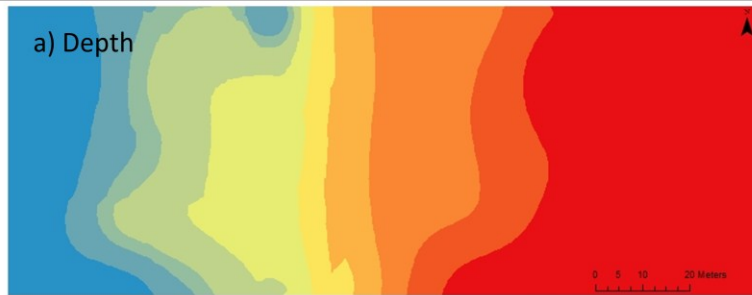
E 1: Water elemental chemistry data

Lake Charlotte	UNITS	7 Cove approx. 9m	7 Cove at approx. 12m	Dug well sample at Bud's Cove	Mine/Bat Cave Entrance	7 Cove at 1.7m	Pit at water table	MINE	Granite Islands at 2m
Total Aluminum	mg/L	1.206	0.163	0.114	0.151	0.150	2.683	0.013	0.170
Total Arsenic	mg/L	0.006	<DL	<DL	<DL	<DL	<DL	0.257	<DL
Total Barium	mg/L	0.011	0.004	0.013	0.004	0.004	0.013	<DL	0.004
Total Beryllium	mg/L	0.0001	<DL	<DL	<DL	<DL	0.0001	<DL	<DL
Total Calcium	mg/L	1.143	0.978	24.372	0.916	0.990	2.511	9.741	0.969
Total Cadmium	mg/L	0.0003	<DL	<DL	<DL	<DL	<DL	<DL	<DL
Total Cobalt	mg/L	0.0008	<DL	<DL	<DL	<DL	<DL	<DL	<DL
Total Chromium	mg/L	0.0007	0.0002	0.0004	0.0002	0.0002	0.0011	0.0002	0.0021
Total Copper	mg/L	0.0013	0.0003	0.0016	0.0004	0.0004	0.0059	0.0003	0.0016
Total Iron	mg/L	1.2610	0.1677	0.5392	0.1514	0.1321	0.7579	0.0068	0.1627
Total Potassium	mg/L	0.276	0.255	2.050	0.241	0.251	0.561	0.582	0.289
Total Lithium	mg/L	<DL	<DL	<DL	<DL	<DL	<DL	0.085	<DL
Total Magnesium	mg/L	0.462	0.413	0.754	0.394	0.410	0.841	1.210	0.405
Total Manganese	mg/L	0.5707	0.0514	0.1645	0.0356	0.0379	0.0295	0.0017	0.0414
Total Molybdenum	mg/L	<DL	<DL	<DL	<DL	<DL	<DL	<DL	<DL
Total Sodium	mg/L	2.448	2.524	3.678	2.414	2.512	3.375	4.193	2.514
Total Nickel	mg/L	0.0014	0.0006	0.0002	0.0004	0.0008	0.0009	0.0008	0.0005
Total Phosphorus	mg/L	0.015	<DL	0.035	<DL	<DL	0.061	0.014	<DL
Total Lead	mg/L	0.0038	<DL	<DL	<DL	<DL	<DL	<DL	<DL
Total Sulfur	mg/L	0.591	0.594	1.246	0.579	0.586	1.784	2.761	0.599
Total Antimony	mg/L	<DL	<DL	<DL	<DL	<DL	<DL	<DL	<DL
Total Selenium	mg/L	<DL	<DL	<DL	<DL	<DL	<DL	<DL	<DL
Total Strontium	mg/L	<DL	<DL	0.083	<DL	<DL	0.013	0.037	<DL
Total Titanium	mg/L	0.012	<DL	<DL	<DL	<DL	0.025	<DL	<DL
Total Thallium	mg/L	<DL	<DL	<DL	<DL	<DL	<DL	<DL	<DL
Total Vanadium	mg/L	<DL	<DL	<DL	<DL	<DL	<DL	<DL	<DL
Total Zinc	mg/L	0.0215	0.0146	0.0393	0.0162	0.0137	0.0127	0.0091	0.0271
Sowden Lake	UNITS	41-A at 5.5m	41-A2 at 6m	41-F at 8.5m	41-H at 7m	46-DD at 11.5m	46-D2 at 4.5m		
WICP3AL	mg/L	0.079	0.085	0.169	0.084	0.101	0.113		
WICP3AS	mg/L	<DL	<DL	<DL	<DL	<DL	<DL		
WICP3BA	mg/L	0.005	0.006	0.008	0.006	0.006	0.006		
WICP3BE	mg/L	<DL	<DL	<DL	<DL	<DL	<DL		
WICP3CA	mg/L	4.549	4.618	4.640	4.535	4.562	4.473		
WICP3CD	mg/L	<DL	<DL	0.0002	<DL	<DL	<DL		
WICP3CO	mg/L	<DL	0.0002	<DL	0.0001	<DL	<DL		
WICP3CR	mg/L	0.0003	0.0003	0.0005	0.0004	0.0004	0.0004		
WICP3CU	mg/L	0.0005	0.0009	0.0006	0.0010	0.0007	0.0007		
WICP3FE	mg/L	0.4445	0.4828	0.7555	0.4577	0.5056	0.5514		
WICP3K	mg/L	0.569	0.555	0.560	0.544	0.549	0.517		
WICP3LI	mg/L	<DL	<DL	<DL	<DL	<DL	<DL		
WICP3MG	mg/L	1.077	1.099	1.109	1.085	1.093	1.064		
WICP3MN	mg/L	0.0118	0.0152	0.1075	0.0152	0.0206	0.0214		
WICP3MO	mg/L	<DL	<DL	<DL	<DL	<DL	<DL		
WICP3NA	mg/L	1.178	1.196	1.194	1.180	1.172	1.121		
WICP3NI	mg/L	0.0007	0.0011	0.0006	0.0007	0.0008	0.0007		
WTOTP	mg/L	0.020	0.016	0.019	0.012	0.024	0.020		
WICP3PB	mg/L	<DL	<DL	<DL	<DL	<DL	<DL		
WICP3S	mg/L	0.492	0.499	0.496	0.501	0.515	0.503		
WICP3SB	mg/L	<DL	<DL	<DL	<DL	<DL	<DL		
WICP3SE	mg/L	<DL	<DL	<DL	<DL	<DL	<DL		
WICP3SN	mg/L	<DL	<DL	<DL	<DL	<DL	<DL		
WICP3SR	mg/L	0.012	0.013	0.013	0.012	0.013	0.012		
WICP3TI	mg/L	<DL	<DL	<DL	<DL	<DL	<DL		
WICP3TL	mg/L	<DL	<DL	<DL	<DL	<DL	<DL		
WICP3V	mg/L	<DL	<DL	<DL	<DL	<DL	<DL		
WICP3ZN	mg/L	0.0268	0.0281	0.0186	0.0188	0.0213	0.0224		
WICP3P	mg/L	<DL	0.017	0.024	0.018	0.019	0.018		
Shebanodowan	UNITS	Small Site	Island Site						
WICP3AL	mg/L	0.008	0.019						
WICP3AS	mg/L	<DL	<DL						
WICP3BA	mg/L	0.007	0.008						
WICP3BE	mg/L	<DL	<DL						
WICP3CA	mg/L	8.778	8.026						
WICP3CD	mg/L	<DL	<DL						
WICP3CO	mg/L	<DL	<DL						
WICP3CR	mg/L	<DL	<DL						
WICP3CU	mg/L	<DL	<DL						
WICP3FE	mg/L	0.0343	0.0540						
WICP3K	mg/L	0.560	0.598						
WICP3LI	mg/L	<DL	<DL						
WICP3MG	mg/L	1.554	1.489						
WICP3MN	mg/L	0.0132	0.0117						
WICP3MO	mg/L	<DL	<DL						
WICP3NA	mg/L	2.157	1.921						
WICP3NI	mg/L	0.0009	0.0006						
WICP3P	mg/L	<DL	<DL						
WICP3PB	mg/L	<DL	<DL						
WICP3S	mg/L	0.858	0.696						
WICP3SB	mg/L	<DL	<DL						
WICP3SE	mg/L	<DL	<DL						
WICP3SN	mg/L	<DL	<DL						
WICP3SR	mg/L	0.017	0.016						
WICP3TI	mg/L	<DL	<DL						
WICP3TL	mg/L	<DL	<DL						
WICP3V	mg/L	<DL	<DL						
WICP3ZN	mg/L	0.0107	0.0216						

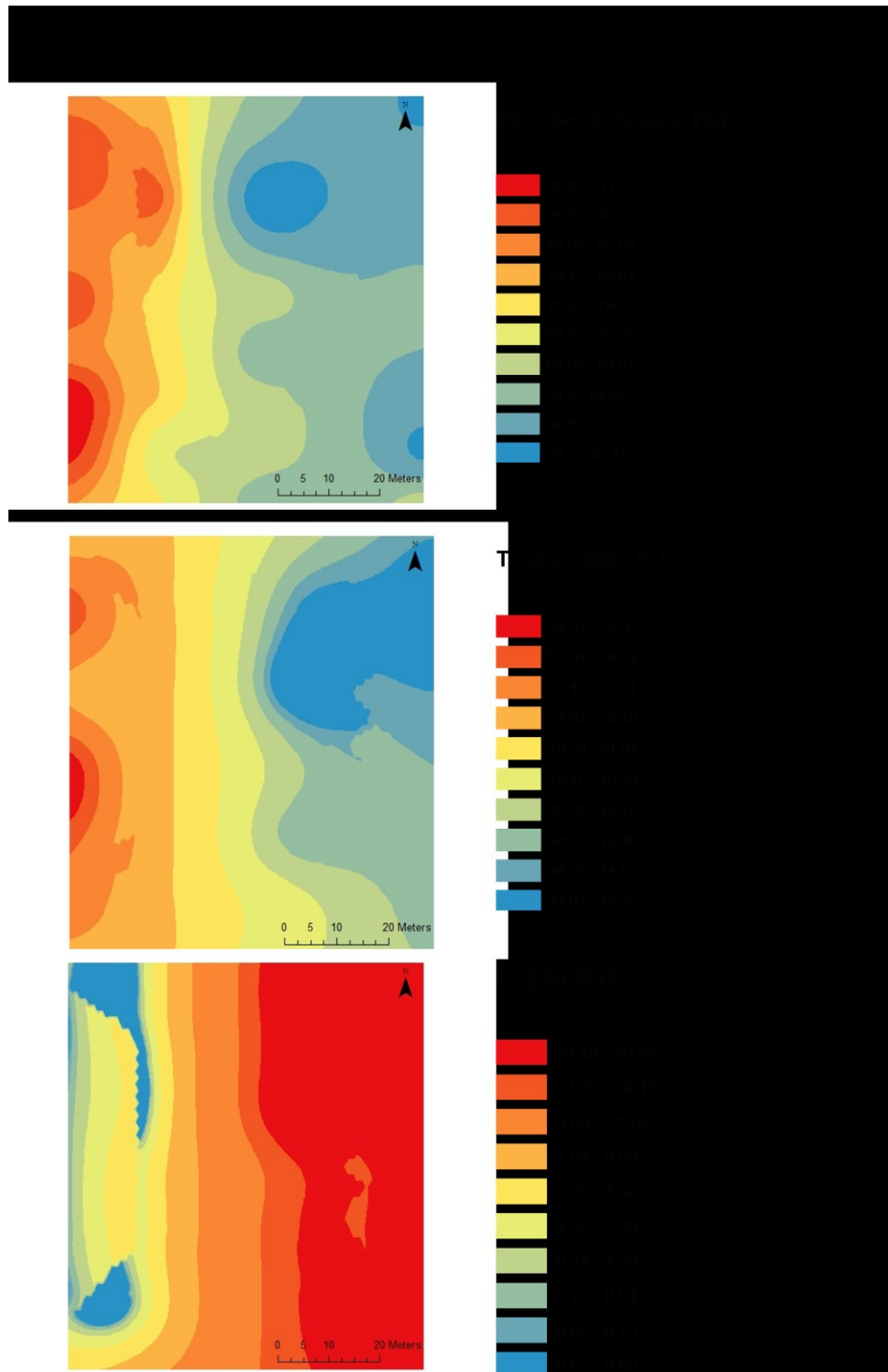
E 2.1: Depth, Temperature and Dissolved Oxygen



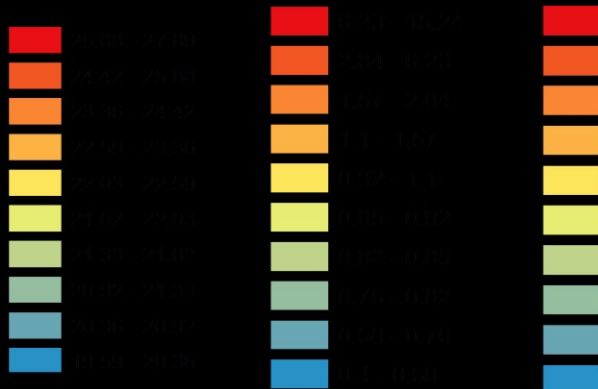
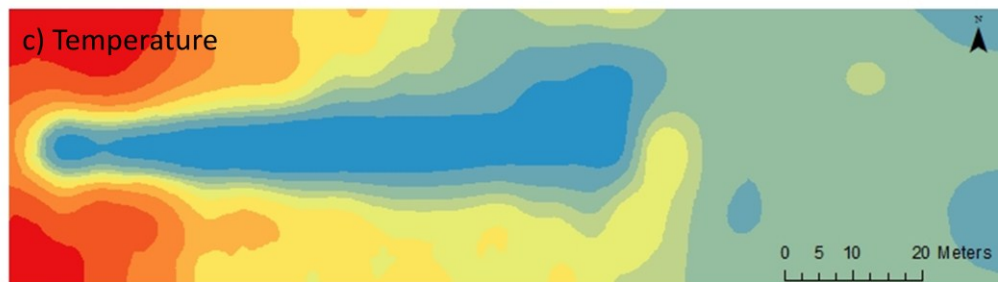
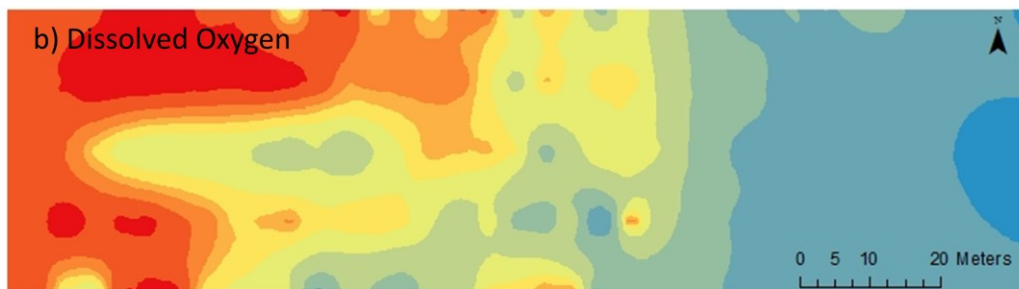
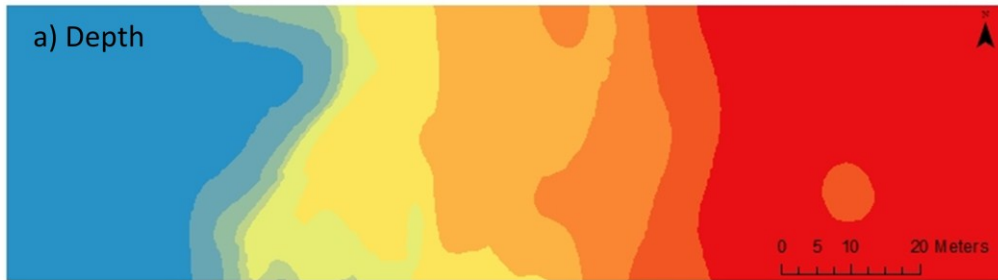
E2.1: Depth, Temperature and Dissolved Oxygen



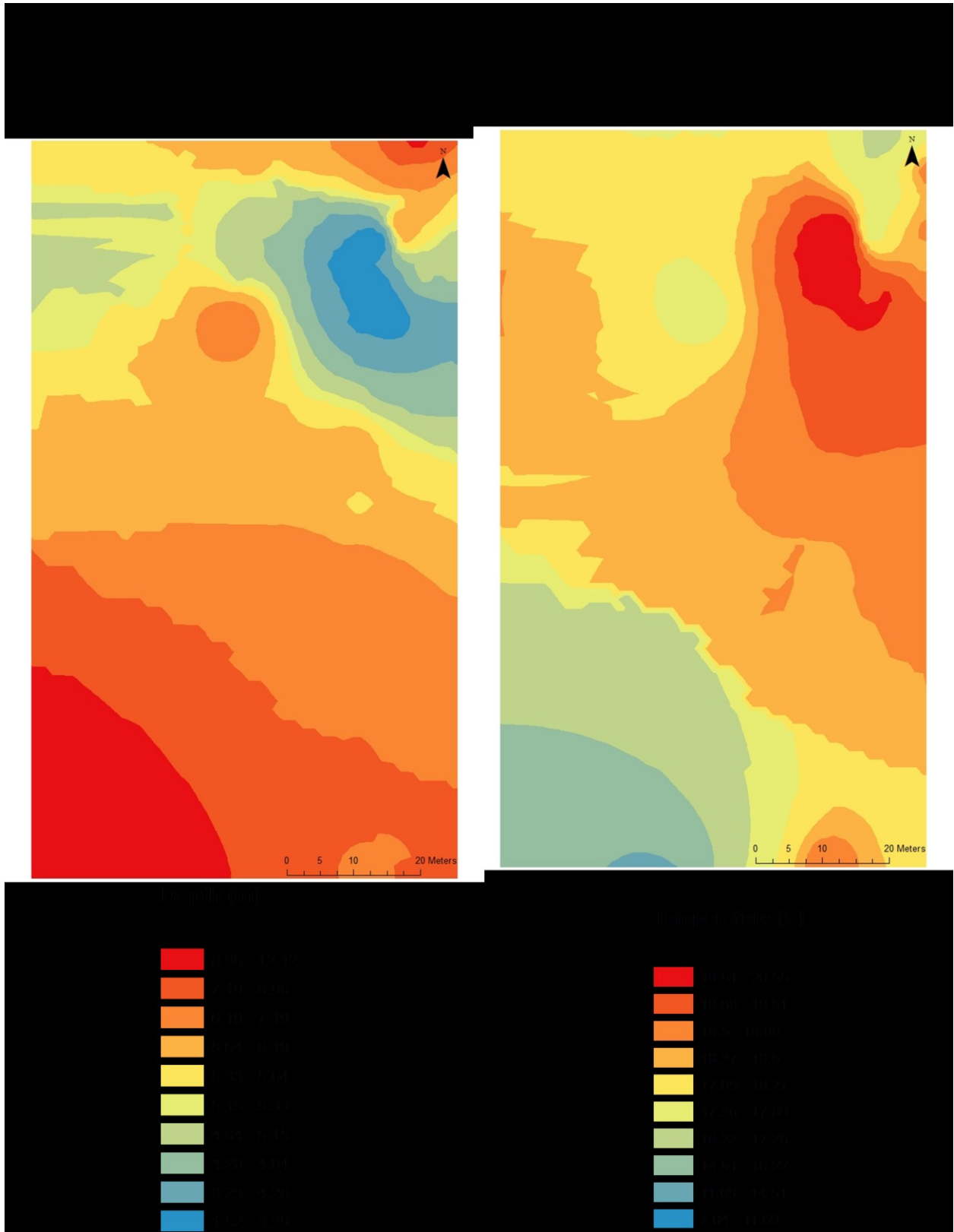
E2.1: Depth, Temperature and Dissolved Oxygen



E2.1: Depth, Temperature and Dissolved Oxygen

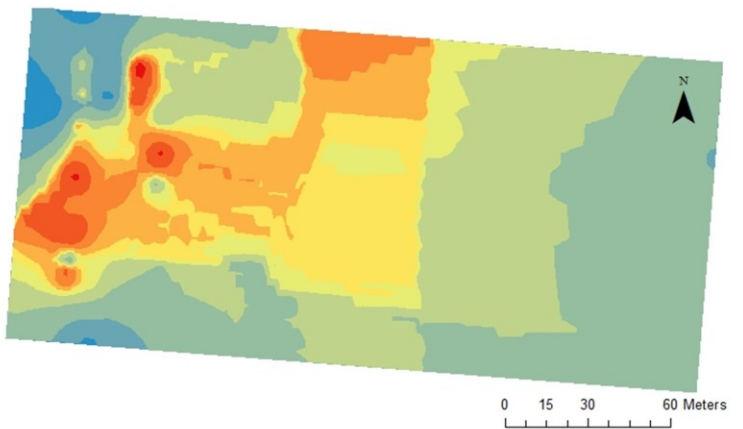
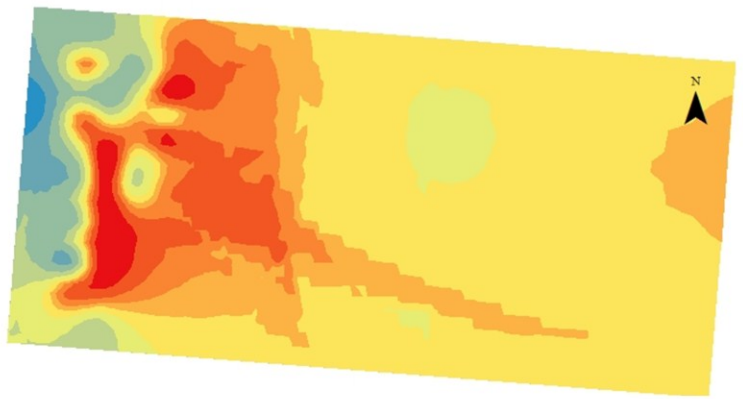
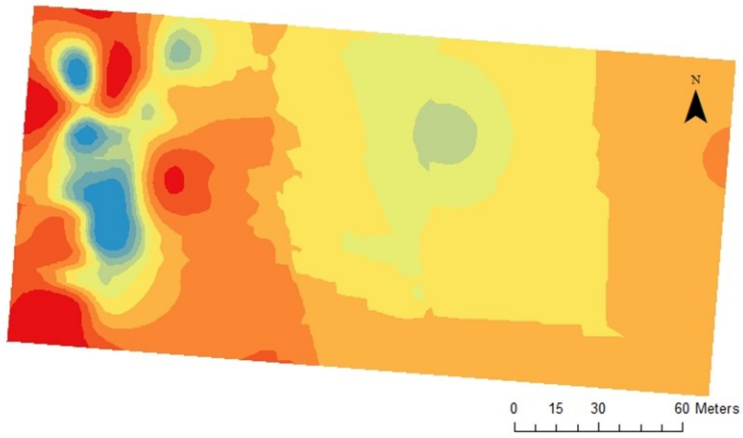


E2.1: Depth, Temperature and Dissolved Oxygen

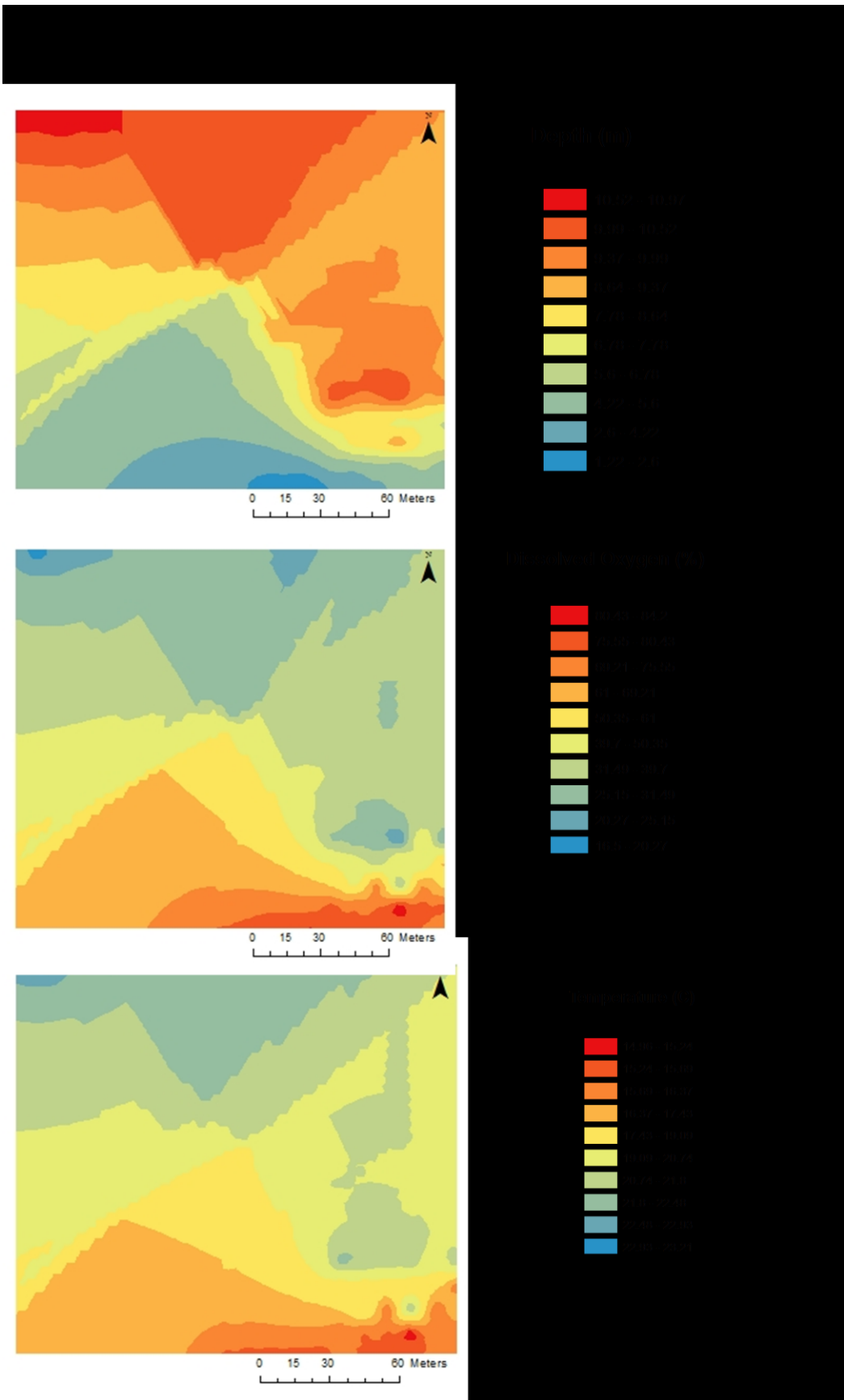


E2.1: Depth, Temperature and Dissolved Oxygen

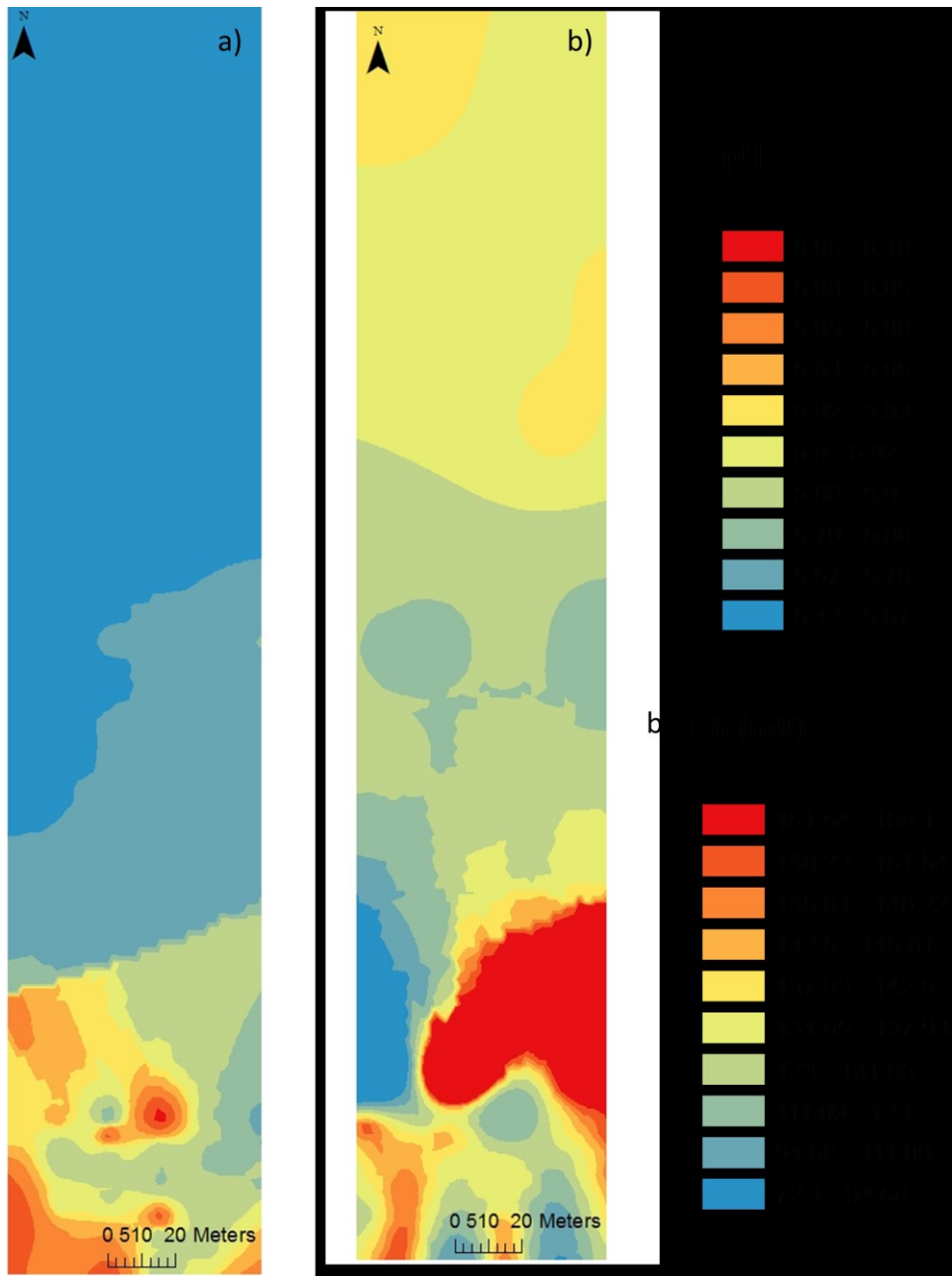
Water Properties at Sowden 41, So



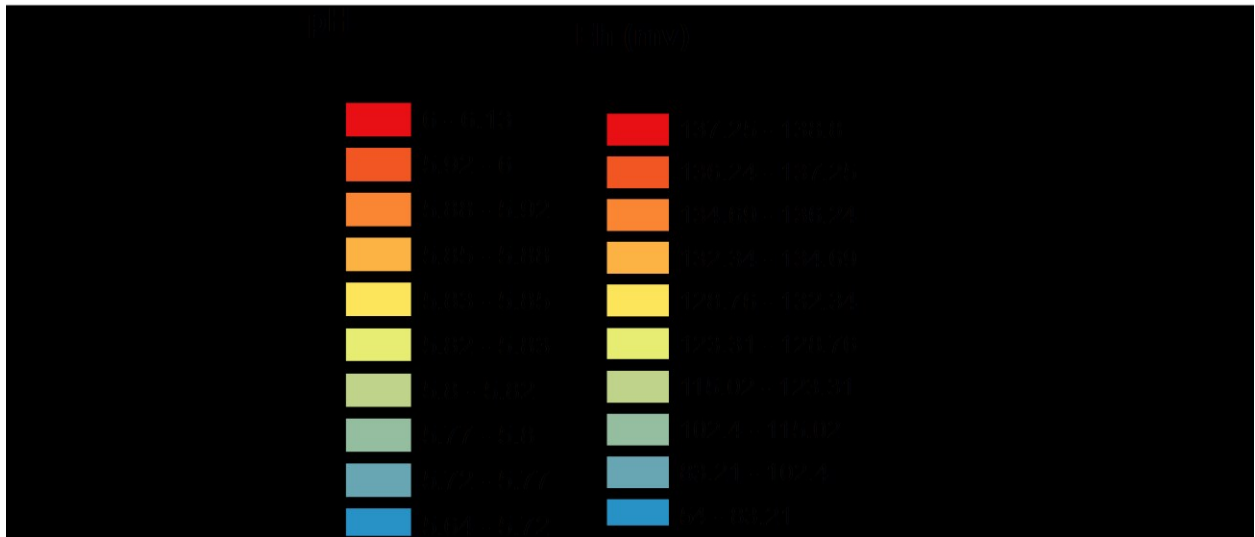
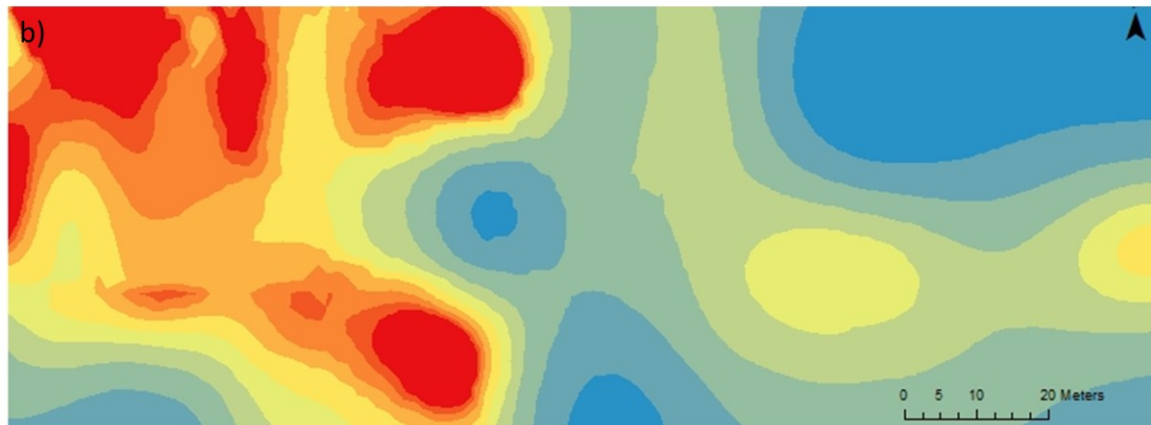
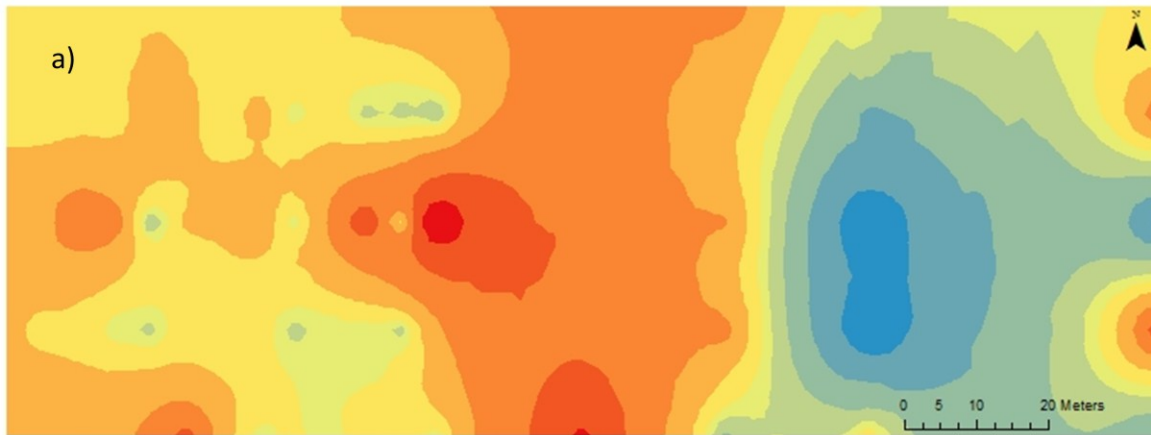
E2.1: Depth, Temperature and Dissolved Oxygen



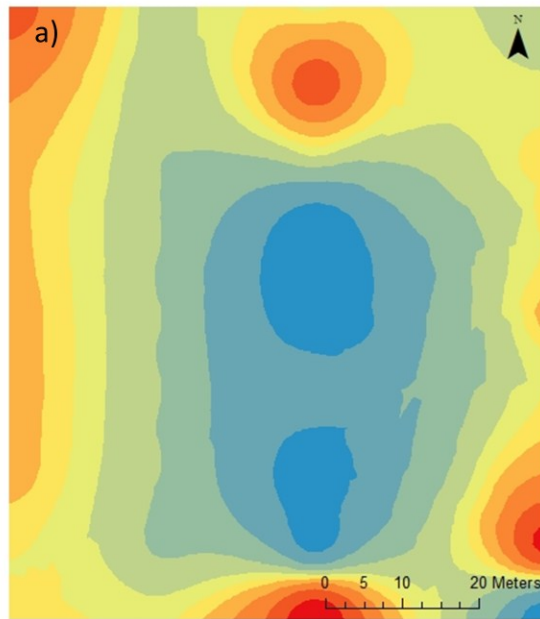
E2.2: Eh and pH Maps: 7 Cove



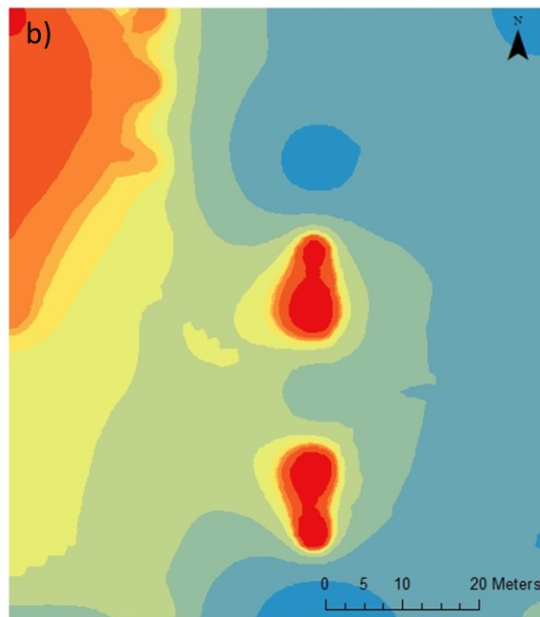
E2.2: Eh and pH Maps Bud's Cove



E2.2: Eh and pH Maps Mine Site



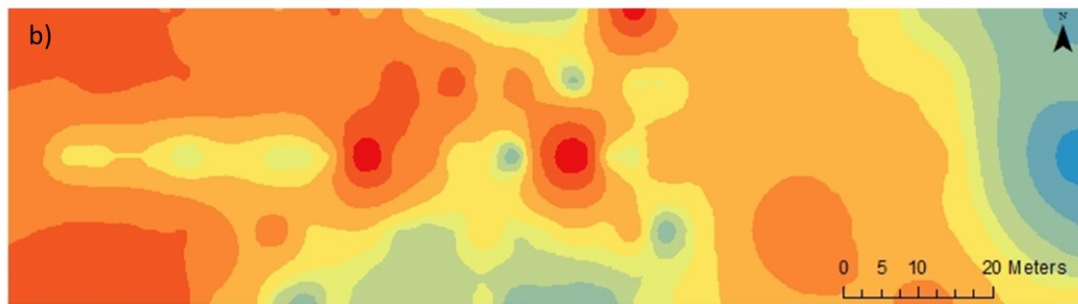
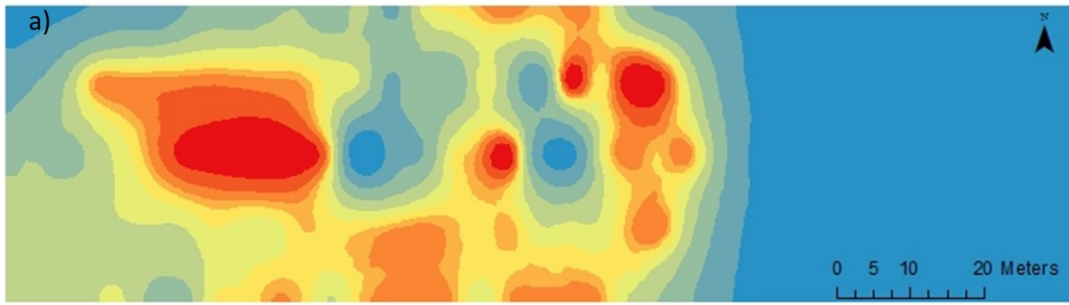
pH



Eh

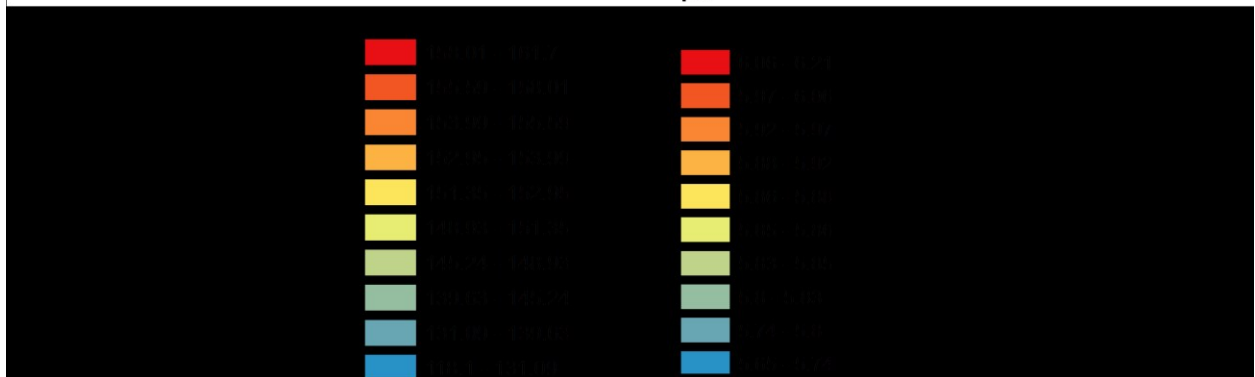


E2.2: Eh and pH Maps My Cove

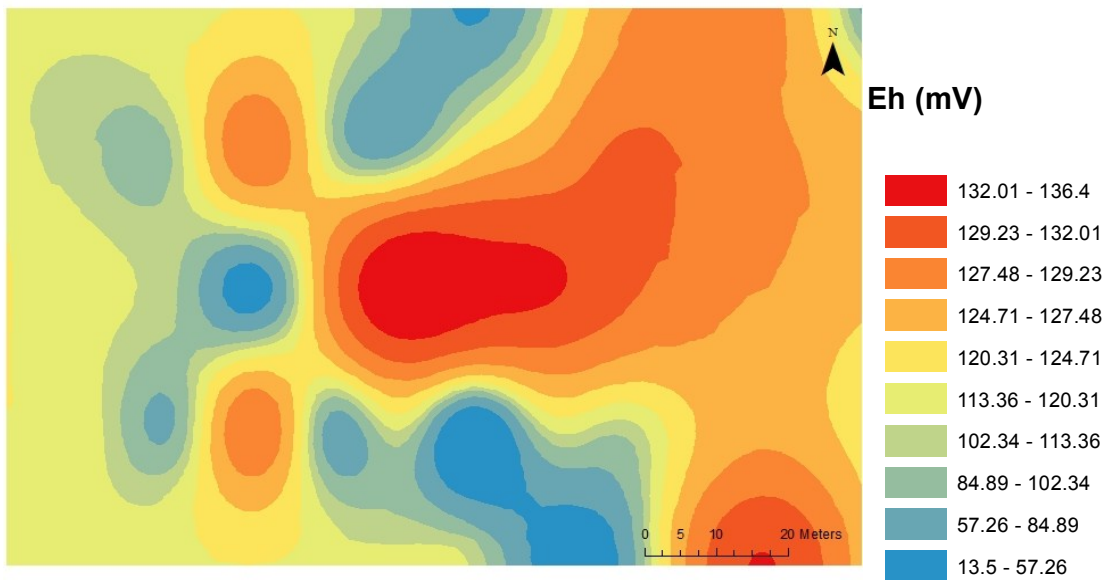
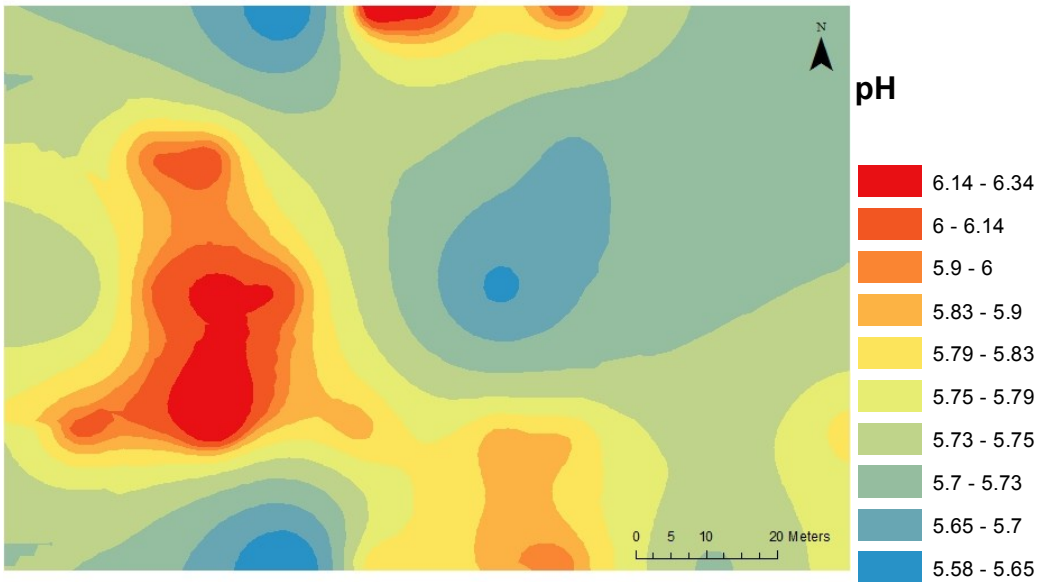


a) Eh (mV)

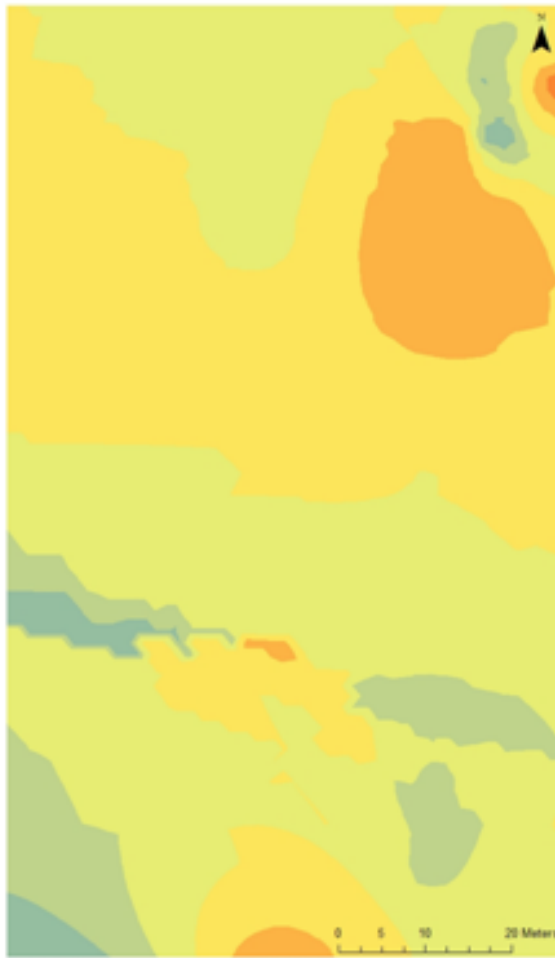
b) pH



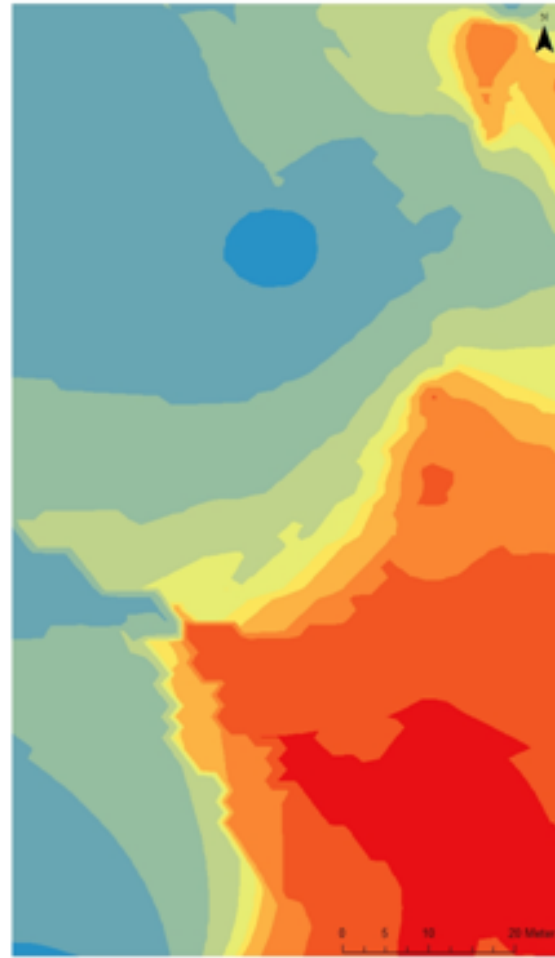
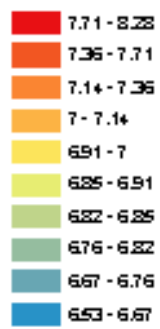
E2.2: Eh and pH Maps Granite Islands



E2.2: Eh and pH Maps: Sowden 46



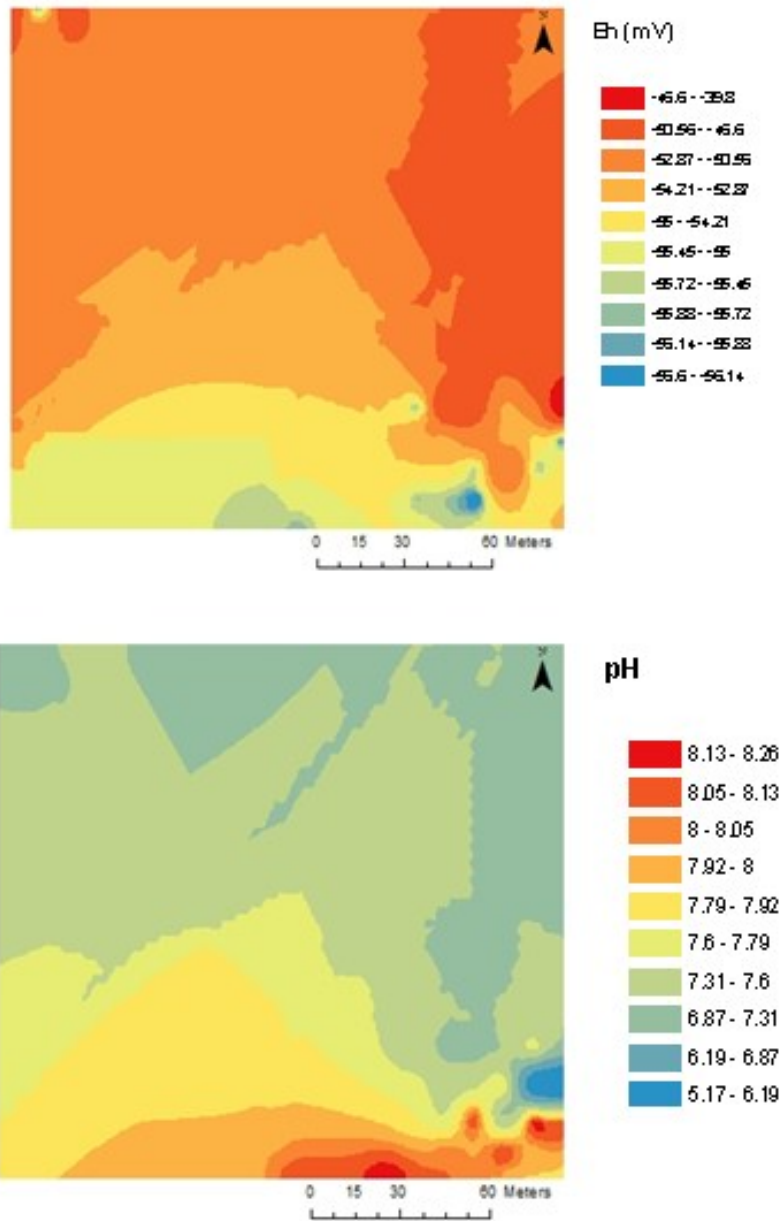
pH



Eh (mV)



E2.2: Eh and pH Maps: Shebandowan Island Site



Appendix F: Environmental Distribution Elemental Maps

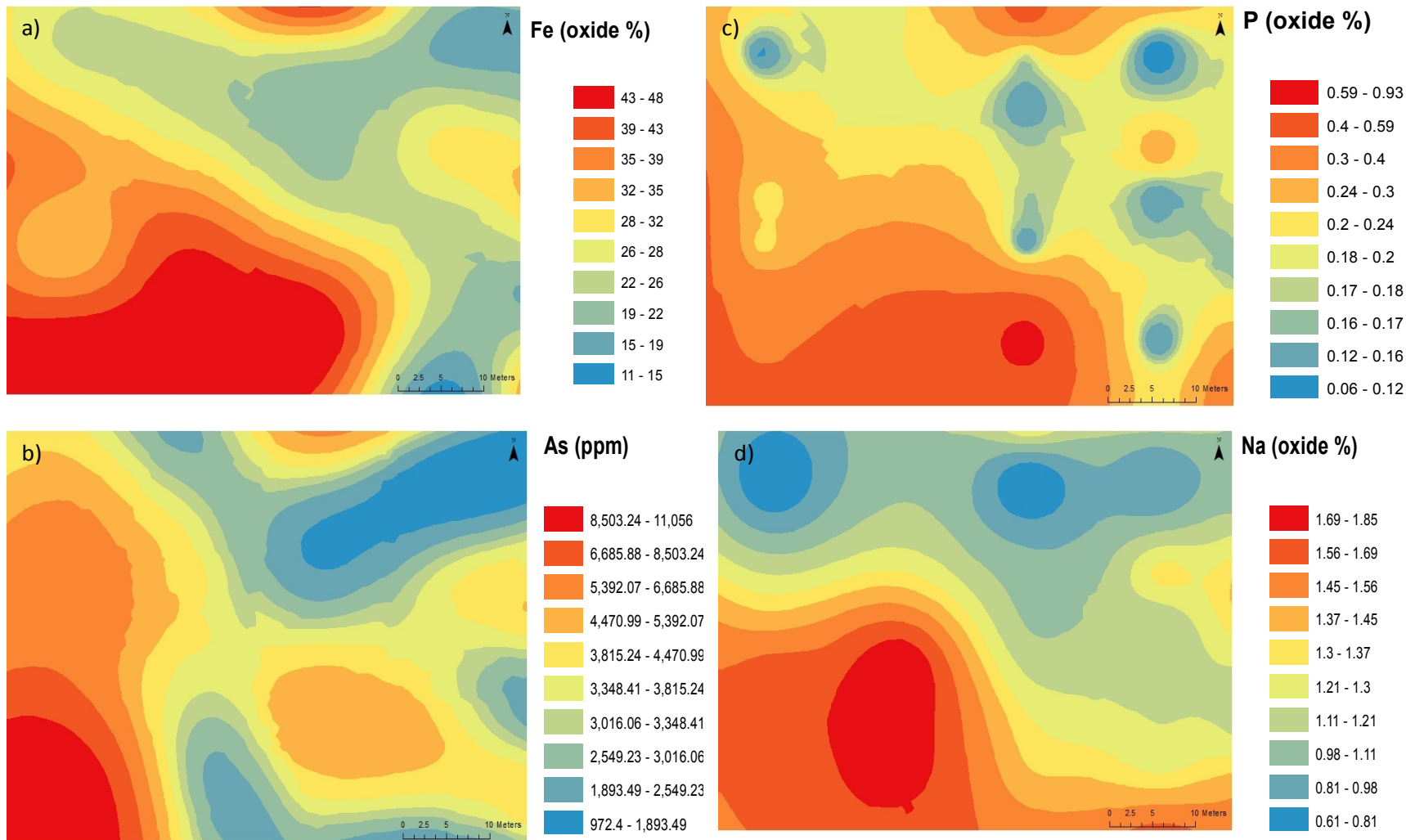
F1: Maps of the three most comparable elements to iron, manganese, aluminum and carbon

F1.1 Iron compatibility.....	55
F1.2 Manganese Compatibility.....	62
F1.3 Aluminum Compatibility.....	71
F1.4 Carbon Compatibility.....	79

F2: Remaining elemental maps

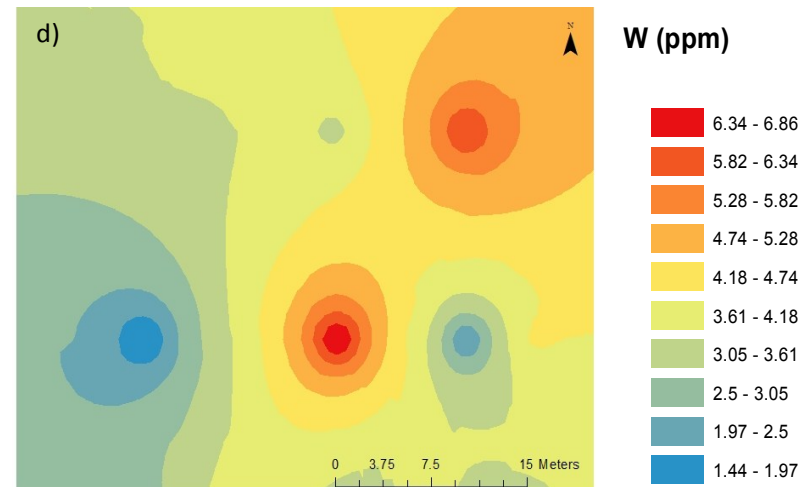
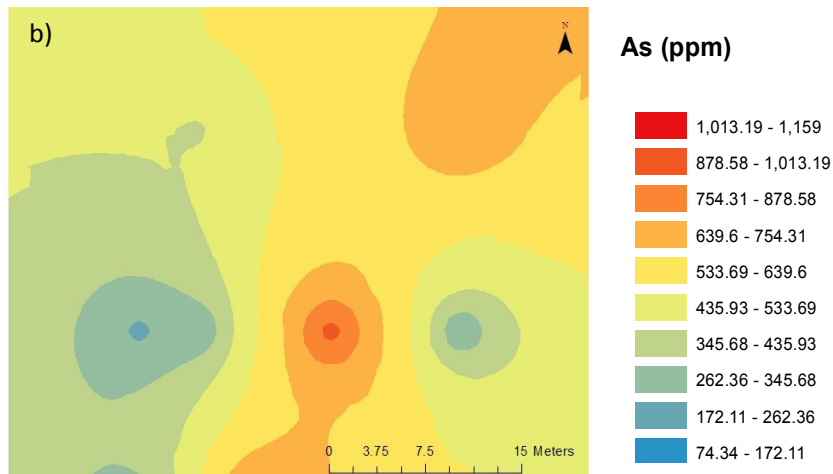
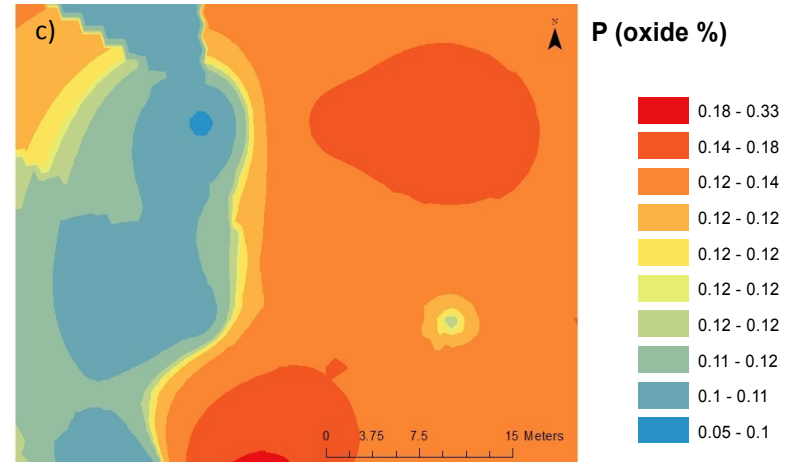
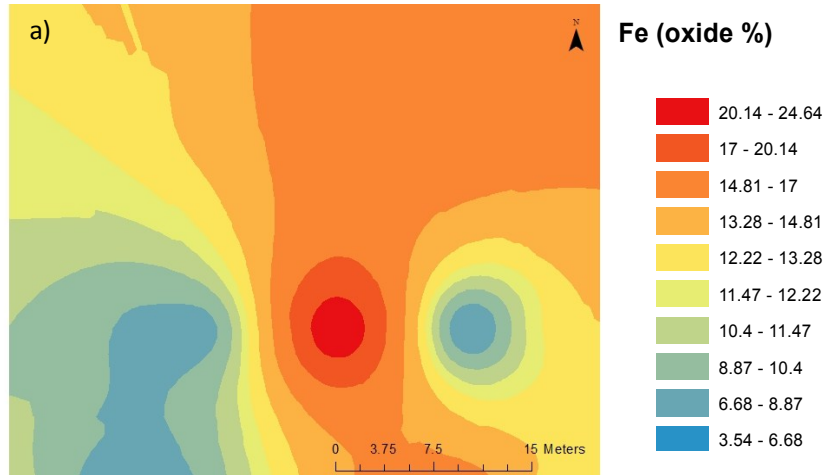
F2.1: 7 Cove (Lake Charlotte).....	82
F2.2: Bud's Cove (Lake Charlotte).....	86
F2.3: Granite Islands (Lake Charlotte).....	90
F2.4: Mine Site (Lake Charlotte).....	95
F2.5 My Cove (Lake Charlotte).....	103
F2.6 Island Site (Shebandowan Lake).....	107
F2.7 Small Site (Shebandowan Lake).....	110
F2.8 Sowden 46 (Sowden Lake).....	111
F2.9 Sowden 41 (Sowden Lake).....	115

F1.1: Iron Compatibility



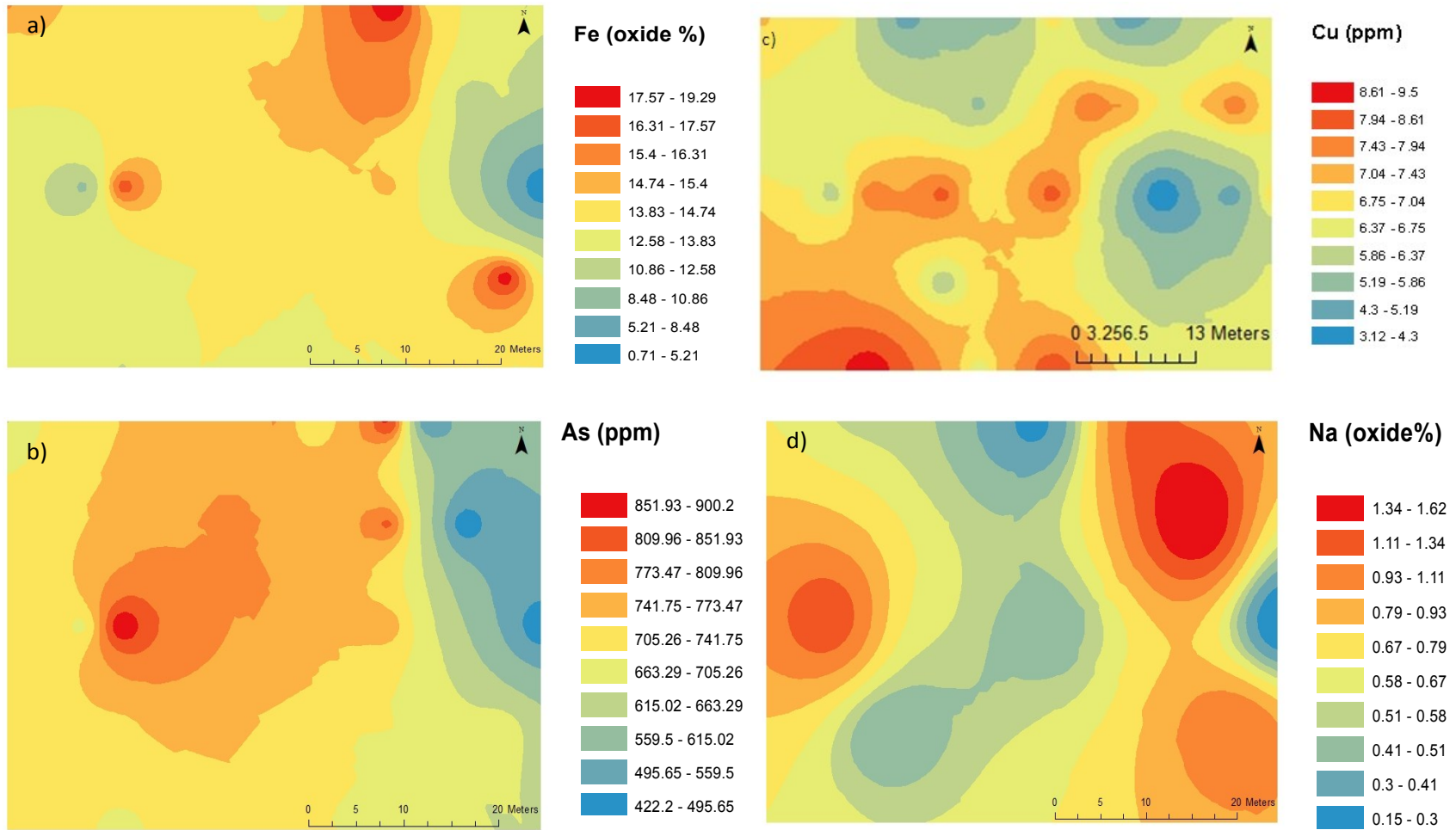
Chemical similarities to Iron at 7 cove a) iron distribution, b) arsenic distribution, c) phosphorus distribution, d) sodium distribution

F1.1: Iron Compatibility



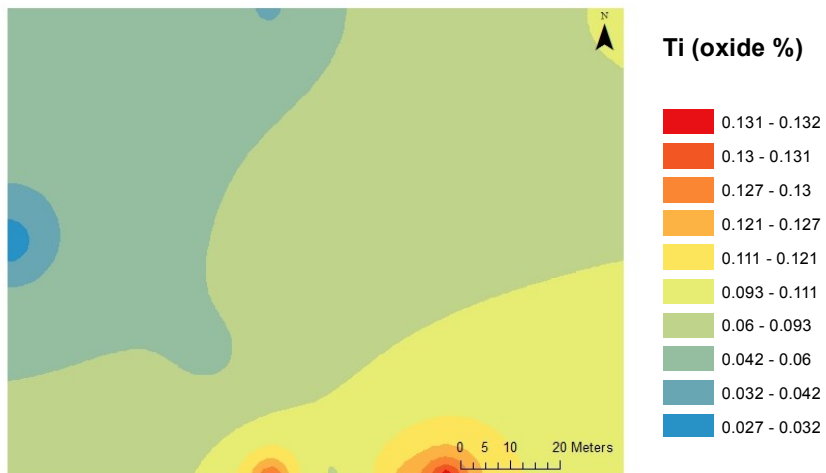
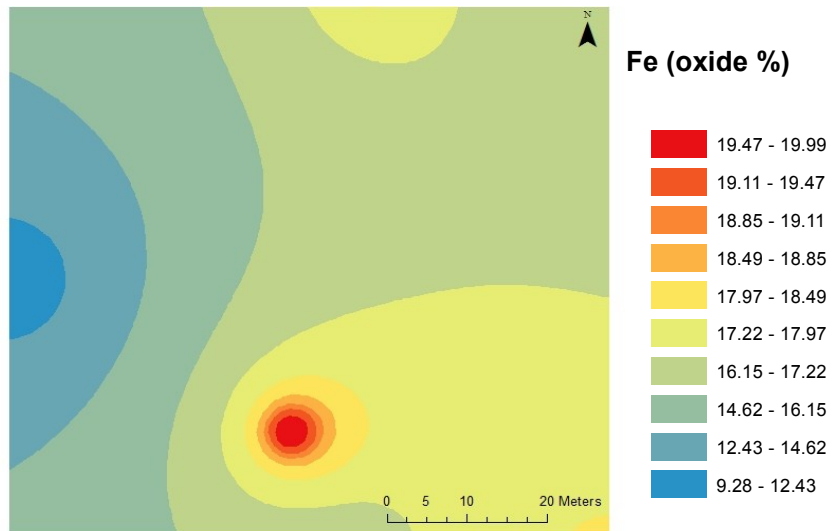
Chemical similarities to Iron at Bud's Cove, a) iron distribution, b) arsenic distribution, c) phosphorus distribution, d) tungsten distribution

F1.1: Iron Compatibility



Chemical Similarities to Iron in My Cove a) iron distribution, b) arsenic distribution, c) copper distribution, d) sodium distribution.

F1.1: Iron Compatibility

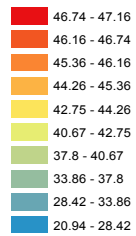


Chemical Similarities to Iron in Granite Islands iron distribution and titanium distribution.

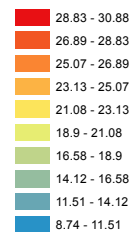
F1.1: Iron Compatibility



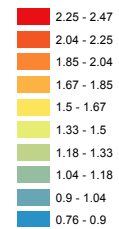
Fe (oxide %)



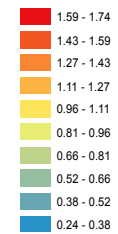
As (ppm)



P (oxide %)

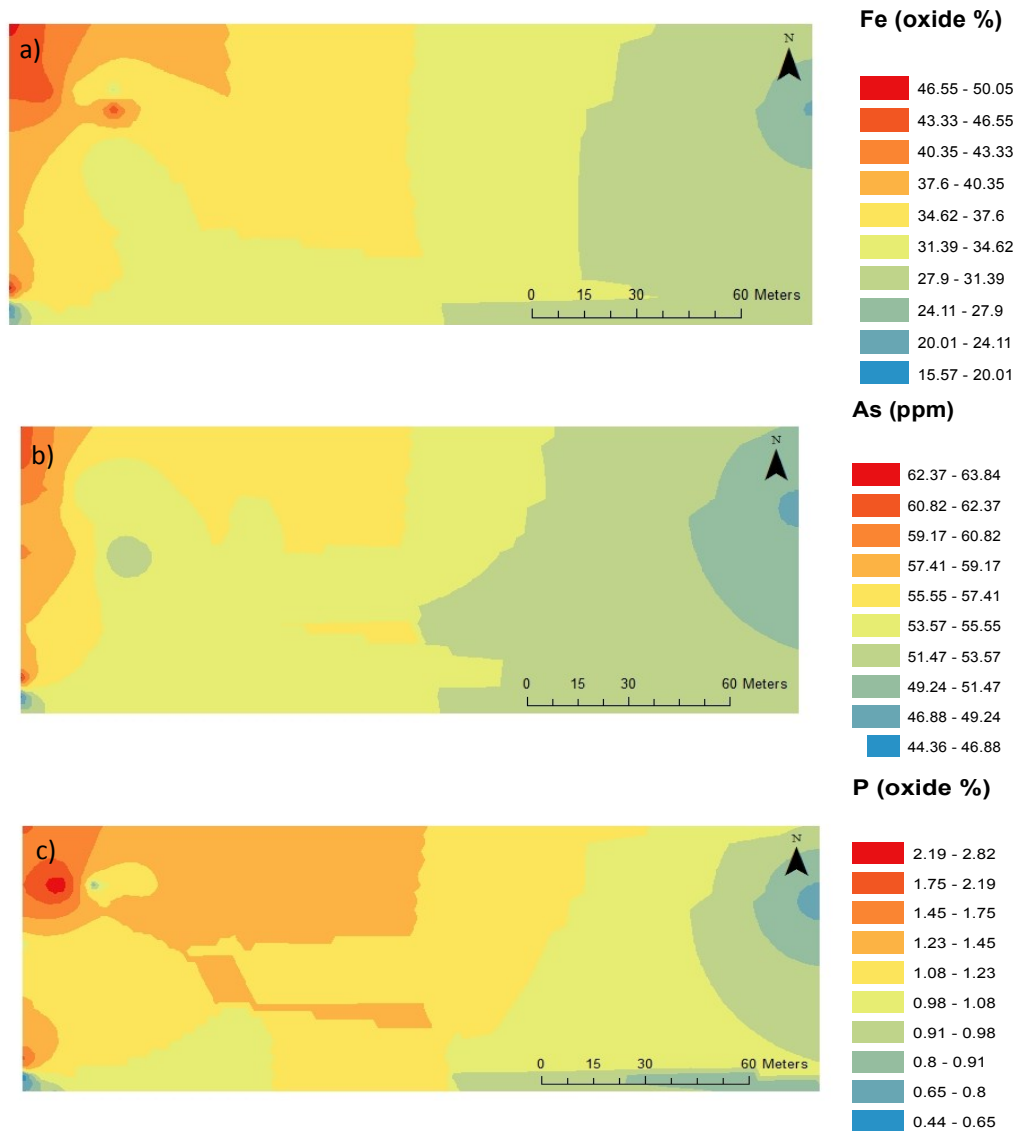


Nb (ppm)



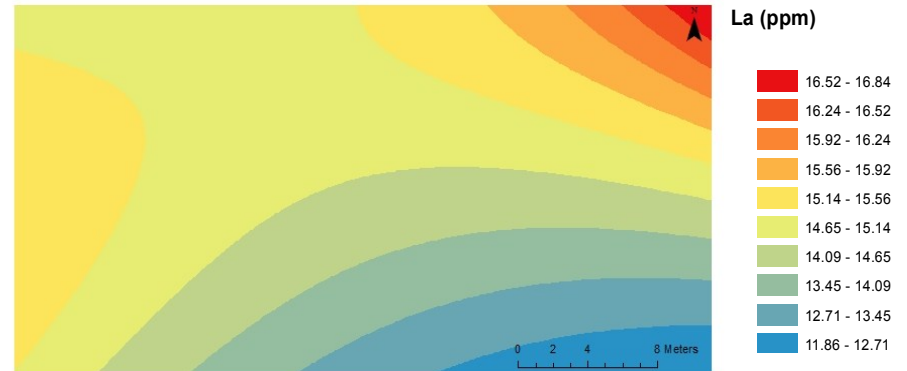
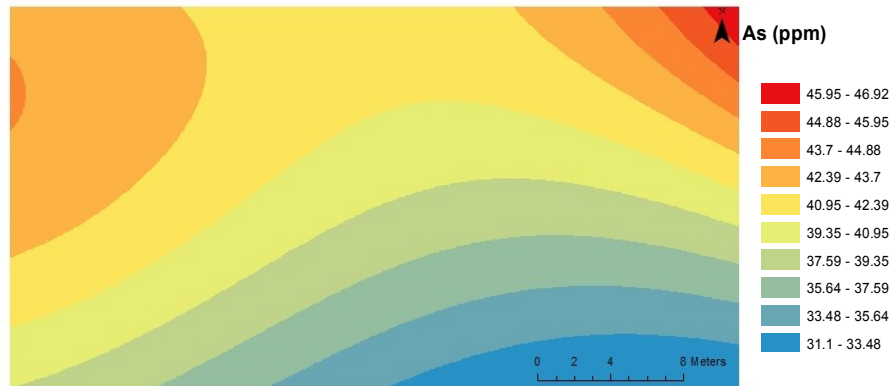
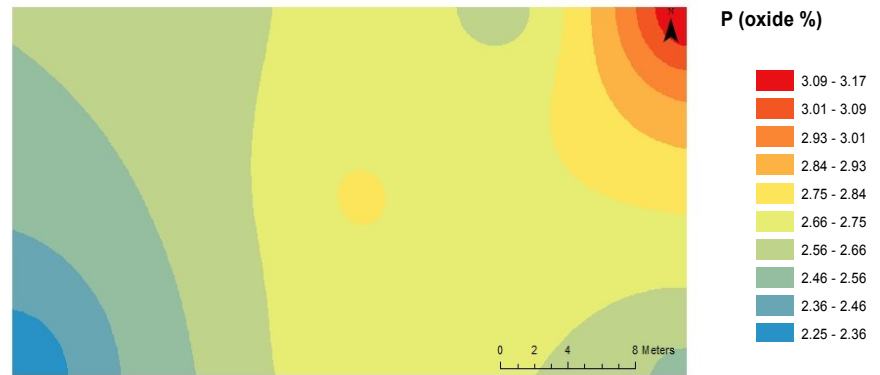
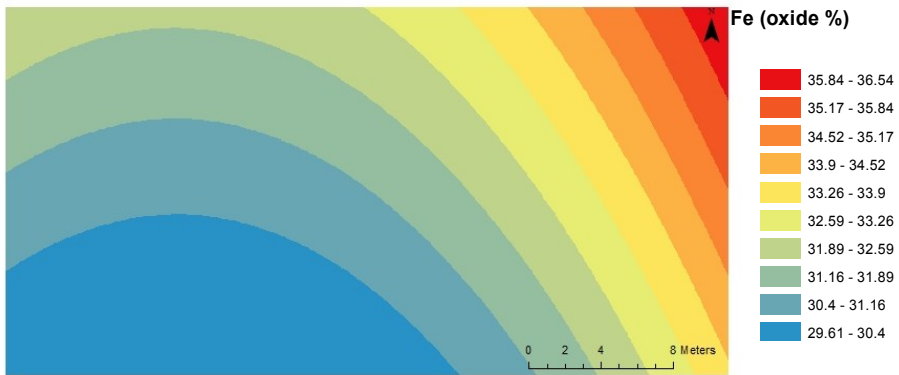
Chemical Similarities to Iron at Sowden Lake 46, a) Iron distribution, b) arsenic distribution, c) phosphorus distribution d) niobium

F1.1: Iron Compatibility



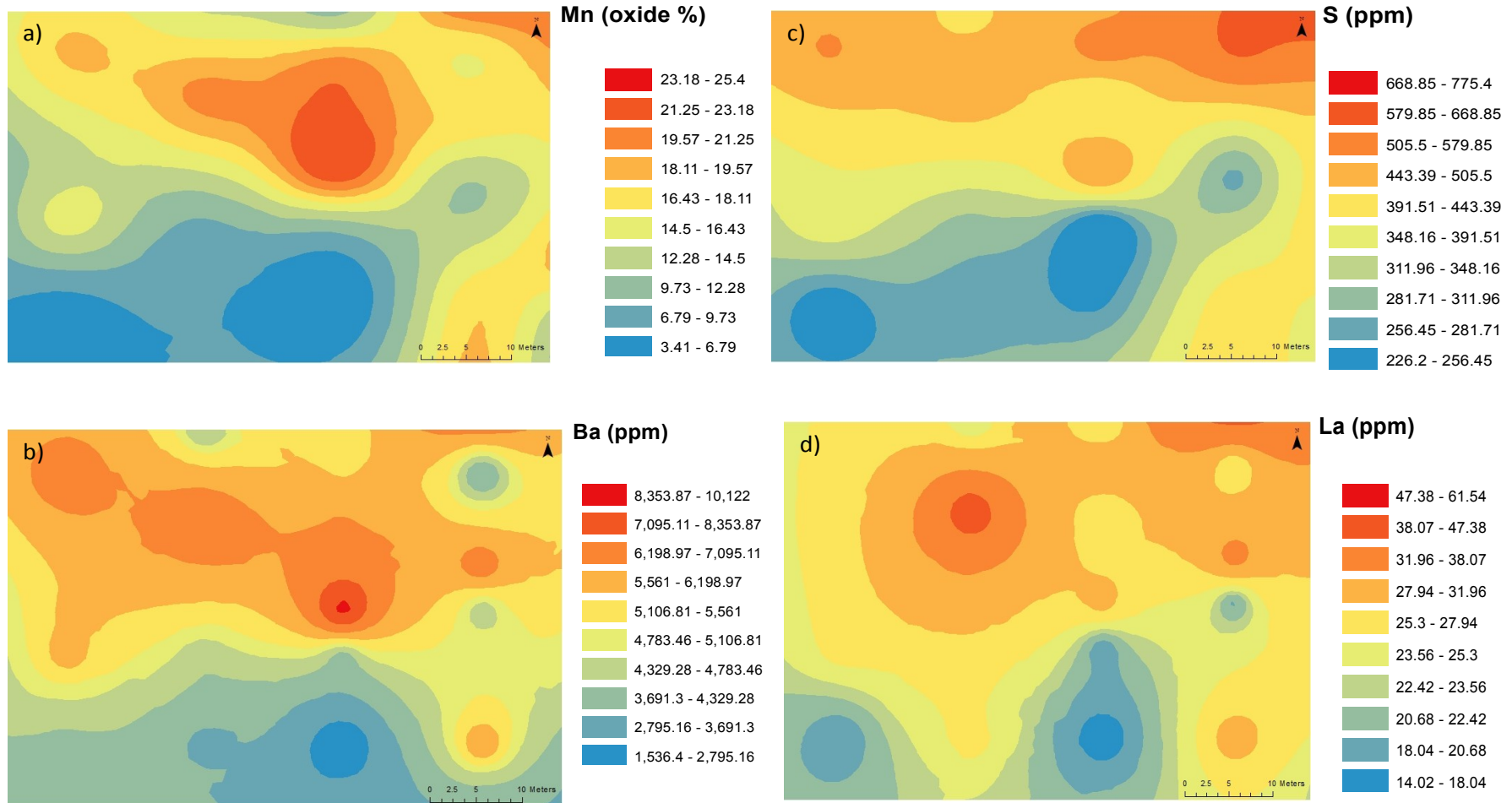
Chemical similarities to iron at Sowden Lake, Area 41. a) iron distribution, b) arsenic distribution, c) phosphorous distribution

F1.1: Iron Compatibility



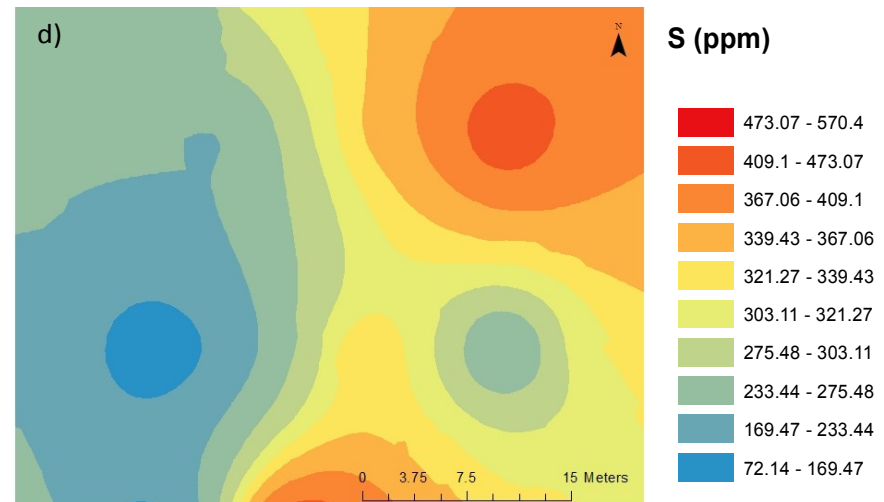
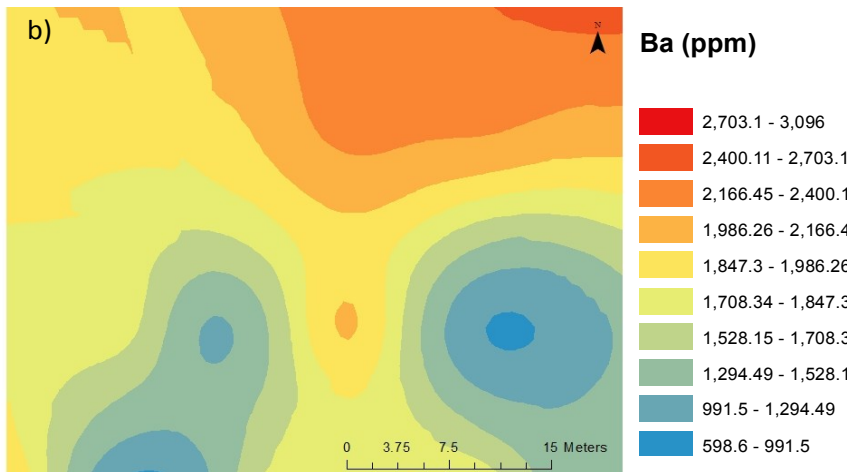
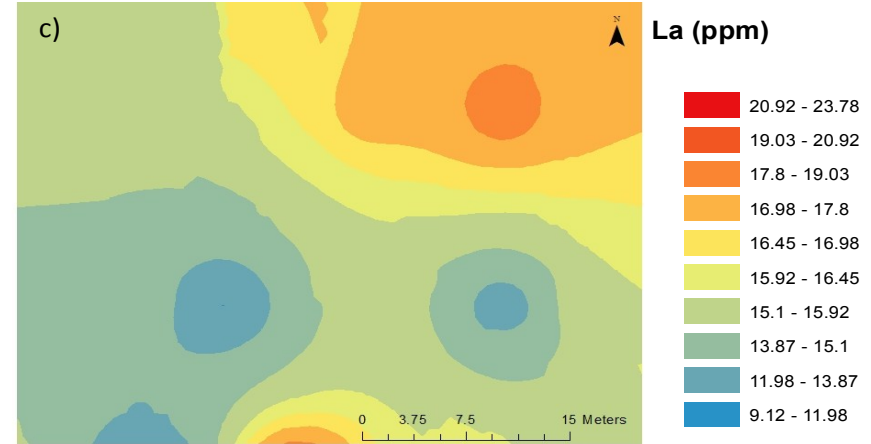
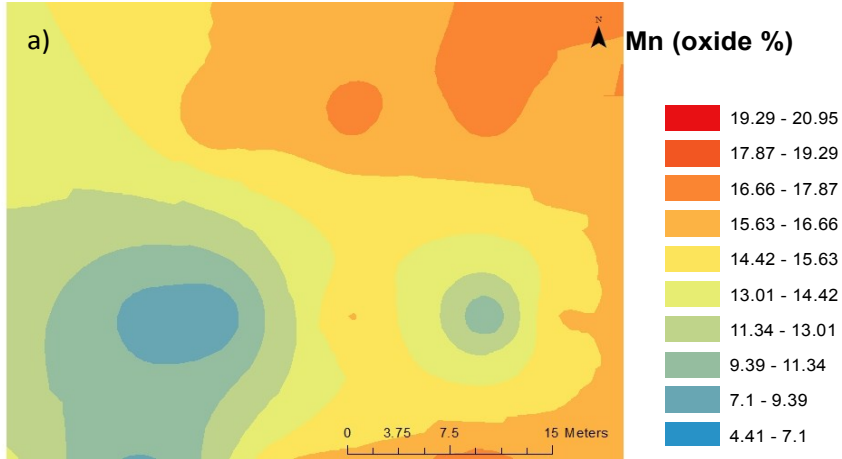
Chemical Similarities to Iron at Island Site, Shebandowan, a) iron distribution, b) arsenic distribution, c) phosphorus distribution, d) lanthanum distribution

F1.2: Manganese Compatibility



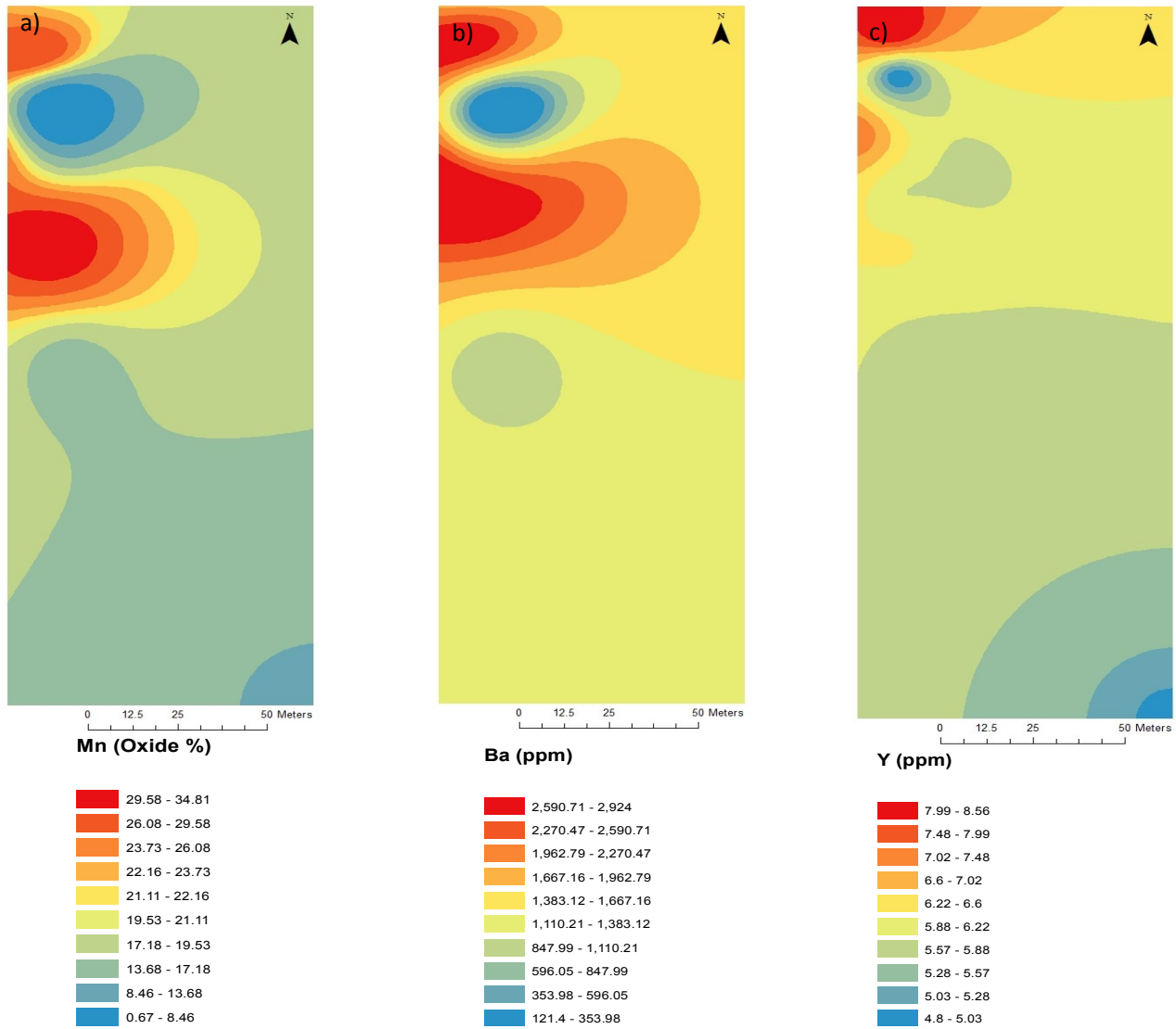
Chemical similarities to Manganese at 7 cove a) manganese distribution, b) barium distribution, c) sulfur distribution, d) lanthanum distribution

F1.2: Manganese Compatibility



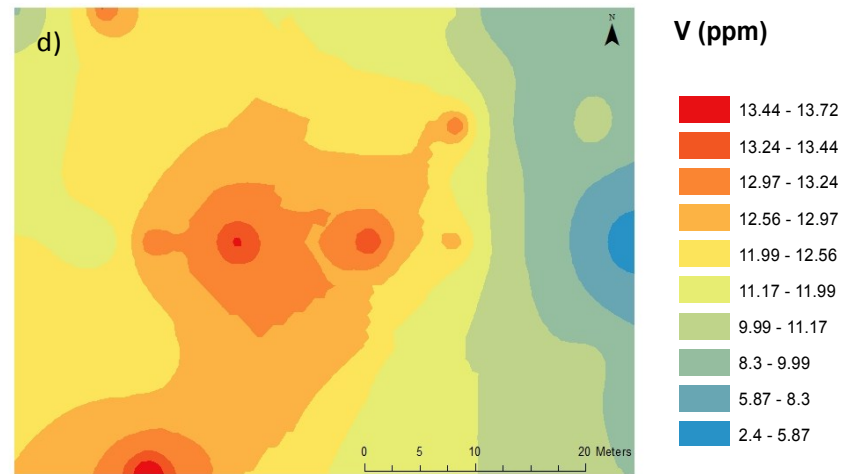
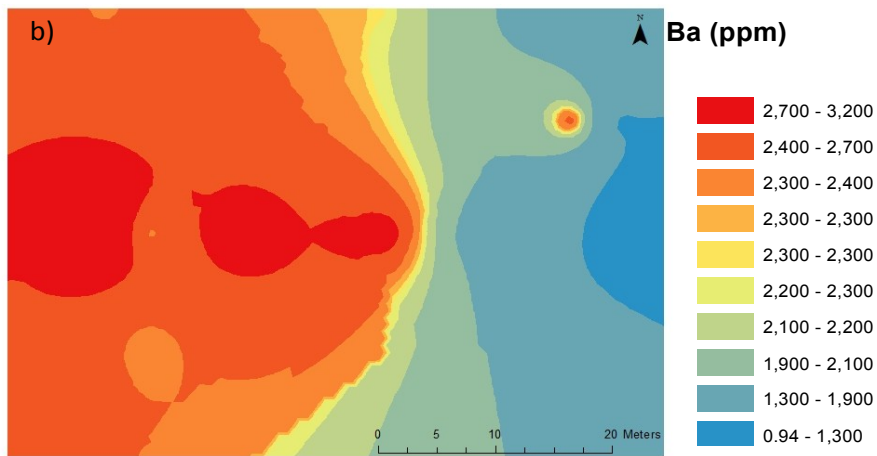
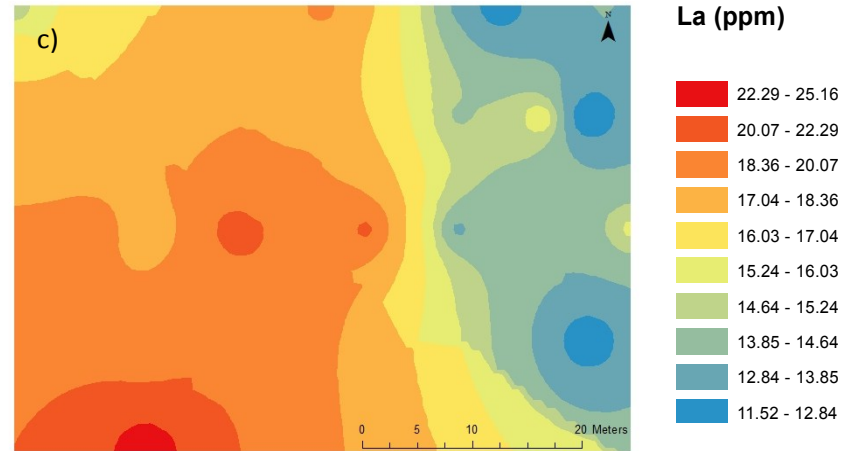
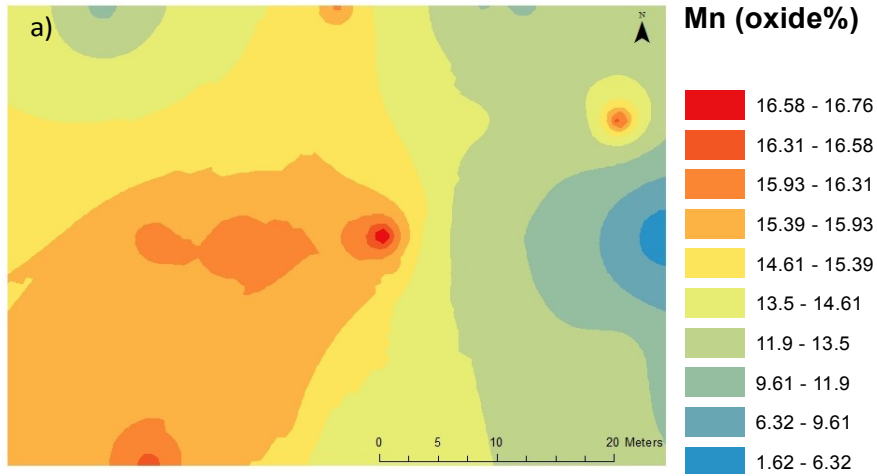
Chemical similarities to Manganese at Bud's Cove a) manganese distribution, b) barium distribution, c) lanthanum distribution, d) sulfur distribution

F1.2: Manganese Compatibility



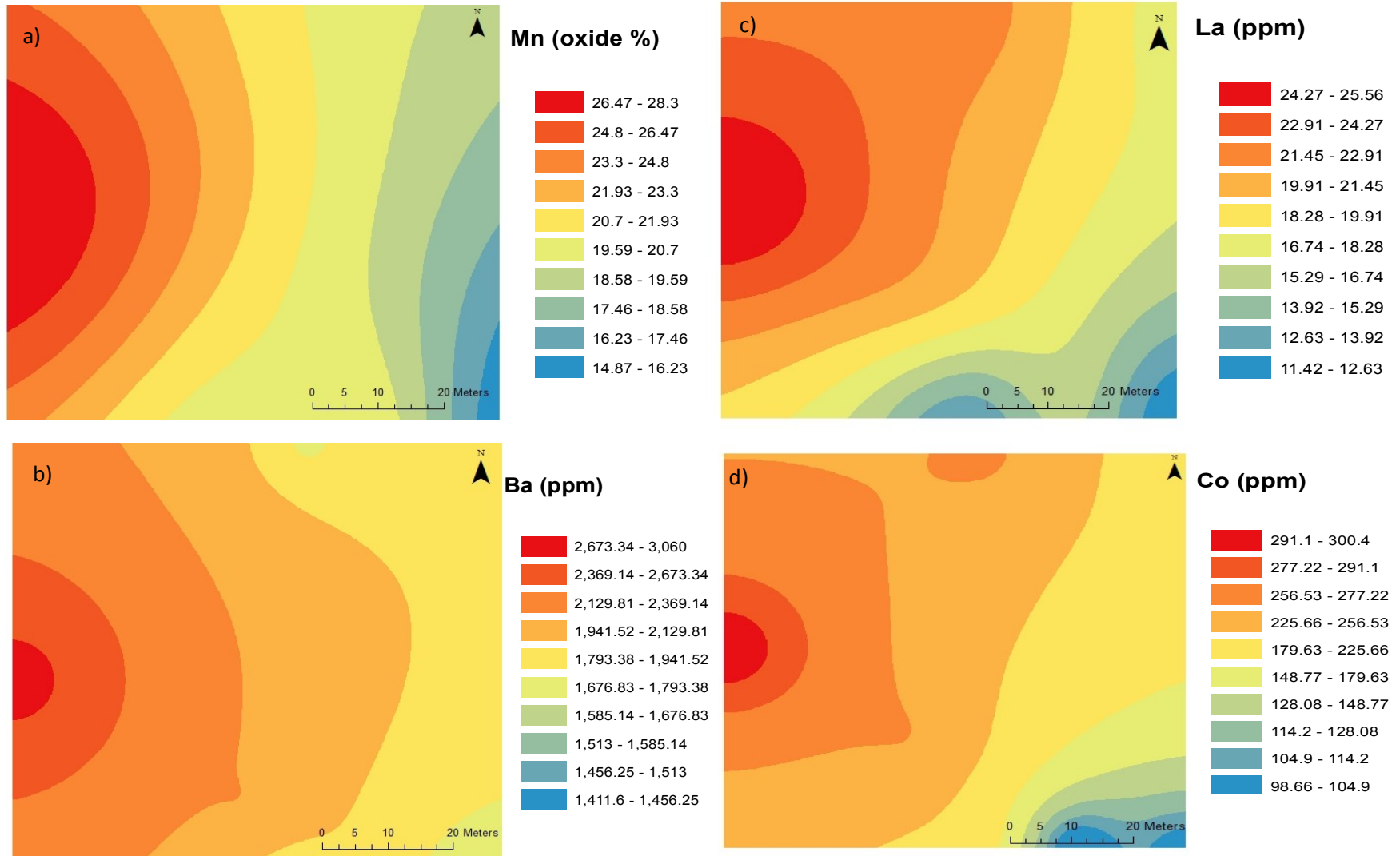
Chemical Similarities to Manganese in Mine Area a) manganese distribution, b) barium distribution, d) yttrium distribution

F1.2: Manganese Compatibility



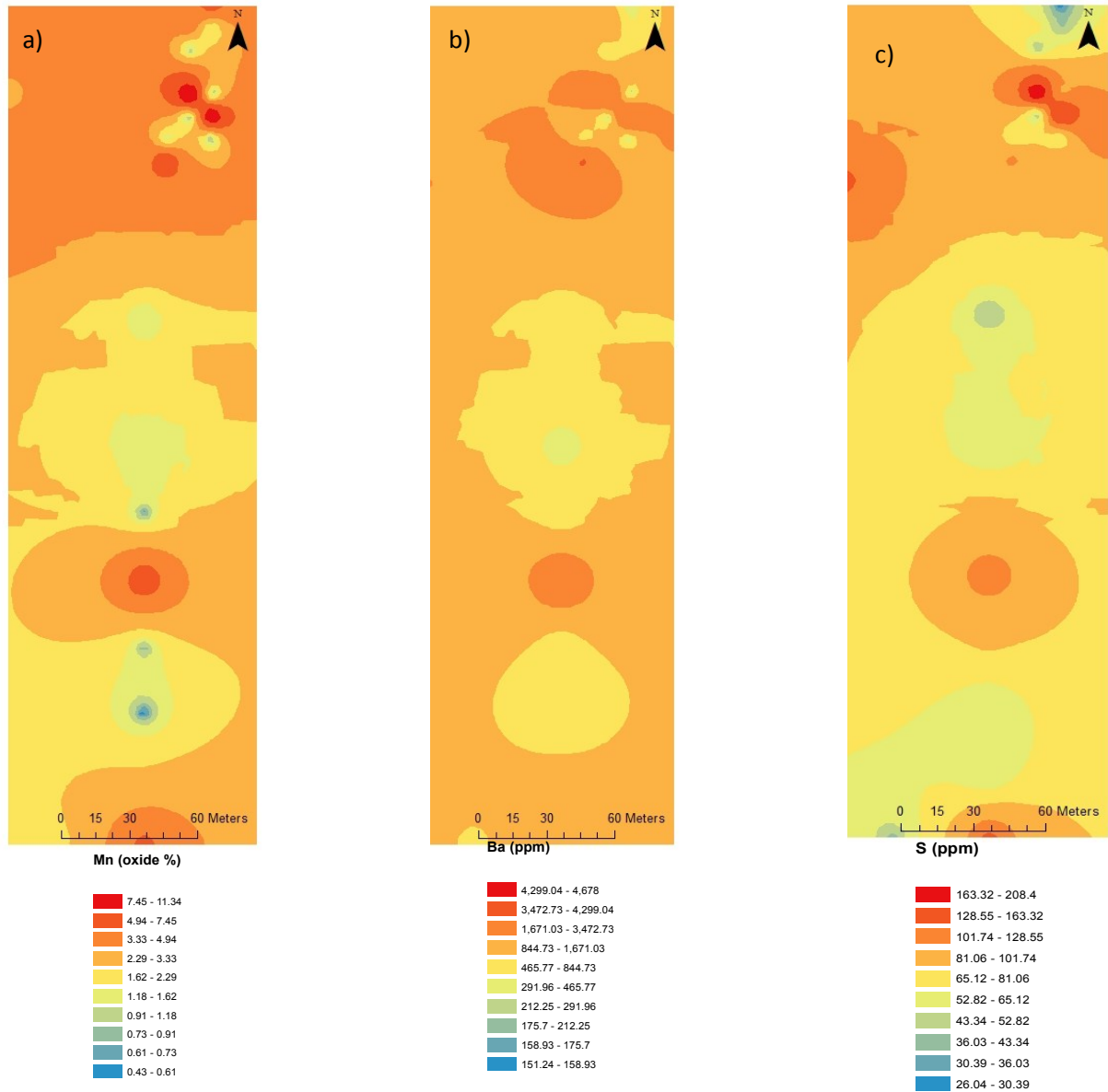
Chemical Similarities to Manganese in My Cove a) manganese distribution b) barium distribution, c) lanthanum distribution d) vanadium distribution. Note there is also a concentration distribution trend from deep water (east) to shallow water (west)

F1.2: Manganese Compatibility



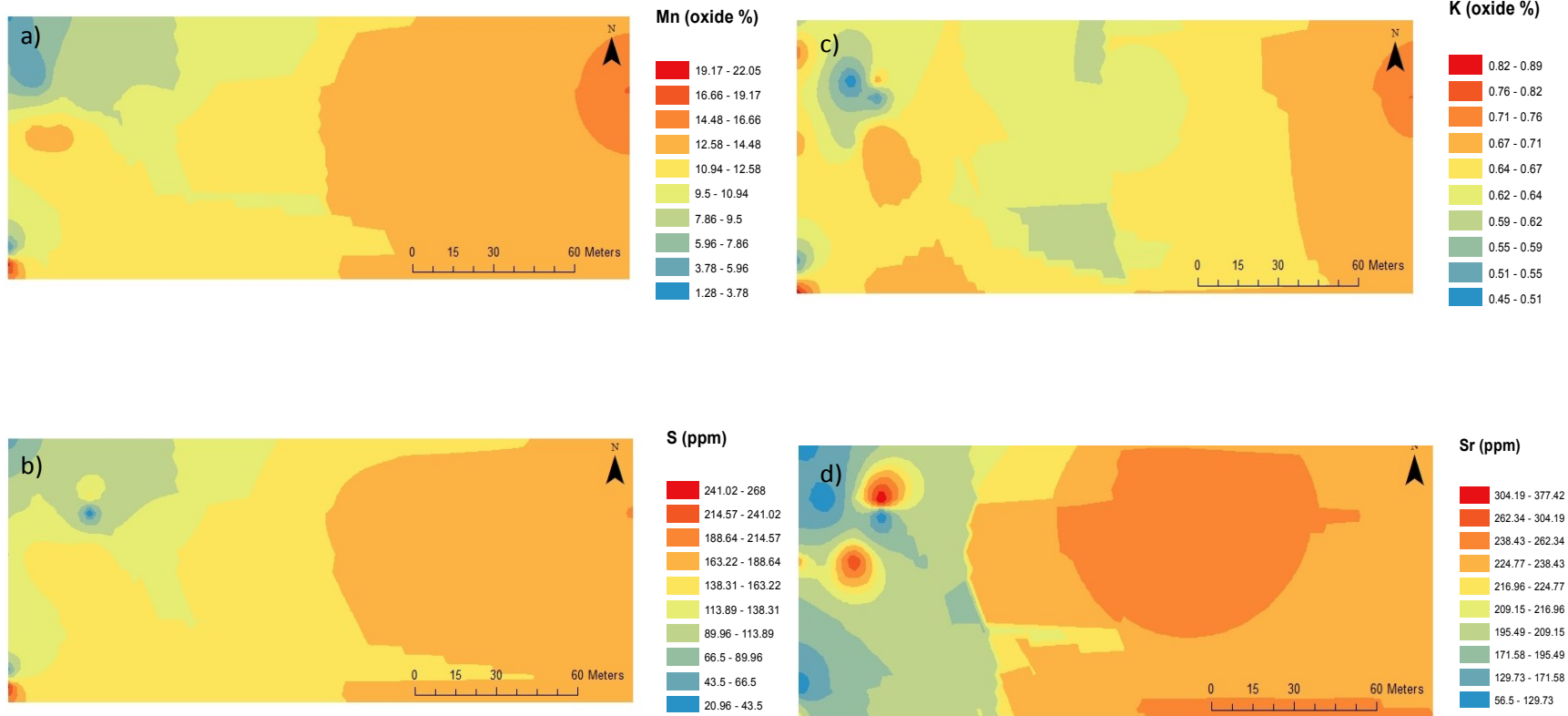
Chemical Similarities to Manganese in Granite Islands a) manganese distribution, b) barium distribution, c) lanthenum distribution, d) copper distribution. Note there is also a concentration distribution trend from deep water (east) to shallow water (west)

F1.2: Manganese Compatibility



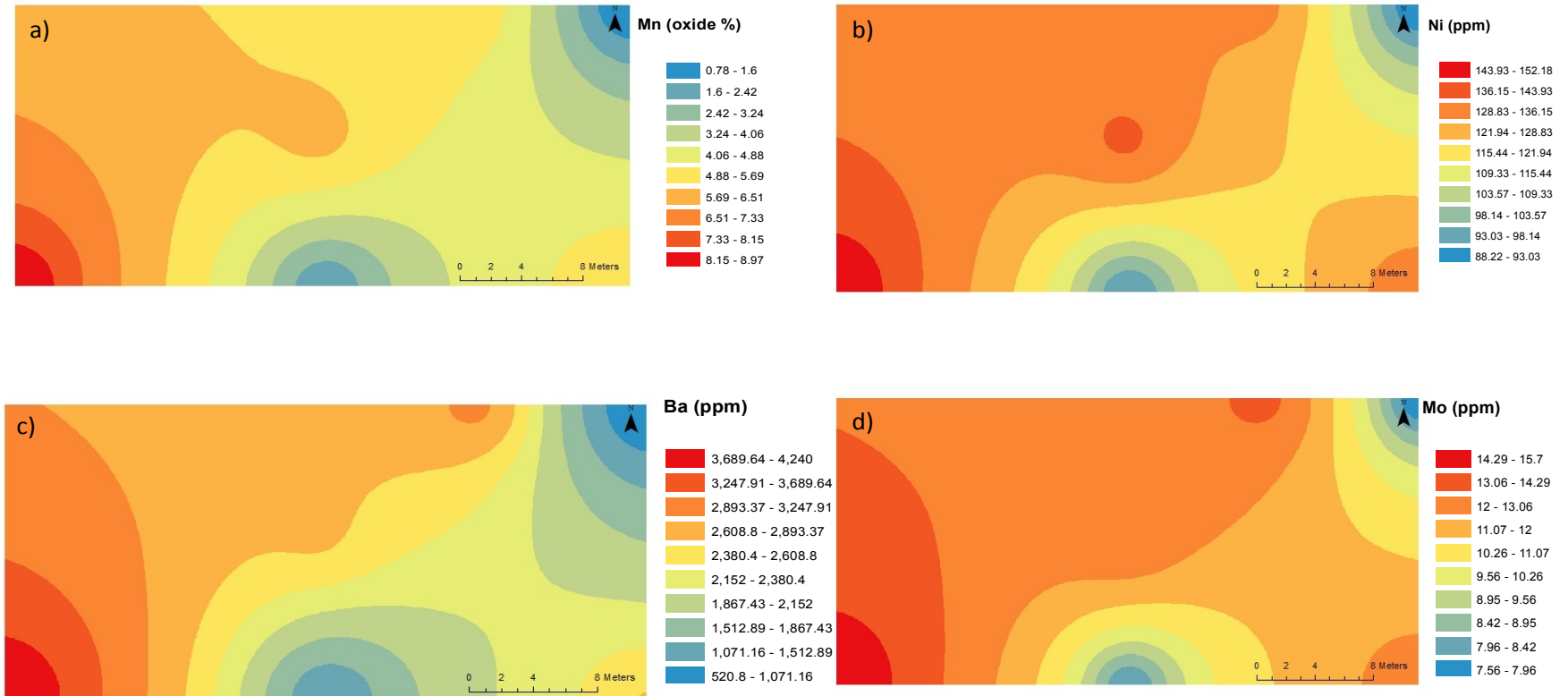
Chemical Similarities to Manganese at Sowden Lake 46 a) manganese distribution, b) barium distribution, c) sulfur distribution

F1.2: Manganese Compatibility



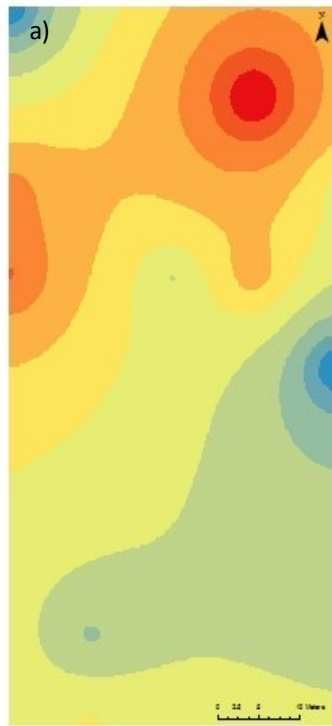
Chemical Similarities to Manganese at Sowden Lake 41 a) manganese distribution, b) sulfur distribution, c) potassium distribution, d) strontium distribution

F1.2: Manganese Compatibility

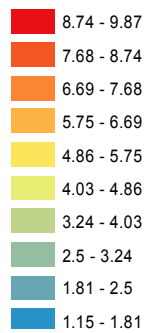


Chemical Similarities to Manganese at Island Site, Shebandowan a) manganese distribution b) barium distribution, c) nickel distribution, Molybdenum distribution

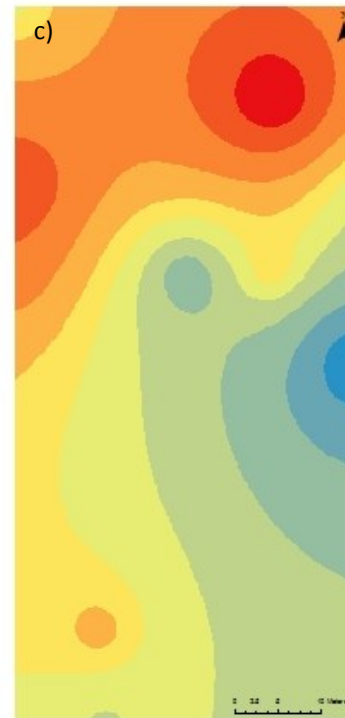
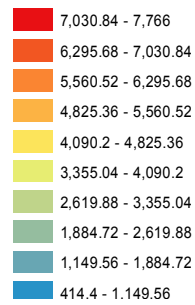
F1.2: Manganese Compatibility



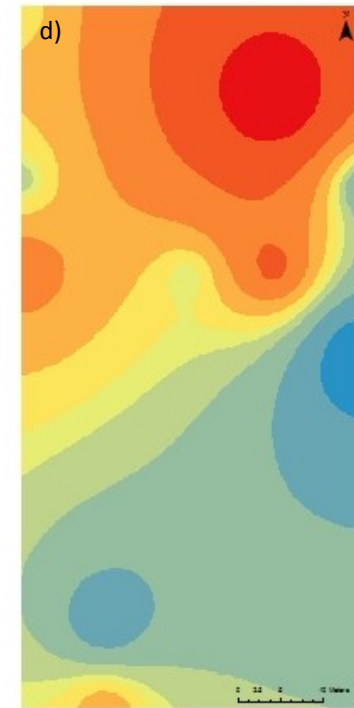
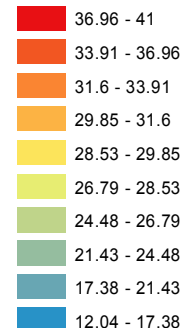
Mn (Oxide %)



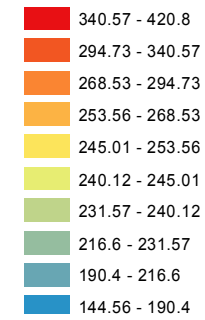
Ba (ppm)



La (ppm)

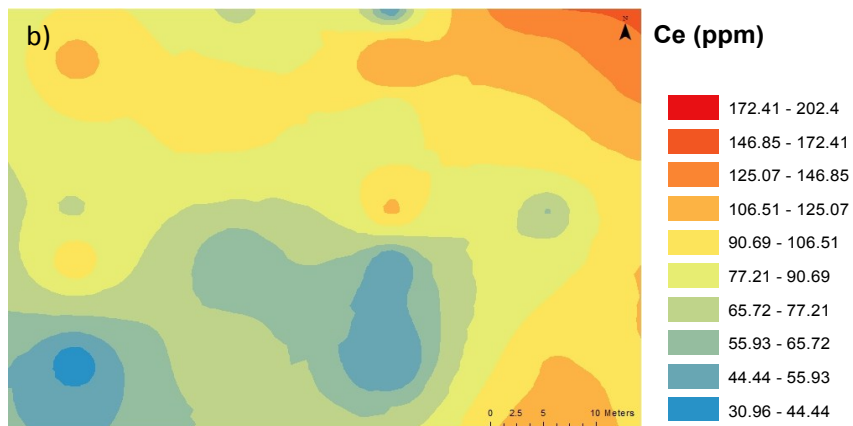
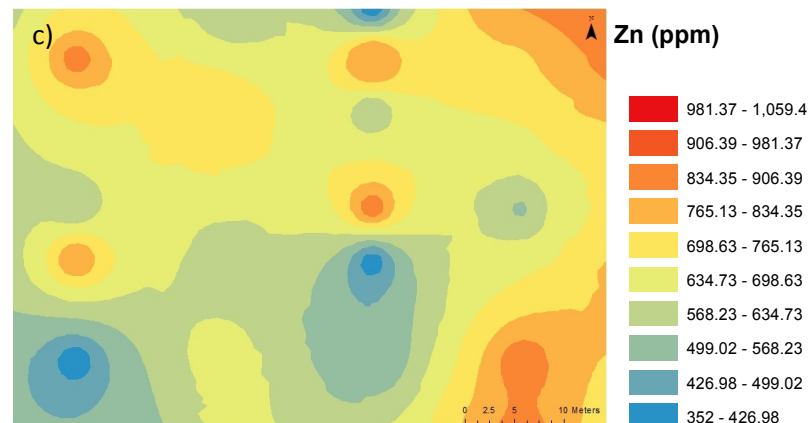
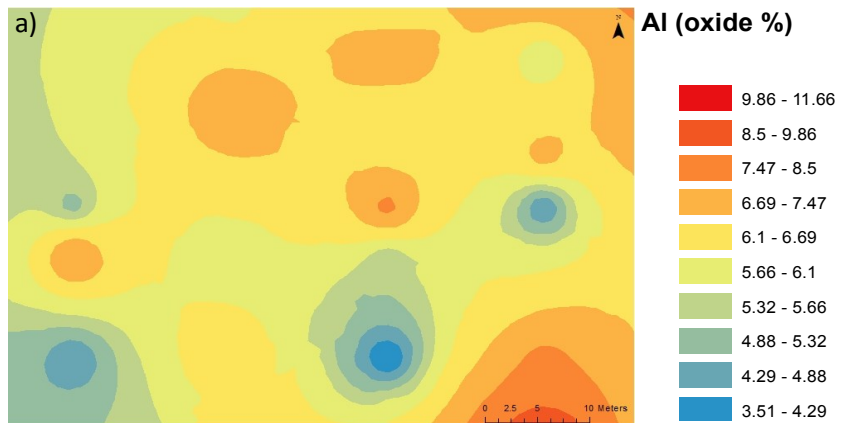


S (ppm)



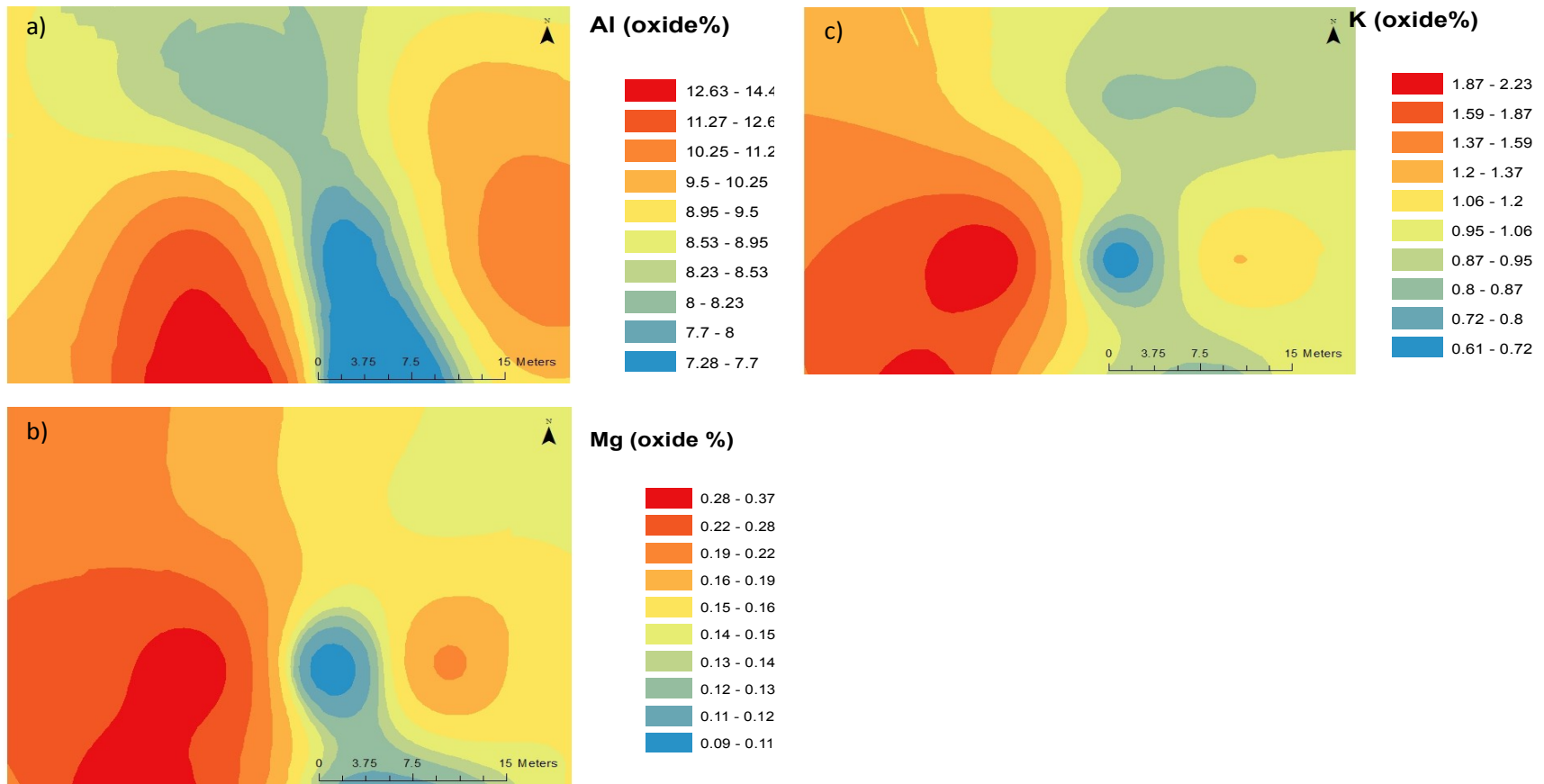
Chemical Similarities to Manganese at Small Site, Shebandowan a) manganese distribution, b) barium distribution, c) lanthanum distribution, d) sulfur distribution

F1.3: Aluminum Compatibility



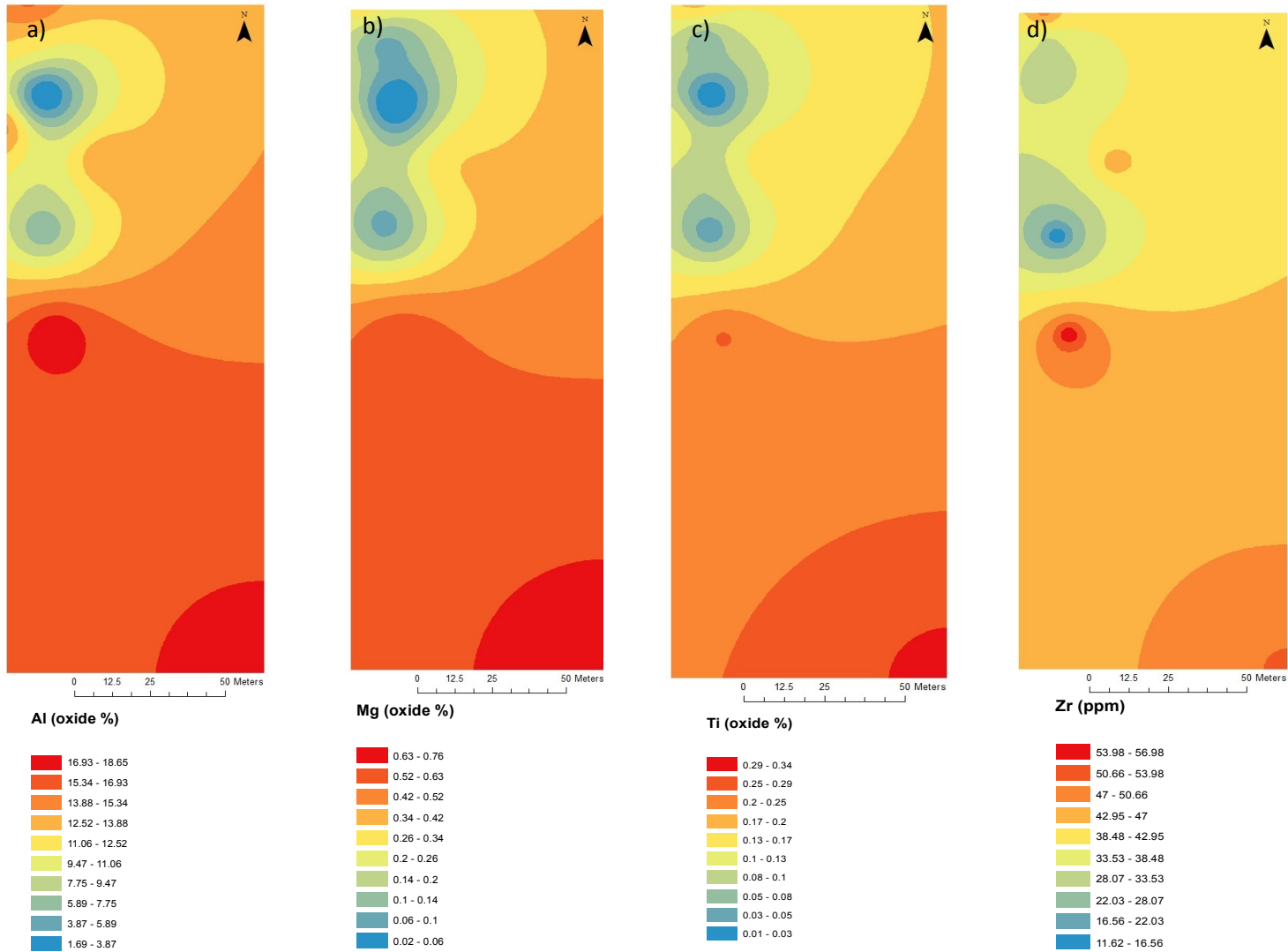
Chemical similarities to Aluminum at 7 cove a) aluminum distribution, b) cerium distribution, c) zinc distribution

F1.3: Aluminum Compatibility



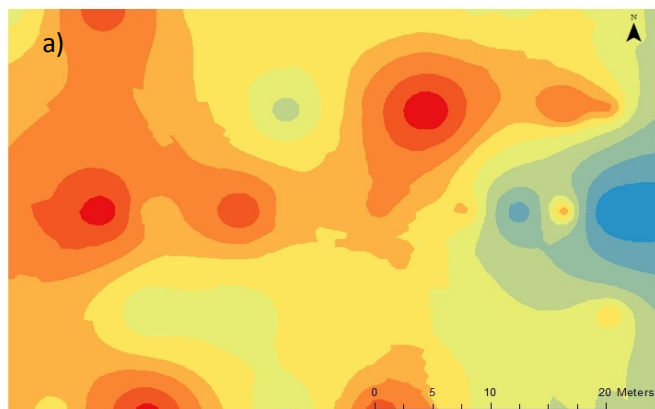
Chemical similarities to Aluminum at Bud's Cove, a) aluminum distribution, b) magnesium distribution, c) potassium distribution.

F1.3: Aluminum Compatibility

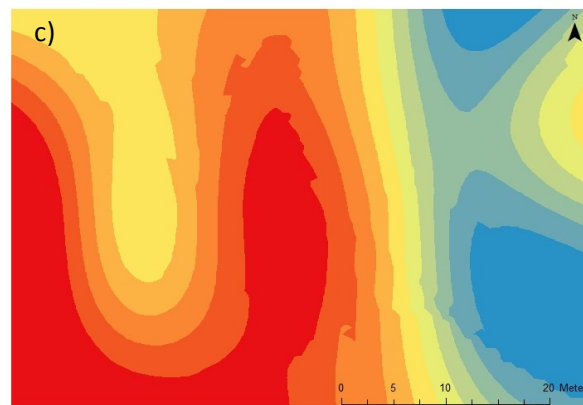
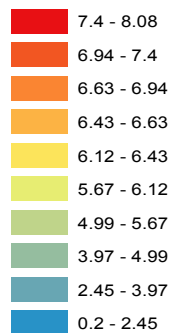


Chemical Similarities to Aluminum in Mine Area, a) aluminum distribution, b) magnesium distribution, c) titanium distribution, d) zircon

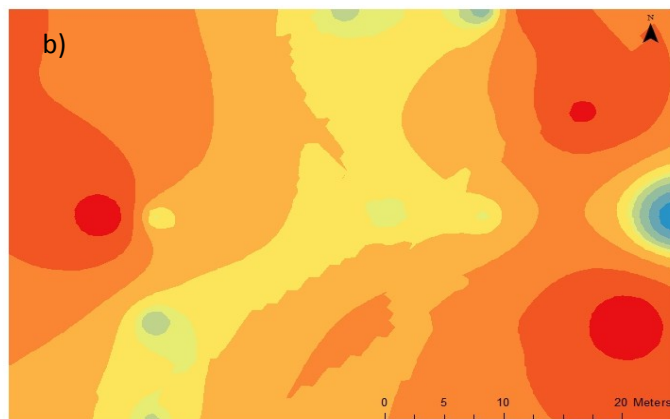
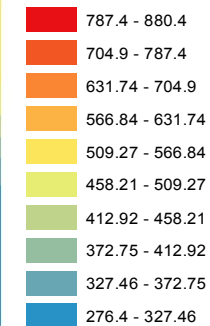
F1.3: Aluminum Compatibility



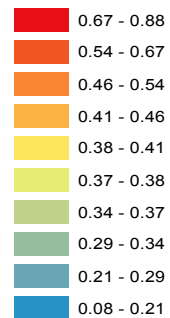
Al (oxide %)



Zn (ppm)

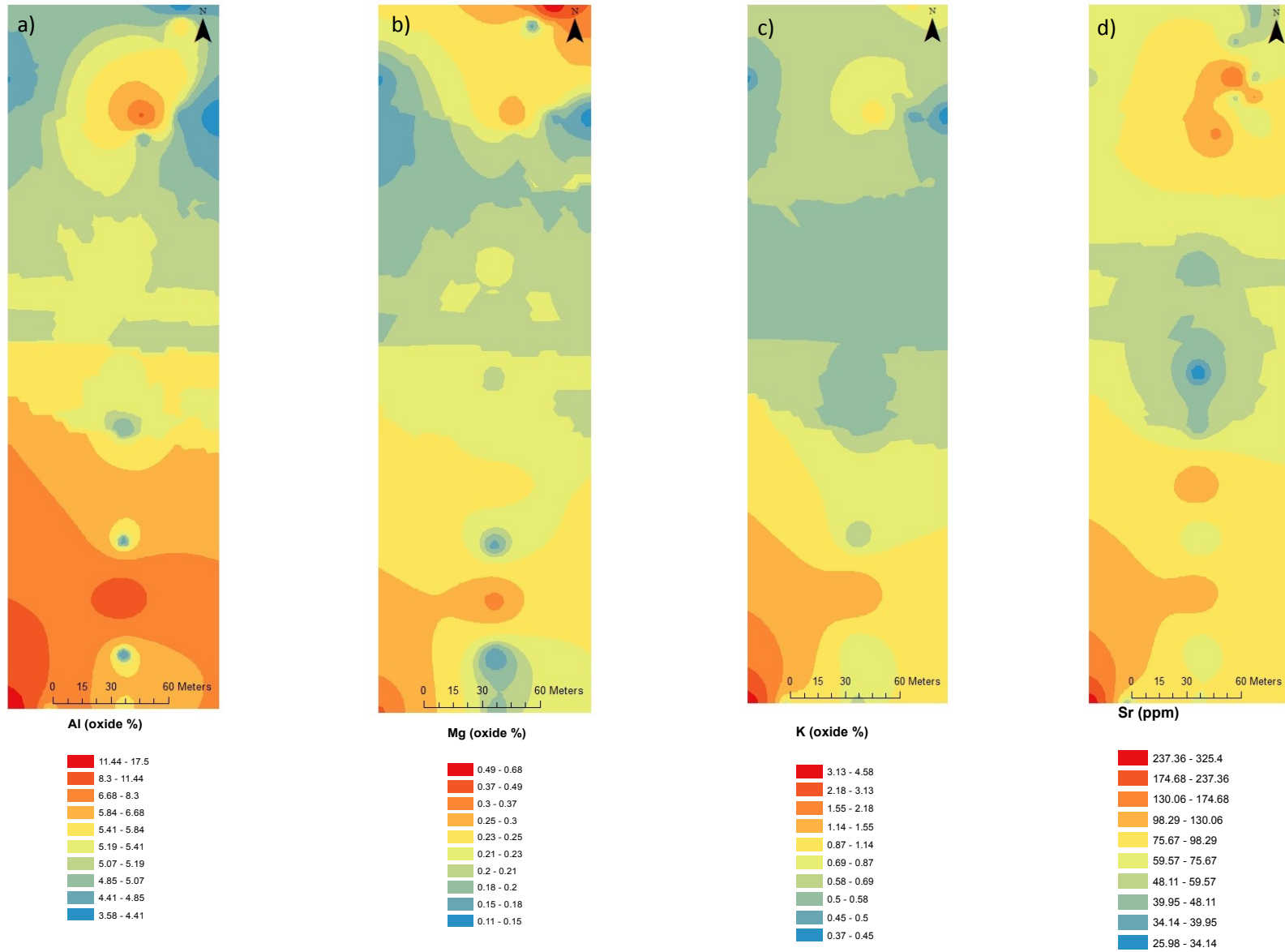


K (Oxide%)



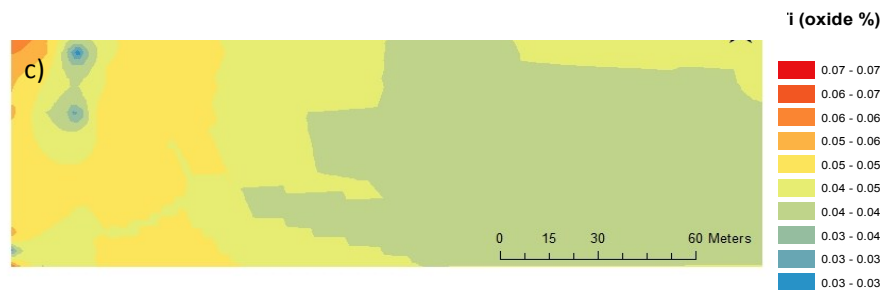
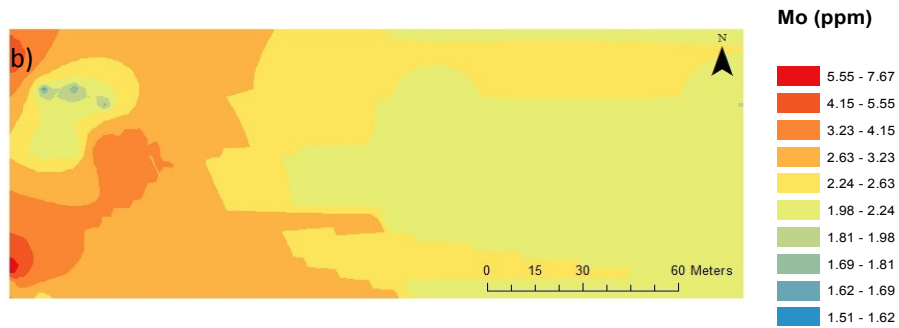
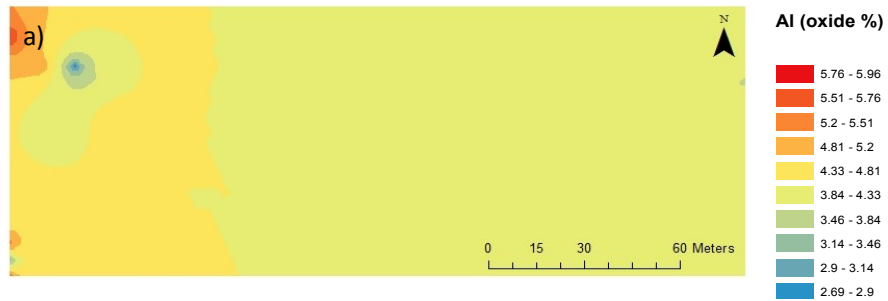
Chemical Similarities to Aluminum in My Cove, a) aluminum distribution b) potassium distribution, c) zinc distribution

F1.3: Aluminum Compatibility



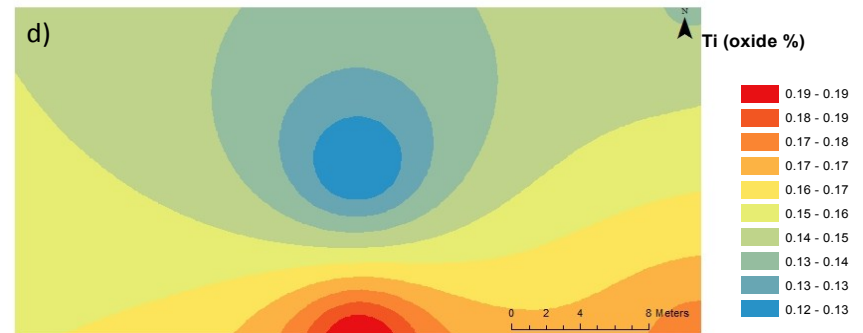
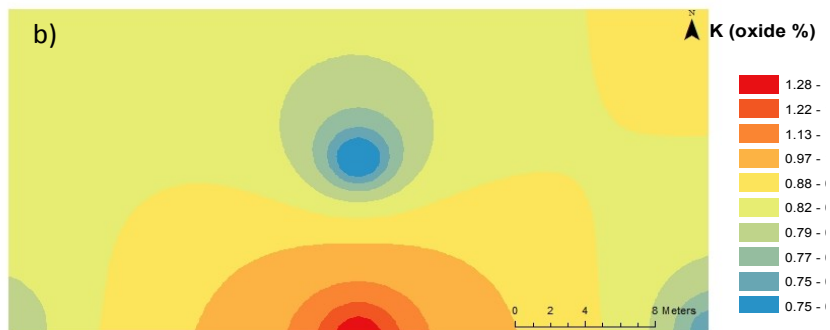
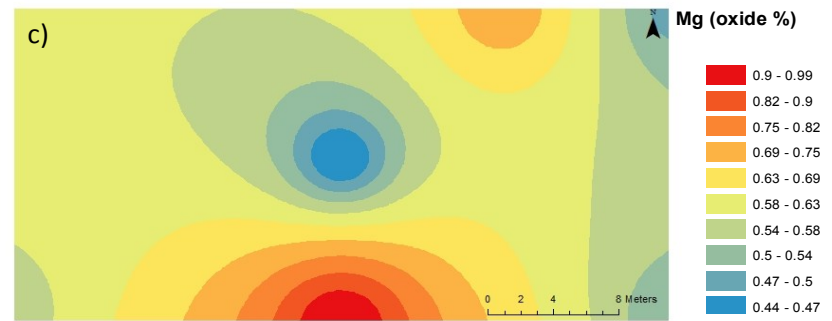
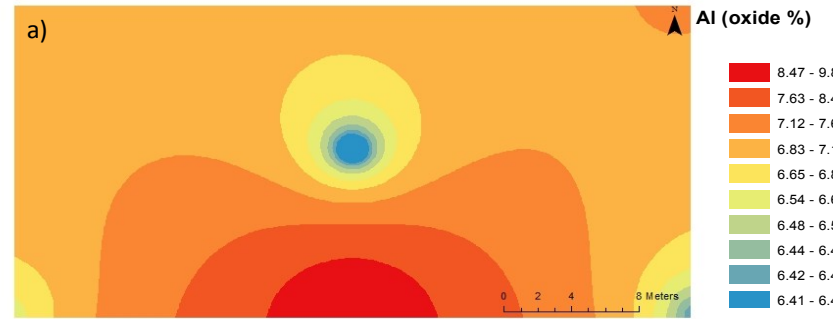
Chemical Similarities to Aluminum at Sowden Lake 46 a) aluminum distribution, b) magnesium distribution, c) potassium distribution, d) strontium distribution

F1.3: Aluminum Compatibility



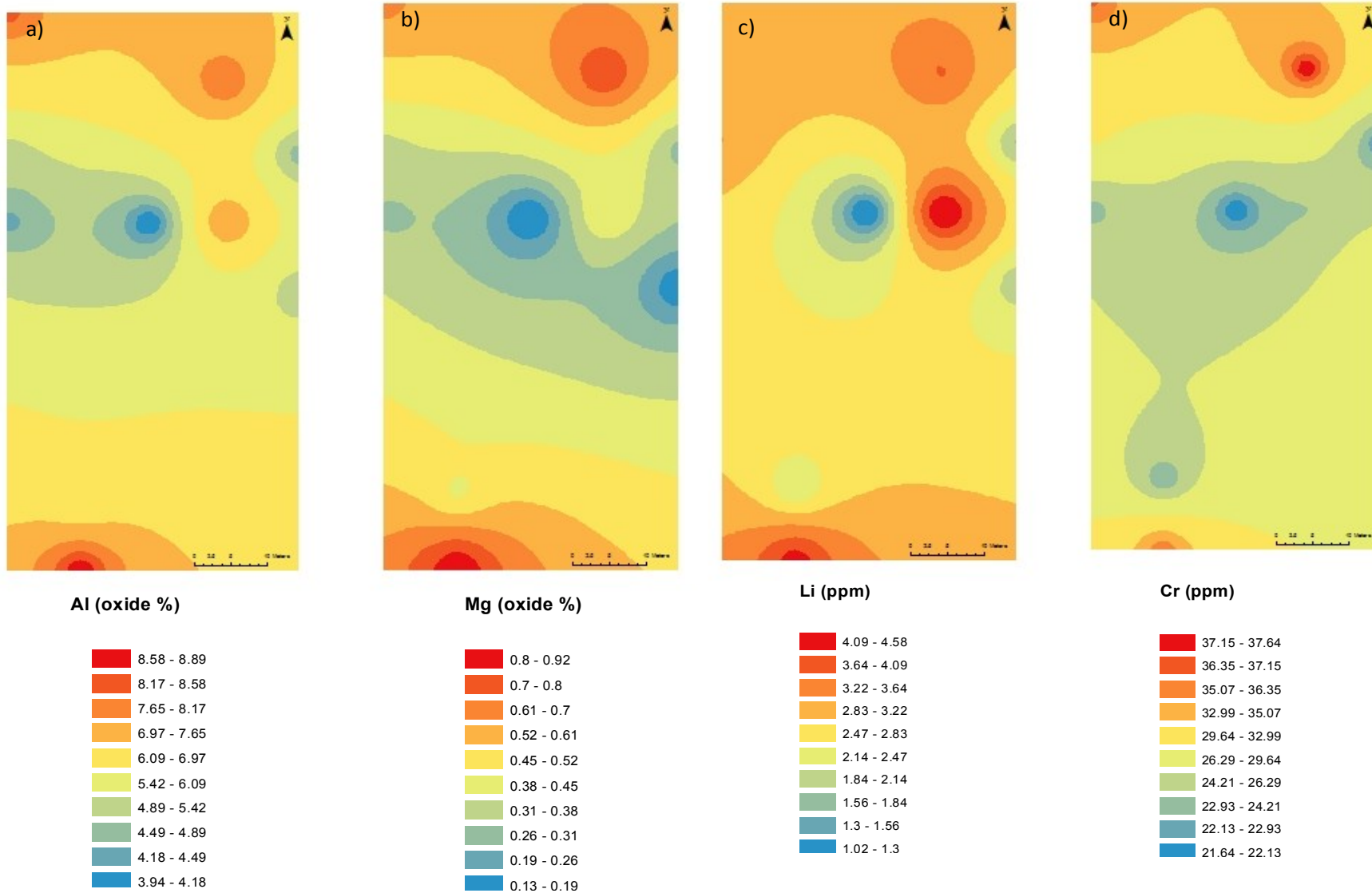
Chemical Similarities to Aluminum at Sowden Lake 41 a) aluminum distribution, b) molybdenum distribution) titanium distribution

F1.3: Aluminum Compatibility



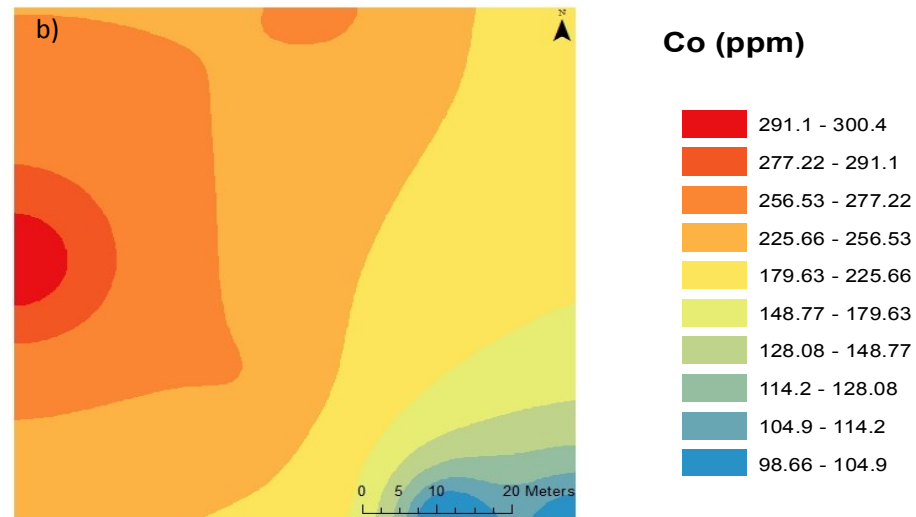
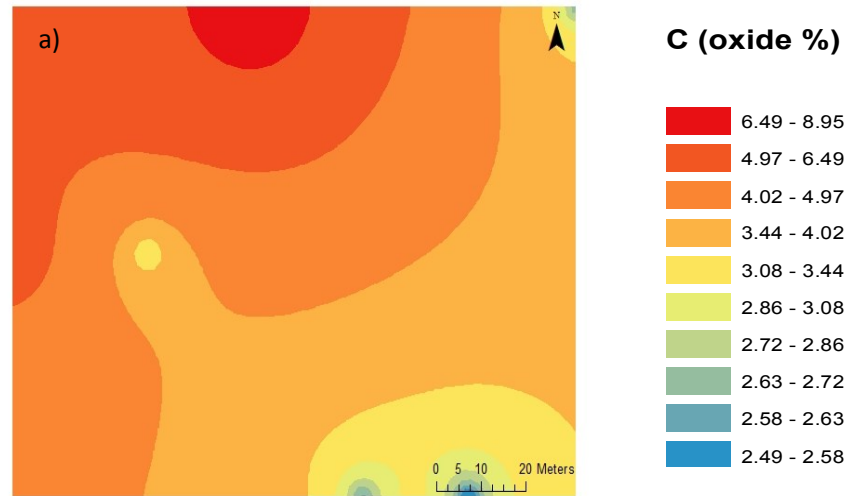
Chemical Similarities to Aluminum at Island Site, Shebandowan a) aluminum distribution, b) potassium distribution, c) magnesium distribution, d) titanium distribution

F1.3: Aluminum Compatibility



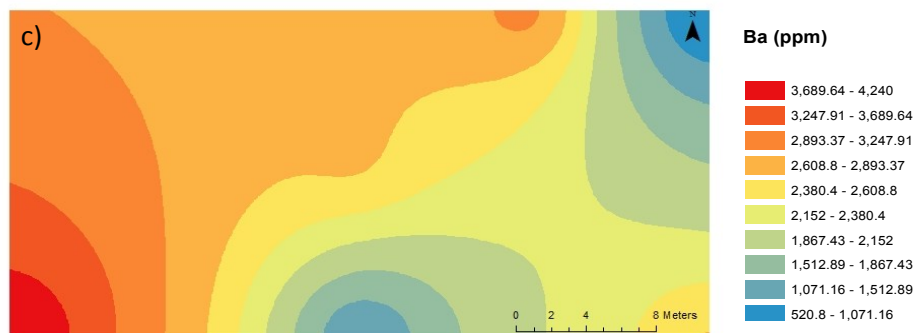
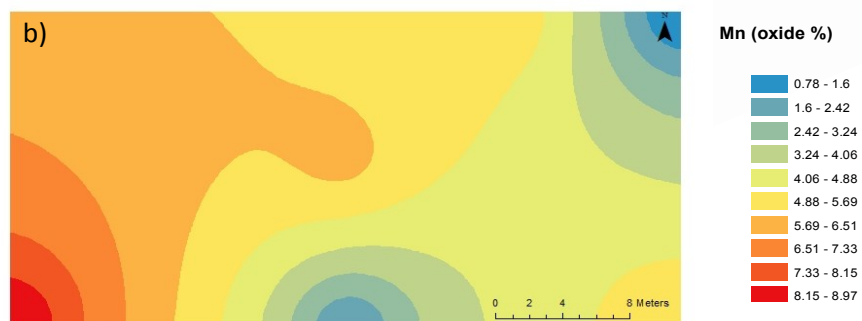
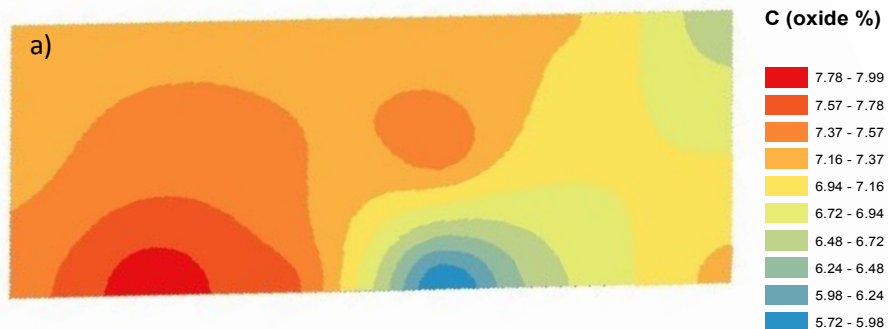
Chemical Similarities to Aluminum at Small Site, Shebandowan, a) aluminum distribution, b) magnesium distribution, c) lithium distribution, d) chromium distribution

F1.4: Carbon Compatibility



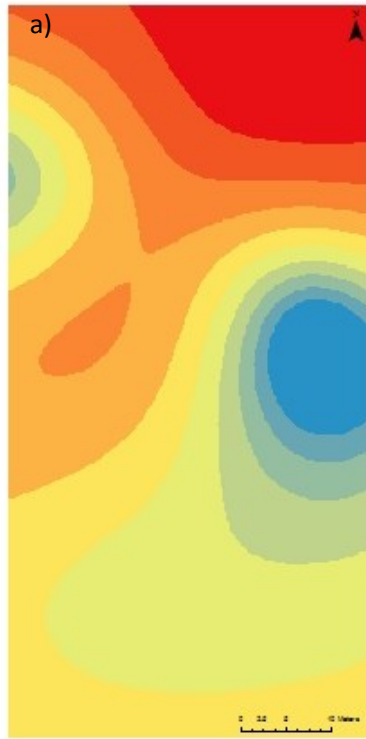
Chemical Similarities to Carbon at Granite Islands, a) carbon distribution, b) cobalt distribution

F1.4: Carbon Compatibility

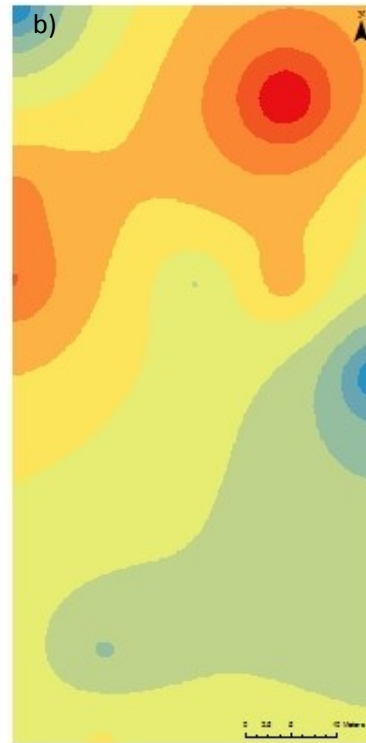
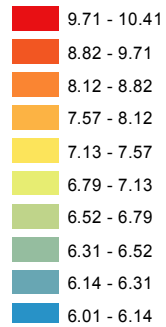


Chemical Similarities to Carbon at Island Site, Shebandowan a) carbon distribution, b) manganese distribution, c) barium distribution

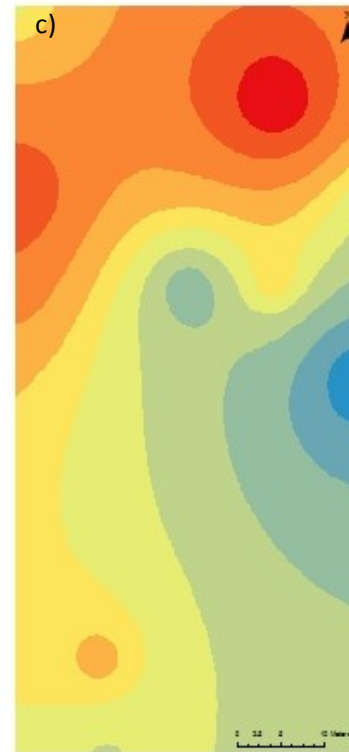
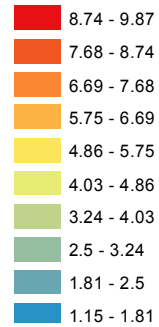
F1.4: Carbon Compatibility



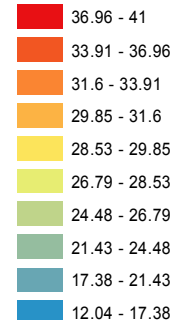
C (oxide %)



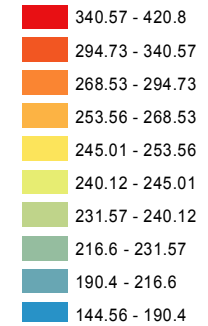
Mn (Oxide %)



La (ppm)

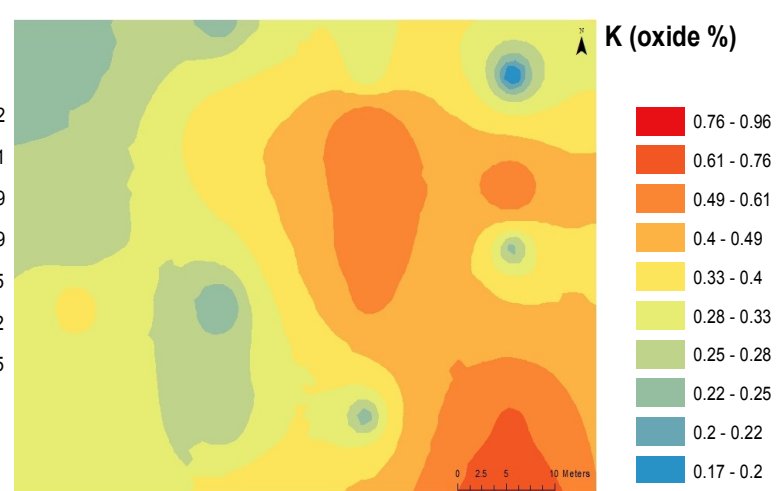
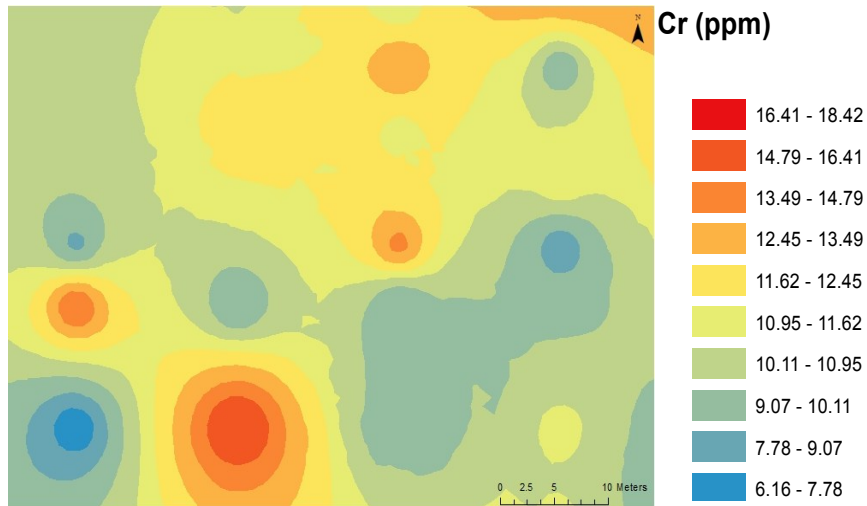
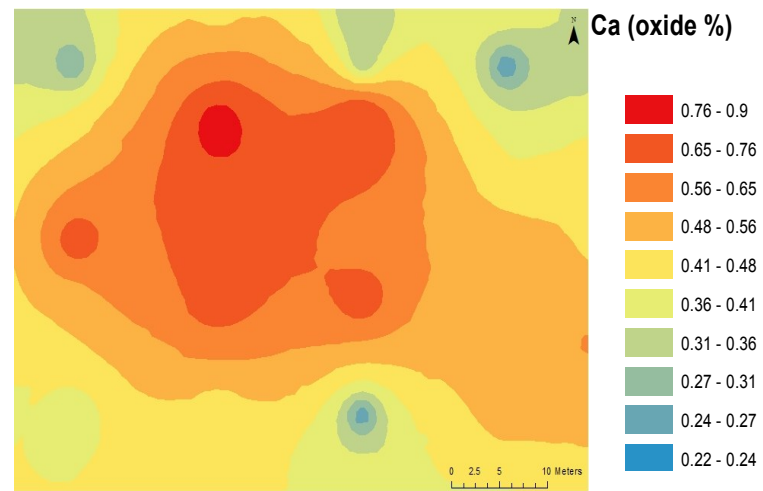
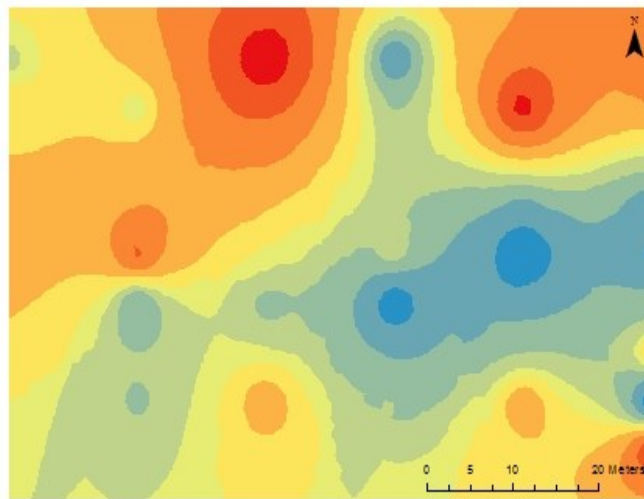


S (ppm)

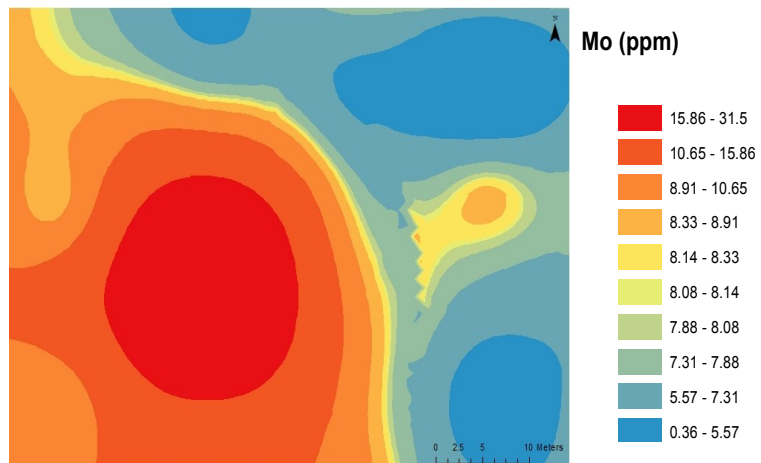
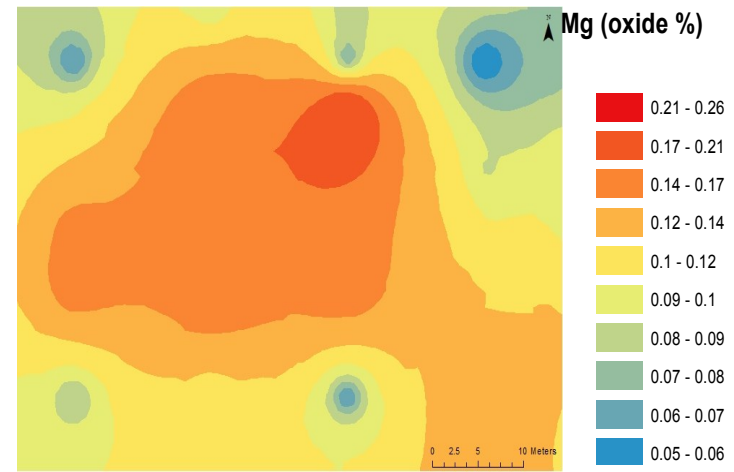
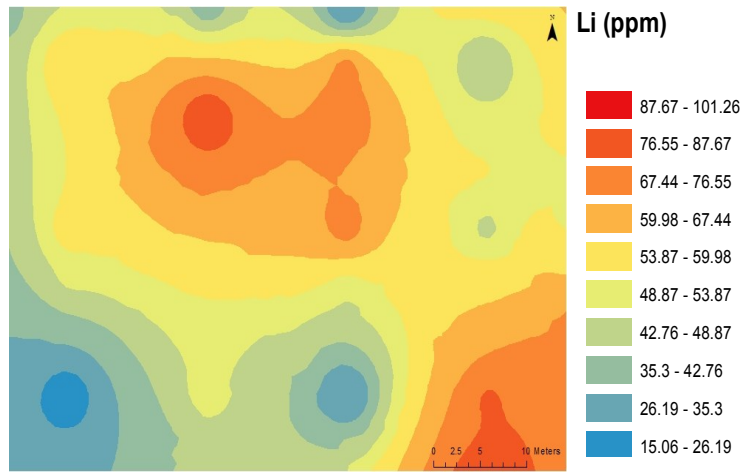


Chemical Similarities to Carbon at Small Site, Shebandowan, a) carbon distribution, b) manganese distribution, c) lanthenum distribution, d) sulfur distribution

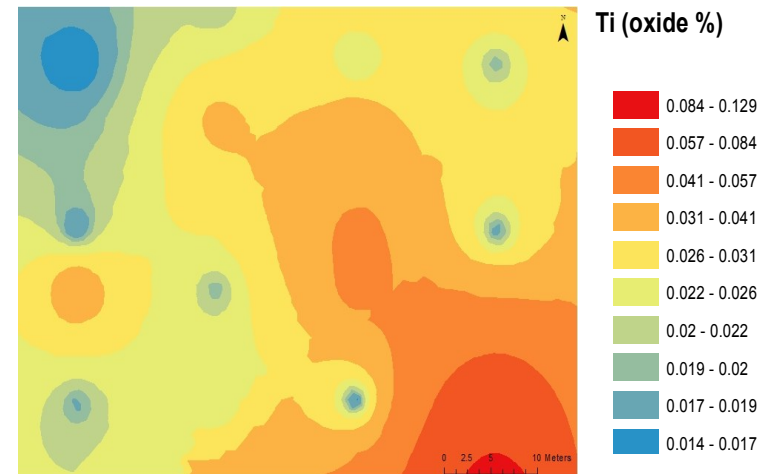
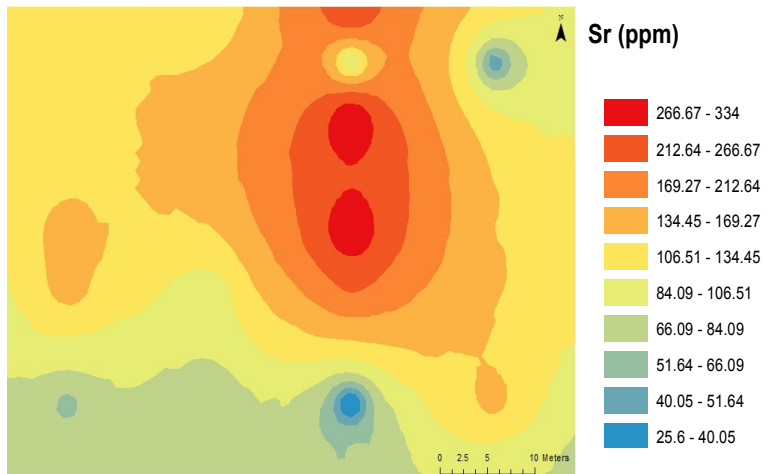
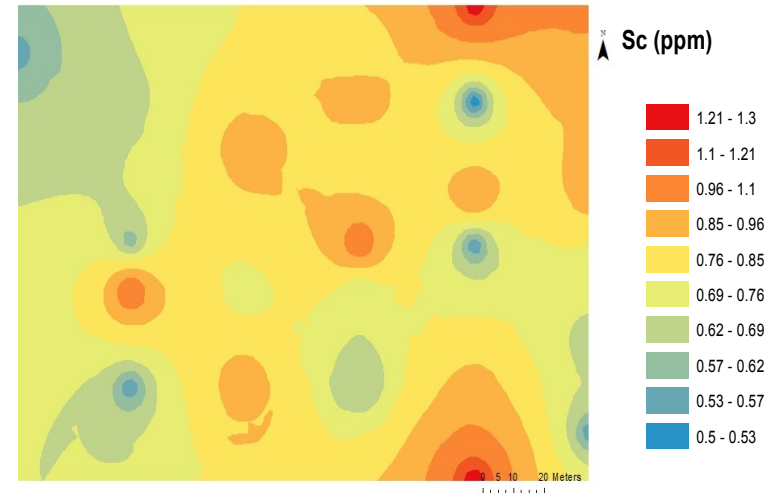
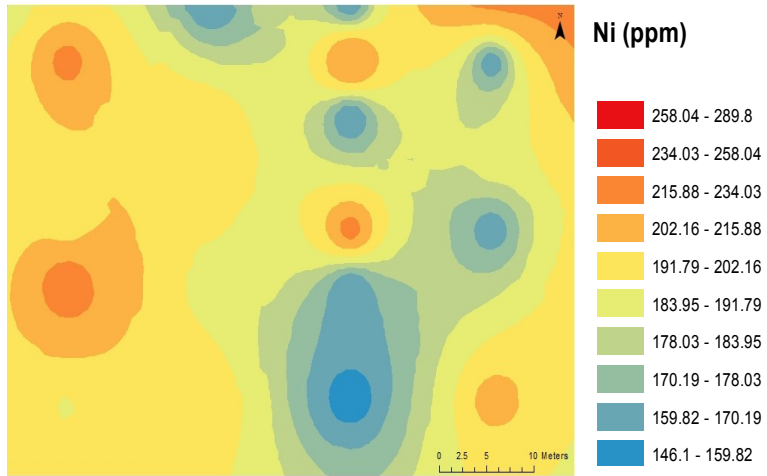
F2.1 7 Cove (alphabetical order)



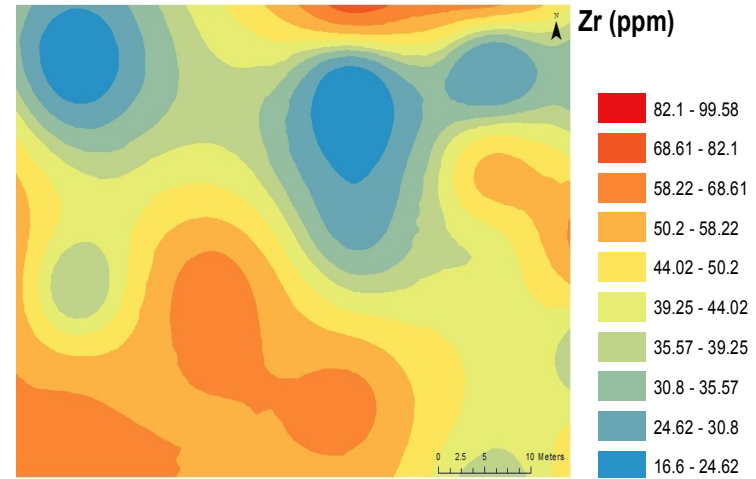
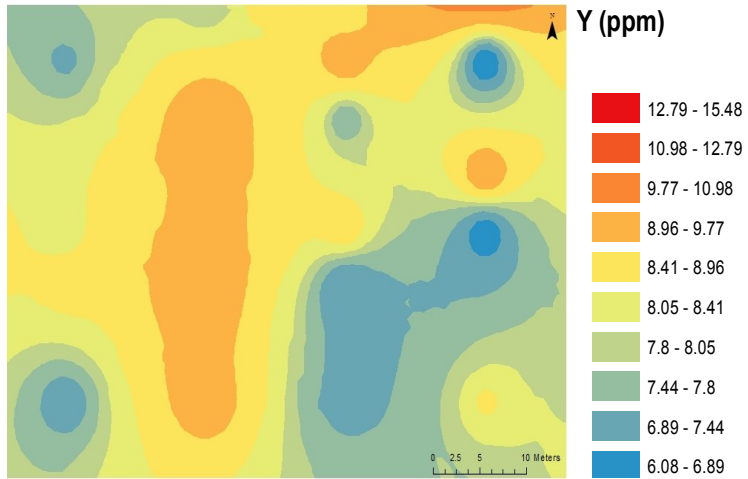
F2.1 7 Cove (alphabetical order)



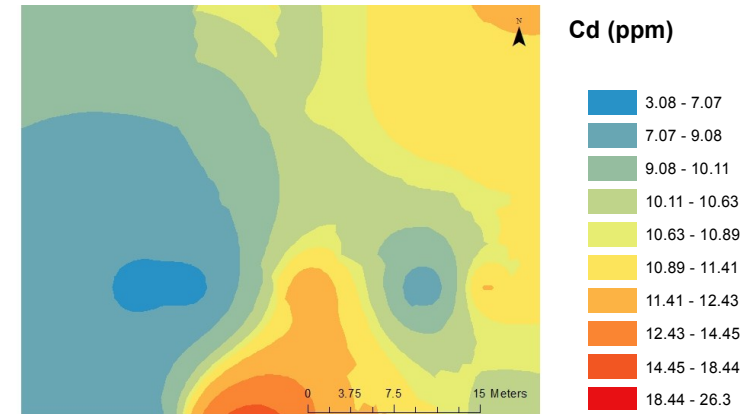
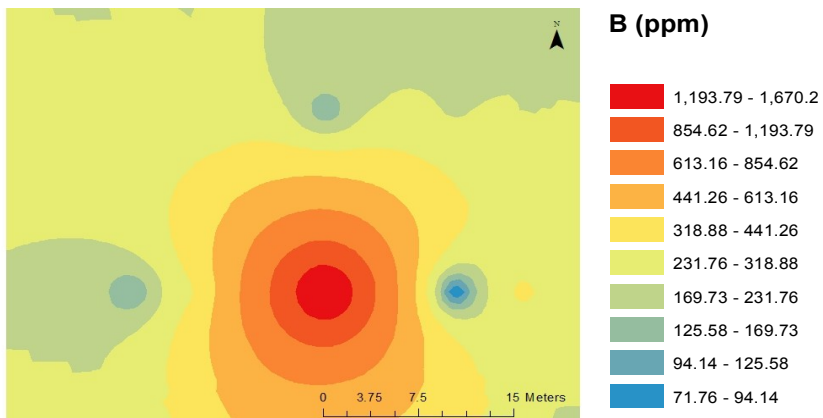
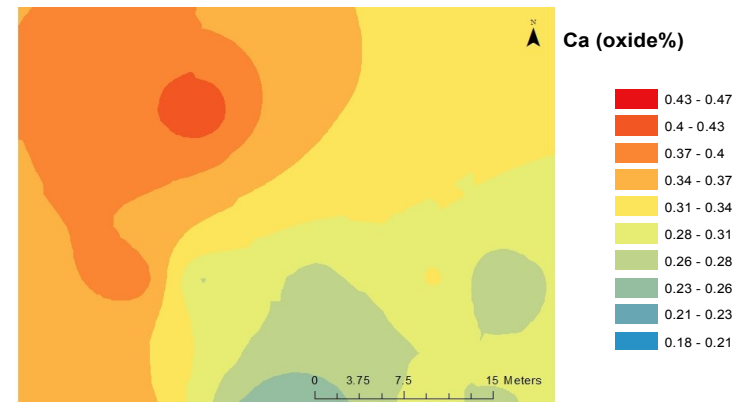
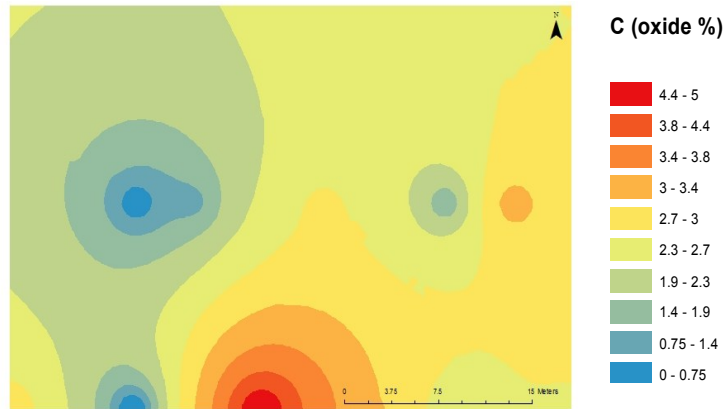
F2.1 7 Cove (alphabetical order)



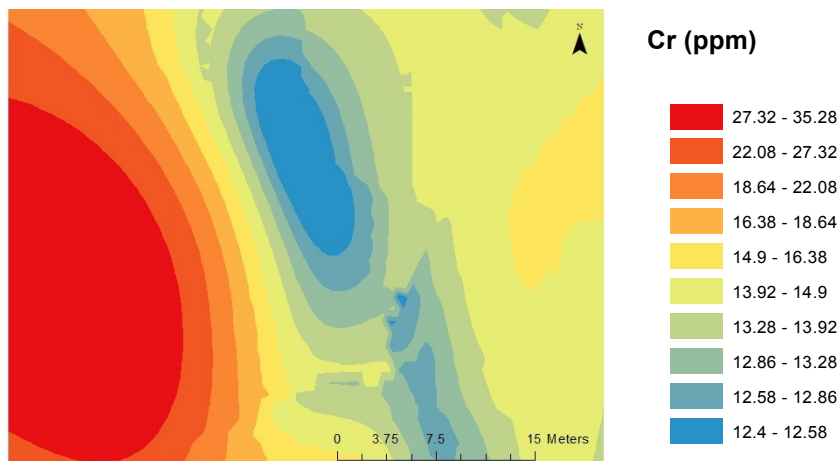
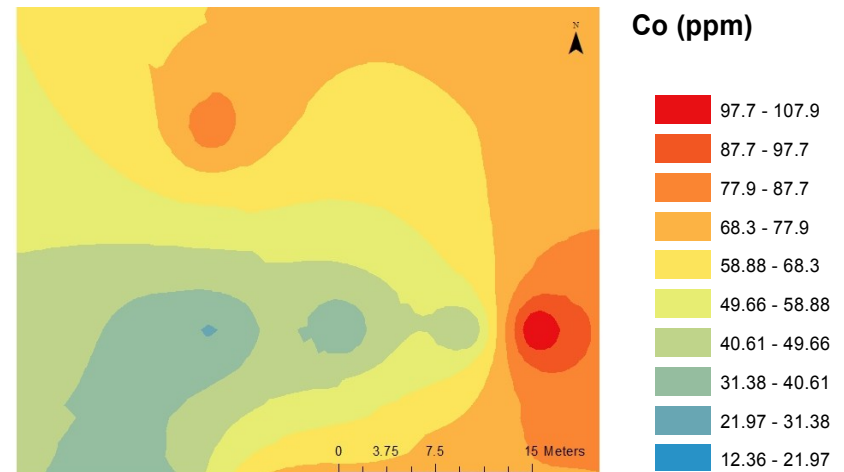
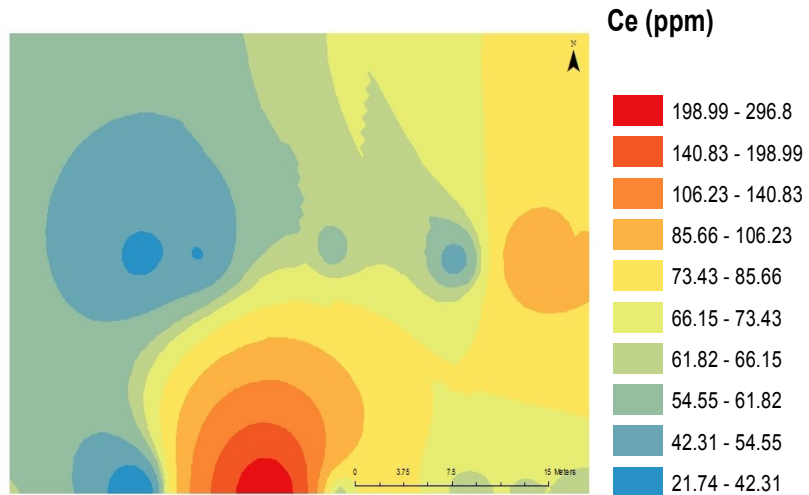
F2.1 7 Cove (alphabetical order)



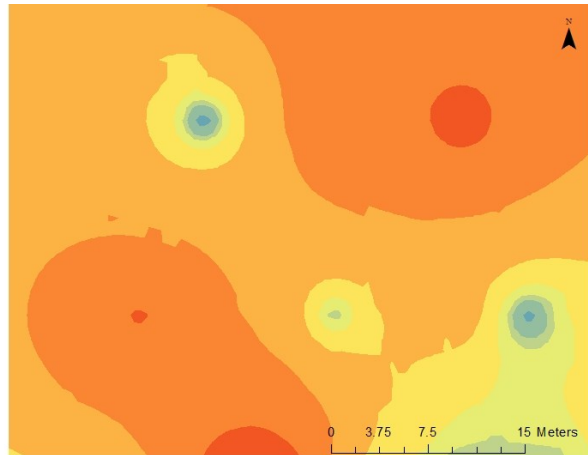
F2.2 Bud's Cove (alphabetical order)



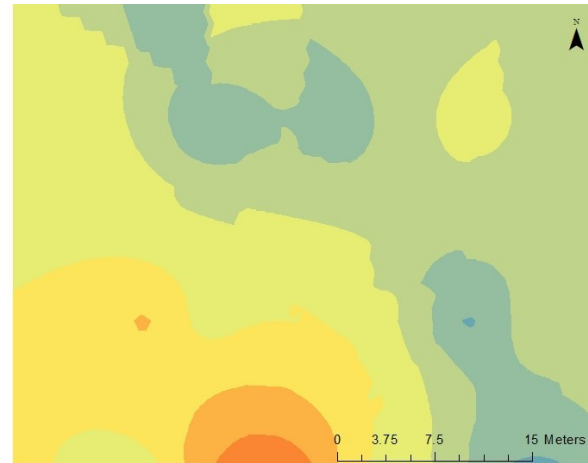
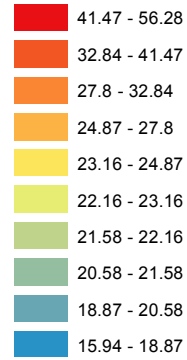
F2.2 Bud's Cove (alphabetical order)



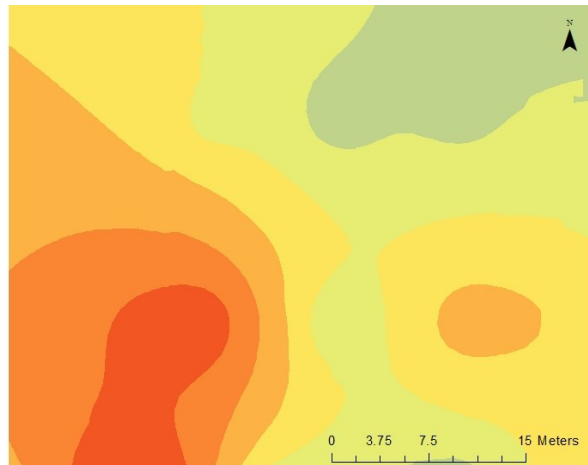
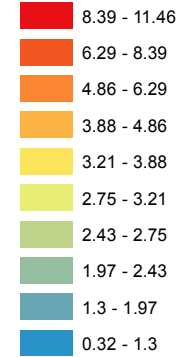
F2.2 Bud's Cove (alphabetical order)



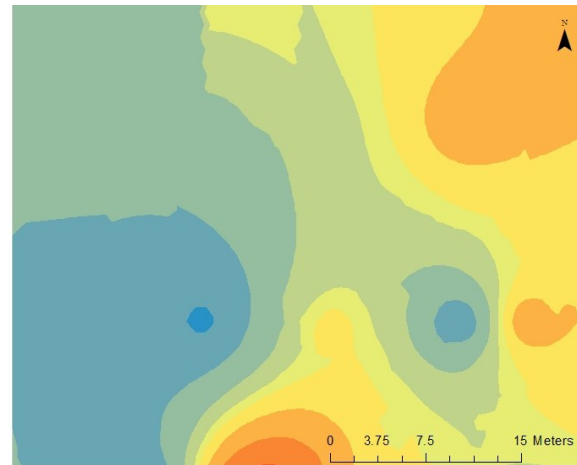
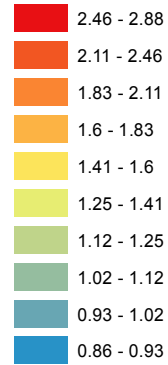
Li (ppm)



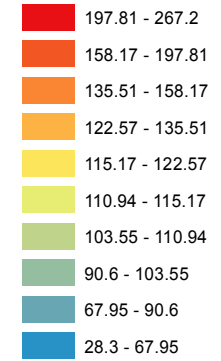
Mo (ppm)



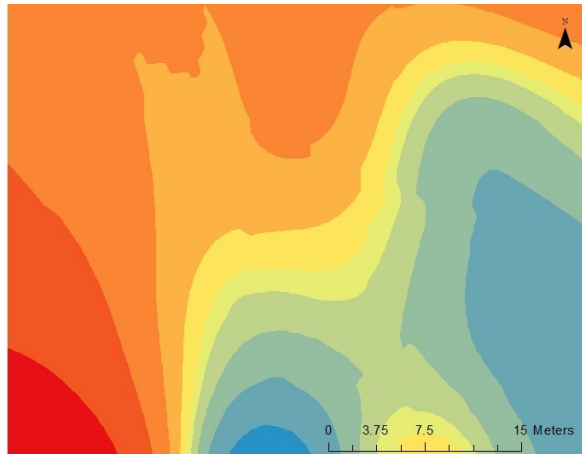
Na (oxide %)



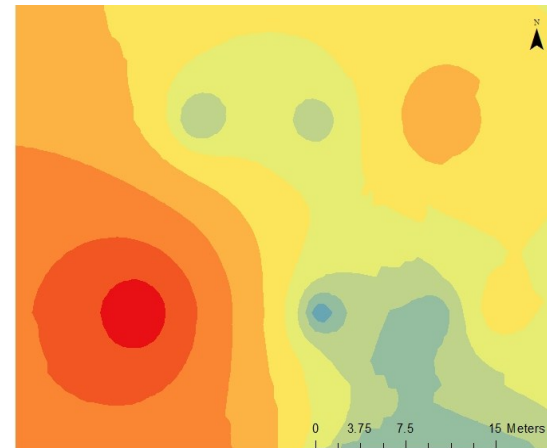
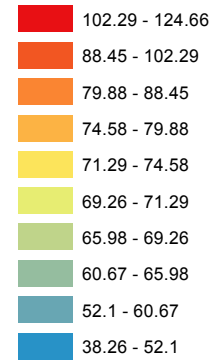
Ni (ppm)



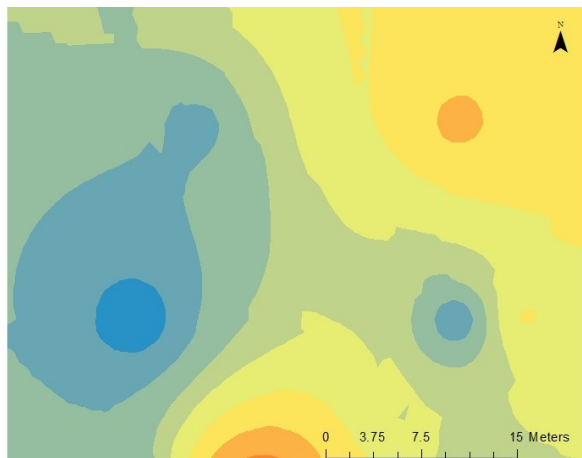
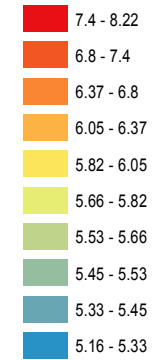
F2.2 Bud's Cove (alphabetical order)



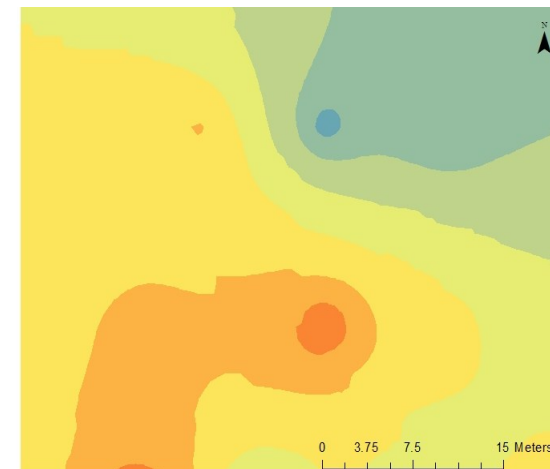
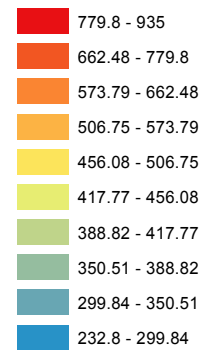
Sr (ppm)



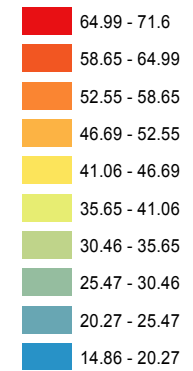
Y (ppm)



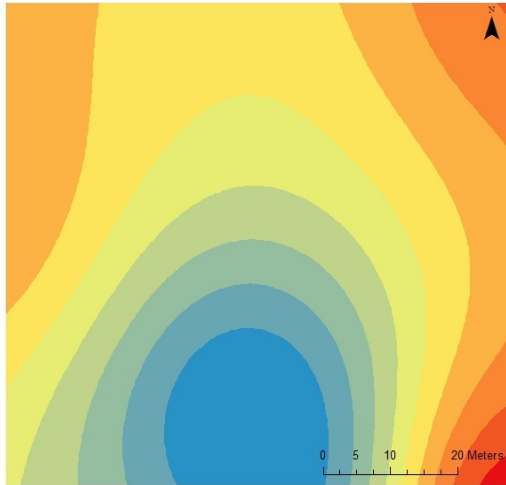
Zn (ppm)



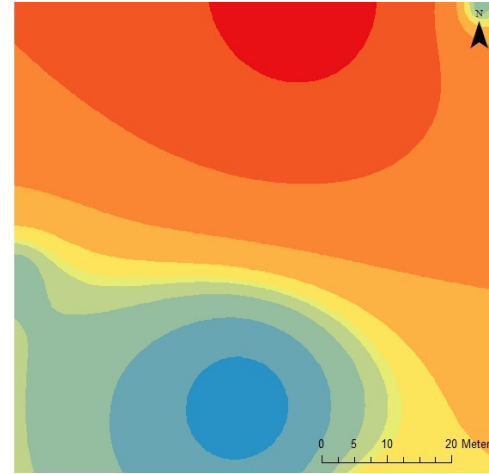
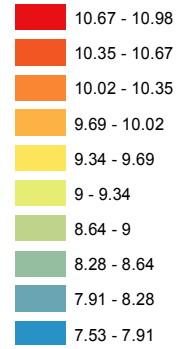
Zr (ppm)



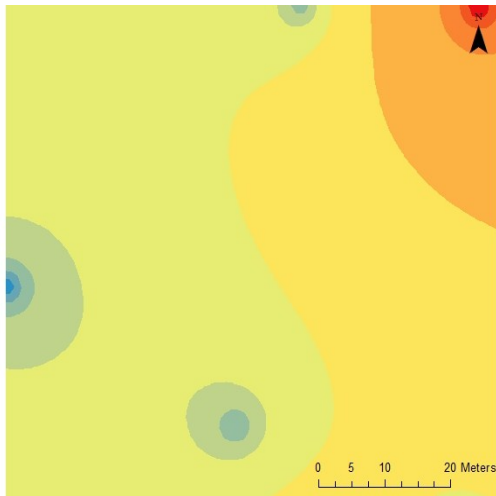
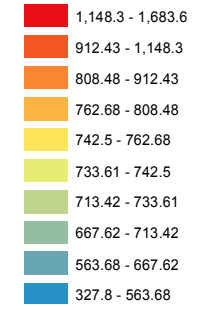
F2.3 Granite Islands (alphabetical order)



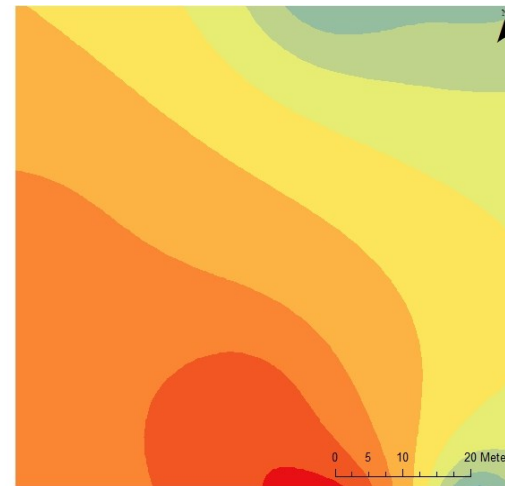
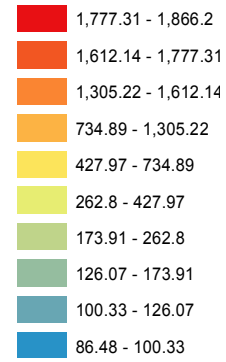
Al (oxide %)



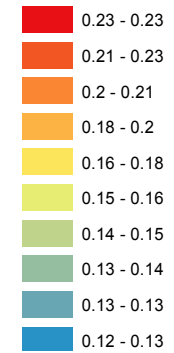
As (ppm)



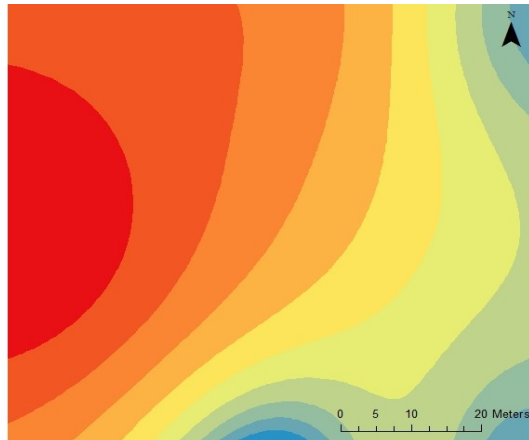
B (ppm)



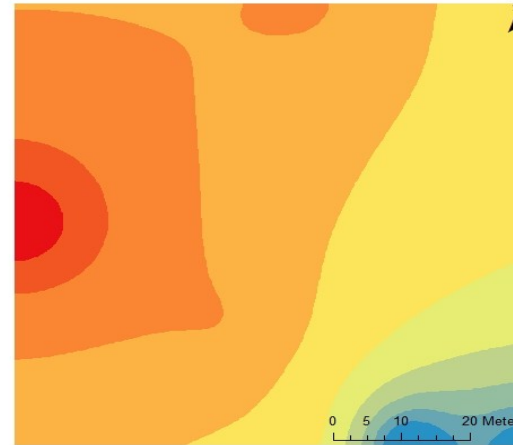
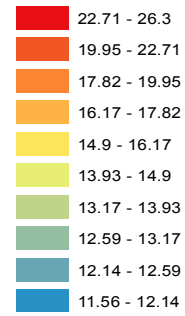
Ca (oxide %)



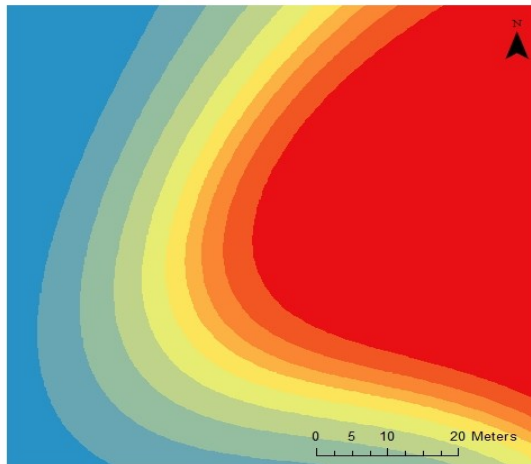
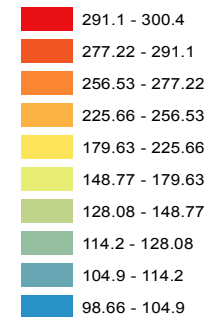
F2.3 Granite Islands (alphabetical order)



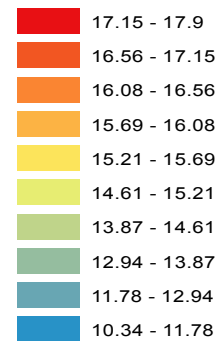
Cd (ppm)



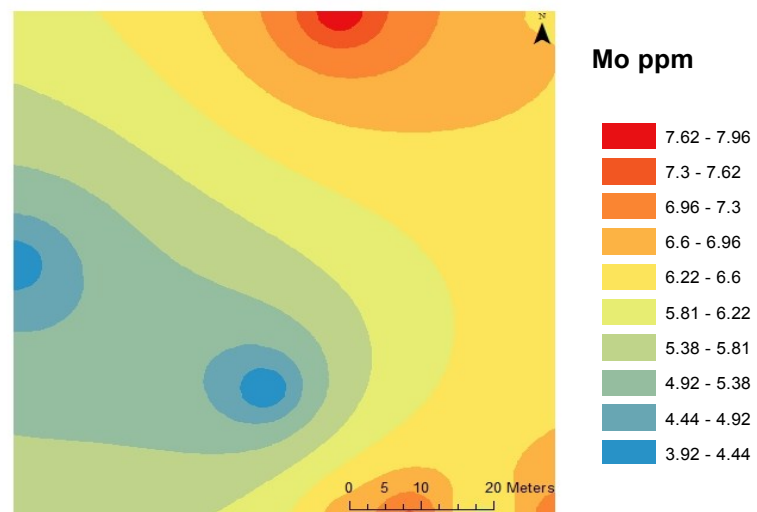
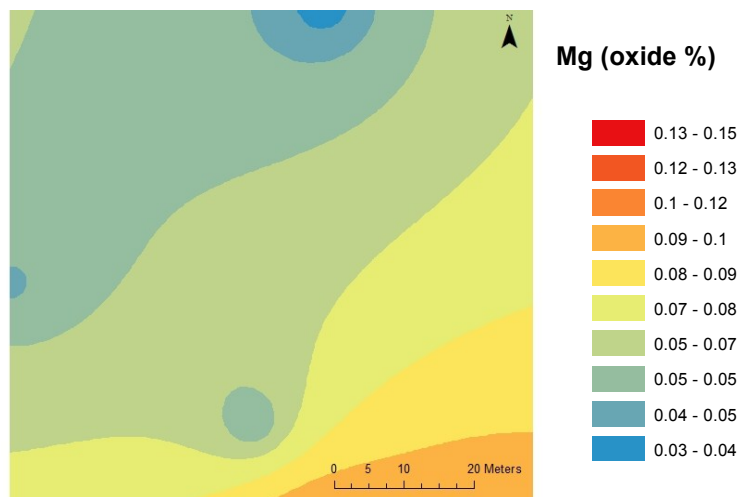
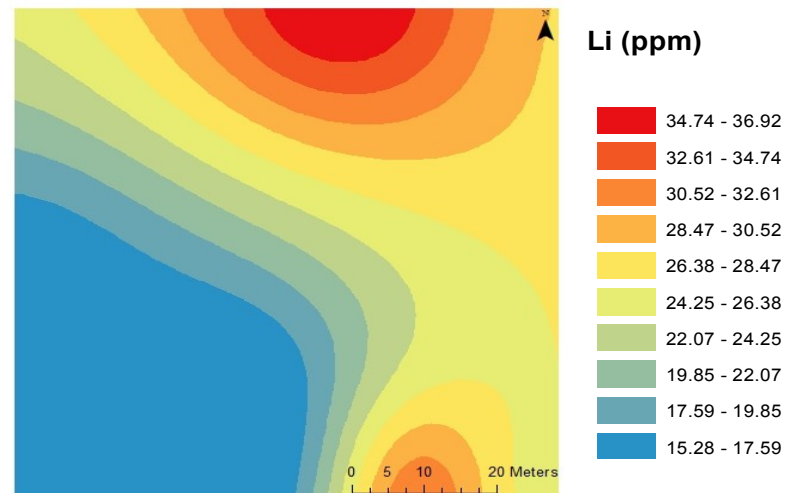
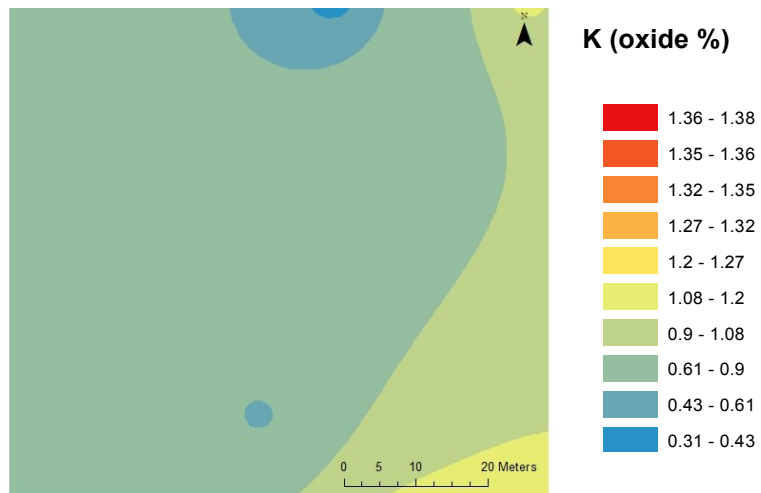
Co (ppm)



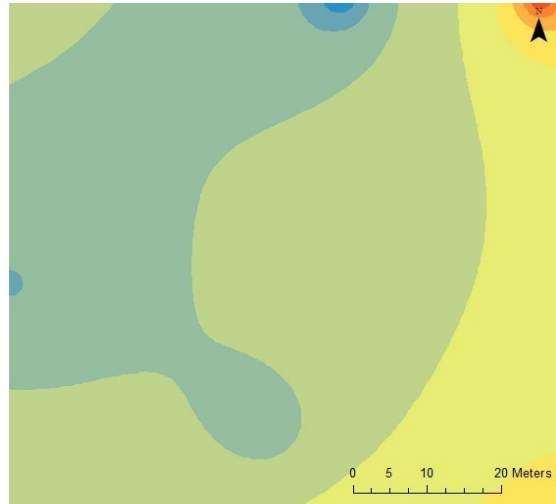
Cr (ppm)



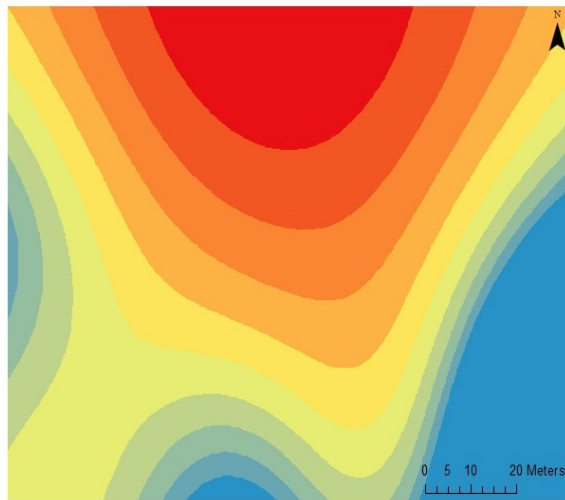
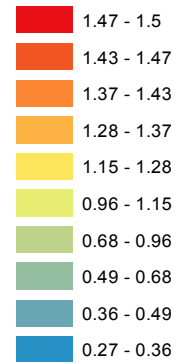
F2.3 Granite Islands (alphabetical order)



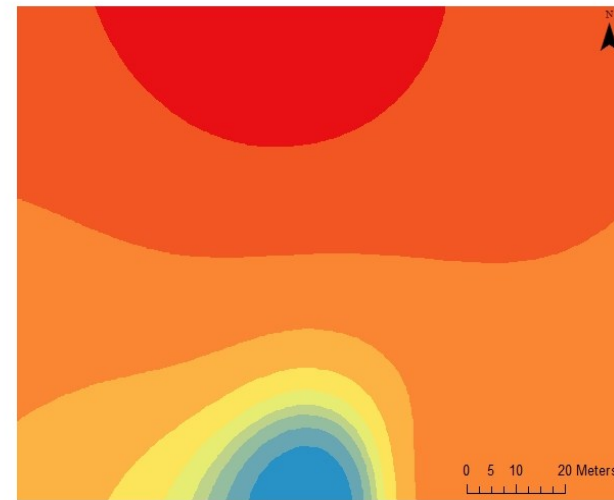
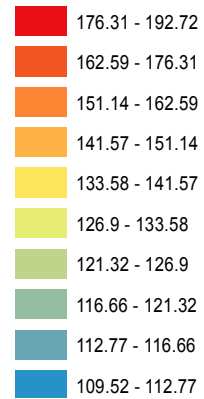
F2.3 Granite Islands (alphabetical order)



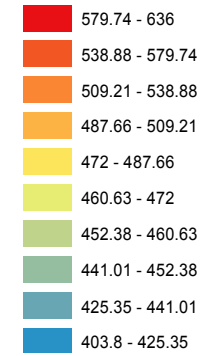
Na (oxide %)



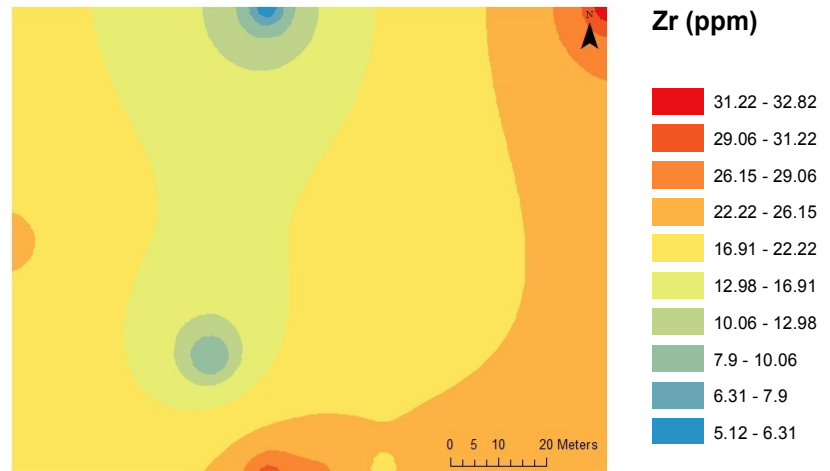
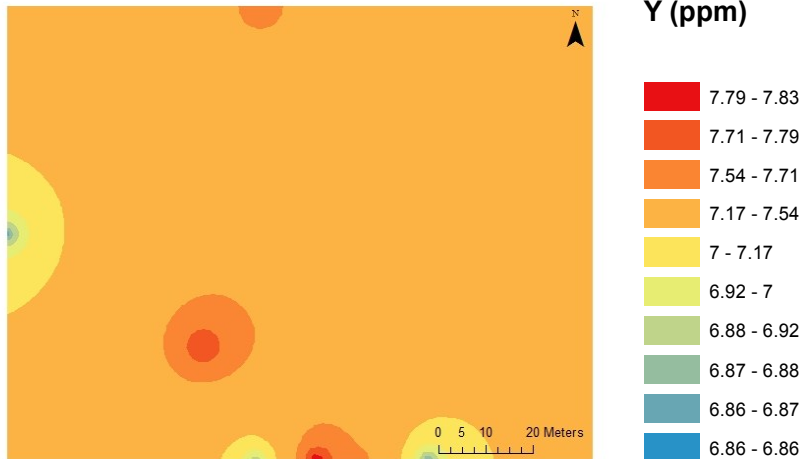
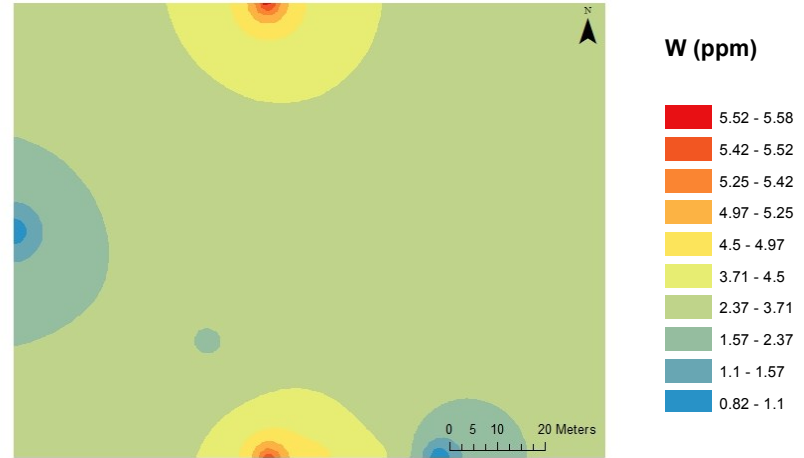
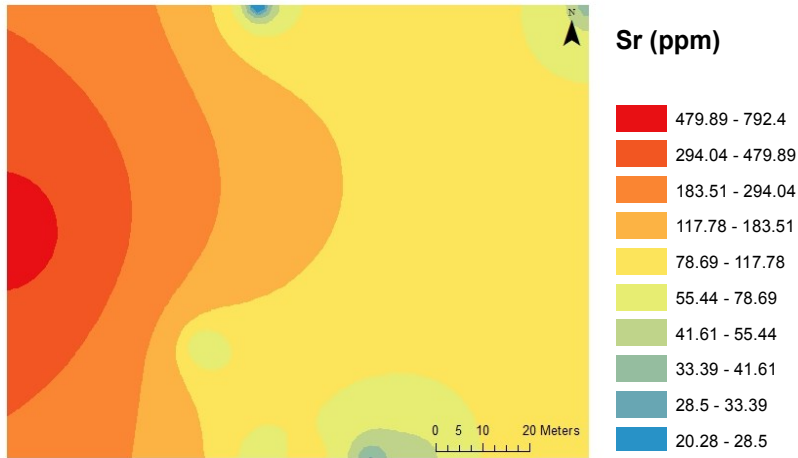
Ni (ppm)



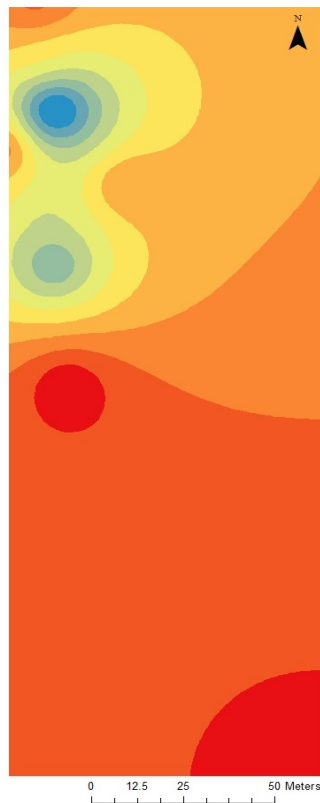
S (ppm)



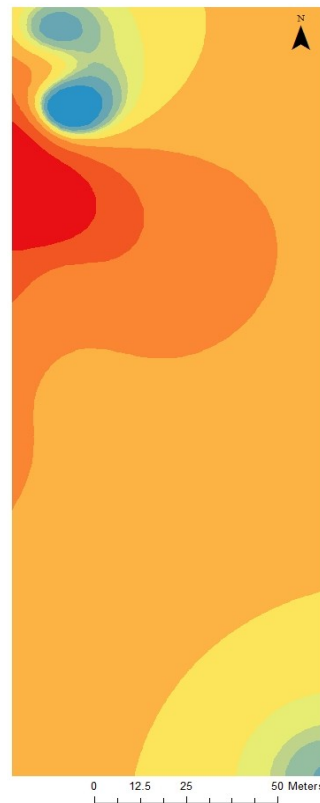
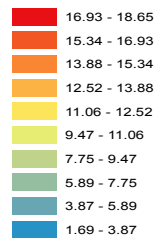
F2.3 Granite Islands (alphabetical order)



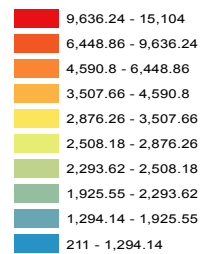
F2.4 Mine Site (alphabetical order)



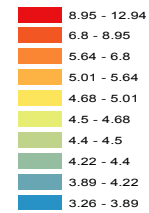
Al (oxide %)



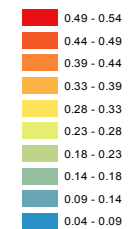
As (ppm)



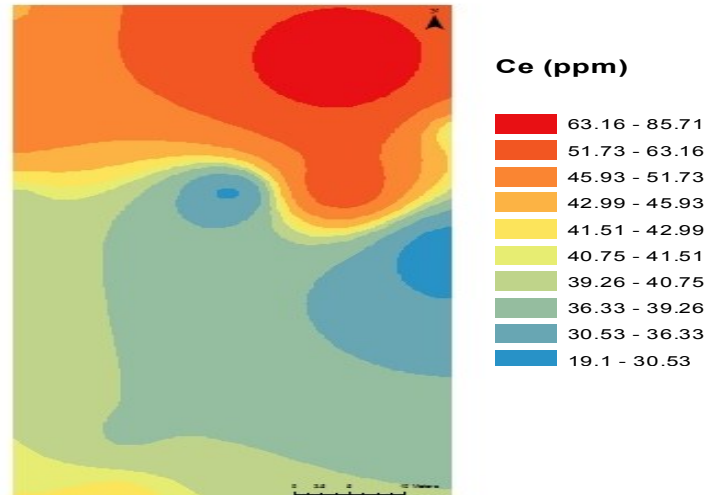
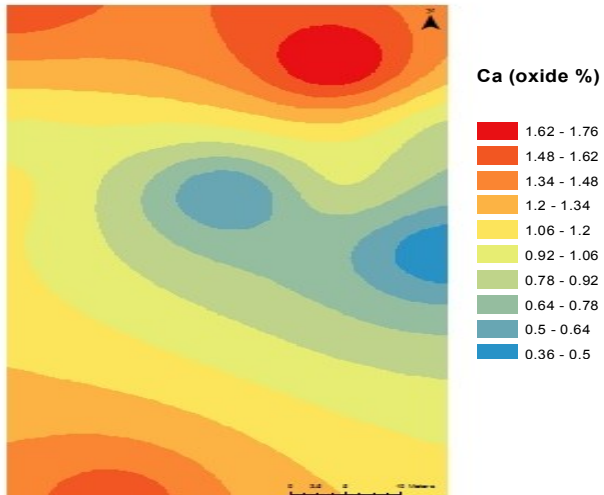
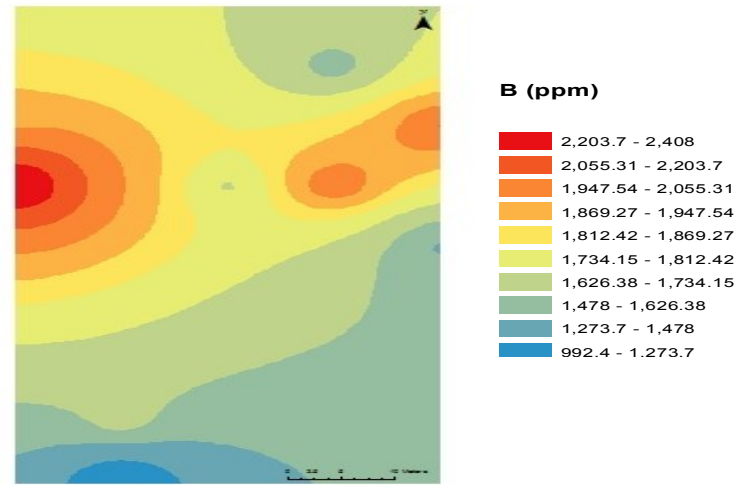
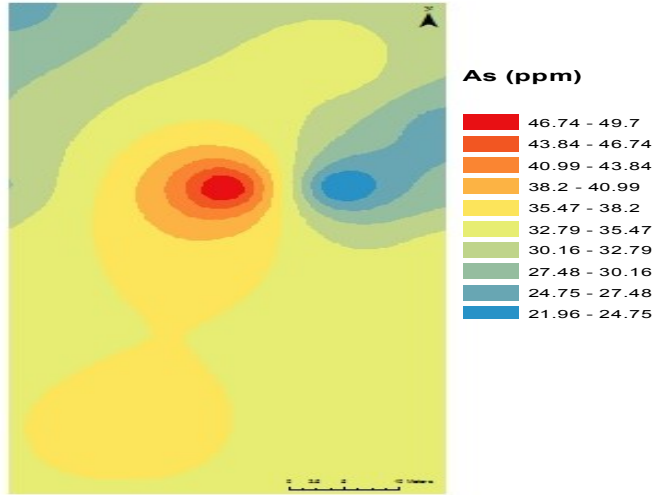
C (oxide %)



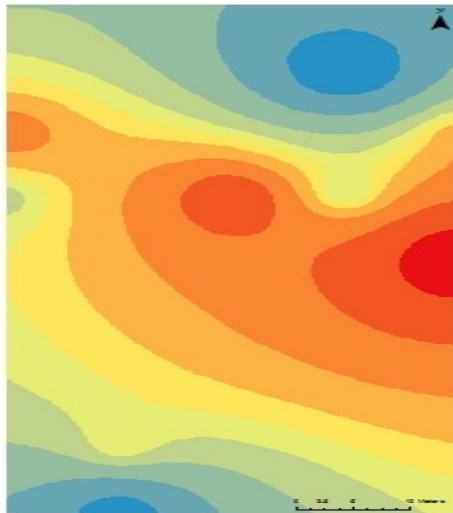
Ca (oxide%)



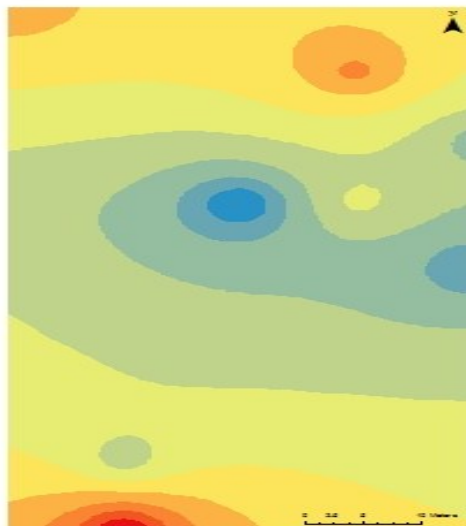
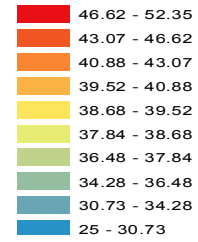
F2.4 Island Site (alphabetical order)



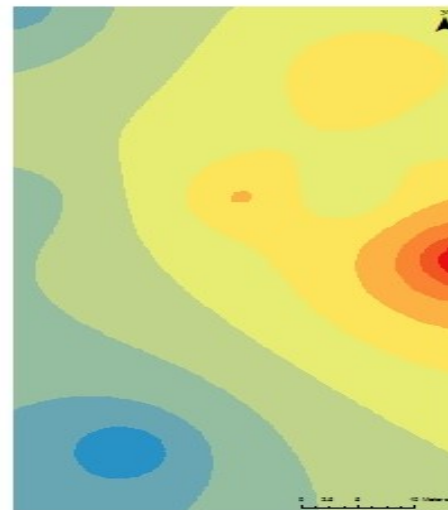
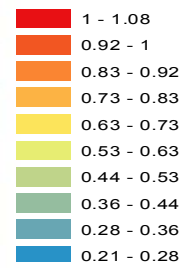
F2.4 Island Site (alphabetical order)



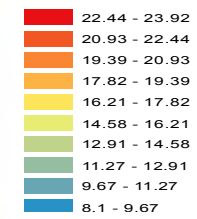
Fe (oxide %)



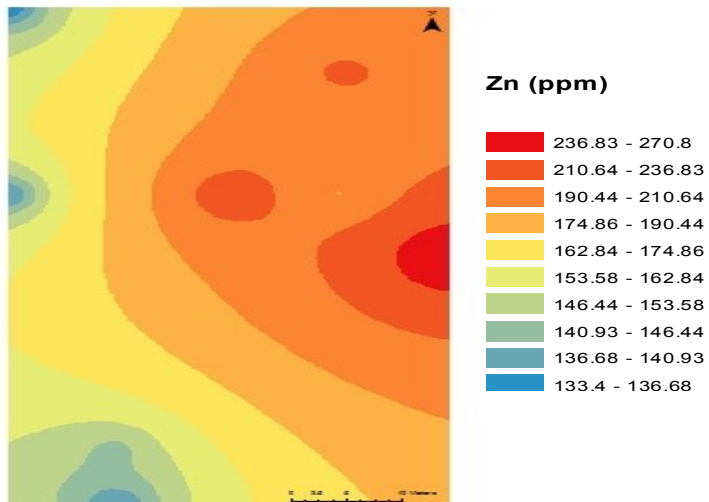
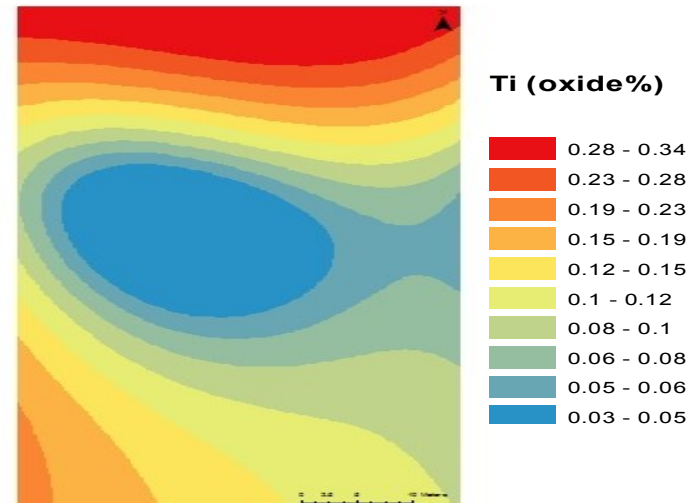
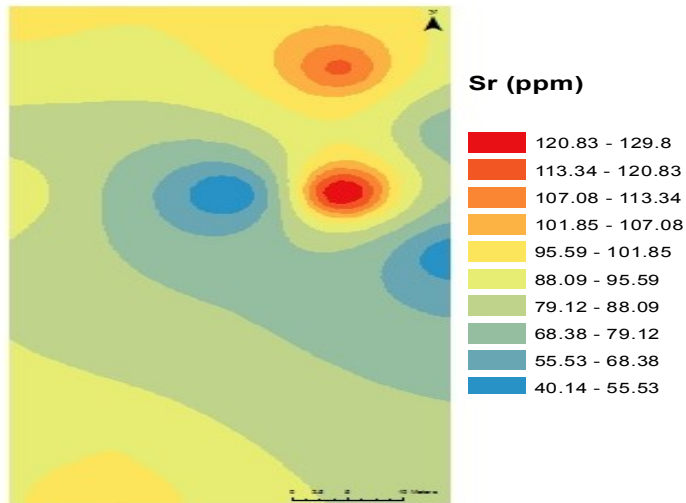
K (oxide %)



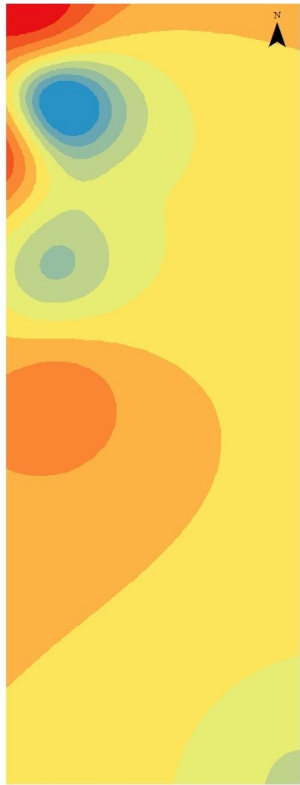
Mo (ppm)



F2.4 Island Site (alphabetical order)

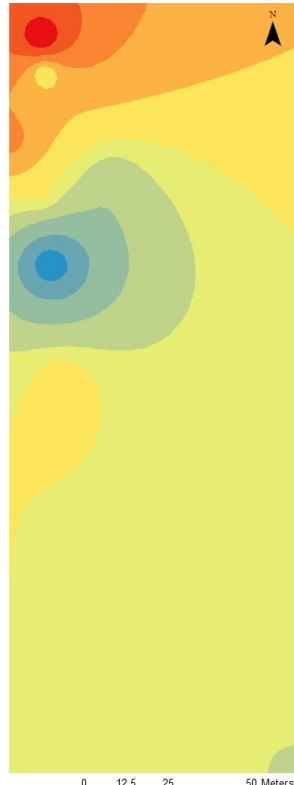
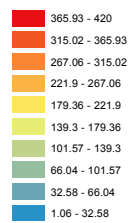


F2.4 Mine Site (alphabetical order)



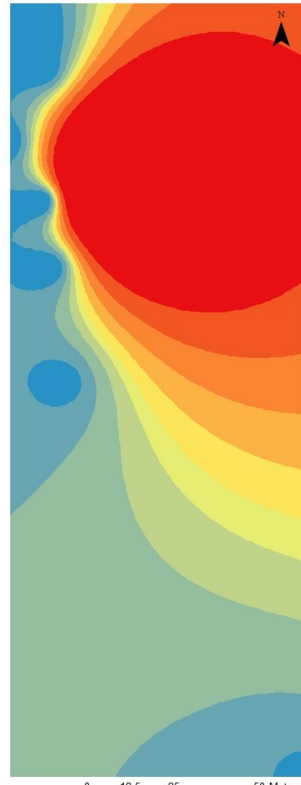
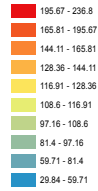
0 12.5 25 50 Meters

Ce (ppm)



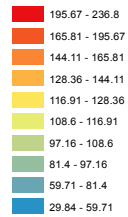
0 12.5 25 50 Meters

Co (ppm)

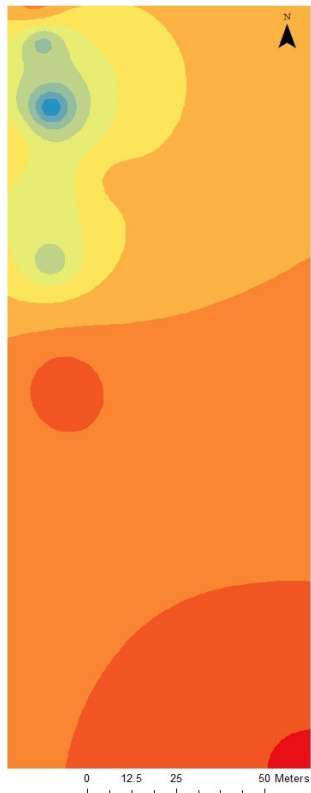


0 12.5 25 50 Meters

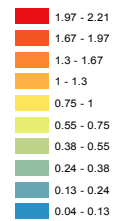
Cr (ppm)



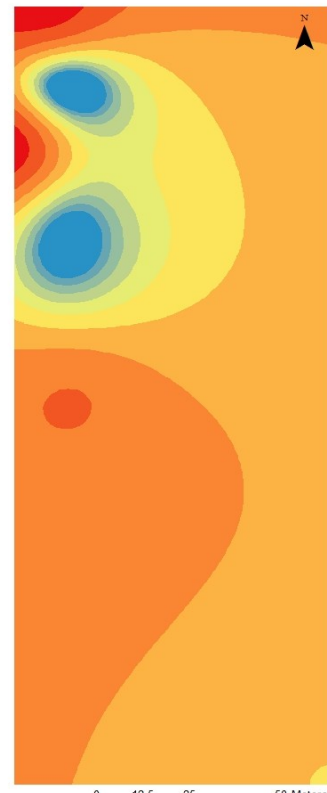
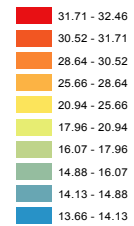
F2.4 Mine Site (alphabetical order)



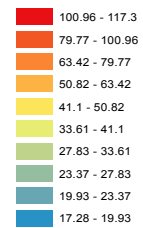
K (oxide %)



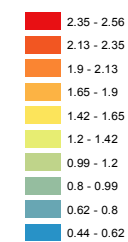
La (ppm)



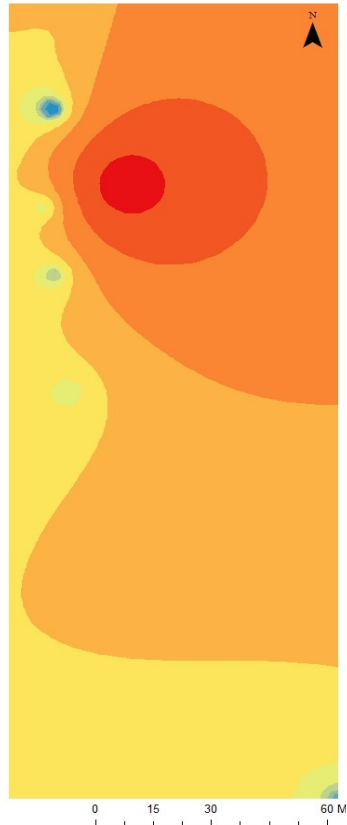
Li (ppm)



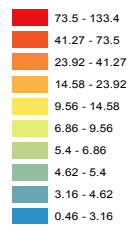
Na (oxide %)



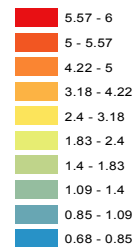
F2.4 Mine Site (alphabetical order)



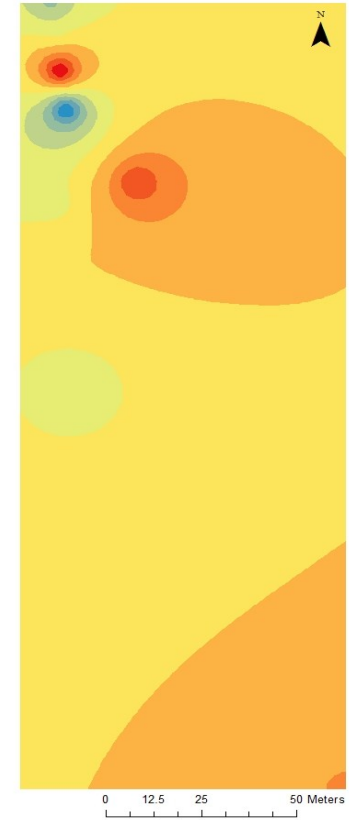
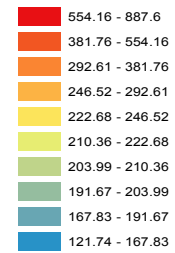
Mo (ppm)



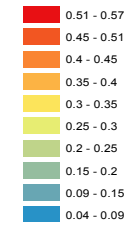
Nb (ppm)



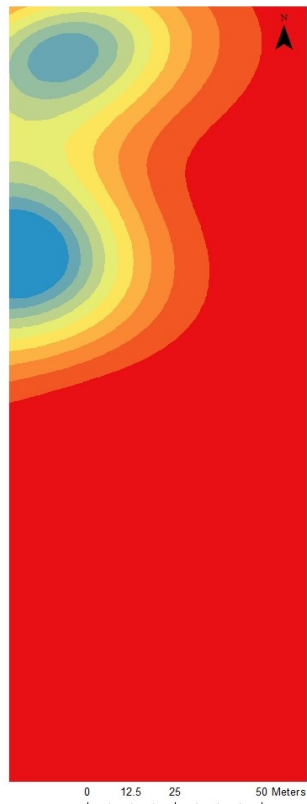
Ni (ppm)



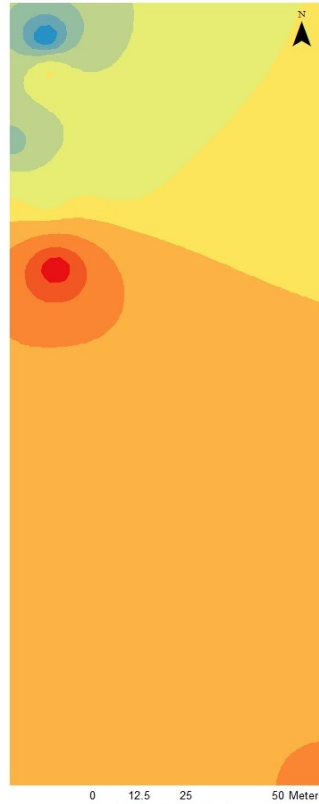
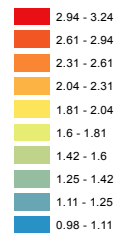
P (oxide %)



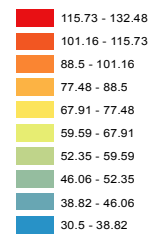
F2.4 Mine Site (alphabetical order)



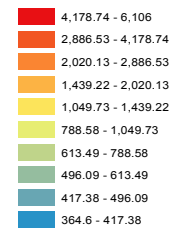
Sc (ppm)



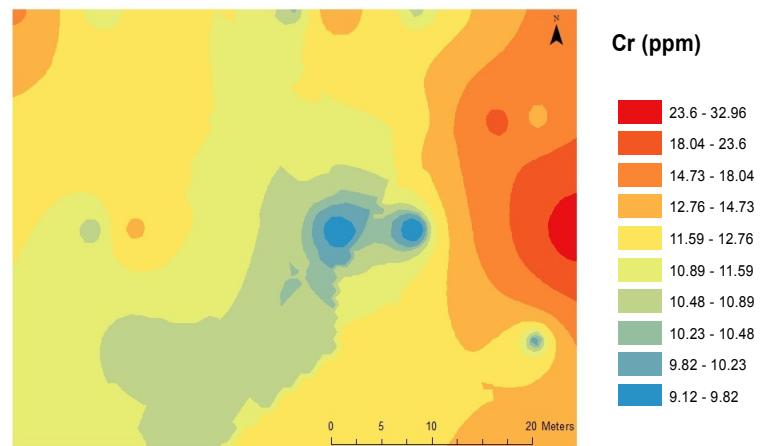
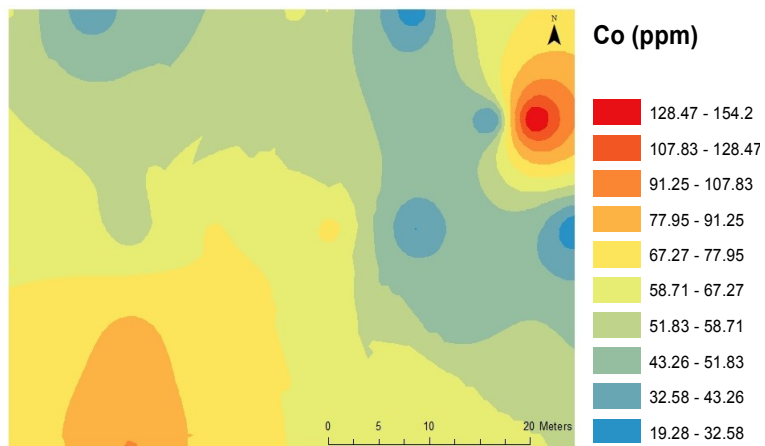
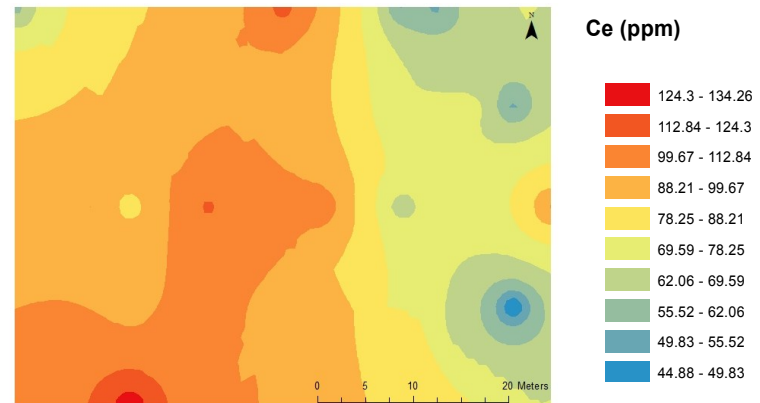
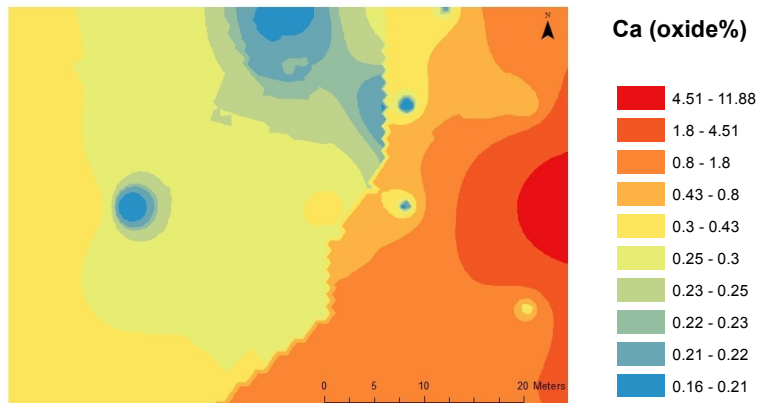
Sr (ppm)



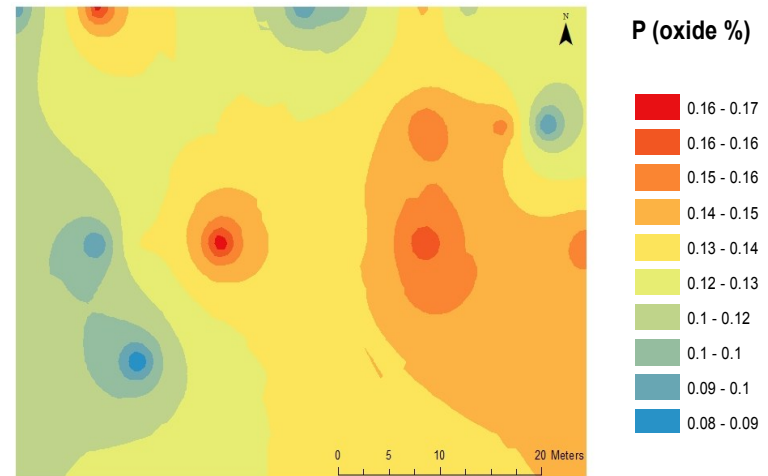
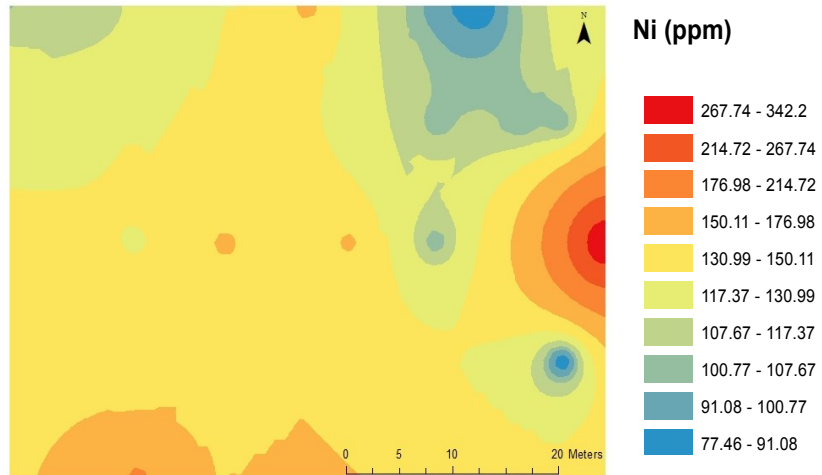
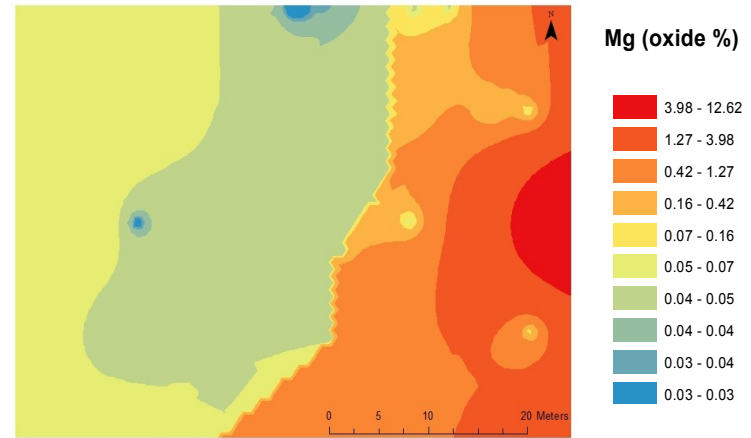
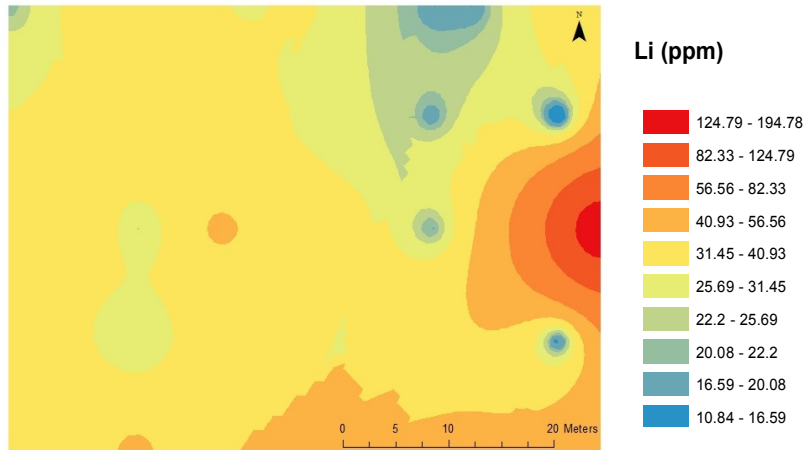
Zn (ppm)



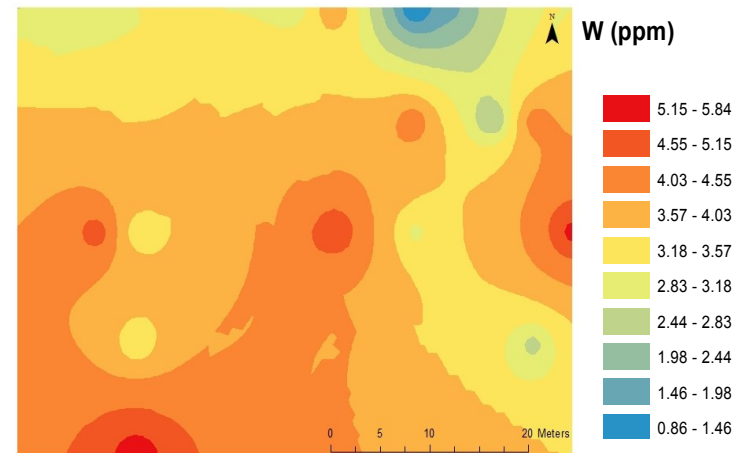
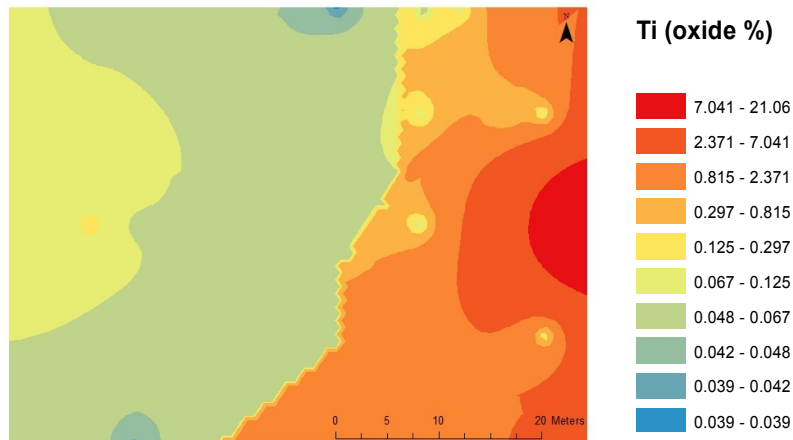
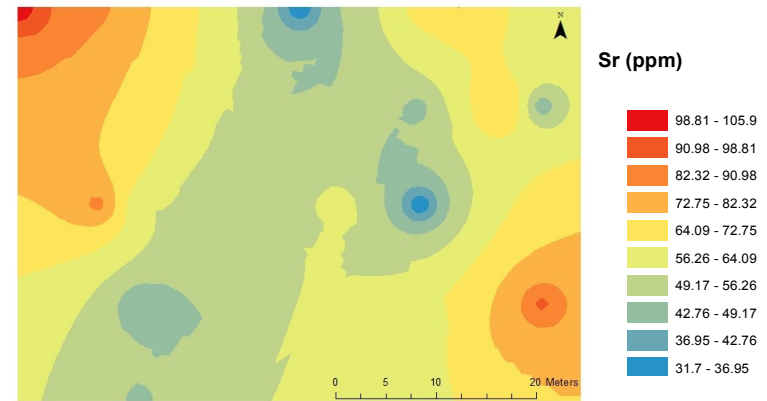
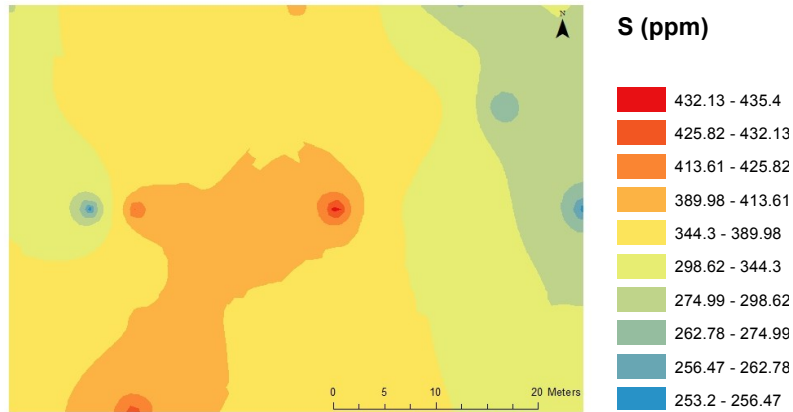
F2.5 My Cove (alphabetical order)



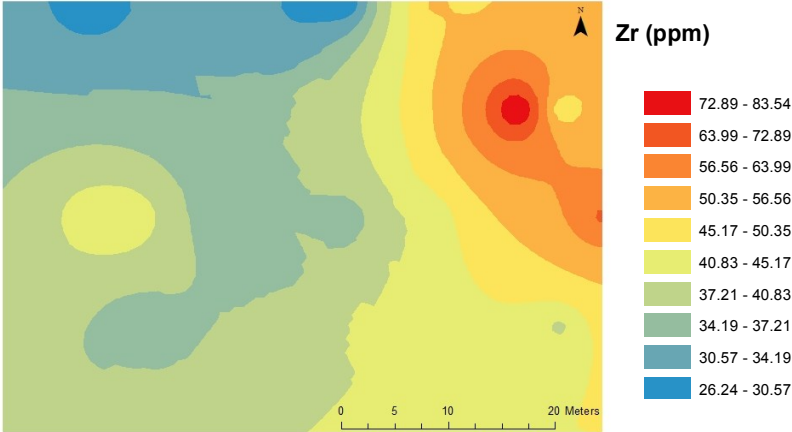
F2.5 My Cove (alphabetical order)



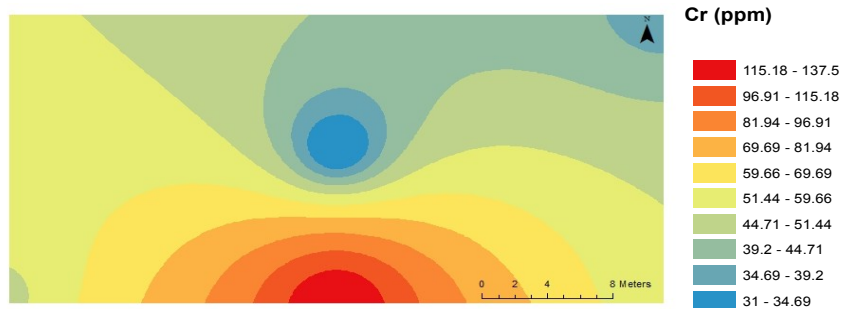
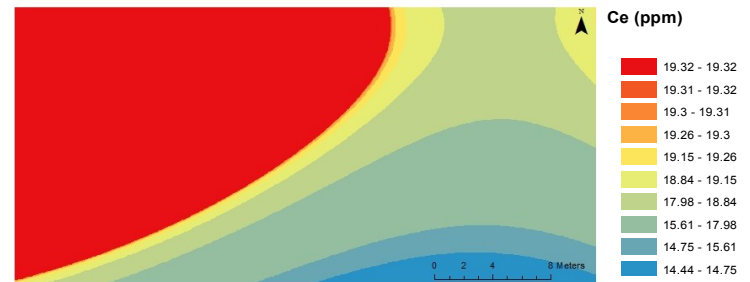
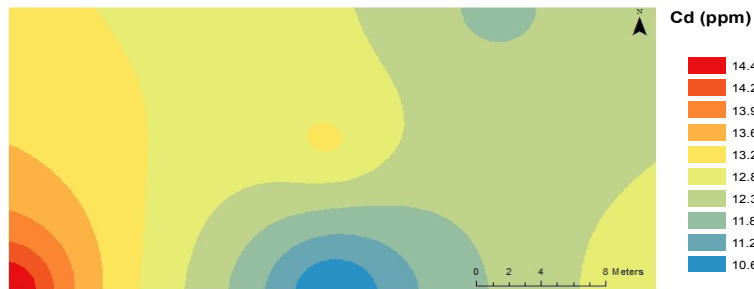
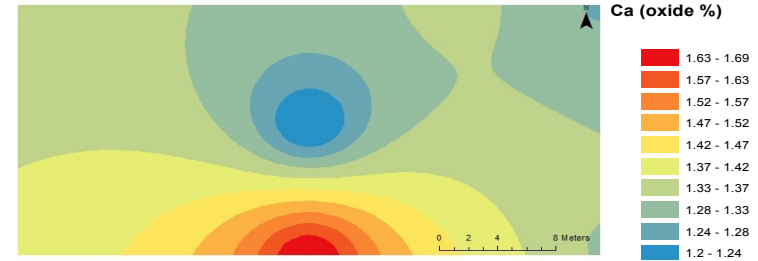
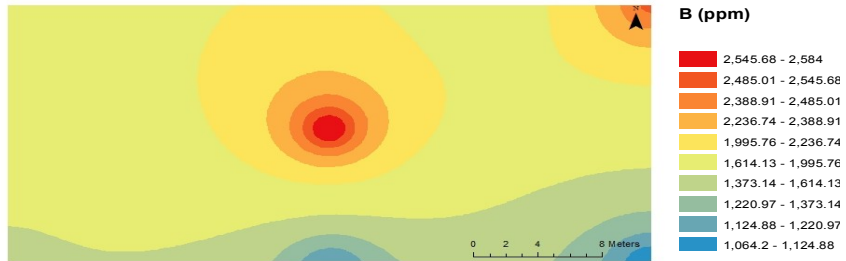
F2.5 My Cove (alphabetical order)



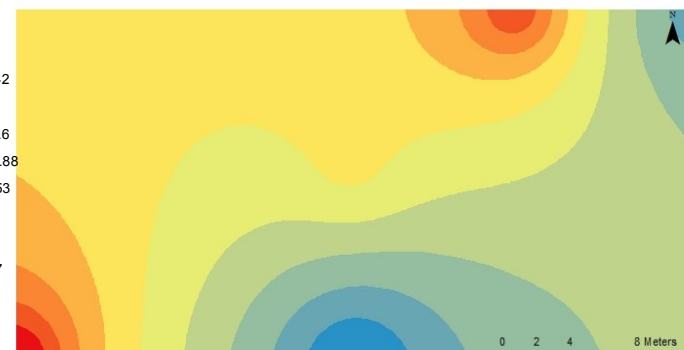
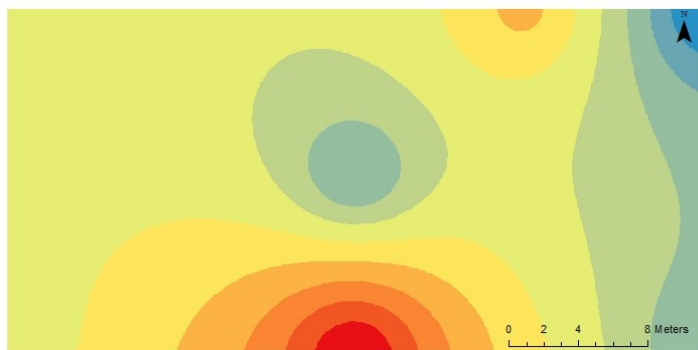
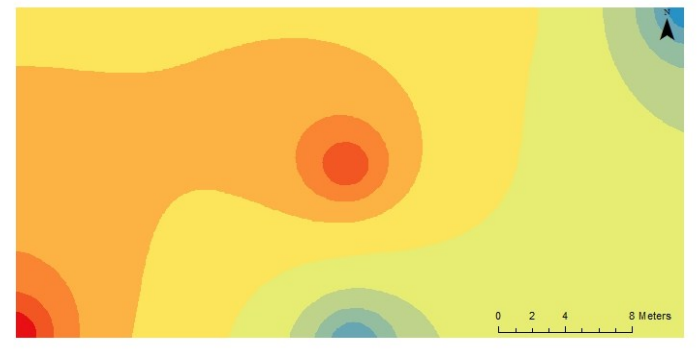
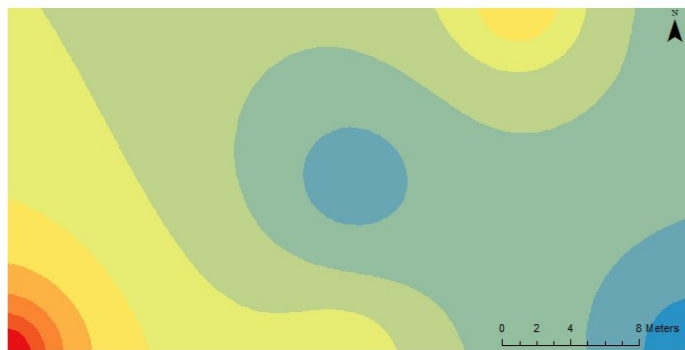
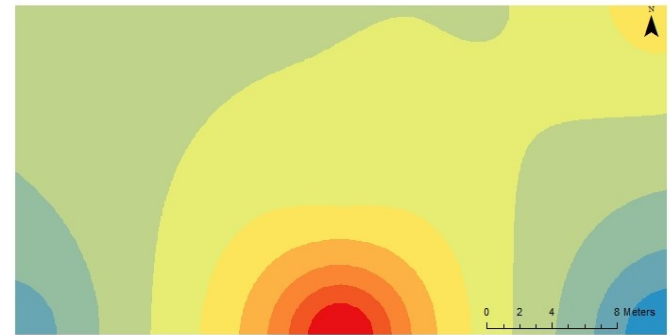
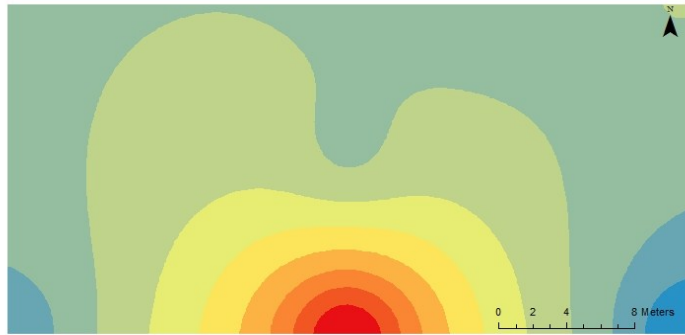
F2.5 My Cove (alphabetical order)



F2.6 Island Site (alphabetical order)



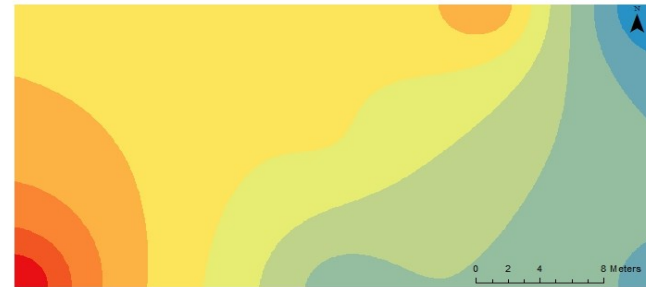
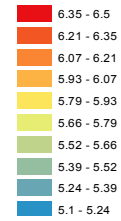
F2.6 Island Site (alphabetical order)



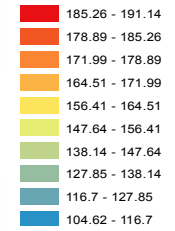
F2.6 Island Site (alphabetical order)



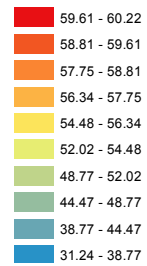
Y (ppm)



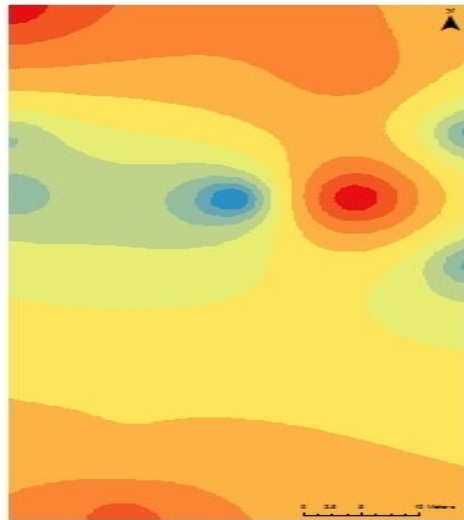
Zn (ppm)



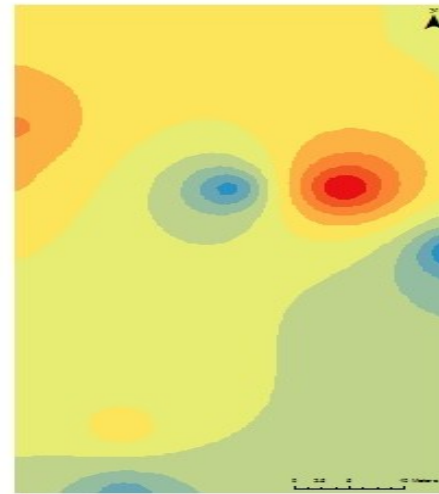
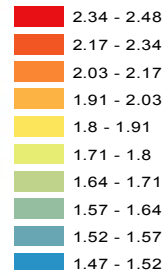
Zr (ppm)



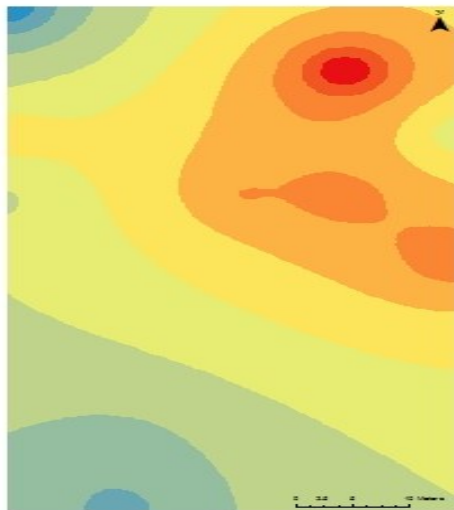
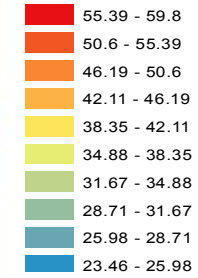
F2.7 Small Site (alphabetical order)



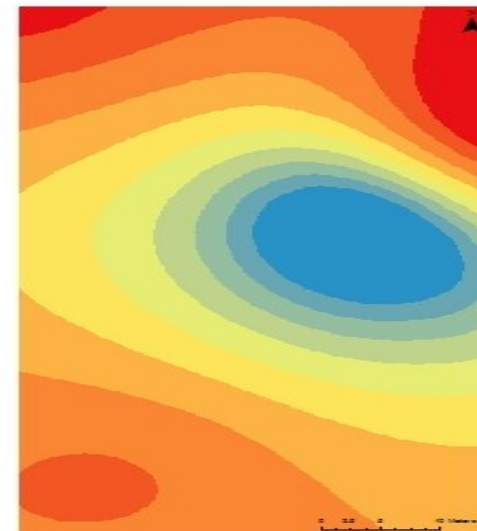
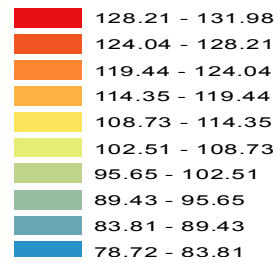
Na (oxide %)



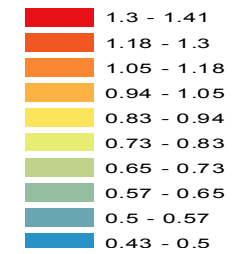
Zr (ppm)



Ni (ppm)



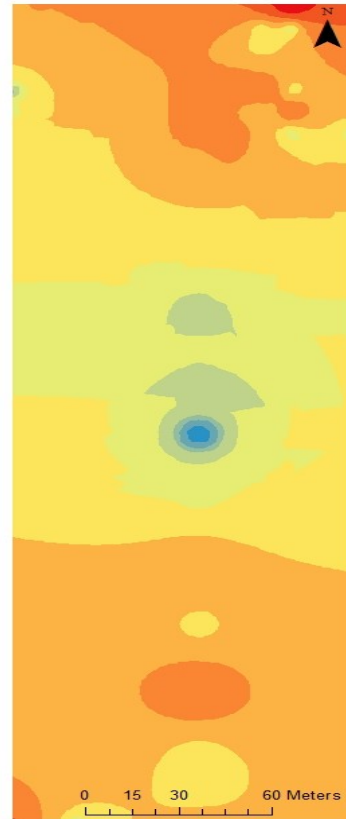
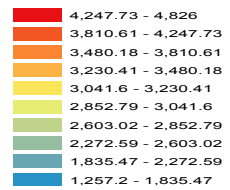
P (oxide %)



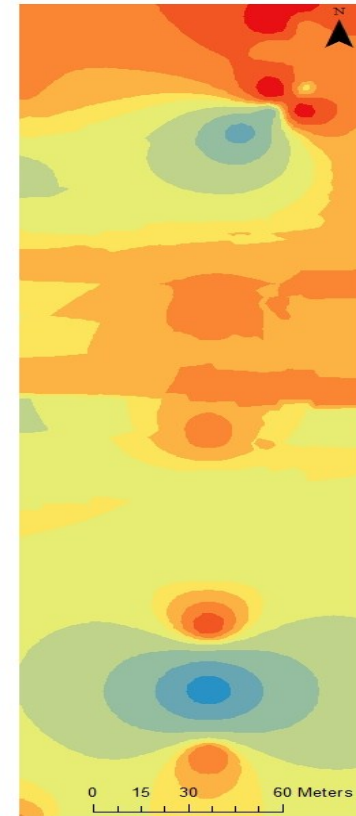
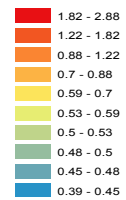
F2.8 Sowden 46 (alphabetical order)



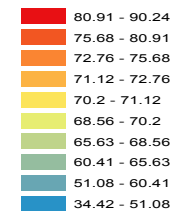
B (ppm)



Ca (oxide %)



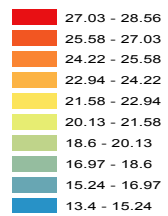
Ce (ppm)



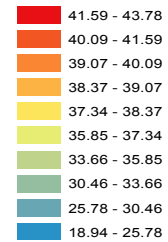
F2.8 Sowden 46 (alphabetical order)



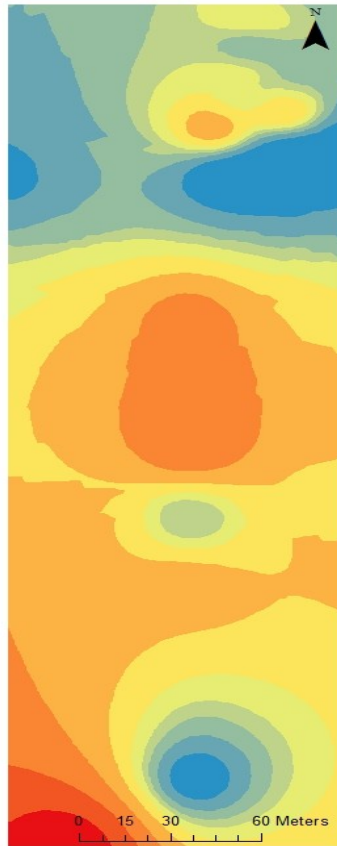
Cr (ppm)



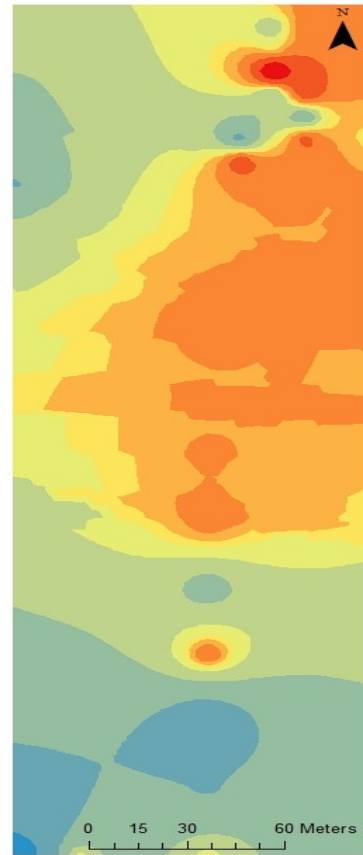
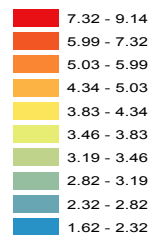
La (ppm)



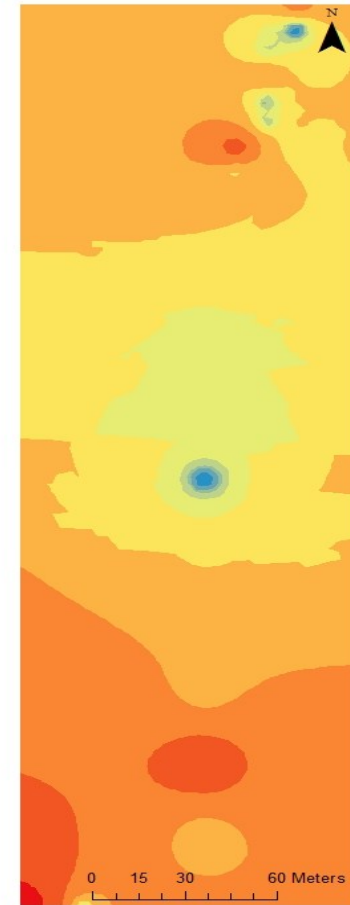
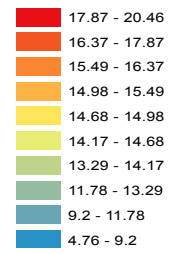
F2.8 Sowden 46 (alphabetical order)



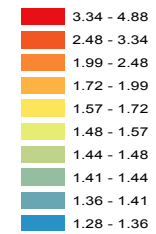
Li (ppm)



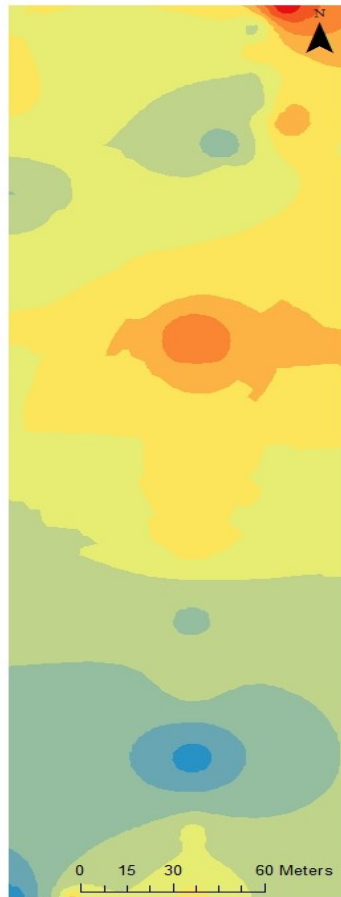
Mo (ppm)



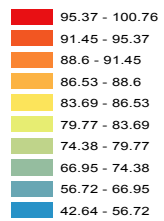
Na (oxide %)



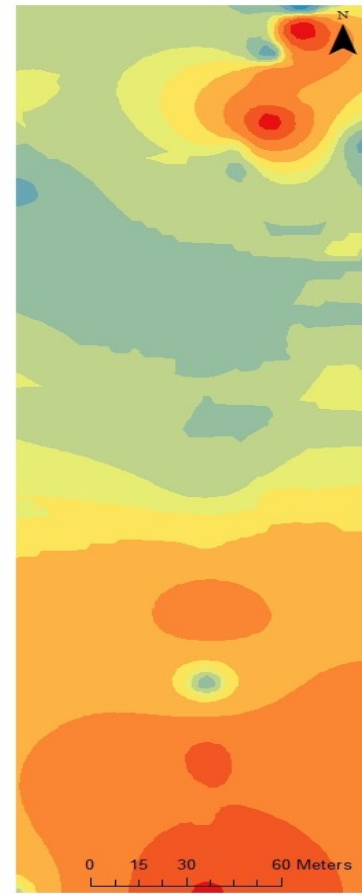
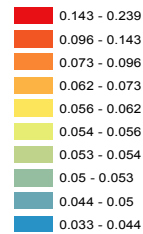
F2.8 Sowden 46 (alphabetical order)



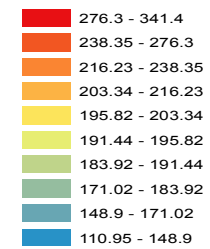
Ni (ppm)



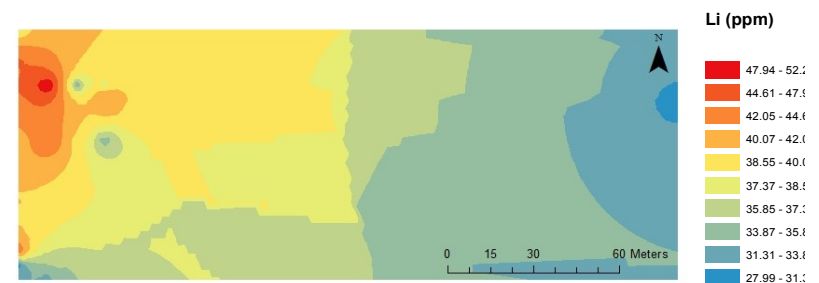
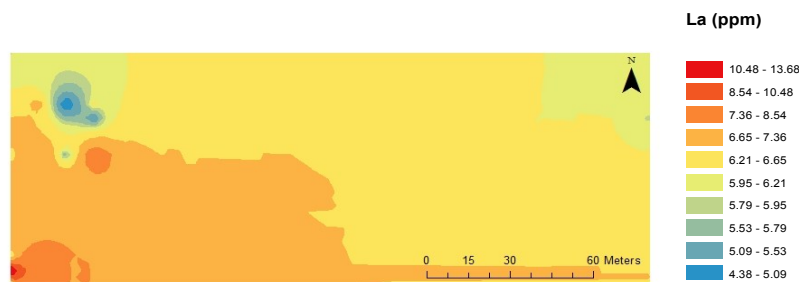
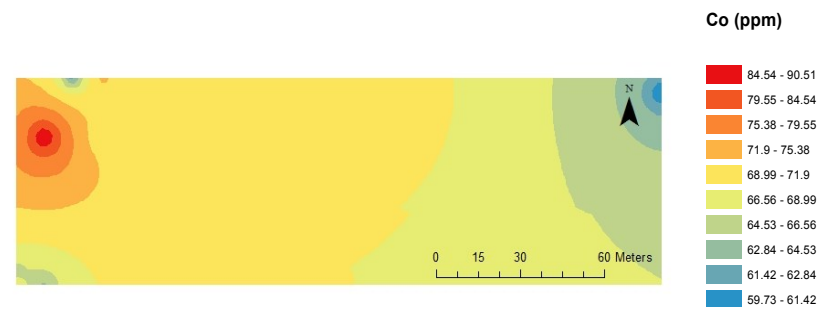
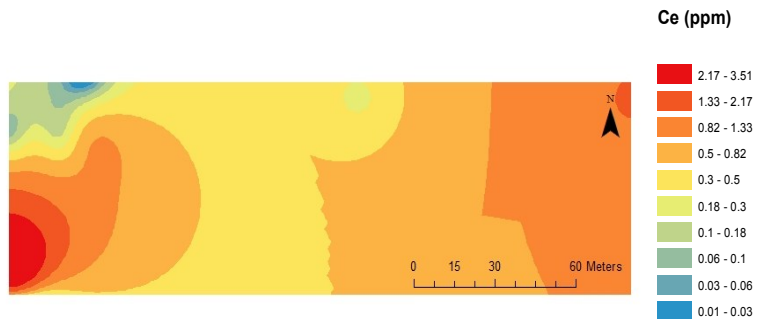
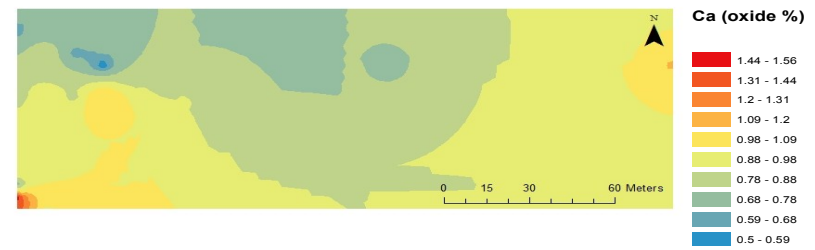
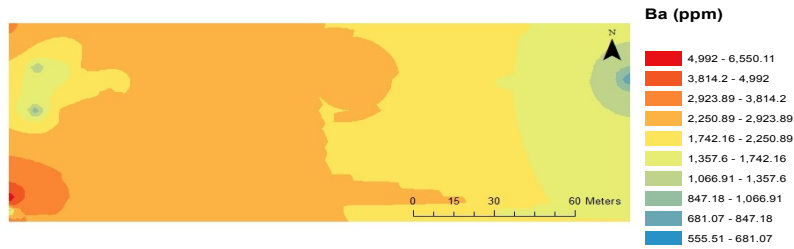
Ti (oxide %)



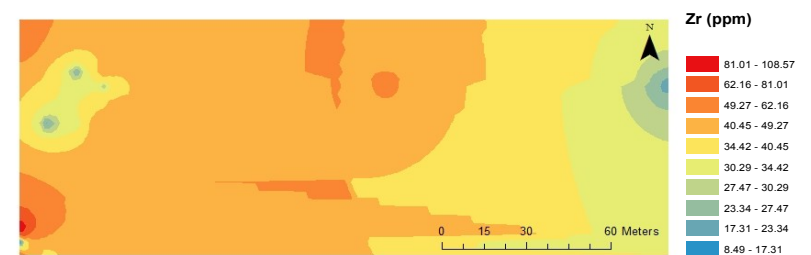
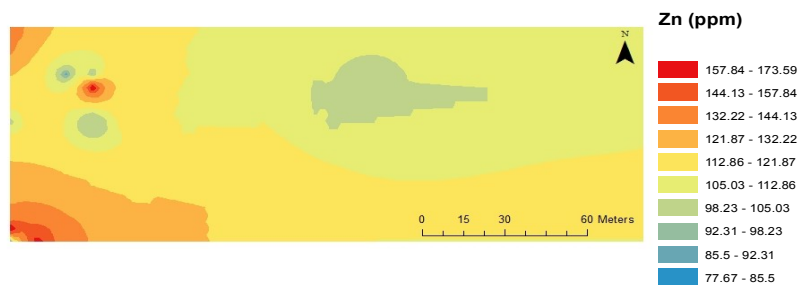
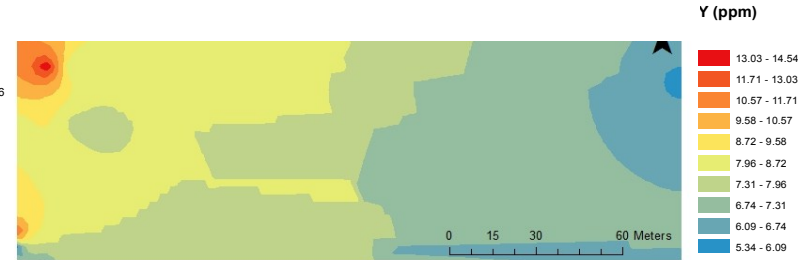
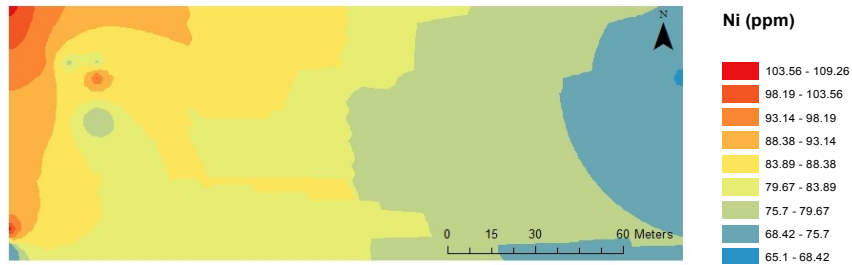
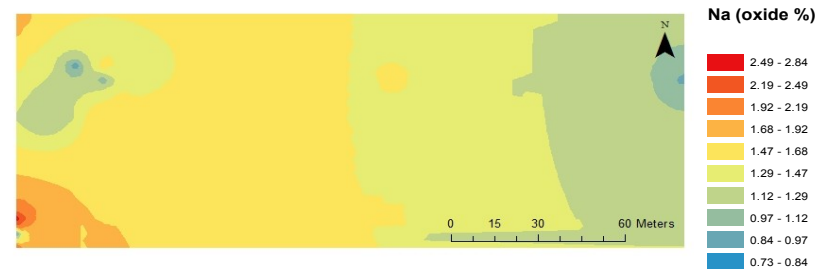
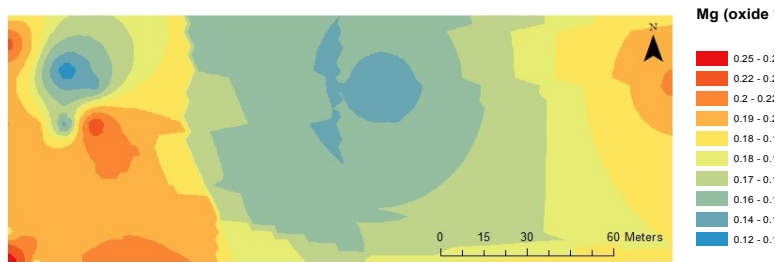
Zn (ppm)



F2.8 Sowden 41 (alphabetical order)



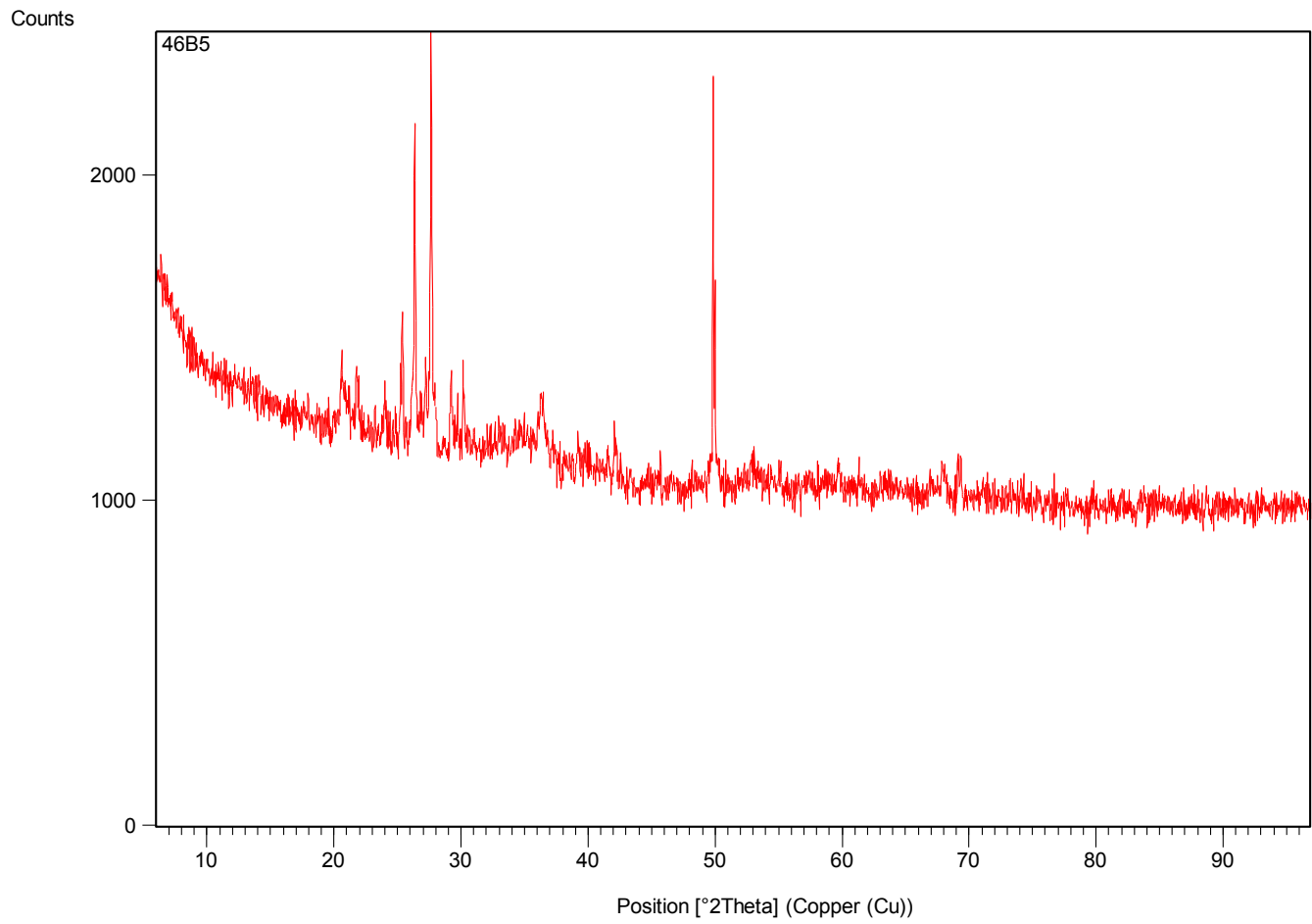
F2.8 Sowden 41 (alphabetical order)



Appendix G: XRD Spectrums

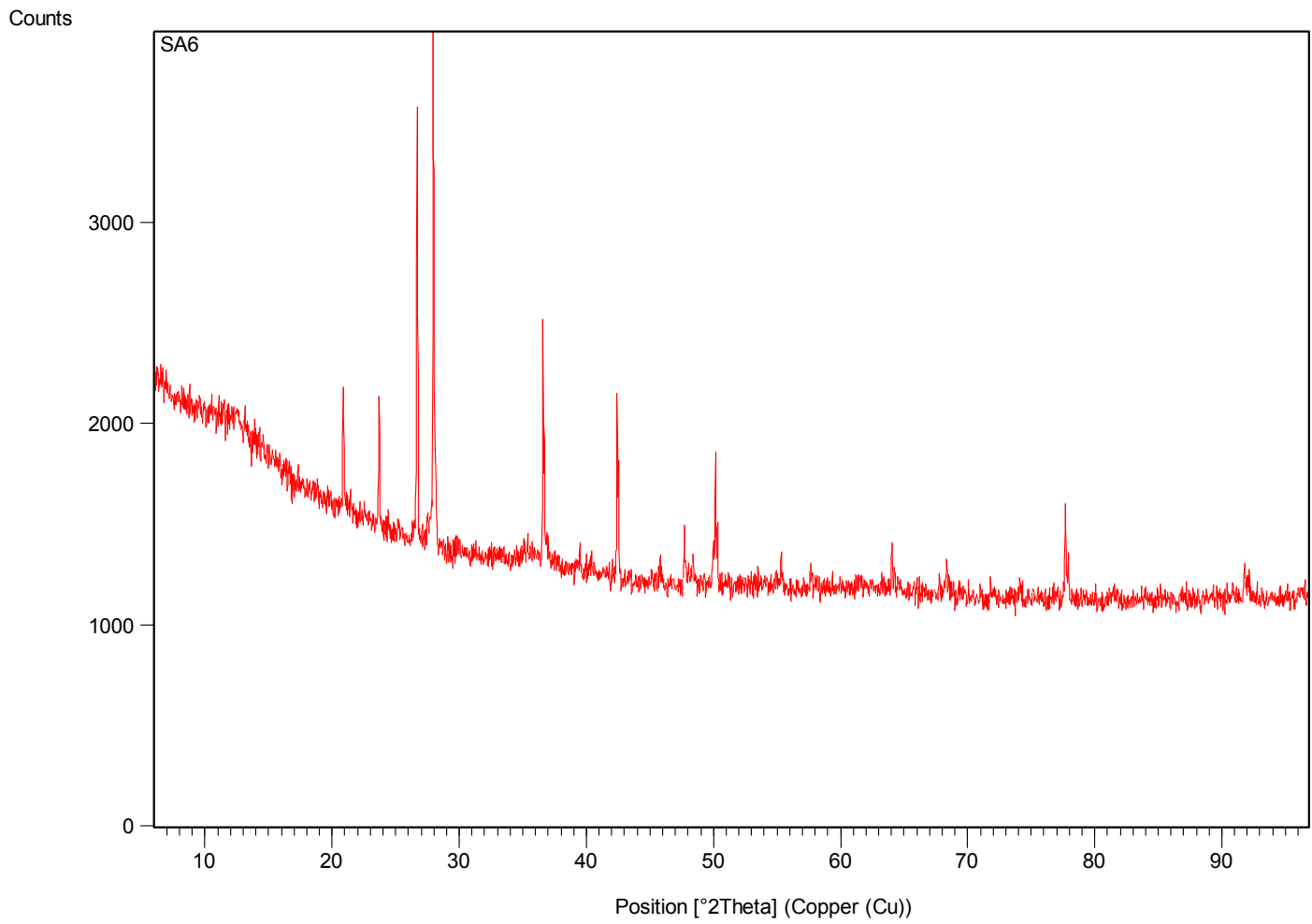
G1: XRD Sowden Lake Spectrum.....	118
G2: XRD Shebandawan Lake Spectrum.....	119
G3: XRD Lake Charlotte Spectrum.....	120

G1: XRD Sowden Lake Spectrum



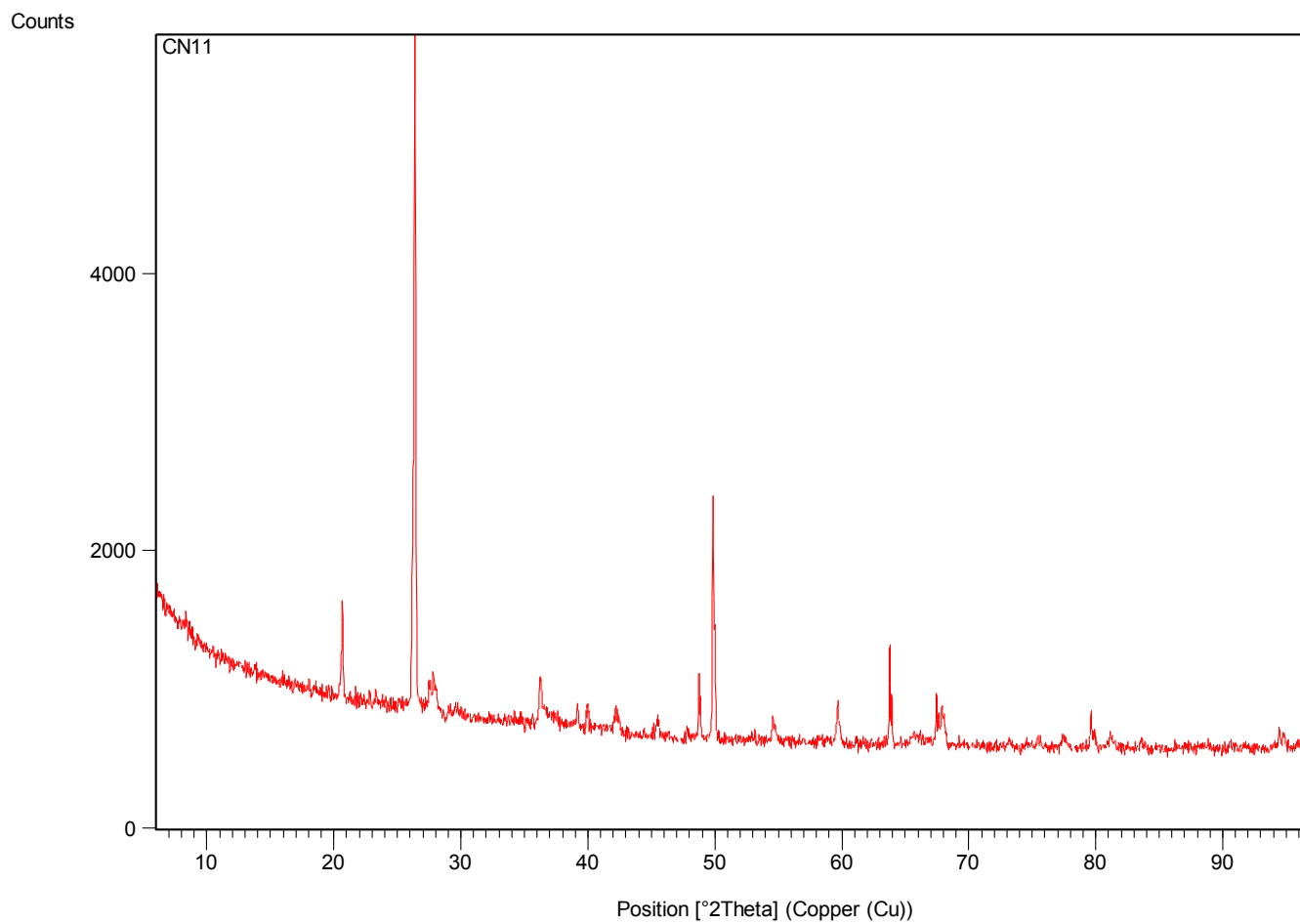
Typical Sowden Lake precipitate XRD spectrum. This spectrum is from Area 46, sample B5.

G2: XRD Shebandawan Lake Spectrum



Typical Shebandowan Lake precipitate XRD spectrum. This spectrum is from Small Site, sample A6.

G3: XRD Lake Charlotte Spectrum



Typical Lake Charlotte precipitate XRD spectrum. This spectrum is from 7 Cove, sample N11.